SYNTHESIS AND CHARACTERISATION OF POLYAMIDE 6 BLENDS - MADE BY REACTIVE EXTRUSION

A Thesis Submitted for the Degree of Doctor of Philosophy

by

Joo Fai TUNG

Department of Materials Technology

Brunel University

August, 1993

Abstract

Continuous anionic polymerisation of catalysed ∈-caprolactam has been undertaken on an intermeshing co-rotating twin-screw extruder for the preparation of polyamide 6. An optimised extruder screw and barrel configuration was used during reactive extrusion process to permit necessary feeding, mixing, devolatilising and pumping requirements. Various screw speeds and barrel temperature profiles were also employed to influence the thermal and shear history of the reaction mixture. Differential scanning calorimetry and wide angle X-ray diffraction techniques were used to characterise the thermal properties and crystalline order of the polymerisation product. It was observed that the extent and form of the crystalline structure can be greatly influenced by the material composition, method of preparation and annealing procedures during and after the polymerisation stage.

Molecular weight, molecular weight distribution and residual monomer content of the reactive polymerised PA6 samples as determined by solution viscometry, gel permeation chromatography and gas chromatography analysis revealed that these properties could be influenced by polymerisation conditions in the extruder, yielding values of M_w up to 100 kg.mol^{-1} and polydispersity index as high as 6 with monomer residue contents of 4-6%. Selected mechanical properties of the PA6 samples as measured using standard test procedures exhibited superior impact and elongational properties under tensile deformation but showed a slightly reduced tensile strength compared to commercial polymer.

A reactive polymerised blend of PA6 with 10 wt% EPR copolymer has been successfully synthesised in a similar manner using the twin-screw extruder at a screw speed of 150 rpm. This elastomer modified blend material exhibits superior tensile and impact strength compared to the pure PA6. Enhancement of the mechanical properties is postulated to be attributed to the formation of a PA6-g-PE graft copolymer which can possibly functioned as an emulsifying agent to lower the interfacial tension between the two phases thereby compatibilising the blend. Experimental evidence from FTIR and phase solubility studies have supported the formation of this graft copolymer. Characterisation studies by DSC, DMA and WAXD suggested structural modification of the EPR copolymer has occurred as a result of chain scission during the polymerisation/blending process leading to the formation of a crystalline PP phase and an amorphous PE component. Macroradicals formed from this mechano-degradation reaction by chain scission of the reacting polymers are postulated to be responsible for the formation of this graft copolymer.

Blends of reactive polymerised PA6 and a commercial grade isotactic PP homopolymer of compositions 10%, 30%, 50% and 70% PP were also prepared with and without the presence of another commercial grade functionalised PP compatibiliser. Results obtained from structural, morphological and mechanical studies obtained for the non-functionalised blend of 10% PP showed apparent "miscibility" of the phase components which is an unexpected observation since PA6 and PP are well known to be incompatible. It is postulated that a branched PP and a PA6-g-PP graft copolymer has been formed, as a result of mechano-degradation reaction during the extrusion/blending process. Reaction blends with higher PP compositions however, showed incompatibility behaviour with coarse blend morphology and poorer mechanical properties. Phase inversion phenomena for this reaction blend is observed at PA6 composition of 30% with evidence of interpenetrating polymer network structure in the blend mophology.

The functionalised reaction PA6/PP blends with 5% compatibiliser showed phase separation of the polymer components in all compositions as evidenced from DSC, WAXD, DMA and SEM studies. No improvement of mechanical properties was observed as compared to the blends without compatibiliser. A PA6-g-PP-g-MA graft copolymer has postulated to have formed between the PA6 and the compatibiliser but this compatibisation effect is not efficient enough to enhance the mechanical behaviour of the blends.

ACKNOWLEDGEMENTS

I am sincerely indebted to my project supervisor Dr. P.R. Hornsby, for his constant encouragement, supervision and technical advice throughout the course of this project. Many thanks are also accorded to the project co-supervisor, Dr. M.J. Folkes, for the many useful discussions and assistance related to the research work.

My grateful thanks also go to all the technicians of the Materials Technology Department, Brunel University for their kind assistance and guidance in my experimental work. Special thanks are convey to Mr. P. Bradbrook and Ms M. Tyce, as well as other administrative staff for their help and kind cooperation.

Special thanks are also due to other research staff and students especially Dr. K. Tarverdi, Dr. Lee, Jian, Aziz, Ian, Chris and Ansgar, who have offered invaluable assistance towards completion of my research programme.

I owed a profound debt to my employer, the Standards and Industrial Research Institute of Malaysia (SIRIM), especially the Director General, Dato' Dr. Ahmad Tajuddin bin Ali, in granting me a scholarship and study leave for the completion of this project. Many thanks are also to be accorded to the staff of the Plastics Technology Group, SIRIM for their kind cooperation and assistance.

I would also like to thank my parents and members of the family for their strong encouragement and confidence in me.

Finally, my wife Sharon Wong deserves my wholehearted thanks for her unlimited support and encouragement during these three years of study. I have no words to express my gratitude and affection for all her sacrifice especially in shouldering the "fatherly" responsibility for our two darling daughters, May Yen and May Jean throughout this endeavour.

CONTENTS

CHAPTER 1

INTRODUCTION

1.1 Reactive Extrusion

Reactive extrusion refers to the performance of chemical reactors during continuous extrusion of polymers and/or polymerisable monomers. It is different from the performance of chemical reactors run in long residence time batch mixers or knead reactors (which are types of reactive compounding), and from Reaction Injection Moulding (which is a type of reactive processing). While not a new or novel process, reactive extrusion has been the subject of vigorous research activity in recent years, both in industry and academe, and has resulted in numerous commercial processes and products.

The primary factor for the success of reactive extrusion is the extruder's unique suitability as a vehicle for performing chemical reactions in the bulk process i.e. without the use of diluents, to produce "value-added" specialty polymers through chemical modification of existing resins or, when appropriate, to produce polymers from monomers. This virtue results from its ability to pump and mix highly viscous materials and to facilitate the staging of multiple process steps in a single machine, including melting, metering, reacting, side-stream addition, venting and under appropriate circumstances, even final product forming.

Although bulk polymerisation processes taking place in stirred tanks are simple, economic and straight-forward, they are useful up to a certain viscosity level of the reactive mixture. As the polymerisation proceeds, melt viscosity increases and after a certain point, the material becomes unmanageable for mixing, and heat transfer limitations become critical. At this stage, the material has to be transferred into an extruder for completion of the reaction.

Screw extruders have been used to resolve these heat and mass transfer problems. The ability of these machines to continuously create new thin surface layers during processing operations can effectively increase the degree of mixing and also minimise the temperature gradients within the polymer being produced. Another factor that can be controlled, via operating and geometrical specifications of screw extruders, is the residence time in the reactor system. Generally the residence time is substantialy lower as compared to that required in a batch reactor for the same reaction. Thus, the problem of long exposure period to high temperatures, that can cause polymer degradation, is minimised.

Furthermore, the ability of an extruder to process polymeric materials with high viscosities without any solvents can also result in a dramatic cost reduction both in raw materials and solvent-recovery equipment.

Finally, for polymer modification reactions, reactive extrusion processes offer natural means for chemical crosslinking and grafting at any reaction stage via stage-feeding of reactive agents along the extruder barrel. This way, one can tailor-make small quantity specialty polymers that are uneconomical to produce in large scale operations.

The combination of chemical reactions and polymer processing as in reactive extrusion, therefore, offers a rich potential means for further development of new and novel polymeric products and processes.

Figure 1.1 illustrates the case of an extruder reactor process in comparison with a typical Continuous Stir Tank Reactor (CSTR) process, done in hydrocarbon solution. Operations unique to the conventional solution process are shown inside the solid circle while the dashed circle shows equipment unique to the extruder process.

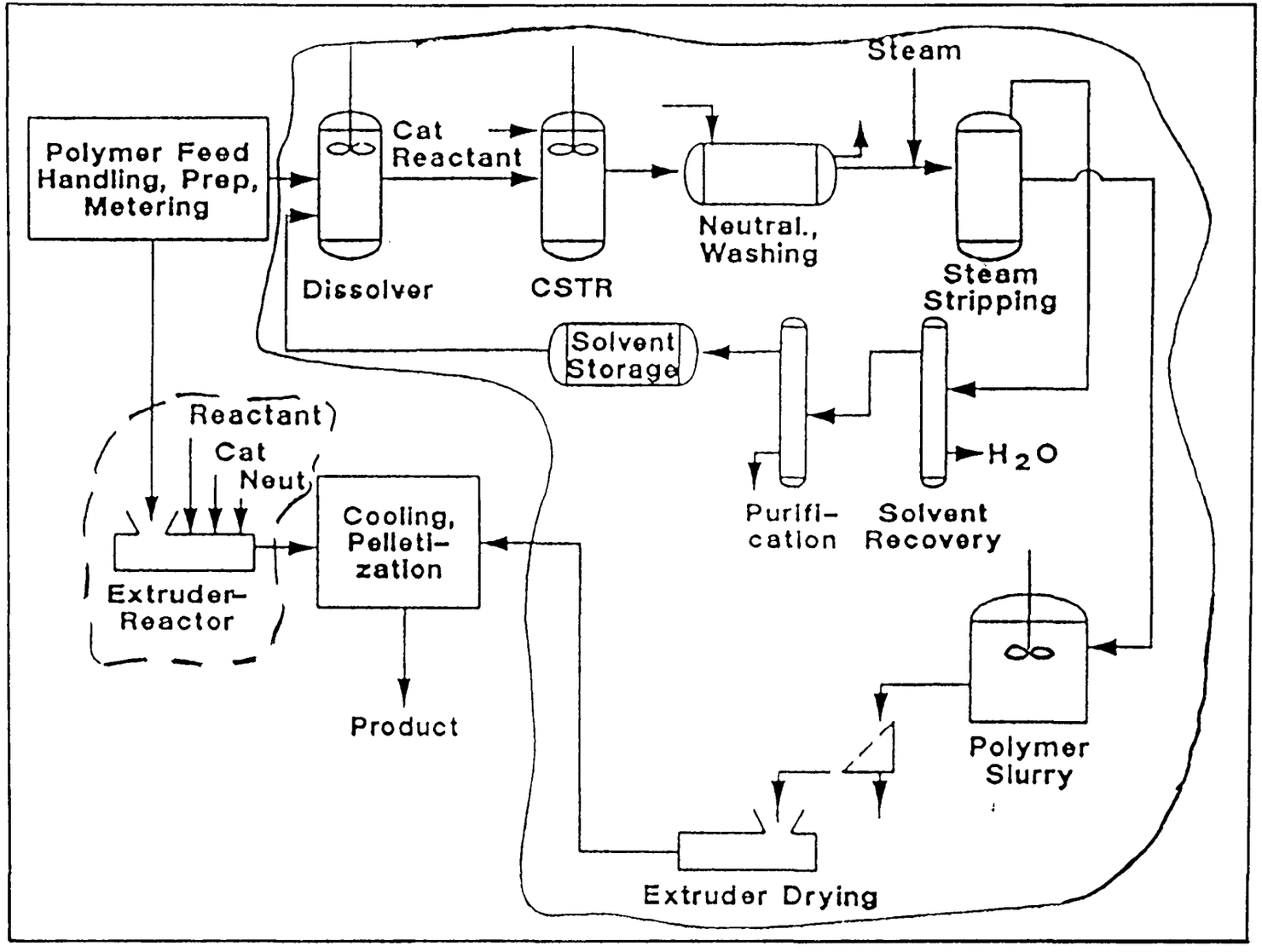

Figure 1.1 Comparision of an extruder and continuous stir tank (CSTR) reactor process

1.2 Polyamide 6

Polyamides are amongst the foremost group of engineering thermoplastics, accounting for almost half the world's consumption of these specialty resins. Polyamides, frequently referred to as "nylons" are the first plastics to be developed that could be considered for engineering applications in areas which are traditionally associated with metals. Even fifty years from their commercial development, the growth rate at 4-5% is still above average and shows no sign of slowing down. The rate of new product development is probably greater in polyamides than in any other group of polymers.

Polyamide 6 is one of the earliest polyamide materials to be developed, and together with polyamide 6,6, have dominated the polyamide group in terms of commercial importance and account for over ninety percent of world consumption of polyamides. Polyamide 6 is the generic term for a synthetic linear polyamide in which the repeating unit of the chemical structure contains six carbon atoms, one belonging to the carbonyl group of the recurring amide group (-CONH-), and five to the $-(CH_2)_5-$ moiety interlinking the amide groups. Today, most of the polyamide 6 is produced in the form of filament yarns and stable fibre yarns for the manufacture of carpets, tyre cords, apparel, hosiery, upholstery, seat belts, parachutes, ropes and industrial cords.

In addition, considerable quantities of polyamide 6 are also used in many commercial injection moulding, extrusion and casting operations for the manufacture of moulded products, tubing, pipes, tapes, sheets, rods and monofilaments to be used as components in automobiles, appliances, machinery, electrical and consumer goods. However, the by far largest uses of all polyamide 6 manufactured are for tyre cords, industrial cords and textile yarns.

Industrial operation for the manufacture of polyamide 6 involves the ring opening polymerisation of ϵ-caprolactam. This process entails initiation by either water or

a strong base. The water initiated process is known as the hydrolytic polymerisation whereas initiation by a strong base is conducive to anionic polymerisation that requires anhydrous conditions [Figure 1.2].

The most important commercial process today for the synthesis of polyamide 6 is the hydrolytic polymerisation which may be performed either batch wise or in a continuous operation. The process flow chart is as shown in Figure 1.3. This polymerisation process is characterised by heating ∈-caprolactam in the presence of water or water releasing substances to temperatures in the region of 250 - 270°C for periods of about 12 hr to more than 24 hr depending upon the reactor configuration and property requirements of the final polymer.

The second approach for commercial synthesis of polyamide 6 is the base initiated anionic polymerisation process, which is characterised by a fast rate of conversion. Two techniques are associated with this manufacturing technique; a "high temperature" polymerisation which is initiated and carried out at temperatures above 220°C and a "low temperature" polymerisation which requires an operation wholly executed at temperatures in the range of 140 - 180°C. Both techniques involve the use of catalytic compounds such as the carbonates, hydrides, amides, alcoholates and hydroxides of alkali and alkaline earth metals as well as metal organic compounds.

However, the low temperature polymerisation process can only proceed satisfactorily in the presence of a strong base and an activator. N-acyl lactams, acyl ureas and imides such as N, N, N'-, N'-tetraacetyl hexamethylene diamine are classes of compounds widely used as activators for this polymerisation reaction. This low-temperature, anhydrous polymerisation prosess for polyamide 6 is frequently referred to as monomer casting since thick commercial polyamide 6 products of solid rod and profile shapes are obtained in essentially one single stage from the monomeric caprolactam.

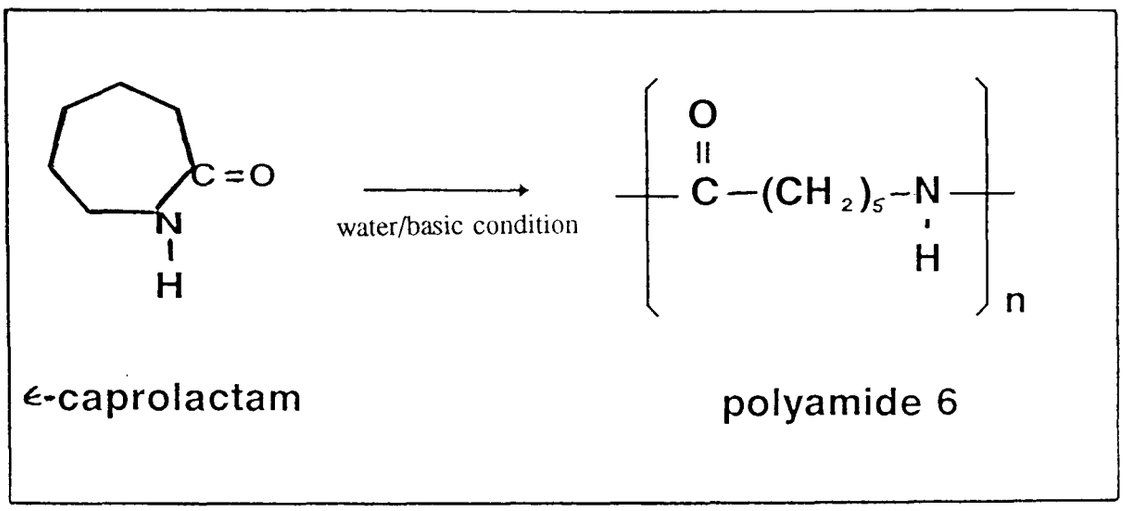

Figure 1.2 Ring opening polymerisation of ∈-caprolactam

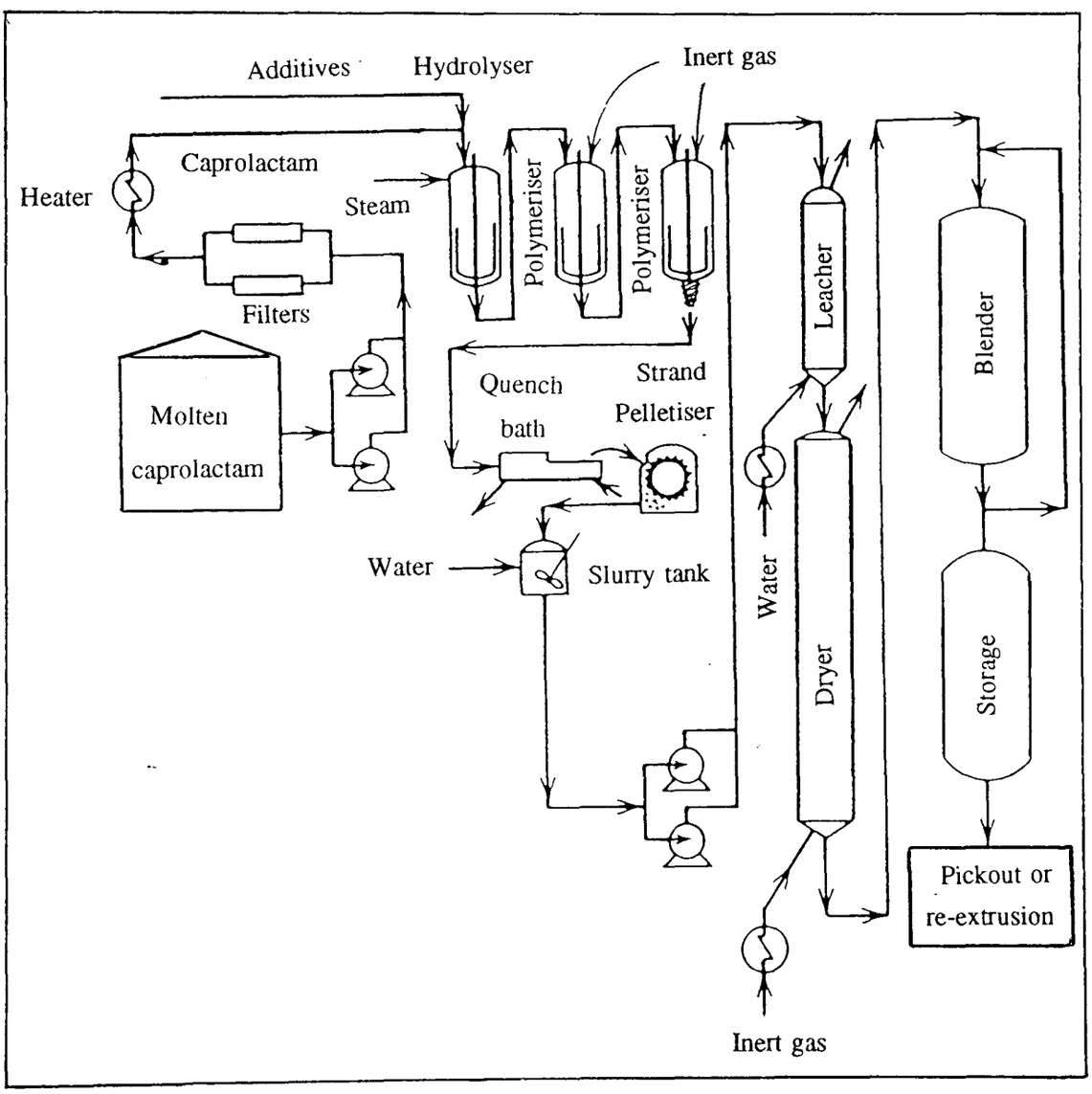

Figure 1.3 Commercial hydrolytic polymerisation process for polyamide 6

In the 1980's , this activated anionic polymerisation process also formed the technological basis for the development of polyamide 6 block copolymers using Reaction Injection Moulding (RIM) technique which has been widely used for the production of elastomer toughened automotive components.

1.3 Polymer Blends

Polymer blending represents one of the fastest growing segments of polymer technology from the standpoint of commercial products application and development. Both the open and patent literature in this area of work is voluminous. In principle, blending two materials together in order to achieve a balance of properties not obtainable with a single one is an obvious and well-founded practice which has been successfully exploited in metallurgical science for decades. With polymers, however, the thermodynamics of mixing do not usually favour mutual solubility and therefore most binary polymer mixtures form two distinct phases. This is a direct consequence of their high molecular mass. In spite of this, many immisible polymer systems form useful commercial products. Some key examples include elastomer toughened plastics such as high impact polystyrene (HIPS) and acrylonitrile butadiene styrene (ABS).

There is no doubt that the main reason for polymer blending is economy, especially due to the ever increasing capital cost involved in the development of new polymeric materials. If a "new" material can be generated at a lower cost with properties meeting specifications, the manufacturer will definitely be glad to use it to remain competitive in business. In general, the following economy-related reasons can be cited for the development of polymer blends:-

* generation of unique material as far as its processibility and/or performance are concerned;
* extending the performance of expensive and specialty resins;

* quick modification of performance properties possibly at a lower cost; and
* reuse of plastics scrap materials

Different processes are being used for the preparation of polymer blends such as mechanical mixing, dissolution in co-solvent then film casting, freeze or spray drying, latex blending, fine powder mixing and the use of monomers together with another blend component followed by polymerisation, as in the preparation of interpenetrating polymer network (IPN) system.

Very often for the blending of two incompatible polymer components, a third component called compatibiliser or interfacial modification agent is used in order to obtain a stable and reproducible dispersion which would lead to the desired blend morphology and properties.

Polyamide 6 with its characteristically high heat resistance, stiffness, tensile strength and oil resistance properties, is widely used in engineering applications. However, it also possess certain inherent disadvantages such as affinity to absorb moisture (which has an adverse effect on their mechanical properties), notch sensitivity and moderate impact strength. Considerable attempts have been made to strengthen and modify the polyamide 6 properties by glass-reinforcement and blending with elastomers, as well as polyolefins. However, it is well known that preparation of either a polyamide 6/polyolefin or polyamide 6/elastomer blend is difficult since these are two incompatible polymers with different molecular polarity and crystalline structures.

In order to overcome this poor interfacial adhesion problem, a third polymer or compatibiliser is used which has reactive chain ends partially compatible with both polyamide and polyolefin phases. The compatibilisers used are usually graft copolymers or block copolymers of polyolefins containing anhydride or carboxyl functionalities to form amide or imide linkages with the polyamide phase.

1.4 Objectives of Study

Adaptation of the fast anionic polymerisation reaction used in the polyamide 6 monomer casting batch process to a continuous, dynamic process involving reactive polymerisation of ∈-caprolactam in a twin-screw extruder reactor, forms a principal objective of this study.

Extrusion processing parameters, including reactant formulation, processing temperature, screw speeds and geometry as outlined in Figure 1.4 are explored and their effects interrelated to the microscopic and macroscopic properties of the polyamide 6 polymer synthesised in the extruder.

A further objective of the work is to consider novel reactive extrusion processes involving in-situ polymerisation of polyamide 6 and subsequent melt-blending separately with ethylene-propylene copolymer (thermoplastic elastomer), as well as commercial grade isotactic polypropylene homopolymer in the twin-screw extruder to produce reactive polymerised polyamide 6 blends. These materials are then characterised to investigate the relationship between structural and physical properties in relation to blend compositions and processing variables.

1.5 Outline of Thesis Structure

Chapter 1 includes a brief introduction on reactive extrusion and properties of polyamide 6 and blends relevant to this work. Study objectives are presented together with an outline of the research programme.

Chapter 2 begins with a literature survey on reactive extrusion followed by a review on studies using extruder (single screw and twin-screws) as polymerisation and chemical reactor for polymer synthesis and chemical modification. Studies on structural forms of polyamide 6 are then reported followed by a comprehensive

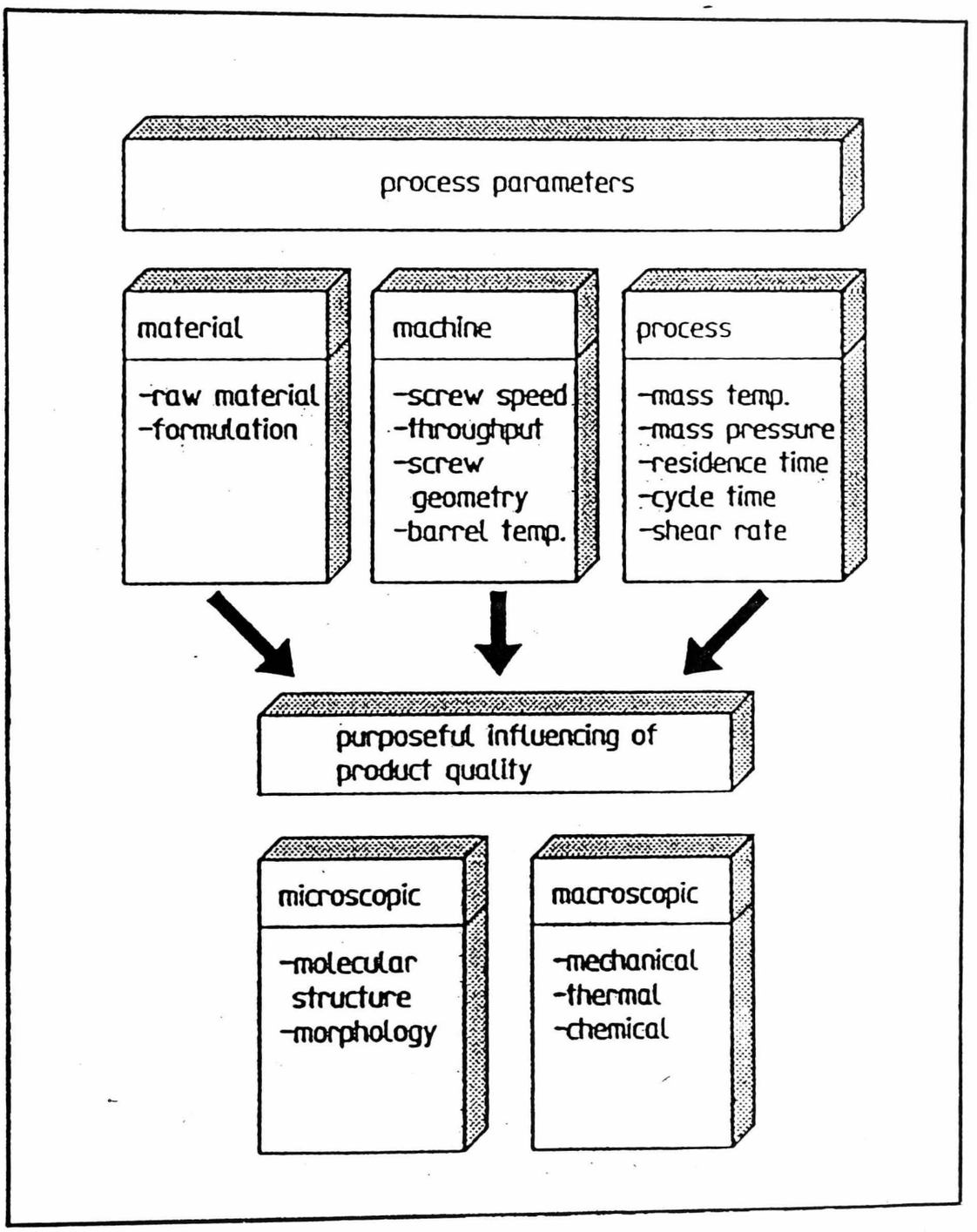

Figure 1.4 Correlation of extrusion processing variables and properties of reactive polymerised polyamide 6

review on work done in the areas of polyamide 6/elastomer, polyamide 6/ polypropylene, and polyamide 6 composites reinforced with glass fibres.

Chapter 3 describes the raw materials, extruder configuration and processing parameters used for the activated anionic polymerisation of ∈-caprolactam to polyamide 6. Characterisation techniques for evaluation of the microscopic and macroscopic properties of the polymer materials are outlined followed by discussion of the properties obtained with respect to extrusion processing conditions used.

Chapter 4 outlines the raw materials used and experimental procedures for the preparation of a 10% composition by weight of elastomer (ethylene-propylene copolymer) modified reactive polymerised polyamide 6 blend. Structural, morphological and mechanical properties of the materials are evaluated with respect to processing parameters and thermal treatment conditions.

Chapter 5 describes the raw materials and reactive processing conditions for the preparation of binary and ternary blends of reactive polymerised polyamide 6/ polypropylene materials. Binary blends are melt mixed during in-situ polymerisation of caprolactam with different compositions of commercial grade polypropylene homopolymer. Ternary blends are obtained under similar reactive processing conditions but with the incorporation of small quantities of an additional commercial grade functionalised polypropylene compatibiliser. Structural and physical properties characterisation of the blend samples are conducted followed by detailed discussions on possible formation of amorphous polypropylene molecules, polyamide 6/ polypropylene graft copolymers and the " apparent compatibility " of the non-functionalised polyamide 6/polypropylene blend with 10% polypropylene composition.

Chapter 6 presents some concluding remarks on the experimental results obtained and proposed suggestions for future work.

CHAPTER 2

LITERATURE SURVEY

2.1 Introduction to Reactive Extrusion

Reactive extrusion is now being viewed as an efficient means of continuously polymerising monomers as well as chemically modifying existing polymers and being defined as an engineering specialty that combines two traditional separate operations: the chemical reaction for the formation or modification of polymeric macromolecules and the processing of the polymer for the purpose of shaping it into a final product [1].

To be considered an example of reactive extrusion, a chemical reaction must take place as a result of mixing in an extruder. Hence, the production of chemically bonded laminates is not included since the actual chemical reaction takes place outside the extruder without the need for mixing. Likewise, production of foams with blowing agents are also not considered since these processes do not involve actual chemical reaction on the polymer itself.

In a typical reactive extrusion process, the reactants are fed into an extruder through a feed hopper and various other liquid or gaseous reactants or additives are then further introduced via other injection ports along the extruder barrel. The reactive mixture is conveyed through the extruder and the reaction is driven to the desired degree of completion. At this point, and after the removal of any volatile by-products (devolatilisation), the molten polymeric product is extruded through a die, water-quenched and then pelletised.

There has been intense recent activity in the field of reactive extrusion, mostly in industrial laboratories and at extruder companies rather than in academic laboratories. More than 500 patents and about 300 published papers on the subject of reactive extrusion have appeared within the last twenty years [2]. The advantages

associated with reactive extrusion based upon criteria such as improved controlled processing, economic factors and the enhancement of material properties have been discussed in short reviews by **Wielgolinski** *et al.* [3], **Kowalski** [4], **Eise** [5], **Frund** [6], **Kamal** *et al.* [7], **Ratzsch** [8], **Lambla** [9], **Brown** *et al.* [2] and more recently **Tzoganakis** [10].

The following types of chemical reactions have been performed by reactive extrusion and can be summarised into six categories [10] :-

(i) Bulk polymerisation (free radical, anionic, cationic, condensation, and co-ordination polymerisation of monomers or oligomers to high molecular weight polymers).

(ii) Controlled degradation and crosslinking of polymers (usually polyolefins) by means of a free radical initiator for the purpose of producing a product with controlled molecular weight distribution and a higher concentration of reactive sites for grafting.

(iii) Functionalisation of commodity polymers for the purpose of producing materials to be used in grafting applications.

(iv) Polymer modification by grafting of monomers or mixture of monomers onto the backbone of existing polymers for the purpose of improving various properties of the starting material. Free radical initiators and ionising radiation can be used to initiate the grafting reactions.

(v) Interchain copolymer formation. Usually, this type of reaction involves combination of reactive groups from several polymers to form a graft copolymer.

(vi) Coupling reactions which involve reaction of a homopolymer with a polyfunctional coupling agent or a condensing agent to build larger molecular mass by chain extension or branching.

2.2 The Extruder As A Polymerisation Reactor

The extruder, which has been traditionally used for continuous mixing, kneading and processing of polymers, has also been known as a polymerisation reactor for a relatively long time. Historically, extruders were used in the 1920s for rubber polymerisation which were described in the patent literature in the 1930s. A comprehensive review on the historical development of extruders in polymer processing technology has been complied by **White** *et al.* [11].

The design of extruders for polymerisation applications involves the manipulation and integration of technical information from several distinct areas. For an extruder to function as a reactive processing reactor, it must be able to deal with the continuously changing melt viscosity of the polymerising monomer . Mixing phenomena will be considerably retarded when the reactive mixture is highly viscous, and the resulting inhomogeneities in chemical composition and temperature can lead to poor product quality.

It is also important to realise that the rate of the polymerisation reaction has to be matched with residence time in the extruder to ensure completion of the polymerisation process. Provision is also has to be made for the continuous removal of unreacted monomers or volatile by-products by devolatilisation of the product at reduced pressure before exiting from the extruder. In this manner, adequate control of the degree of polymerisation may be achieved and consistent uniform product may be obtained.

Although both single and twin-screw extruder configurations are used in reactive polymerisation processes, twin-screw variants are increasingly being favoured over the single screw types. The main reasons are the extended control of residence time distribution, mixing and the superior heat as well as mass transfer capabilities. The main difference between single and twin-screw extruders is the melt conveying mechanism. In single screw extruder, the conveying depends on frictional forces in the solids conveying zone and viscous forces in the melt pumping zone. As for twin-screw extruder, the conveying mechanism depends very much on the screw geometry configurations and it is of a positive displacement character (intermeshing screws type). The relative merits and the performance of different forms of twin-screw extruder have been appraised [12, 13].

Depending on the direction of rotation of the two screws, twin-screw extruders can be categorised into co-rotating and counter-rotating extruders. As co-rotating screws are rotating in the same direction, the material is transported from one screw to the other in a figure of "8" action. This results in good dispersion and because of the high screw speeds used, higher shear rates can be achieved. By contrast, the screws of the counter-rotating extruder turn in opposite directions and the melt is moved forward axially and partially kneaded in the inter-screw clearance as experienced in a rolling mill.

Based on the degree of intermeshing operation between the screws, twin-screw extruders can be further divided into intermeshing and non-intermeshing types. The latter are extruders (often called tangential counter-rotating extruders), where the flights of one screw do not protrude into the channel of the other screw. These extruders cannot form closed or semi-closed compartments and, therefore, do not have positive conveying characteristics.

Bulk polymerisation in an extruder has been considered in review articles by **Mack** [14] and **Siadat** *et al.* [15]. In bulk polymerisation, a monomer or a mixture of monomers is converted to high molecular molecular mass polymer with little or no

solvent dilution. Extruder reactors for bulk polymerisation have been designed to convey simultaneously in different barrel segments both starting material and product with a large difference in melt viscosity, and to control within narrow limits the temperature gradient in the reaction mixture arising from the exothermic heat of polymerisation.

Generally, two types of bulk polymerisation have been performed in extruder reactors: condensation polymerisation and addition polymerisation.

Condensation polymers can arise through a repeated condensation process of two distinct monomers to give high molecular mass polymer and a low molecular mass by-product such as water or a low boiling alcohol. To ensure high conversion to polymer, the reaction equilibrium must be optimised by efficient removal of low molecular mass by-product. Extruder reactors for condensation polymerisation typically provide for vacuum venting at one or more barrel segments to remove volatile by-products.

On the other hand, addition polymer formation does not result in a low molecular mass by-product and the synthesis of addition polymers by bulk polymerisation in an extruder is often done with vacuum venting to remove unreacted monomer.

2.2.1 *Single Screw Extruder*

The single screw extruder is the most common type used for the analysis of reactive polymerisation mechanism. Early work by **Stober** *et al.* [16] in 1950, described the final polymerisation of styrene prepolymer in a single screw extruder operated at 10 rpm and 120-200°C temperature gradient over the length of the barrel with average material residence time about 18 minutes.

Martens *et al.* [17] carried out experiments on polyurethane production in a single screw extruder, employing a solution polymerisation method. The reaction was carried out at room temperature and samples obtained both from the extruder and a batch reactor were compared in terms of molecular mass. It was observed that the extruded product yielded a broader molecular weight distribution, a higher weight average molecular weight, and a lower number average molecular weight.

Streetman [18] synthesised melamine-formaldehyde prepolymer in a single screw extruder at 130°C. A typical feedstock of 2:1 para formaldehyde to melamine yields 95-100% conversion from 3 minutes extruder residence time. Final curing of the extrudate was carried out in a heated reaction chamber where water by-product was removed.

Siadat *et al.* [13] analysed the residence time behaviour on polycondensation reaction in a single screw extruder as an example having approximated the extruder by a tubular reactor. Using the increase in temperature due to the dissipated energy, they developed a model for the computation of parameters which depend on the residence time, such as degree of conversion, polymerisation and polydispersity.

Tadmor *et al.* [19] computed molecular weight and molecular weight distribution for a polymerisation with and without interruption, as well as for a polycondensation reaction, by taking into consideration the mixing behaviour and the residence time distribution in a single screw extruder. Here again, the results of the computations show that the single screw extruder can be approximated by a tubular reactor.

Hyun *et al.* [20] studied the polymerisation of thermoplastic polyurethane in a single screw extruder. Their experiments confirmed the data pertaining to the reaction kinetics as well as the dependence of the viscosity function on the conversion, temperature and shear rate. The computed results show clearly interdependency of the velocity, temperature and pressure profiles in the screw channel based on the

selected process parameters used during the synthesis of the polymer. The experimental observations are in agreement with the data obtained by computation.

Mizuno *et al.* [21] reported low molecular weight polybutylene terephthalate copolymers with terminal hydroxyl groups polymerised with diisocyanates to give polyurethane in a single screw extruder with 65 mm screw diameter and 2 minutes residence time. The isolated product formed had molecular mass about 25,000.

A study has been published by **Gozdz** *et al.* [22] on extruder copolymerisation of styrene/divinyl benzene in the presence of polyethylene. Analysis of the pressed films obtained showed 0.09 wt.% styrene monomer remaining. After a typical reaction time of 7-21 minutes, only 3.8-5.9 wt.% material could be extracted with ethyl acetate. Copolymer as detected by infrared technique is about 30% depending upon initial monomer and initiator level.

2.2.2 *Tangential Counter-rotating Twin-screw Extruder*

The tangential or non-intermeshing, counter-rotating twin-screw extruder exhibits operating characteristics which are practically identical to that of a single screw extruder. It has been claimed that this type of twin-screw extruder can provide some 25% more free volume per unit length than fully intermeshing geometries, this being due to the greater centre line distance, the apex volume, and also because of the fact that the flights of the screw do not occupy part of the channel volume of the opposite screw [23]. This increase in free volume makes it possible to increase mean residence time inside the extruder, facilitating complete polymerisation during the extrusion process.

There have been only two studies reported on reactive polymerisation using non-intermeshing counter-rotating twin-screw extruders. **Gouinlock** *et al.* [24] have demonstrated the use of this extruder type to advance the molecular weight of low

molecular weight copolyester from bisphenol A, neopentyl glycol and terephthaloyl chloride. A 20 mm diameter extruder was used with residence time of 15-30 minutes for screw speeds of 100 and 50 rpm respectively.

Tucker *et al.* [23] have reported the use of a 20 mm screw diameter non-intermeshing counter-rotating twin-screw extruder for anionic polymerisation of caprolactam to form polyamide 6 (PA6). Production rate in excess of 9.1 kg hr^{-1} has been obtained with screw speed of 525 rpm. No structural details of the product were given, however.

2.2.3 *Intermeshing Counter-rotating Twin-screw Extruder*

There are only a few reactive polymerisation processes performed using fully intermeshing, counter-rotating twin-screw extruders reported in the patents and published literature. **Schuddemagge** *et al.* [25] described the process of dissolving polybutadiene rubber in styrene followed by addition of acrylonitrile. The styrene and acrylonitrile copolymerise by a peroxide induced free radical mechanism.

Komazawa *et al.* [26] described the polymerisation of trioxane to polyformaldehyde using a special continuous reactor involving shafts with intermeshing counter-rotating paddles.

A study of methyl methacrylate polymerisation using a 34 mm diameter, self-wiping, fully intermeshing, counter-rotating twin-screw extruder has been published by **Stuber** *et al.* [27]. The initiator used in this free radical polymerisation reaction was not reported, however. Residence time distributions and product molecular mass were used to construct models predicting product polydispersity, extruder pressure generation, and throughput efficiency with varying degree of success.

Pressure sensitive adhesives have been polymerised by **Kotnour** *et al.* [28] and **Engler** *et al.* [29] based on isooctyl acrylate in a 34 mm diameter counter-rotating twin-screw extruder with Teflon-coated screws and barrel surface. The extruder was operated at screw speeds between 20-200 rpm to give residence times of between 20 and 1.5 minutes. The extruded polymer had molecular mass of 1.2×10^6.

More recently, **Ganzeveld** *et al.* [30] studied the mixing mechanism of polyurethane polymerisation inside a fully intermeshing counter-rotating twin-screw extruder with 40 mm diameter screws and a L/D ratio of 15. An throughput of 4.1 kg hr^{-1} was reported. The workers concluded that an increase in the screw speed and overall throughput rate have the effect of decreasing the conversion efficiency, while an increase in die resistance increases the monomer conversion.

2.2.4 *Intermeshing Co-rotating Twin-screw Extruder*

Some 90% of all the reactive polymerisation processes reported in patents and published literature involve the use of intermeshing co-rotating twin-screw extruders as the chemical reactor. These extruders operate on the building block principle since the screw elements can be individually selected and assembled depending on the requirements of the mixing task required. Each screw configuration furnishes a different extruder with unique conveying, pressurisation, devolatilisation and mixing capabilities. Reviews on the operational principles and mixing studies are described by **Rauwendaal** [31], **Kalyon** *et al.* [32] and **Hornsby** [33-35].

The condensation polymerisation of bisphenol A dianhydride with different aromatic diamines to yield polyetherimides using co-rotating twin-screw extruders has been described by **Takekoshi** *et al.* [36], **Banucci** *et al.* [37] and **Schmidt** *et al.* [38].

Polyesters have also been synthesised in co-rotating twin-screw extruders from low molecular weight prepolymers. **Kosanovich** *et al.* [39] used condensation

prepolymer from a continuous stirred tank reactor and completed the polymerisation in the twin-screw extruder reactor. The polymer had an intrinsic viscosity 40% higher than the starting material.

Numerous studies on the synthesis of polyurethanes using co-rotating twin-screw extruders, have been reviewed by **Xanthos** [40]. Since these reactions proceed by step-growth polymerisation, stoichiometry matching among the reactants is important for production of high molecular mass polymer and because of this process requirement, the reactants are often fed into the extruder as melts or liquids.

Sutter *et al.* [41] prepared atatic polybutene by polymerisation of 1-butene in a 24 mm co-rotating twin-screw extruder. Polymerisation occured in a reaction zone at 100°C giving a final product with density of 0.85 kg m^{-3}, and good tensile properties.

Bruzzone *et al.* [42] and **Carbonaro** *et al.* [43] produced butyl rubber by polymerising a mixture of isobutylene and isoprene dissolved in a mixture of methyl chloride and non-halogenated hydrocarbon solvent. The polymerised mixture containing 50-65 wt % polymer exited the extruder through a vertically mounted discharge screw feeding to a devolatilising extruder where excess monomer and solvent were removed.

Heinemeyer *et al.* [44] described polymerisation of bisphenol A diglycidyl ether in the presence of ethyl triphenyl phosphonium acetate and acetic acid complex in an extruder at 185°C. A residence time of 3 minutes is reported to yield product with molecular mass of 30,000.

Seddon *et al.* [45] described a process for polymerising polyacetal in a co-rotating twin-screw extruder with residence time of 3.1 minutes and a degree of conversion of about 70%.

Semanchik *et al.* [46] also reported the polymerisation of trioxane to polyoxymethylene using a similar type of extruder. At a polymerisation temperature of 120°C, polyoxymethylene was produced at 80% conversion and the conversion was observed to decrease steadily with increasing feed rate.

Todd [47] has published a study on the polymerisation of trioxane to polyoxymethylene using a 50 mm screw diameter extruder. The feed consists of trioxane with 2-4 wt % of unspecified comonomer and some catalysts such as boron trifluoride dibutyl etherate. The energy balance of the process was considered in great detail. Conversion as a function of feed rate was reported at 65°C. Key issues in this polymerisation process include provision of efficient mixing for prevention of solid formation that could possibly block the extruder and limit transport of monomers to the growing polymer chain. Finally, the removal of heat of polymerisation was discussed to keep the temperature sufficiently low for an efficient monomer conversion of >90%.

2.3 Synthesis of Polyamide 6 in an Extruder Reactor

Synthesis of polyamide 6 (PA6) in extruder reactors by ring-opening polymerisation of lactams has been mentioned in a number of publications. In an early report, **Illing** [48] polymerised lactams such as caprolactam or dodecalactam in a twin-screw extruder equipped with co-rotating, intermeshing screws. The reaction was initiated with 0.2-0.3 wt % sodium lactamate and an accelerator was also added. The components were either all preblended for throat feeding, or channeled through two separate feed streams consisting of lactam/initiator and lactam/accelerator which are introduced into the extruder hopper simultaneously.

Feedstock materials were first melted at 90 - 100°C in the melting zone designed with kneading blocks and conveyed to a polymerisation zone held at 140-160°C. In this section, the shear forces on the PA6 melt formed could be varied using an

adjustable valve, which controlled the clearance between the screw elements and the outer sleeve of the extruder barrel. The PA6 polymer produced was conveyed through a melt seal and expanded into the devolatilisation zone at 230°C. Throughput rate was reported to be 200 kg hr^{-1} for an extruder with 83 mm screw diameter. Average residence time was only 2-3 minutes. PA6 with molecular mass of 85,000 was subsequently used to produce filament, ribbon and extruded profile.

A similar but more detailed study was reported recently by **Bartilla** *et al.* [49] and **Menges** *et al.* [50] in which caprolactam was polymerised in a 30 mm co-rotating twin-screw extruder with a L/D of 28. The feedstock materials were pumped into the extruder hopper in two molten caprolactam streams containing sodium caprolactamate (catalyst) and hexaminediisocyanate (co-catalyst).

The screw configurations used had different conveying elements for feeding, melting, reaction and discharging. Thorough mixing of the reactants was accomplished through a set of kneading blocks just prior to the reaction zone. With this particular screw configuration, the molecular mass of the PA6 formed could be adjusted through controlled degradation in a second set of kneading blocks located after the reaction zone. Product characteristics were found to depend strongly on processing conditions with typical molecular mass of 80,000 produced at a maximum output rate of 10 kg hr^{-1}.

In the work of **Bartilla** *et al.* [49], preliminary tests on the reaction characteristics were performed in cast systems and in a cone and plate rheometer. The aim of these experiments was to determine suitable catalyst/activator systems at an optimal temperature that would allow completion of the reactions in the extruder in about 1-3 minutes. Useful information was obtained from the temperature rise versus time curves, and viscosity against time curves obtained at different reaction temperatures. In a particular promising system as reported, a peak temperature of about 188°C was reached in 1.8 minutes, at which time the viscosity recorded a rapid exponential increase. The reaction temperature for this polymerisation was 160°C and the

undisclosed catalyst and activator used were recorded at 3 and 7 pph respectively. Polymerisation experiments carried out in the cone and plate viscometer showed that the conversion to high molecular mass PA6 was strongly dependent on extruder shear rate, increasing initially (attributed to better mixing) and decreasing thereafter, presumably the result of polymer degradation.

Procedures have also been reported for combined polymerisation of ∈-caprolactam in a twin-screw extruder together with die forming of the resulting PA6 into a semi-finished product, with claimed economic and technical benefits [51]. The forming processes were conducted with a PA6 polymer still in the plasticised state from polymerisation. The comparatively high molecular mass of the material provides not only good further processing attributes (melt rigidity and stretching behaviour) but also improved mechanical properties for the finished product. The possibilities for further processing based on industrial fabricating techniques such as blow moulding, compression moulding and profile extrusions were outlined.

Van Buskirle *et al.* [52] have also briefly described caprolactam polymerisation and copolymer formation in a 34 mm diameter co-rotating twin-screw extruder of L/D 40. The screw design incorporated four kneading block segments for increased shear and also reversed screw elements for increased residence time of the reacting material. In a typical example, caprolactam was fed to the extruder with 1% bromomagnesium caprolactam as catalyst and 1.5% terephthaoyl-bis-caprolactam as co-catalyst at 250°C, 150 rpm screw speed, 5.5 kg hr^{-1} throughput and 85 seconds residence time. PA6 was produced at 92-95% conversion with solution intrinsic viscosity of 1.84-2.30.

Block and graft copolymers were also prepared similarly during in-situ polymerisation of caprolactam in the presence of polyetherimide derived from dianhydrid and m-phenylene diamine. The extrusion conditions used were 250°C, 150 rpm and 8 kg hr^{-1} which gave a reported yield of 87% caprolactam conversion.

The copolymer formed was assumed to arise through chain scission or imide ring opening of polyetherimide followed by polyamide chain growth.

PA6 copolymerised with polybutadiene has been prepared by **Hergenrother** *et al.* [53] by polymerisation of caprolactam in the presence of functionalised 1,2-butadiene in a 30 mm co-rotating twin-screw extruder. For example, a solution of 1 part polybutadiene of molecular mass 25,000 neutralised with caprolactam and 2 parts of isocyanate-terminated polybutadiene which has been end-capped with caprolactam in a prior step (molecular mass of 3,000), was prepared in hexane solution at 79% solid. The rubber solution so prepared was then fed at 10 gm min^{-1} to the first zone of the extruder where the solvent was stripped, followed by dowmstream addition of 8.6 gm min^{-1} caprolactam containing 1% antioxidant. The extruder was operated at 25 rpm and the temperature used was 182 - 194°C. Residence time was reported at 5 minutes and the final product had 42.3% PA6 content.

Polymerisation of caprolactam using a co-rotating twin-screw extruder in the presence of 0.25 mol % sodium bis(2-methoxyethyoxy)-di-aluminium hydride and 0.5 mol % cyclic trimer of phenyl isocyanate has been described by **Kubanek** *et al.* [54]. The extrusion temperature profile used was 220°-230°C (inlet zone), 230°-240°C (middle) and 215°-225°C (outlet zone). A mixture of caprolactam and laurolactam in the ratio 95:5 by weight could also be polymerised by this process.

Polymerisation of dodecalactam in the presence of sodium hydride at 250°C in an extruder reactor equipped with a gear pump between the last extruder zone and the die has been described by **Biensan** *et al.* [55]. The gear pump was set to produce 35 kg hr^{-1} extrudate. This constant output rate enables the continuous production of extruded profile sections.

Tucker *et al.* [23] described the polymerisation of PA6 in a 20 mm screw diameter, counter-rotating, non-intermeshing twin-screw extruder with screw configured only

with conveying elements. A throughput rate of 9.1 kg hr^{-1} was reported with a polymer of consistent molecular mass independent of screw speeds up to 525 rpm. The uniformity of molecular mass attained was attributed to the continuous distributive mixing process which is rather unique with the counter-rotating, non-intermeshing twin-screw extruder. Apparently, distributive mixing could promote a *uniform reaction* at lower shear rate without polymer degradation.

2.4 Formation and Structure of Polyamide 6

2.4.1 *Anionic Polymerisation of Caprolactam*

In 1941, **Joyce** *et al.* [56] obtained a patent on the base catalysed polymerisation of caprolactam. They described the reaction of a small amount of sodium or other alkali metal with caprolactam to form sodium caprolactamate and the rapid, exothermic polymerisation of caprolactam at a temperature above 200°C to form molten PA6.

In 1955, exploratory research was focused on the base catalysed polymerisation of lactam. A two-stage mechanism for the thermally-initiated anionic polymerisation was disclosed [57]. This mechanism was tested by a simple procedure of adding a pre-formed acyllactam to caprolactam containing sodium caprolactamate at 160°C. Very rapid polymerisation was observed and a solid polyamide casting resulted within 4-5 minutes of reaction time. It was observed that in the absence of the acyllactam initiator, polymerisation did not occur.

The anionic polymerisation of lactams has been explored in great depth by **Sebenda** *et al.* [58-61]. These workers studied the basic reaction mechanisms involved in the initiation and propagation reactions of the anionic polymerisation of caprolactam and reaction rates determination based on the types and concentrations of the lactam salt (catalyst) and the substituted lactams (activator).

The behaviour of different initiators in a two-step anionic polymerisation of caprolactam was compared by **Stea** *et al.* [62]. In the first step, the reaction was carried out above the polymer melting point and in the second, it was carried out at lower temperature. This was done to investigate the difficulties which might occur when two solutions of caprolactam containing the catalyst and co-catalyst respectively, are mixed at temperatures below the melting point of the polymer formed. More recently, the effects of initiator structures on physical and thermal properties of PA6 were also studied by **Desai** *et al.* [63].

Iobst [64] studied the kinetics of the activated anionic polymerisation of caprolactam to PA6 using an adiabatic temperature rise technique. The reaction rate was reduced when the activator concentration exceeded the catalyst concentration. Other kinetic studies have also been made [65, 66] which report different polymerisation rates with different levels and ratios of catalyst and initiator used.

2.4.2 *Structural Analysis*

Studies on the crystal structure of PA6 were first carried out by **Brill** [67], who reported a monoclinic structure corresponding to what is now universally referred to as the α form. Later researchers, notably **Wallner** [68] and **Holmes** *et al.* [69] confirmed the basic characteristics of the α phase and further refined its structure. The generally accepted prototype of the α phase is the monoclinic structure of **Holmes** and the chains are assumed to be fully extended and occur in anti-parallel hydrogen bonded sheets.

A second well established crystalline form has been described and studied by **Kinoshita** [70] and **Arimoto** [71]. This crystalline γ phase, is readily formed in PA6 by chemical treatment in iodine-potassium iodide solution followed by a de-iodization treatment in sodium thiosulphate solution. The prototype structure for this

γ phase corresponds to a "kinked" or pleated hydrogen bonded sheet structure in which the hydrogen bonding occurs between parallel rather than anti-parallel chains.

In addition to these two well established phases, the literature contains numerous references to phases that differ in various ways from either the α or γ prototypes described above. **Roldan** *et al.* [72] have noted that the unit cell dimensions of the α phase can vary with material processing history and called this phase α-paracrystalline. Other studies on PA6 structures have reported that the ß phase which has a shortened chain axis repeat distance as compared to the γ phase, but possesses a hexagonal or pseudohexagonal symmetry. The ß form as described by **Roldan** *et al.* [72] is typical of this group. It seems clear in retrospect that such a phase is not basically different from the γ form but is slightly less well crystallised than the monoclinic sample of **Arimoto** [71]. **Ziabicki** [73] has used the symbol ß to describe the pseudohexagonal form occurring in melt spun filaments. The chain axis repeat distance in these filaments is presumably close to 17Å and would seem more related to the extended chain α form.

Illers *et al.* [74] in a study utilising X-ray diffraction, infrared spectroscopic, density and calorimetric techniques, expressed doubt on the existence of a well crystallised ß phase that differs substantially from the γ phase. Experimental results showed that the γ phase formed by iodide treatment cannot be readily transformed to α form by dry annealing. The study therefore, concluded that a poorly crystallised γ^* phase of pseudohexagonal form exists in unoriented samples quenched from the melt which can be readily transformed to α phase by annealing treatment.

Parker *et al.* [75] did an extensive literature review on the crystal structures of PA6. Based on this review and their own experience with spun and drawn fibres, it was concluded that there are two basic types of structures: (i) extended chain structures with hydrogen bonding primarily between anti-parallel chains (α-type) and structures in which the hydrogen bonding tended to be primarily between parallel chains and the chain axis crystallographic repeat distance is significantly shortened (γ-type).

Stepaniak *et al.* [76], studied and proposed the existence of a "pleated α" structure in filaments that have been melt spun with low orientation. This phase presumably has hydrogen bonding between anti-parallel chains as in the α phase, but exhibits a shortened repeat distance and pseudohexagonal symmetry. The study showed that such a structure would readily transform to α form on annealing or drawing, since no breaking of hydrogen bonds between parallel chains and reforming them between anti-parallel chains is necessary, as in the case when forming the α phase from the γ phase. The results further suggested that this phase could correspond to the γ* phase of **Illers** *et al.* [74] and also to the ß phase of **Ziabicki** [73]. However, no substantial experimental evidence was provided for the shortened repeat distance, and it is not clear how this phase differs from an otherwise highly imperfect, poorly developed α form.

Kyotani [77] reported wide-angle X-ray diffraction (WAXD), differential scanning calorimetry and density studies on the crystalline forms of PA6 obtained from the glassy state under different crystallisation conditions. It was disclosed that the weight fraction of the γ form decreases with increasing crystallisation temperature above 160°C and that of the α form increases. Growth of the γ form is found to be predominant in crystallisation temperature of 100°C and of the α form at temperature of 200°C. A large amount of a thermally unstable form is included in the γ form crystallised from the glassy state at lower crystallisation temperatures which is readily transformed into the α form upon annealing at 200°C.

In another study, **Kyotani** *et al.* [78] reported WAXD investigations of the relative amounts of α and γ crystalline forms of PA6 obtained from the melt under different crystallisation conditions. The weight fraction of the γ form was found to decrease with increasing crystallisation temperatures and that the corresponding α form increases.

In another more recent paper, **Kyotani** [79] investigated solution crystallisation of PA6 using electron microscopy and WAXD techniques. Lamellar single crystals and

spherulites of the γ form are obtained by crystallisation from 1,2,6-hexametriol. The morphology of the single crystals is reported to be different from that obtained from glycerine solution. Sheaf-like crystals of the α form are also obtained from both solvents. The melting behaviour of the crystals and the effects of solvents on the growth of the two crystalline forms are also discussed.

Hirami [80] performed on-line wide-angle X-ray scattering and birefringence experiments to study structural development of PA6 during the melt spinning process. A mechanism is proposed such that hydrogen bonds are formed between adjacent molecules which are packed together due to primary nucleation during the melt-spinning process. As for the as-spun fibres on the take-up bobbin, this same trend is enhanced further due to secondary nucleation caused by moisture regain. Simultaneously, the crystallisation of molecular chains also accelerates the orientation along the fibre axis which directly enhances the rate of crystallisation.

In a related report, **Hirami** [81] presented data on structural changes of the γ form crystals quenched from the melt at various crystallisation temperatures using small-angle X-ray diffraction measurements.

Multhy *et al.* [82] reported lattice distortion of the γ form of PA6 with various processing conditions. The results showed that on annealing the PA6 fibres, the α form is produced primarily by γ→α conversion in high orientation fibres, while additional α form can also be crystallised from the amorphous phase in low orientation fibres. Experimental evidence was presented to show α crystallites are favourably formed during conditioning of poorly cystallised fibres in a humid atmosphere and fibres with α phase as the major crystallite form are produced upon drawing these conditioned fibres. Fibres drawn without lag time contain primarily γ phase crystallites.

Studies on high speed melt-spun PA6 filaments were carried out by **Heuvel** *et al.* [83]. Increasing crystallinity and high orientation was observed with increased take-

up velocity. The results obtained were rather similar to those obtained from high speed spinning of polyethylene terephthalate where an increase in γ phase with increasing take-up speed was also reported. At take-up velocities greater than 2500 m min^{-1}, γ crystals were mainly generated from orientation induced nuclei and α crystals grew slowly after moisture pick up.

The molecular weight effect on the melt spinning of PA6 was investigated by **Ishibashi** *et al.* [84] by on-line temperature and diameter measurements. Number average molecular mass in the range 18,500-24,000 were found to be independent of the temperature and diameter profiles.

Gurato *et al.* [85] also investigated the annealing effect on PA6 filaments with two different molecular masses of 4,700 and 17,000 and observed lower crystallinity for the higher molecular mass sample.

In another study, **Koyama** *et al.* [86] investigated the relationship between structure and properties developed in as-spun PA6 filaments. Differential scanning calorimetry, wide and small-angle X-ray scattering, and tensile tests were conducted. Structural characterisation results and properties of the filaments were found to be strongly dependent on molecular weight. Generally, higher molecular weight leads to higher modulus and filament tenacity and lower elongation to break in the as-spun filaments.

The transition of γ phase PA6 crystals to the α phase on stretching in the chain direction was first reported by **Miyasaka** *et al.* [87]. The γ phase fibre prepared by iodine treatment was stretched under constant load and the crystal deformation was observed by an X-ray diffraction method.

It is well known that during the production of films, fibres and engineering components, a polymer is exposed to varying degree of heat and humidity. The processing conditions have significant influence on such properties as the mechanical

behaviour, dimensional stability, appearance and dye diffusion. The structural basis for these changes in the performance of the material can be studied in the laboratory by controlled annealing of the specimen. In this aspect, several studies have been reported on the effect of annealing on the structure of PA6.

Bankar *et al.* [88] investigated the structure developement and mechanical properties of as-spun PA6 filaments by separately annealing in air, treatment in water and formic acid solution. Transformation from the pseudohexagonal γ form to the α monoclinic form was also reported. The tensile strength of spun and conditioned filaments were observed to increase with higher take-up velocity and spineline stress, while elongation to break decreased with these variables.

Park *et al.* [89] studied PA6 fibres which were annealed while subjected to a constant stretch and analysed the subsequent mechanical and structural results. A paracrystalline structure model of PA6 was proposed in which folded chains, fully extended chains, partially folded and partially extended chains coexist in the highly drawn high strength fibres. A correlation between small-angle laminar spacing and a crystalline perfection index derived from WAXD data was also developed.

Stamhuis *et al.* [90] reported the effect of reequibration reactions on the annealing of PA6 under elevated pressure. Chain scission is believed to have constituted a predominant step in the annealing of polyamides under elevated pressure which is followed by an enhanced rearrangement of the chains leading to growth of the polymer crystals in lateral and chain directions.

Murthy *et al.* [91] studied the changes upon annealing of the inter- and intra-lamellar structures in PA6 and discussed the mechanisms which led to these changes. Surface premelting and the accompanying changes in the surface structure of the lamellae, selective melting, and more importantly, the longitutional motion of the PA6 chains and the resulting folding of interfibrillar extended amorphous chains are

considered to account for the shrinkage of the fibre, disorientation of the crystallites, increase in crystalline perfection and the increase in lamellar spacing observed.

Khanna *et al.* [92-95] have studied the processing history effects on the crystallisation rate of PA6 from the molten state. Characterisation data from differential scanning calorimetry and optical microscopy studies were presented to show parameters such as molecular weight, impurities, monomer and oligomers were not responsible for the observed changes in crystallisation behaviour upon processing. However, processing treatments such as melt extrusion or freeze-grinding (high shear rate) or solution precipitation are required to overcome the H-bond stabilised disordered environment in virgin PA6 in order to introduce locally ordered regions (nucleation sites) which could lead to an increase in the crystallisationn rate.

A novel process for enhancing the crystallisation rate of PA6 from the melt by incorporation of nucleating agents comprising finely divided inorganic mineral, fatty amides and low molecular weight polymers is also described by **Khanna** *et al.* [96]. It is claimed that PA6 comprising mainly the α crystalline phase can be produced by this process.

Brucato *et al.* [97] investigated the morphology and crystal structures of nucleated PA6 quenched from the melt. The results revealed that samples were essentially amorphous at high cooling rates of larger than 200°C sec^{-1}. The γ crystalline form was observed for cooling rates in the interval 70°C to 200°C sec^{-1}, whereas α crystalline structure was dominant at lower cooling rates.

Kyotani [98] prepared PA6 crystals grown from stirred 1,2,6-hexanetriol solution and observed filmy aggregates around the stirrer and suspended crystals in solution. Fibrous crystals are observed to present in filmy aggregates and their molecules are folded and oriented perpendicular to the fibre axis. These crystals have α monoclinic crystal structure with the hydrogen bonds parallel to the fibre axis.

Lee *et al.* [99] examined the relationship between J-1 polymer (a semi-crystalline polyamide homopolymer) and carbon fibre as a composite matrix. The crystalline behaviour of the sample was observed to be influenced by its thermal history. Matrix cracks due to the thermal expansion mismatch between the fibre and matrix were reduced by slowly cooling the composite from the melt. During slow cooling, the matrix remains in a softened state for a longer period of time, allowing greater relaxation of internal stresses.

Engler *et al.* [100] studied the influence of molecular weights on the crystallisation rate of oriented , glassy PA6 using differential scanning calorimetry and wide- angle X-ray diffraction techniques. The workers concluded that both the crystallisation rate and the degree of cystallisation of the samples depend on the fraction of high molecular weight components present in the sample. Given two samples with the same molecular weight, the one with the broader distribution crystallises more rapidly. Similarly, samples having the larger molecule weight crystallises to a greater extent when two samples have the same molecular weight distribution.

Todoki *et al.* [101] studied reorganisation of PA6 crystallised during the DSC heating process. Double melting peaks of PA6 are observed and these are considered to be the consequence of superposition of three processes which occur successfully during heating; perfection of the original crystals, melting of the perfected crystals concurrently with recrystallisation and melting of the recrystallised crystals.

The melting behaviour of drawn PA6 yarns which were prevented from shrinking during heating was also studied by **Todoki** *et al.* [102]. The DSC thermogram obtained exhibits only a single melting endotherm at a higher temperature instead of the double peaks for samples made in the unconstrained state. These experimental results obtained inferred that single melting peak of PA6 results from the absence of the partial melting/recrystallisation process which constitute the appearance of double endothermic melting peaks.

2.4.3 *Polyamide 6/Polypropylene Blends*

Blends of polyolefins and engineering polymers combining properties of both components can tailor product properties to specific end-product applications. For example, by blending polypropylene (PP) and polyamide 6 (PA6), it might be able to combine the thermal and mechanical properties of PA6 and the insensitivity to moisture that characterises PP. In this way, a blend material with low moisture absorption, improved processability, as well as good impact resistance and flexural modulus can be obtained [103].

Several reports on PA6/PP blends have been published on compatibilisation of the blend morphology leading to an improvement of physical properties [104 - 113]. Blends based on PA6/PP have been compatibilised by reactive extrusion, where functionalised PP can act as interfacial agent to form copolymers that bridge the two incompatible phases. The bridging by these compatibilisers is analogous to the role of surfactants in oil-oil emulsions as observed by **Molau** [115].

Ide *et al.* [104] first reported the use of maleic anhydride grafted PP as a compatibiliser to improve the physical properties of a PA6/PP blend. The formation of a graft copolymer was observed between maleic anhydride in PP chain and the terminal amino group of PA6. The existance of such a copolymer was confirmed by solvent extraction followed by identification of the amine group by differential scanning technique. The existance of the graft polymer was identified by a decrease of crystallinity caused by difficulty in polymer chain arrangement, whereby the movement of segments was prevented by the branched chain. The mechanical properties of the compatibilised PA6/PP blend material were remarkably improved with increasing amount of maleic anhydride added to the blend.

Liang *et al* [105] studied the melt flow and solification of PA6/PP fibre blends including the structure of the product produced. Blends of PA6/PP compositions 75/25, 50/50 and 25/75 were prepared in a 20 mm single screw extruder combined

with a static mixer head. The size of the two phases observed by scanning electron microscopy showed that they decrease with increasing extrusion rate through the die. The crystalline phases of both PP and PA6 blend melt spun fibres were also characterised by wide-angle X-ray diffraction. Extracting the melt spun blend fibres with formic acid yielded small diameter PP minifilaments.

Willis *et al.* [106, 107] studied the processing - morphology relationship of PA6/PP blends with ionomer compatibilisation agents prepared from single step and two steps mixing operations. The results showed that morphology of the compatibilised blends was observed to be significantly dependent on the compatibiliser concentration. For a dispersed phase content of 10% by weight, a maximum reduction in phase size was observed when only 0.5% by weight of ionomer was added to the blend. The interactions of the compabiliser with the phases were confirmed by Fourier transform infrared spectroscopy. In comparision to one-step mixing, blends prepared by two-step or batch mixing were characterised by a smaller dispersed phase when PA6 was the matrix and a larger particle size when PA6 was the minor phase. The results obtained were explained in terms of strong interactions between PA6 and the ionomer compabiliser.

Park *et al.* [108] studied melt blends of PA6/PP and PA6/PP with 5 wt % maleic anhydride grafted PP prepared using a Brabender plasticorder. Structural analysis of the blend materials were reported based on DSC thermal properties and their morphology determined by electron microscopy.

Dagli *et al.* [109] investigated the effect of different modified PP compatibilisers on the PA6/PP blends prepared in an intensive batch mixer with roller blades. Structural analysis of the blend products were made by melt flow rates, differential scanning calorimetry, infra-red spectroscopic and microscopic techniques. Experimental results showed that the grafting reaction possibly occurred between the amine end group of PA6 and the carboxyl group of the functionalised PP. A significant decrease in the melt flow rate and differences in the infrared results

indicated the presence of an acid-amine reaction although results obtained from morphological investigation did not show any compatibilising effect.

Nishio *et al.* [110] reported for the first time, a study on maleic anhydride grafted PA6/PP blends prepared in a 30 mm diameter, counter-rotating twin-screw extruder of L/D 40. The amount of PA6 in all the blend components was fixed at 30%. The graft block copolymer formed was extracted with xylene and characterised by transmission electron microscopy and differential scanning calorimetry. The melting peaks of both the PA6 and PP components of the blend were observed to shift a little to lower temperature possibly due to the formation of a copolymer. Electron microscopy showed a decrease in the size of PP particles with increasing copolymer content.

Modic *et al.* [111] described the use of a styrenic block copolymer functionalised with maleic anhydride (FSBC) as a compatibiliser and impact modifier for a PA6/PP blend system prepared using a 25 mm diameter, co-rotating twin-screw extruder. For a blend with composition 50/50, the addition of FSBC causes a distinct change in the blend morphology. The morphology transformed from a co-continuous structure to one which contains discrete particles of PA6 in the PP matrix. The addition of only 5 wt % of FSBC has led to a dramatic reduction in PA6 particle size. Based on morphological observations, it was concluded that FSBC is located at the interface of the PA6 particles and is clearly functioning as a compatibilising agent. The compatibilising effect is due to the reaction between the amine end groups of PA6 with the anhydride functional groups of FSBC. The results showed an improvement of impact resistance properties at both ambient and sub-ambient temperatures. The tensile properties of the blends however, are not been affected by the modifier present.

Holsti-Miettinen *et al.* [112] described the compatibilisation of PA6/PP blends used with four different compatibilisers including maleic anhydride functionalised PP, maleic anhydride grafted styrene-ethylene butylene-styrene block copolymer, fumaric

acid and glycidyl functionalities. Physical and structural properties of the blends formed are characterised by mechanical, morphological and thermal techniques. The results concluded that all the compatibilisers are effective as interfacial agents and generally, only about 5 wt % of the compatibilser is suffice to form the copolymer. Interactions between the blend components, as a result of compabilisation, were evident from the blend morphology, increase melt viscosities and improved mechanical properties.

Ishida *et al.* [113] and **Adur** *et al.* [114] described the effect of a filler on the compatibility of an immisible PA6/PP blend. The fillers used were glass beads and glass fibres. They concluded that an improvement of the properties towards surface-induced compatibilisation is observed when the filler surface is being treated with a suitable silane coupling agent. In these systems, the filler takes not only the usual role of a reinforcing material but also a new role as modifier of the interface structure.

More recently, **Lambla** *et al.* [116] reported studies of co-crystallisation structure and properties of PA6/PP blends prepared in a twin-screw extruder using graft copolymer PA6-g-PP and block copolymer PA6-B-PP. The formation of co-crystallisation (disapperance of the PA6 crystallisation peak) at 7% compatibiliser content for a PA6/PP blend of composition 50/50 has been attributed to the presence of the copolymer which has been observed to play an important role of nucleating inhomogeneity in the co-crystallisation process. DSC is being proposed to be used for the characterisation of compatibility between the phases of the blend. It was suggested that if only one melting or crystallisation peak is observed, the blend can be considered to be a homogeneous dispersion. On the other hand, if two distinct melting or crystallisation peaks are detected which are associated with the individual blend components, then a heterogeneous dispersion blend has been formed.

2.4.4 *Polyamide 6/Elastomer Blend*

Improvements in the physical and mechanical properties of thermoplastic polyamide resins has been the subject of matter of research and development over a considerable period of time. In the unmodified state, polyamide 6 resin has a sufficient combination of good tensile and flexural properties, high heat distortion temperature, and average notched Izod impact strength in the order of 50 $J.m^{-1}$. Based on these properties, it has been considered to be among the first "engineering resins". By chemically grafting the polyamide 6 to a dispersed elastomer phase, heterophase blends with impact strengths on the order of 1000 $J.m^{-1}$, well in excess of the so-called "high impact" resins can be obtained. Much of such earlier research and development has been addressed to the admixture of the polyamides with a variety of additives, including elastomer-like or elastomeric materials, such as ethylene-propylene copolymers (EPR) or ethylene-propylene diene monomer (EPDM), and other modified and unmodified resins with various degrees of success. The desired level of improvement has not been achieved with the addition of such elastomeric materials due primarily to the relative incompatibility between the elastomeric materials and the polyamide resins.

Attempts have been made to overcome this problem and increase the compatibility between the hydrocarbon elastomeric materials and the polar polyamide resins by modification of the elastomeric materials to provide reactive sites that enable the polyamide resins to adhere to the elastomeric materials [117-119].

Both crazing and shear banding are believed to occur during the fracture of polymers upon impact. The elastomer contributes to the toughness of the blend by retarding craze growth and concentrating stresses in the elastomeric domains. However, strong adhesion between the continuous matrix and the dispersed elastomeric phase, a low interfacial energy, and critical dimensions of the elastomeric domains are required in order to minimise the decay of tensile mechanical properties of the material formed by blending. In 1979, **Flexman** [120] recognised this phenomenon

and reported crazing and shear banding behaviour upon deformation of an elastomer-toughened polyamide 6,6.

Wu [121] described a mechanism for toughness of polyamide 6,6 with elastomeric particles by measuring the impact energy dissipated in the notched fracture surface and established an energy balance for the mechanism. It was concluded that about 25% of the impact energy is dissipated by matrix crazing and 75% dissipated as heat by matrix yielding.

In another study, the effects of elastomer particle size and elastomer-matrix adhesion on notched impact toughness of polyamide 6,6/elastomer blends are analysed [122]. A sharp tough-brittle transition is found to occur at a critical particle size, when the elastomer volume fraction and elastomer-matrix adhesion are held constant. The critical inter-particle distance is observed to be a material property of the matrix, independent of elastomer volume fraction. It was also observed that, the general condition for polymer toughening by elastomer is that the inter-particle distance must be smaller than a critical value. For polyamide/elastomer blends, this critical interparticle distance was found to be 0.304 μm for notched Izod impact fracture. Van der Waals attraction can provide sufficient adhesion for toughening while interfacial chemical bonding is not always necessary. Even if there is interfacial chemical bonding, a polymer/elastomer blend will still be brittle, if the inter-particle distance is greater than the critical value. This study concludes that this criteria for toughening is proposed for all polymer/elastomer blends which dissipate impact energy mainly by increased matrix yielding.

Cimmino *et al.* [123] described the modification of an amorphous random ethylene-propylene copolymer (EPR) by solution grafting of maleic anhydride (MA) molecules onto the elastomer chain. The resulting EPR-g-MA was used together with EPR to obtain binary PA6/EPR, PA6/EPR-g-MA and ternary PA6/EPR/EPR-g-MA blends by melt mixing in a Brabender-like apparatus. Structural analysis and mechanical properties were evaluated. The results showed that binary and ternary

blends containing 20 wt % of total elastomer indicate a significant improvement of impact properties at room temperature when the elastomer phase is partly or entirely EPR-g-MA. In the case of the binary blends, these results were related to the presence of elastomer domains of very small size thoroughly adhered to the PA6 matrix. In the ternary blend, a much more complicated morphology is observed which is characterised by the presence of large EPR domains, likely containing some EPR-g-PA6 graft molecules acting as an interfacial agent, as well as domains of EPR-g-PA6 of smaller size strongly adhere to the matrix similar to that observed for the PA6/EPR-g-MA blend morphology mentioned earlier.

Cimmino *et al.* [124] later described a new method of obtaining an elastomer-modified PA6 directly during hydrolytic polymerisation of caprolactam to PA6. Both binary and ternary blends containing EPR and EPR-g-MA were prepared and morphology/mechanical properties analysed as function of composition and reaction conditions. The results showed that tensile strengths and elongation at break of binary and ternary blends are slightly lower than those of pure PA6. It was observed that the morphology of the blends is strongly dependent on the method of preparation. The impact properties of both the binary and ternary blends were similar to those obtained by melt mixing of the PA6 polymer.

Cimmino *et al.* [125] also investigated the effect of mixing procedures on the properties of binary and ternary blends of PA6, EPR and EPR-g-MA. Two kinds of processing routes have been discussed : (a) one-step mixing in which the three blend components were simultaneously introduced in the mixer; (b) two-step mixing in which the two elastomers were separately premixed before final mixing with PA6. The results showed that the blends obtained by one-step mixing exhibit a coarse morphology and poor impact resistance properties, whereas the ones prepared by the two step mixing procedures showed very fined morphologies and excellent impact performance. These observations have been attributed to the influence of the interfacial agent formed during the melt mixing of the two premixed elastomers with PA6.

Martuscelli *et al.* [126] studied the morphological, kinetic, structural and thermodynamic properties of PA6/EPR and PA6/EPR/EPR-g-MA blends. Results showed that EPR-g-MA can act as a nucleating agent for the PA6 spherulites and also causes a drastic depression of the overall kinetic rate constant for crystallisation which is related to the increase of melt viscosity observed for the PA6/EPR-g-MA blend. The elastomer does not seem to have any influence on the thermal behaviour of PA6 and the results concluded that in the melt state, PA6 is incompatible with both EPR and EPR-g-MA.

Borggreve *et al.* [127, 128] described the influence of elastomer concentration and particle size on the impact behaviour of PA6/EPR-g-MA blends prepared in a 40 mm single screw extruder. The results showed that with increasing concentration and decreasing particle size, the brittle-tough (BT) transition temperature decreases and hence the impact behaviour improves. A relationship between the BT temperature and the inter-particle distance (ID) has been proposed.

In a subsequent paper [129], it was shown that ID is not the only parameter which determines the impact strength of a PA6/modified elastomer blend. The mechanical properties of the pure modified elastomer were also shown to have a decisive influence. On the other hand, the concentration of the coupling agent, maleic anhydride, apparently does not affect the impact toughness of PA6/EPDM blends [130]. The observed stress whitening in all the deformed elastomer modified PA6 blends was found to be attributed to a voiding process and crazing was not observed as a result of certain deformation mechanism.

More recently, **Borggreve** *et al.* [131] described tensile dilatometry tests on PA6/modified elastomer blends with various elastomer concentrations, particle sizes and types of impact modifiers. The results showed that whereas elastomer concentration and particle size do not affect the onset of voiding in the blends during a tensile test, the type of elastomer used has a considerable effect. A correlation exists between the stress at which the elastomer particle cavitate in the tensile test

and the impact behaviour of the blend. A toughening mechanism is proposed in which the cavitation stress of the elastomer and the inter-particle spacing play crucial roles.

Greco *et al.* [132, 133] studied the influence of composition and functionalisation degree of the elastomer-modified PA6 blends obtained directly during the hydrolytic polymerisation of ϵ-caprolactam. An ethylene-propylene elastomer (EPR) and dibutyl succinate (DBS) grafted EPR (EPR-g-DBS) were used as elastomeric components to yield binary PA6/EPR-g-DBS and ternary PA6/EPR/EPR-g-DBS blends having about 20% by weight of total elastomer. Model reactions and selective extraction of the blends indicated that (EPR-g-DBS)-g-PA6 copolymers are formed during the caprolactam polymerisation. A fine and homogeneous dispersion of rubbery domains has been formed for the binary blends, while ternary blends exhibit a quasi-bimodal distribution of rubbery domains. The impact properties of ternary blends are enhanced with the increase of the relative amount of functionalised elastomer. Direct correlation between the mode and state of dispersion of the elastomer domains and impact properties were not obtained.

Greco *et al.* [134] also investigated the influence of degree of grafting of EPR-g-MA on the morphology and mechanical properties of the binary and ternary PA6 blends prepared by melt mixtures. Again fine and more homogeneous dispersion of the elastomeric domains and better impact properties are observed with increasing degree of grafting in the blends. At equal degree of grafting for the compositions used, the binary PA6/EPR-g-MA blends exhibit better properties than the ternary ones. These results are attributed to the presence of an (EPR-g-MA)-g-PA6 graft copolymer formed which is acting as an interfacial agent.

Oshinki *et al.* [135, 136] described the toughening of PA6 using triblock copolymers of the type styrene-(ethylene-co-butylene)-styrene (SEBS), and a maleic anhydride functionalised version (SEBS-g-MA) as compared to a conventional maleated ethylene/propylene elastomer. The results showed that combinations of the

SEBS and SEBS-g-MA elastomer blends with PA6 yields higher levels of toughening than that achieved with the functionalised elastomer alone. The particles of pure SEBS were about 5 μm in diameter which is considered to be too large for PA6 toughening, whereas SEBS-g-MA alone yield particles of about 0.05 μm which appears to be too small for good toughening effect. However, on combination of these two types of elastomers, a continuously varying particle sizes between those extreme limits is observed. These results suggest that the two different elastomers form essentially a single population of mixed elastomer particles. The study concludes that the order of mixing during blend preparation did not significantly affect the mechanical properties of the ternary blends.

Lawson *et al.* [137] described the preparation, analysis, testing and structure determination of ultra-high impact elastomer-modified PA6 blends. Ten different partially unsaturated hydrocarbon elastomers which are functionalised either in solution or in bulk with maleic anhydride to give rubbery "ene" adducts containing varying amounts of pendent succinic anhydride were used for the investigation. Tough, rigid, thermoplastic engineering resins with notched Izod impact strength of 750-1000 J m^{-1} were prepared by melt blending those adducts with PA6. Properties of these blends were observed to be much affected by the type and amount of elastomer used, the anhydride content, mixing as well as the testing conditions.

2.4.5 *Glass Reinforcement during In-situ Caprolactam Polymerisation*

It is well established that incorporation of high modulus fibres into thermoplastics leads to significant increases in the modulus of rigidity, tensile yield and fracture strength as well as heat distortion temperature [138]. Commercial moulding grades of PA6 synthesised by hydrolytic polymerisation of caprolactam is a well established polymer matrix material and PA6/glass composites have known to have excellent combination of high stiffness, tensile strength, toughness and creep resistance

properties. Most of the PA6/glass composites are used in engineering applications such as automotive components and industrial parts.

In most commercial practices, chopped glass fibres are compounded into PA6 matrix by melt blending in a single or twin-screw extruder or kneader to produce pellets for subsequent moulding operations. Since chopped glass fibres are brittle and can be easily damaged during the compounding operation, therefore, today's state of the art is to feed these materials downstream into the already formed melt. However, this feeding sequence could sometimes caused poor wetting of the fibres on the PA6 matrix which may affect the final properties of the composite [139].

PA6 is a semi-crystalline material and there has been some evidence that the reinforcing glass fibres can promote heterogeneous nucleation of the crystalline regions and the formation of transcrystallinity [140, 141]. This crystallinity effect can also result in the variation of mechanical properties in PA6 composites.

The formation of glass-reinforced PA6 sheet composites during in-situ activated anionic and hydrolytic polymerisations of ϵ-caprolactam have been reported by **Otaigbe** *et al.* [142], **Goettler** *et al.* [143] and **Ishida** *et al.* [144].

Otaigbe *et al.* [142] described the anionic polymerisation of ϵ-caprolactam with up to 55 wt % loading of planar-random continuous glass mat reinforcement using a technique similar to reaction injection moulding.

Goettler *et al.* [143] described the fabrication and mechanical characterisation of PA6 composites made by incorporating various types of glass in the form of beads or fibre mat into an activated polymerised caprolactam melt. The results showed that high molecular weight, better wet-out and adhesion to the reinforcement, as well as cold drawing of the PA6 resin has led to homogeneous cavitation that improves the composite toughness in comparision to epoxy or other polymer matrices of equivalent stiffness.

Ishida *et al.* [144] described the design of the reaction injection moulding (RIM)-pultrusion process for the fabrication of continuous reinforced composite. This novel process combines the advantages of both RIM and the pultrusion process, while avoiding their inherent shortcomings. The very low viscosity of the reactive precursors enables excellent fibre wet-out and adhesion. This technique has been applied successfully to obtain unidirectional reinforced PA6 and elastomer-toughened PA6 composites. The composites also exhibited excellent wetting and strength properties.

Menges *et al.* [50] described a laboratory scale manufacturing process for PA6 semi-finished products with glass-mat reinforcement. The low viscosity PA6 prepolymer melt exited from the extruder was used to impregnate the glass-mat and distributed over a sealing film. Further polymerisation reaction is then continued "in-situ" by an infra-red heating source. The final products formed were suggested to be used as carrier and sealing films.

To-date, however, no patent information or published literature is available on PA6/fibre composites formed by "in-situ" anionic polymerisation of caprolactam using extruder as the chemical reactor.

CHAPTER 3

SYNTHESIS AND CHARACTERISATION OF REACTIVE POLYMERISED POLYAMIDE 6

3.1 Introduction

A series of reactive polymerised polyamide 6 (PA6) materials are synthesised by activated anionic polymerisation of ∈-caprolactam in a twin-screw extruder using a range of screw speeds from 50 rpm to 150 rpm. The influence of polymerisation processing parameters on the molecular mass, residual monomer content and crystalline structures of PA6 which in turn have a critical bearing on the material properties are discussed.

3.2 Experimental

3.2.1 *Materials*

The raw materials feedstock composition for the reactive polymerisation of polyamide 6 (PA6) consists of 95% by weight of the monomer, ∈-caprolactam $\underline{CH_2(CH_2)_4CONH}$, 3% of a catalyst, sodium caprolactamate $NaN\underline{(CH_2)_5CO}$, and 2% of an activator V5, bis-acyllactam hexamethylene diamine $O\underline{C(CH_2)_5}NCONH(CH_2)_6HNCON\underline{(CH_2)_5CO}$. The raw materials used are commercial products manufactured by DSM Chemicals, Netherlands. The ratio of catalyst and activator used is based on the recommendation of the raw material supplier for the synthesis of commercial PA6 monomer castings (Appendix I).

Five hundred gramme batches of solid feedstock were accurately weighed and thoroughly tumble mixed before being introduced into a K-tron volumetric blender-feeder at the feed port of the twin-screw extruder.

For comparative studies, a commercial grade PA6 resin CAPRON 8202C (Allied Chemical Corp.) supplied in pellet form is also used for all the characterisation studies.

3.2.2 *Preparation of Polyamide 6*

Polymerisation was undertaken in a 40 mm screw diameter intermeshing co-rotating twin-screw extruder (BTS 40-Betol Machinery Ltd). This was assembled in a 21/1 length over diameter (L/D) ratio with screws configured to permit specified functions of feedstock conveying, melting, mixing, devolatilisation and melt delivery to the die (Figure 3.1). A reaction zone was also defined using segmented discs and trilobal kneading elements to provide a melt seal at the entrance and exit portions of this zone, in addition to contributing to compositional homogeneity. Screw sections in this design are trapezoidal, which result in positive material conveyance together with cross-channel and inter-channel mixing [34].

During the early stages of the work several different screw assemblies were evaluated, the configuration shown in Figure 3.2 gives optimum operating performance. In the devolatilisation zone, a reduced pressure of 50 mm Hg was applied to facilitate volatile extraction as well as removal of the unreacted caprolactam monomers.

A pre-blend of the monomer/catalyst/activator feedstock was delivered at a constant rate to the extruder using a K-Tron twin-screw volumetric feeder. After polymerisation stage, PA6 was die-formed into a 4 mm diameter rod and quenched in water at 23 $^{\circ}$C (Figure 3.3). In some experiments, samples for structural analysis were also prepared by allowing extrudates to cool slowly in air to room temperature.

Temperature profiles along the length of the extruder barrel were set according to the functional requirements of the particular zones. Hence, as the caprolactam

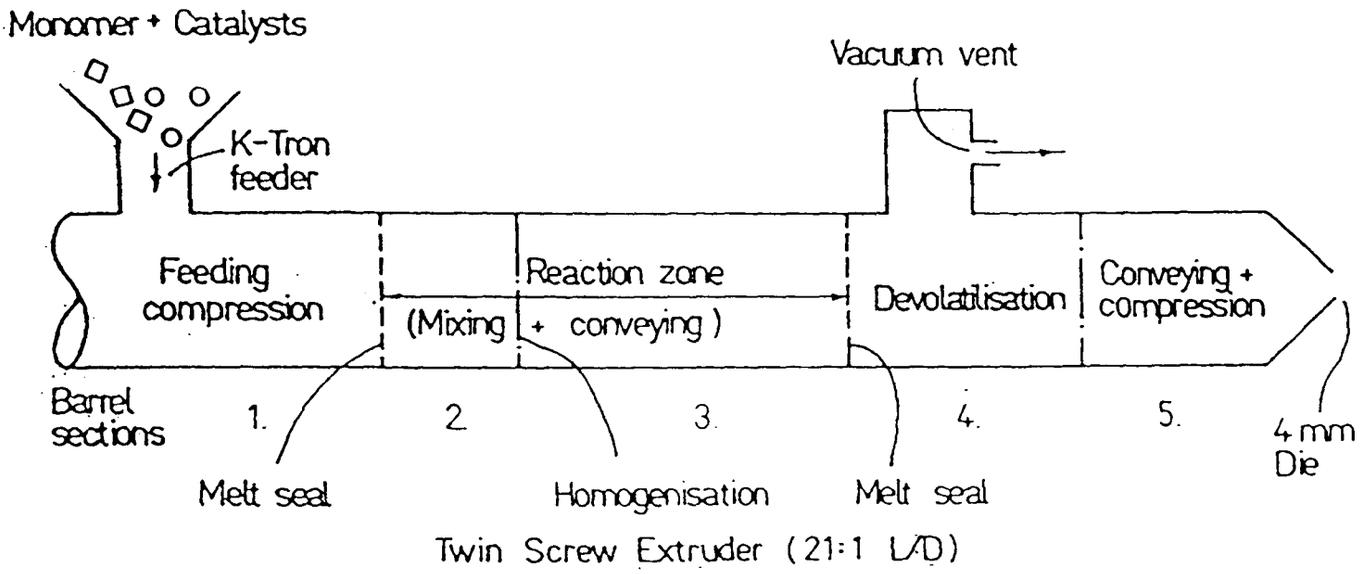

Figure 3.1 Schematic diagram of twin-screw extruder for reactive polymerisation

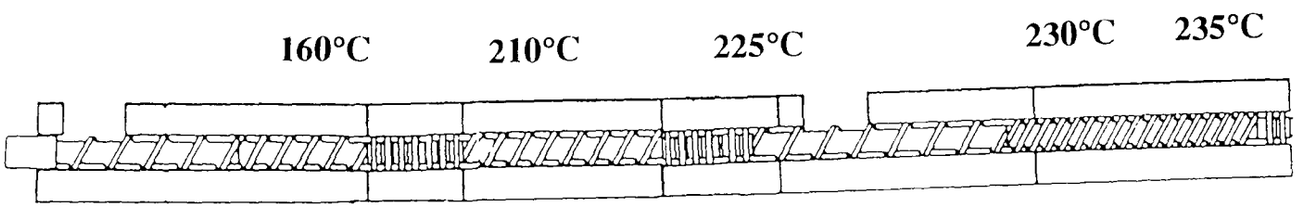

Figure 3.2 Extruder screw profile and barrel temperatures

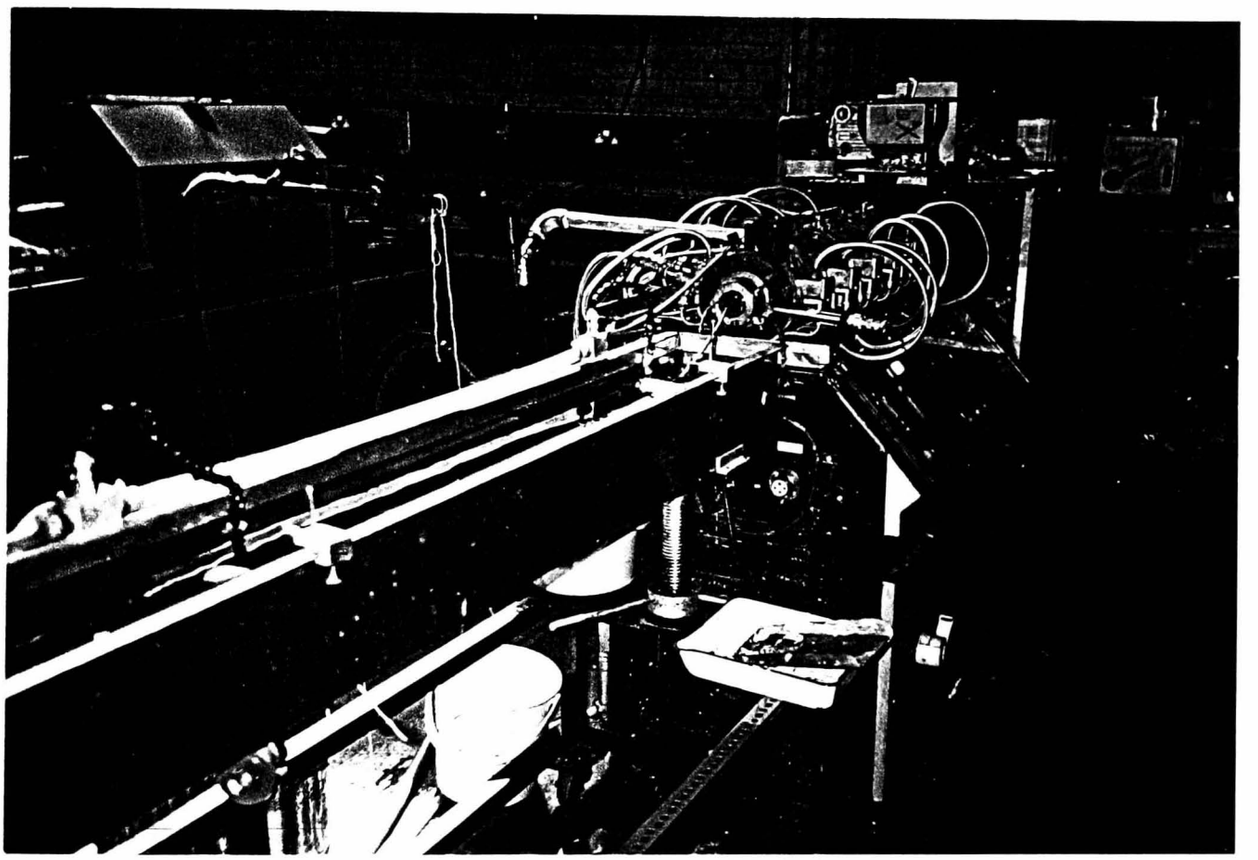

Figure 3.3 Water-quenching the PA6 extrudate after reactive extrusion

monomer melts and polymerises to PA6, the temperature conditions must accommodate the changing rheology of the material. Based on results obtained from model experiments undertaken to determine the effects of temperature and reaction time [64] and practical observations on the extrudates, the barrel temperature profile shown in Figure 3.2 was selected and used for reactive extrusion procedures at extruder screw speeds ranging from 50 to 150 rpm. Material throughput rates of 4 kg h^{-1} were obtained at an extruder screw speed of 150 rpm.

3.2.3 *Preparation of Test Specimens*

The extrudates collected were subjected to hot water extraction using Soxhlet apparatus for 24 hr to remove residual caprolactam monomer and low molecular weight oligomers, followed by drying in vacuo at 110°C for 24 hours. The washed and dried materials were then stored in dessicators at room temperature (23°C) prior to test specimen preparation by injection moulding. Some samples after the extraction process were also subject to further thermal treatment by annealing at a temperature of 180°C for 90 minutes in a vacuum oven prior to structural characterisation.

Tensile and impact test specimens were prepared by injection moulding in accordance with procedures stated in ISO 1874-2 "polyamide 6 homopolymers for moulding and extrusion - preparation of test specimens and determination of properties". All the materials were dried in oven at 90°C for 48 hours prior to the injection process. A Battenfeld 200/50CD Unilog 4000 injection machine (20 ton) was used together with a single end gated, two cavity mould for the production of a ASTM D638 Type 1 tensile test and a 3.17 x 12.7 x 127 mm Izod impact test specimens.

The injection moulding conditions used were:

Temperature settings:

i) At nozzle	240°C
ii) At front of screw	240°C
iii) At middle of screw	235°C
iv) At rear of screw	235°C
v) Mould temperature	82°C

Injection pressure	100 bar
Total cycle time	39.5 seconds
Mould open time	6.5 seconds
Mould closed time	29.5 seconds
Injection time	1.51 seconds
Pressure dwell time	3.55 seconds
Cooling time	28.5 seconds
Clamping pressure	140 bar
Mass of moulding (including sprue and runners)	23.8 gm

3.2.4 *Molecular Weight and Molecular Weight Distribution*

3.2.4.1 *Solution Viscometry*

This was done by measuring the limiting viscosity number (intrinsic viscosity) of a pure PA6 solution in 90% formic acid in accordance with procedures of ISO 307:1984 "Polyamides-Determination of Viscosity Number".

0.25 gm of the previously hot water extracted, dried polymer granules were dissolved in 50 ml of formic acid solution and thoroughly shaken at room

temperature until a clear solution was obtained. Nine concentrations of PA6 from 0.003 to 0.0002 $gm.l^{-1}$ in 90% formic acid solution were prepared in a similar manner. Each solution was then pipetted into a suspended-level viscometer (size no. 2) clamped in a thermostat water bath maintained at 25°C. The efflux times of the solutions through the horizontal timing marks of the viscometer were taken in triplicate and the average time recorded. The efflux times of the pure formic acid were also determined in the same viscometer under similar experimental conditions.

The viscosity ratio, η_r (relative viscosity), defined as the ratio of the polymer solution viscosity η to the pure solvent viscosity η_0, was obtained from the following equation:

$$\eta_r = \eta / \eta_0 = t / t_0 \qquad [3.1]$$

where t = flow time of solution

t_0 = flow time of solvent

Knowing the viscosity ratio of the solution, it was possible to calculate the viscosity number (reduced viscosity) from equations [*3.2*],

$$\text{Viscosity number} = [(\eta - \eta_0)/\eta_0].c^{-1} \qquad [3.2]$$

where c is the polymer solution concentration in $g.ml^{-1}$.

The limiting value of Equation [*3.2*] at infinite dilution is known as the limiting viscosity number (intrinsic viscosity) $[\eta]$, where:

$$[\eta] = \lim_{c \to 0} [(\eta_r - 1)/c] \qquad [3.5]$$

$[\eta]$ is obtained by extrapolating a graph of $[(\eta - \eta_0)/\eta_0].c^{-1}$ versus concentration c to the zero concentration intercept.

The relationship between the limiting viscosity number and viscosity average molecular weight M_v is expressed by the **Mark-Houwink** equation:

$$[\eta] = K \bar{M}_v^a$$

where K and a are constants valid at a specified testing temperature and a specified polymer/solvent system. In this study, values of K and a are taken as 3.77×10^{-2} $g.ml^{-1}$ and 0.80 respectively for the unfractionated PA6 samples [145].

3.2.4.2 *Molecular Weight Distribution*

Gel permeation chromatography (GPC) was used for the determination of molecular mass distribution of the PA6 samples prepared at various extruder screw speeds. This characterisation technique involves a dilute solution of the PA6 being injected into a column of porous gel beads. During the flow of the solution down the column, larger molecules spend less time within the porous gel and therefore are eluted first whereas smaller molecules are retarded and will ellute last. Subsequent analysis of the elluted solution using refractive index or low angle light scattering technique reveals a distribution of the sample molecular weights. This work was carried out at RAPRA Technology Ltd. UK.

The chromatograph conditions used were:

Instrument: Waters 150 CV

Columns: PL gel 2x mixed bed B, 30 cm, 10 μm

Solvent: 1, 2 cresol, with antioxidant

Flow rate: 1.0 (nominal)

Temperature: 120°C (nominal)

Detector: refractive index

Injection: 200 μl

Sample solutions of PA6 prepared at various extruder speeds were prepared by adding 4 ml of solvent to 16 mg of sample in a special vial for the instrument's autosampler. The sample solutions were left overnight at room temperature, to dissolve the samples and then kept at 120 °C within the instrument for approximately 90 minutes prior to use. The special vials incorporate a 0.5 micron steel filler which was used to filter all solutions prior to the chromatography runs. Each solution was run in duplicate for all the experiments.

The molecular weight distribution (MWD) curves for all the samples determined by GPC were as listed in Appendix II.

3.2.5 *Caprolactam Monomer Content*

Anton [146] and **Ongemach** *et al.* [147] described a quantitative infra-red spectrophotometric determination technique for determining free caprolactam in PA6. This method proved lengthy and time consuming however, since it required solution concentration of liquid-liquid extraction of the aqueous concentrate with carbon tetrachloride before subjected to infra-red spectrophotometric determination.

More recently, **Ongemach** *et al.* [148] described another rapid and more precise method based on gas chromatography for the determination of caprolactam monomer residue content. This method uses the well known technique of an internal standard bis-[2-(2-methoxyethoxy)ethyl] ether for calibration and measurement of the elluant.

For accurate determination of the caprolactam monomer residue content of PA6 samples produced in this study, a modified gas chromatography technique was devised which involved using only distilled water as an internal standard.

Gas chromatogram analyses were made using a single column flame ionisation detector attached to a Pye Unicam series 104 gas chromatograph. The single column used was of 2.1 meter length with a 3 mm outer diameter stainless steel column packed with Apiezon L on 60 mesh Diatoport S.

The following instrument settings were used throughout the experiments:

Flow rate, H_2 = 60 ml minute^{-1} at 10 psig

Flow rate, air = 400 ml minute^{-1} at 50 psig

Column temperature = 185°C

Detector temperature = 280°C

Chart speed = 0.1 m min^{-1}

Monomer residue remaining in the extrudate was measured by gas chromatography based on monomer concentration in distilled water. Firstly, a calibration curve (Figure 3.4) of elluant peak areas as a function of monomer contents was contructed from known aqueous caprolactam solutions containing 1 to 12% by weight of monomer. Caprolactam solutions with known concentrations were initially analysed in duplicate with two micro-litre injections of each, giving quadruplicate analysis. After each injection, the ellution peak due to distilled water first appeared at 0.9 minutes average residence time, followed by the caprolactam peak which appeared after 2.2 minutes residence time. Excellent reproducibility of results were recorded ($\pm$3 sec) for all the experimental runs.

For the determination of monomer residue content in the PA6 samples, weights of 0.5 gm of the as-extruded pellets were first extracted in 500 ml of distilled water using Soxhlet apparatus at 100°C for periods of 24 hours. The extracted aqueous solutions were then injected into the gas chromatograph and analysed for caprolactam content in a similar manner as described above. The elution data in terms of peak areas from the recording chart were then compared against the

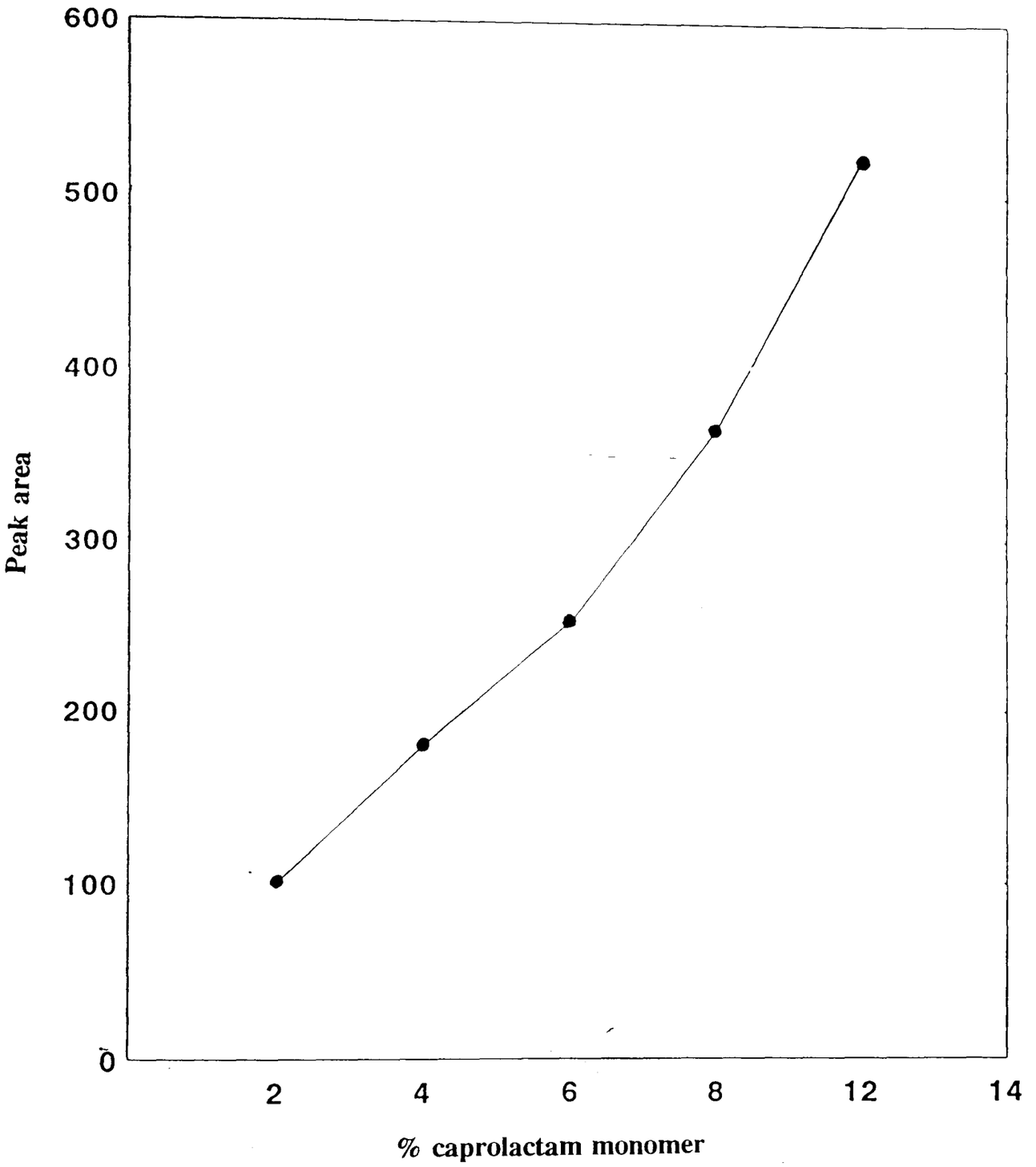

Figure 3.4 Calibration curve for caprolactam monomer content by GC

calibration curve to determine the residual monomer concentration present in the as-extruded pellets.

3.2.6 *Structural Analysis*

3.2.6.1 *Wide Angle X-Ray Diffraction*

Semi-crystalline polymers such as PA6 are known to contain both glassy amorphous phases and ordered crystalline phases. In order to characterise these multi-phase systems that exist in semi-crystalline polymers, the technique of wide-angle X-ray diffraction (WAXD) is frequently used. X-rays of wave-length λ will only be diffracted from a system of parallel lattice planes in a crystal of spacing d if the Bragg equation is satisfied, i.e $n\lambda = 2\ d\ \sin\theta$

where n = an integer which defines the order of diffraction
θ = Bragg diffraction angle
d = distance between lattice plane

Wide-angle X-ray diffraction (WAXD) pattern in an equitorial mode was recorded on a Philips PW1050 Goniometer at room temperature of 23°C over the range of diffraction angles (2θ) from 10° to 30° using nickel filtered copper K_α radiation. The samples used were in the form of thin sheets cut perpendicular to the flow direction of the rod extrudate. The samples were rotated around a fixed axis during diffraction runs. The conditions of the X-ray scattering were 40 kv, 30 mA, time constant 4, slit 1°x1° and 0.6° min^{-1} sweep.

3.2.6.2 *Differential Scanning Calorimetry*

Differential scanning calorimetry (DSC) is a technique in which the difference in energy input into a substance and a reference material is measured as a function of temperature while the substance and the reference material are subjected to a controlled temperature programme. The record obtained is the DSC curve or thermogram. In this investigation, DSC technique is used to evaluate the melting and crystallisation temperatures of the various PA6 samples prepared, in accordance with procedures of ASTM D 3417 "Standard test method for heats of fusions and crystallisation of polymers by thermal analysis".

To this end, representatives samples of PA6 with differing processing history were analysed on a Perkin-Elmer DSC-2B differential scanning calorimeter, by thermal cycling under specified conditions of heating and cooling. During the first heating cycle (Stage I) between 5 mg and 10 mg of samples were heated from 40°C to 250°C at a rate of 10°C min^{-1}, in order to monitor melting behaviour. Temperature was then maintained at 250°C for 15 minutes before cooling to 40°C at a rate of 5°C min^{-1} to determine the onset of crystallisation. A second melting thermogram was subsequently obtained immediately after the cooling cycle (Stage II) using the same conditions as the first heating run.

Throughout the analysis, samples were held in closed aluminium pans under a nitrogen blanket. Duplicate runs were performed for all the samples to ascertain reproducibility of the results estimated to be ± 0.5°C. The apparatus was earlier calibrated with Indium standard reference material with the same heating rate.

3.2.6.3 *Fourier Transform Infrared Spectroscopy*

Infrared (IR) spectra is often used as polymer fingerprints since comparison of characteristic absorption bands in the IR spectrum can lead to identification of the bonds and functional groups present in the polymer. Polyamides are usually characterised by absorption bands in the 670-4000 cm^{-1} region arising from the peptide linkage. For instance, the 3302 cm^{-1} band is due to the NH stretching vibration of the secondary amide [159]; the 1642 cm^{-1} band due to the carbonyl stretching frequency and the 1545 cm^{-1} band is due to the NH deformation vibration [157].

Infrared spectra were recorded with a Perkin Elmer 1720 Fourier transform infra-red spectrometer equipped with a room temperature DTGS detector. A high signal-to-noise ratio was obtained by scanning the samples and reference 256 times at a resolution of 4 cm^{-1}.

Thin films of thickness (5μm) wre prepared from different reactive polymerised PA6 samples using a constant thickness film maker P/N 15620 SPECAC (Perkin Elmer).

3.2.6.4 *Microscopic Analysis*

Microscopic analysis with scanning electron and optical microscopy have been used to identify the morphological pattern of polymer surfaces such as phase separation, crystalline arrangement, fracture characteristics and thermal history. The data obtained was then relate to the processing variables that can possibly lead to less than optimum mechanical properties of the material. In general, the microscopic methods can be divided into three categories i.e. scanning electron microscopy, transmission electron microscopy and light or optical microscopy.

Fracture surfaces of PA6 rod extrudate were examined using a scanning electron microscope (SEM - Cambridge S250) with an acceleration voltage of 10 kV. All the samples were sputter-coated with gold palladium alloy prior to viewing under the microscope (1000-2000x magnification).

Selective PA6 samples prepared by reactive polymerisation of caprolactam were microtomed from the rod extrudate perpendicular to the polymer flow direction for analysis by transmission electron microscopy (TEM). Microtomy was first performed at room temperature using an ultramicrotome and glass knife. However, great difficulty was encountered in an attempt to produce ultra-thin (< 100 nm) sections. This problem was attributed to the inherent toughness of the material and its natural wetting characteristics. It was found that when the specimen approached the cutting edge of the knife, the trough liquid was drawn up between the knife edge and the sample face forming a lubricating barrier which inhibited cutting. Even when cuttings were performed successfully, the sections obtained were observed to be strongly sheared and compressed. These samples were considered non-representative of the true structure since the surface morphology had been greatly distorted, see for example Figure 3.5. Sample preparation was subsequently facilitated using a diamond knife, and ultra thin samples with thickness 50-100 nm were successfully sectioned.

Thin films of the microtomed samples captured on a specimen grid were stained with 2% phosphotungstic acid by floating on a drop of the solution for a period of 30 minutes. The specimen was then washed in distilled water with three rinses before subjected to structural investigation using a Jeol 100C TEM operating at 100 kV (30,000x magnification).

For optical microscopic examination, thin samples of 5 μm thickness were sectioned from the centre of the PA6 rod extrudate perpendicular to the polymer flow direction

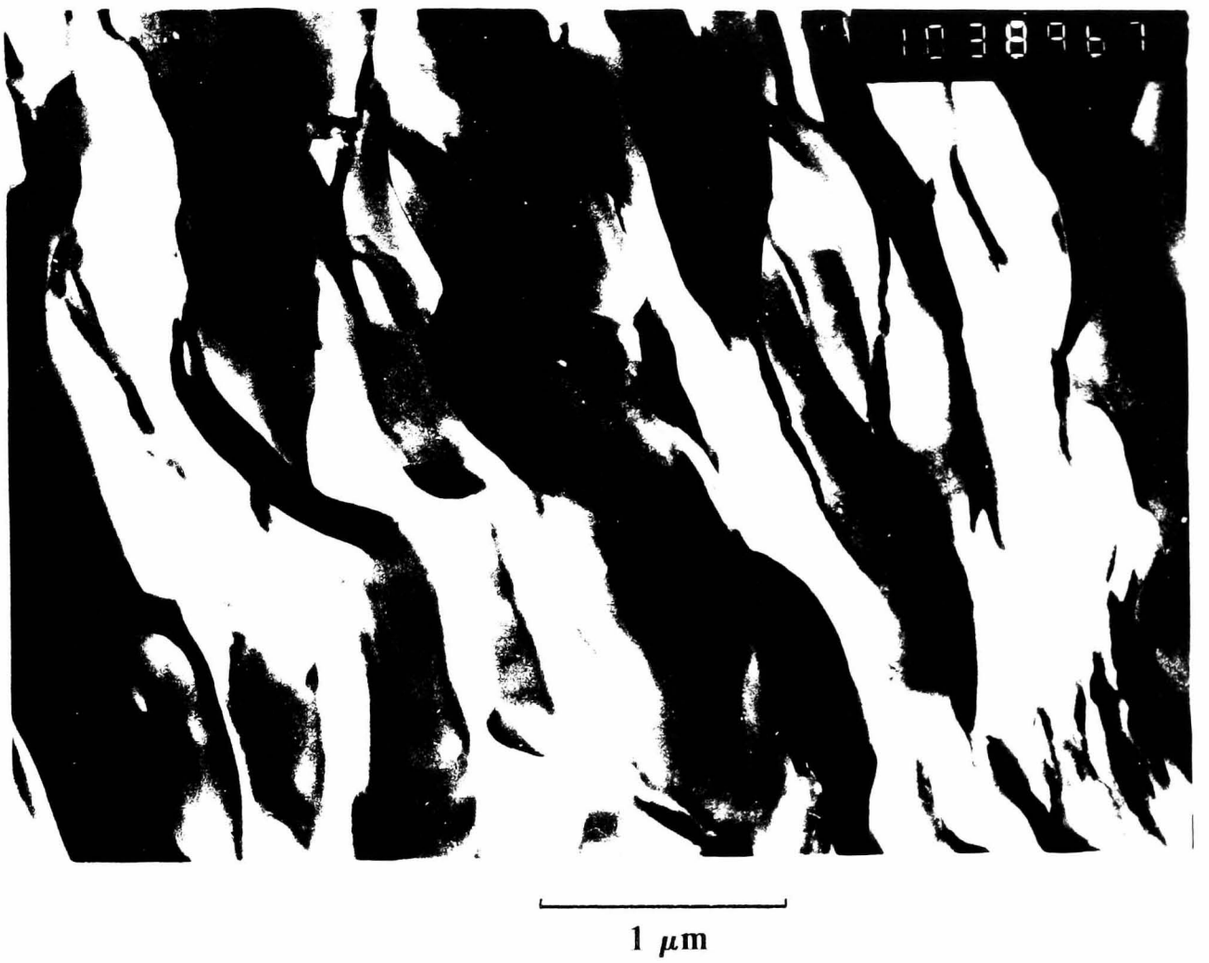

Figure 3.5 TEM micrograph of PA6 showing damage caused by sectioning

using a Leitz sledge microtome and a steel knife. The samples were placed on microscopic slides and examined with a transmission optical microscope (Type: Reichert Zeopan) in plane polarised light (200x magnification). Photomicrographs were taken of all slides for the asssessment of the specimen microstructures.

3.2.7 *Determination of Physical Properties*

3.2.7.1 *Mechanical Behaviour*

Tensile test specimens were prepared by injection moulding of the pellets which have been extracted with water to remove the residual monomers, dried in vacuo for 24 hr, then stored in dessicator at room temperature [Section 3.2.3]. Prior to injection moullding, the PA6 pellets were dried at 90°C in vacuo for 48 hr. Immediately after the injection moulding process, the test pieces were wrapped in plastic bags and stored in a dessicator for 7 days before testing in a state of dry, as-moulded condition.

Stress-strain measurements were made in tension mode at 23°C using a Lloyd L1000S tensometer at a strain rate of 50 mm $minute^{-1}$ with a load cell of 5kN. The tensile test specimen is of ASTM D 638-Type 1 with a gauge length of 50 mm. Five specimens were evaluated for each sample and the mean result reported.

Elongation of the specimen was determined using an infrared non-contacting extensometer on the two gauge marks. Modulus, tensile stress at yield and percentage elongation at break were evaluated.

Flexural tests was performed in accordance with ASTM D790 Method 1 Procedure B viz. three point loading system utilising centre loading on a simply supported

beam. The test specimen used is a rectangular beam (modified Izod impact test bar) with dimensions 80 x 12.7 x 3.17 mm. The support span used was 50 mm and measurements were made at a test speed of 2 mm min^{-1} in compression mode with a 100 N load cell using a Lloyd L1000S tensile/compression machine.

Maximum force and loads at specified strains of 0.7% and 1.0% respectively were obtained for calculation of flexural modulus, E_f according to

$$E_f = L^3m/4bd^3$$

where
- L = support span
- b = width of beam tested
- d = depth of beam tested
- m = slope of the tangent to the initial straight-line portion of the load deflection curve of deflection.

Izod impact resistance of the PA6 samples were conducted on standard, notched test pieces (Type A - 0.25 mm notch @ 45°) at 23°C in accordance with ASTM D 256. The basic principle of the Izod test is to allow a pendulum of known mass to fall through a known height and strike a standard specimen at the lowest point of its swing, and to record the height to which the pendulum continues its swing. Notching of the specimen bar was carried out using a notch cutting apparatus (Davenport, UK). All impact tests were performed using a 2 J hammer with a CEAST 6546 Izod tester. Ten specimens of each PA6 samples were used and the mean of the results reported.

A dynamic mechanical instrument Rheometrics Solids Analyser RSA II was used for the measurement of dynamic mechanical properties of the PA6 samples (dynamic storage modulus E' and the loss factor tan δ) as a function of temperatures from -100°C to 130°C. Dynamic mechanical testing provides a method for determining elastic and loss moduli as a function of temperature, frequency or time, or both. A plot of elastic modulus and loss modulus of the material versus temperature provides a graphical representation of elasticity and damping as a function of temperature or frequency.

This procedure can be used to locate transition temperatures of plastics which involves changes in the molecular motions of a polymer. In the temperature ranges where significant changes occur, elastic modulus decreases rapidly with increasing temperature (at constant frequency), or increases with increasing frequency (at constant temperature). A maximum is observed for the loss modulus.

Testing was carried out in the three-point bending (flexure) mode using a frequency of 6.28 rads s^{-1} (1 Hz). The magnitude of E' and tan δ were measured at every 5°C with increasing temperature. All the test specimens used were rod samples of the reactive polymerised PA6 materials (after monomer extraction and drying) of length 48 mm and 3 mm diameter. All the samples were conditioned at 23°C in the dessicator for 72 hours prior to testing in accordance with Procedure A of ASTM Practice D618. Duplicate specimens were tested to ensure reproducibility of test results. Some "as-polymerised" polymerised PA6 sample extruded at 150 rpm i.e. without monomer extraction but dried in vacuo at 110°C for 24 hr, were also tested to investigate the the effect of monomer on the dynamic mechanical properties of the polymer.

3.2.7.2 *Melt Flow Index*

The basic principle employed in the melt flow index test is that of determining the rate of flow of molten polymer through a closely defined extrusion plastometer. Melt flow index (MFI) is basically defined as the weight of the polymer in grams extruded in 10 minutes interval through a capillary of specific diameter and length by pressure applied through a dead weight under prescribed temperature conditions. MFI of the PA6 samples were determined using a Zwick 4105 melt flow indexer in accordance with ASTM D 1238 procedures. An applied load of 2.16 kg was used at a barrel temperature of 230°C with a die of internal diameter 2.095 mm. Duplicate specimen were evaluated and the mean of the results reported.

3.2.7.3 *Moisture Content*

The amount of water content is of importance in connection with the processing and subsequent properties evaluation of PA6. The moisture content of the reactive polymerised samples and the commercial PA6 material were determined by an initial extraction process using a mixture of 3-methylphenol and toluene followed by analysis of the solution based on the Karl Fisher method. All test procedures were performed as stated in ISO 960 "polyamide 6 - Determination of water content".

3.3 Results and Discussion

3.3.1 *Polymerisation of ∈-Caprolactam*

It is well known that the polymerisation of ∈-caprolactam in the presence of alkaline catalysts such as sodium caprolactamate produces high molecular weight PA6 in just a few minutes, by contrast to "classical" hydrolytic polymerisation which requires reaction time of several hours [58].

After a short induction time, polymerisation of caprolactam to PA6 proceeds with a high rate, at a reaction temperature of about 200°C. The reaction commences with the ionic catalyst (sodium caprolactamate) attaching itself to the caprolactam as shown in reaction (I) of Figure 3.6. A new, reactive sodium salt forms, which in turn reacts with any free caprolactam available to generate acyllactam [Figure 3.6 reaction (II)]. This reactive acyllactam growth centre will further react very rapidly with sodium caprolactamate and the reaction proceeds to form a high molecular weight PA6 [Figure 3.6 reaction (III)].

In the absence of impurities such as air or oxygen, there is no termination reaction. Polymerisation stops when the monomer level is reduced to an equilibrium which is a function of temperature [64].

In order to generate the acyllactam growth centres and proceed with the fast polymerisation reaction at a lower temperature of 140-160°C, an acyllactam based activator is required in additional to the sodium caprolactamate catalyst and caprolactam monomer present. The chemical mechanism for this bis-acyllactam initiated reactive polymerisation of caprolactam to PA6 is as shown in Figure 3.7.

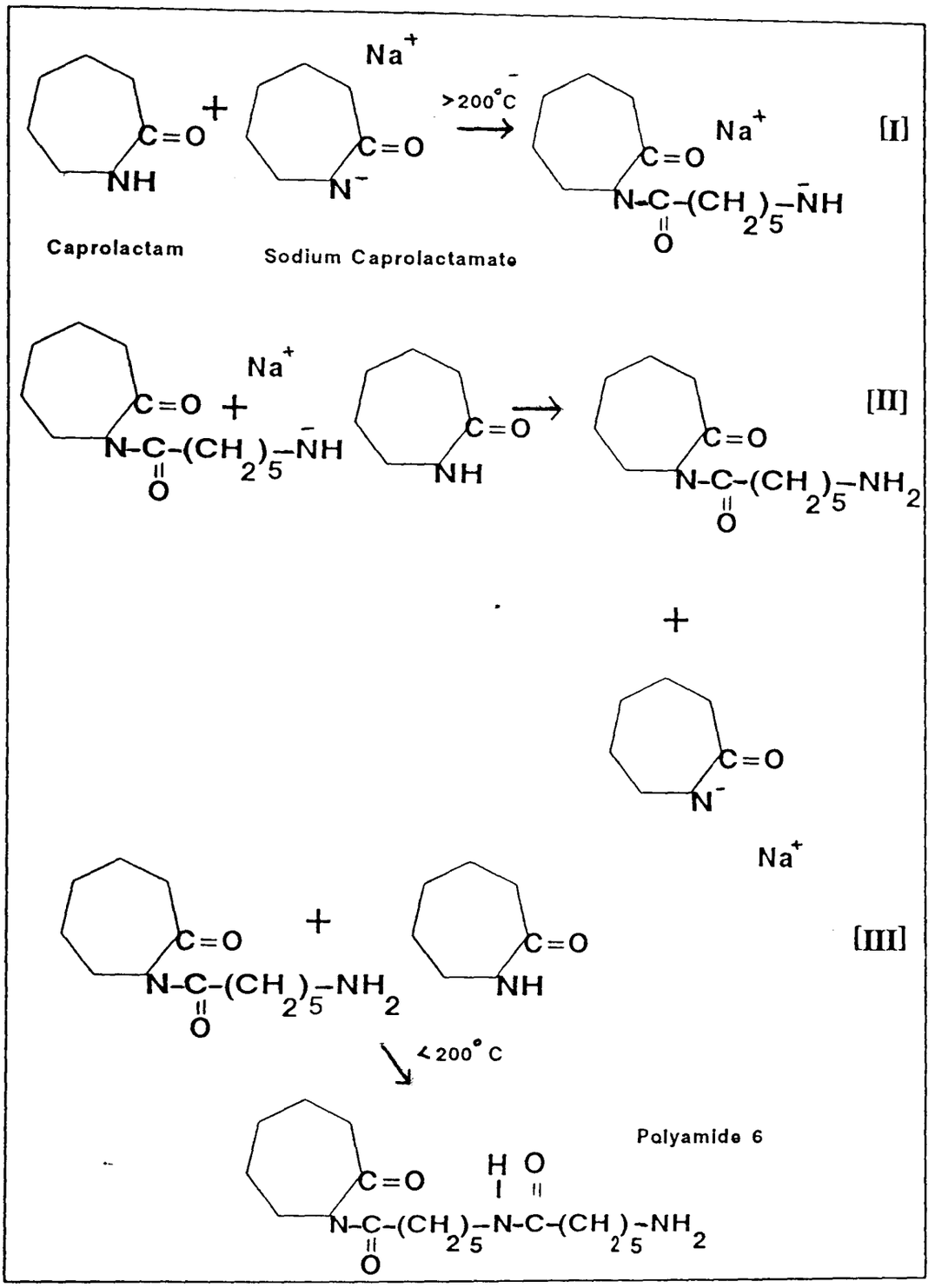

Figure 3.6 Reaction mechanism for anionic polymerisation of caprolactam (adapted from [49])

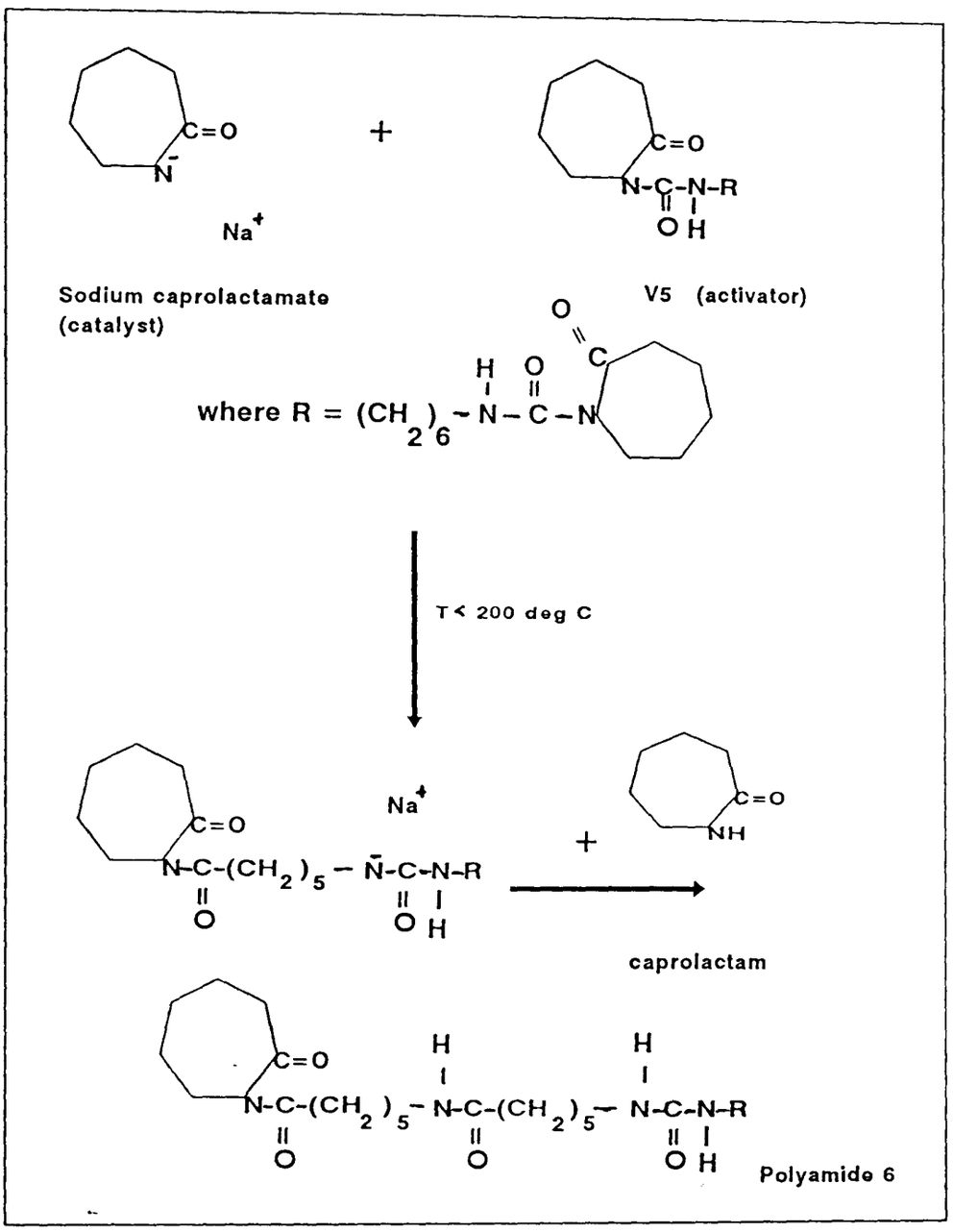

Figure 3.7 Reaction mechanism for activated (acyllactam) anionic polymerisation of caprolactam (adapted from [49])

The investigations presented here were conducted in a co-rotating, intermeshing twin-screw extruder using ϵ-caprolactam (monomer), sodium caprolactamate (catalyst) and a hexamethylene based bis-acyllatam (activator), with consistent material blend compositions by % weight of 95:3:2. Polymerisation of ϵ-caprolactam to PA6 occurred in the reaction zone of the extruder at temperature of 160°C as shown in Figure 3.1. Preliminary experimental trial-runs using other blend compositions of 95:4:1 and 95:2.5:2.5 were not successful since only soft extrudates were obtained indicating only very low polymerisation conversion had occurred. These findings also confirm that the concentration of both the catalyst and activator have a considerable influence on the reaction kinetics and the quality of the polymer formed [49].

The estimated average residence time in the reaction zone of the extruder was 15-20 seconds while total residence time in the extruder was about 80-92 seconds for the highest (150 rpm) and lowest (50 rpm) screw speed used. **Kao** *et. al* [149] studied residence time distribution in a fully intermeshing, corotating twin-screw extruder and reported that throughput, screw rotation speed and screw configuration have great effect on mean residence time, while barrel temperature profile has almost no effect.

Feed composition by weight of 95:3:2 could probably constitute the theoritical equilibrium for the conversion of ϵ-caprolactam monomer to PA6 expected at a reaction temperature of 160°C. It has been reported that 92% conversion of monomer to polymer could be obtained at this equilibrium reaction condition [64].

During the course of the experiment, it has also been observed that precision feeding of the blend components into the feed zone of the extruder was important to ensure consistent polymerisation at the reaction zone. This was done by maintaining a fixed

quantity of the raw materials blend in the K-tron feeder at any time during the polymerisation process.

The other observed extrusion operating parameter essential for the reproduction of consistent quality PA6 materials is minimum level of moisture present in the raw material feedstock since it can easily deactivate the catalyst effect.

3.3.2 *Molecular Weight Determination*

The limiting viscosity number η of the samples were determined by extrapolating the concentrations of PA6 samples in 90% formic acid solution to zero as shown in Figure 3.8. The results observed are unusual since the viscosity number for all the reactive polymerised PA6 samples at any particular solution concentration appears to increase with concentration only up to around 0.001 or 0.0015 $g.ml^{-1}$, decreasing in value thereafter. However, with commercial PA6 material produced by hydrolytic polymerisation, the viscosity number is found to increase continuously with solution concentration even up to 0.01 $g.ml^{-1}$ [150]. Indeed, result for Capron 8202C PA6, carried out under similar experimental conditions, demonstrate this expected trend as shown in Figure 3.8.

It is important to note that ISO 307:1984 does not advocate the use of its test procedures for PA6 materials obtained by anionic polymerisation of lactams, or for polyamides produced with crosslinking agents, on account of their frequent insolubility in the specified solvents of formic acid, sulphuric acid or m-cresol. However, the present experimental work has demonstrated that the intrinsic viscosity of high molecular mass PA6, made by anionic polymerisation of ϵ-caprolactam can be successfully determined by solution viscometry in 90% formic acid solution. Meaningful results are only obtained when polymer solution concentrations are less

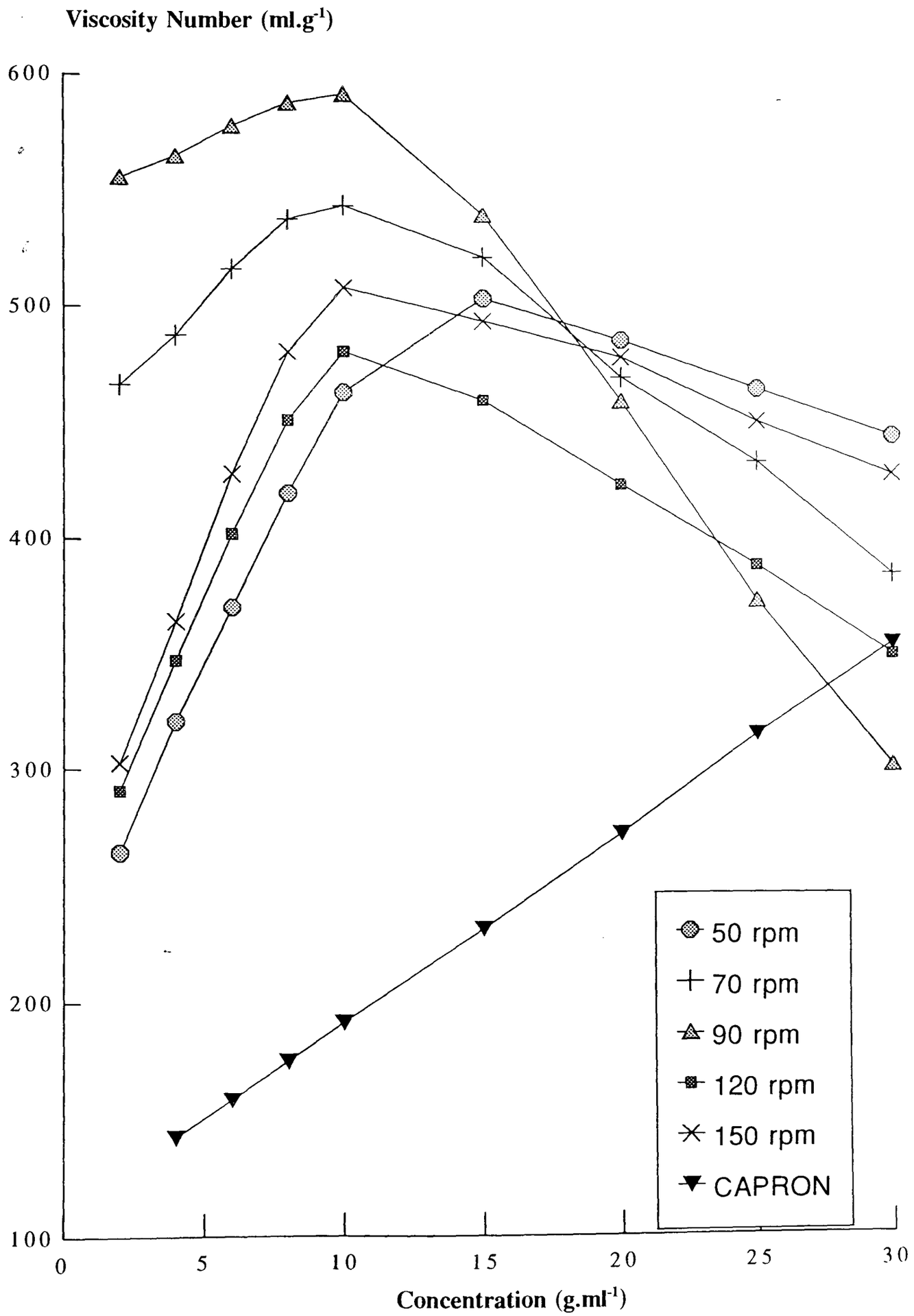

Figure 3.8 Viscosity number of Polyamide 6 variants

than 0.001 $g.ml^{-1}$, well below the concentration level specified in the ISO 307 document.

A likely explaination for the observed phenomena is a polyelectrolyte effect imparted on the formic acid solution, due to the extraordinary high molecular mass of the PA6 obtained by reactive extrusion. Indeed, in an acid medium capable of dissociation, protonation of the amide linkage may occur, resulting in the formation of positively charged PA6 chains which have a tendency to repel each other and hence expanding the polymer coil [151]. However, at very low PA6 concentrations, this effect is possibly been suppressed, thus enabling the determination of limiting viscosity number.

Limiting viscosity number $[\eta]$, obtained for these PA6 samples by extrapolating the data given in Figure 3.8 to zero concentration, are listed in Table 3.1, together with corresponding values of viscosity average molecular mass $\overline{M}_v$, determined from

$$[\eta] = K \overline{M}_v^a$$

where values of the constants K and a are taken as 3.77×10^{-2} $g.ml^{-1}$ and 0.80 respectively for this polymer/solvent system under consideration [145].

To check the validity of these PA6 results, molecular mass data were also analysed by gel permeation chromatography (GPC) using 1, 2 cresol at 120°C. Good agreement is seen between results obtained by solution viscometry and GPC, as seen in Table 3.1. PA6 samples made by anionic polymerisation were observed to yield much higher degrees of polymerisation than polymer produced by a commercial hydrolytic preparation route.

Table 3.1 Limiting viscosity number and viscosity average molecular weight of PA6 variants, determined by solution viscometry and GPC

Screw speed* (rpm)	GPC		Viscometry	
	Limiting viscosity number (ml g^{-1})	$\overline{M}_v$ (kg mol^{-1})	Limiting viscosity number (ml g^{-1})	$\overline{M}_v$ (kg mol^{-1})
50	221	53.7	215	49.6
70	412	110.3	443	122.3
90	562	140.5	540	156.7
120	201	55.8	232	54.5
150	235	60.5	241	57.2
Capron 8202C +	100	25.1	110	21.4

Table 3.2 Molecular weight and molecular weight distribution of PA6 variants determined by GPC

Screw speed* (rpm)	$\overline{M}_w$ (kg.mol^{-1})	$\overline{M}_n$ (kg.mol^{-1})	$\overline{M}_w/\overline{M}_n$
50	53.7	16.7	3.2
70	110.2	18.5	5.9
90	140.5	19.0	7.4
120	55.8	16.6	3.4
150	60.5	17.4	3.5
Capron 8202C +	25.1	14.0	1.8

* Conditions used during reactive extrusion process.
+ Commercial grade PA6 made by hydrolytic polymerisation process.

Other results obtained from GPC determination for all the PA6 samples are summarised in Table 3.2. It is significant that whilst the commercial grade PA6 moulding resins synthesised by hydrolytic polymerisation are supplied with average molecular weights, $\overline{M}_w$ of some 20,000-30,000 g mol^{-1}, the reactive polymerised PA6 synthesised in this study by anionic polymerisation using a twin-screw extruder have attained much higher molecular weights in the range 50,000-140,000 g mol^{-1}.

Table 3.2 showed that the samples prepared at screw speeds of 70 and 90 rpm recorded the highest molecular weights in the region 110,000-140,000 g mol^{-1} with molecular weight distribution (expressed as polydispersity index) of >6. Samples obtained at other screw speeds yield molecular weights of 54,000-60,000 g mol^{-1}, which is still about 80% higher than the commercial grade PA6 resin.

Higher screw speeds of 120 and 150 rpm formed lower molecular weight polymers due possibly to the reduced residence time spent inside the reaction zone of the extruder. More severe shear stresses experienced at higher screw speeds could also contributed to the formation of lower $\overline{M}_w$ polymerisates due to scissioning of polymer chains. On the other hand, at lower screw speed of 50 rpm, a counteracting effect could occur due to longer extruder residence time which will result in poor reaction rates leading to the formation of lower M_w products.

3.3.3 *Residue Caprolactam Monomer*

A calibration curve obtained from a series of standard caprolactam solutions in distilled water with gas chromatogram output peak areas is as shown in Figure 3.4. From this calibration curve, the caprolactam monomer residues of the different PA6 samples were determined and the results displayed in Figure 3.9.

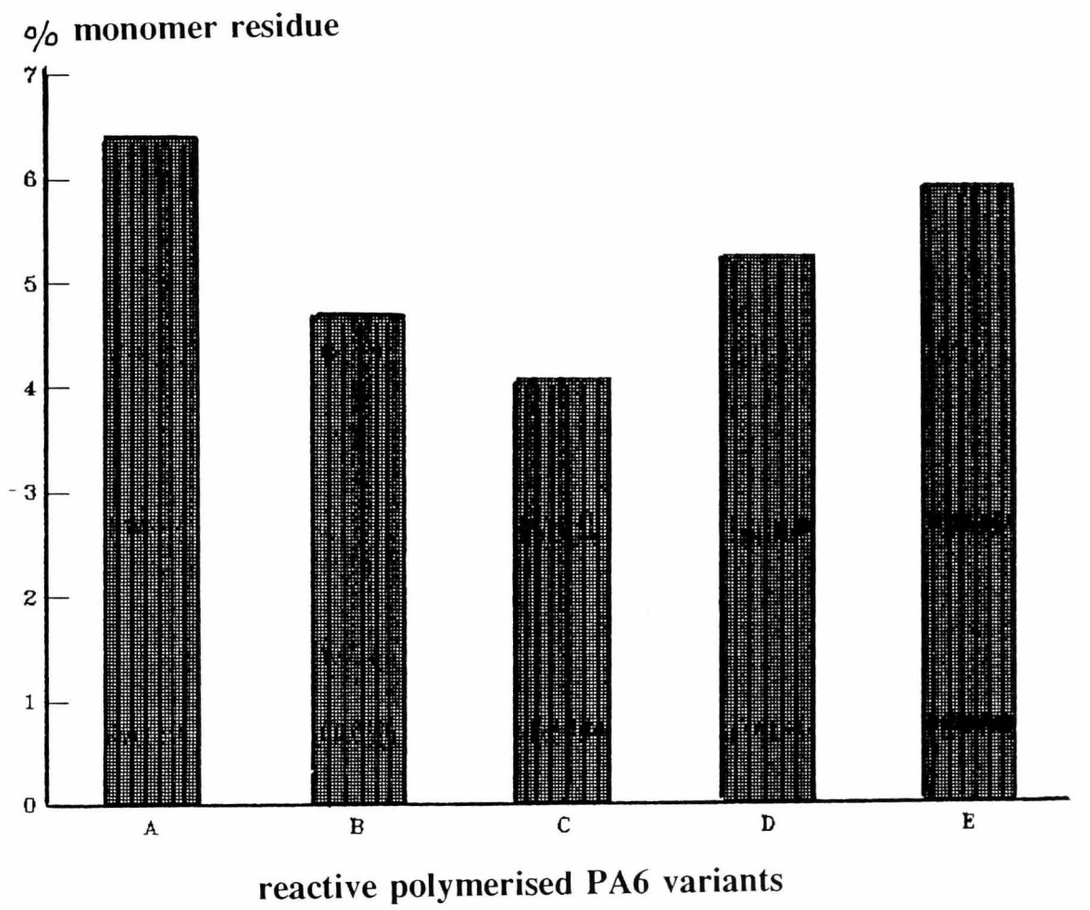

Figure 3.9 Residual caprolactam monomer content of reactive polymerised PA6

(A, B, C, D, E = reactive polymerised PA6 extruded @ 50, 70, 90, 120, 150 rpm)

PA6 samples prepared at the lowest and highest extruder speeds of 50 rpm and 150 rpm were observed to yield the highest monomer residue contents. At these two extremes of extruder speeds employed for these reactive polymerisation experiments, the rates of polymerisation reactions were not optimised due either to exceptional long residence time or inadequate residence time inside the extruder reactor. Long residence time and poor reaction rates of the monomer melts at 50 rpm can lead to low molecular weight polymers with higher level of unreacted monomer residues. On the other hand, high screw speed of 150 rpm could reduce considerably the residence time of the reacting materials inside the polymerisation zone. This, coupled with high sensitivity of the reaction mechanism to higher shear stress at screw speed of 150 rpm could again contributed to the formation of lower molecular weight products with higher level of residue monomers.

3.3.4 *Structural Characterisation*

3.3.4.1 *Wide Angle X-Ray Diffraction Analysis*

Typical WAXD equitorial reflection profiles of the water-quenched PA6 samples which have been subjected to monomer extraction and dried in vacuo at 110°C for 24 hr are shown in Figure 3.10(i). Two sharp reaks were observed characteristics of α crystalline phases with interplanar spacing of d_{200} = 4.4Å and d_{002} = 3.8Å, corresponding to Bragg angles (2θ) of $\approx 19.6^{\circ}$ and $\approx 23.5^{\circ}$ respectively. All air-cooled samples except for the one extruded at 150 rpm, showed similar WAXD patterns as that obtained for the water-quenched samples. The WAXD reflection profile of the air-cooled, 150 rpm sample showed the presence of an additional γ peak at d_{100} = 4.2Å (Bragg angle $2\theta \approx 21.3^{\circ}$) together with the two characteristic α_1 and α_2 peaks [Figure 3.10 (iii)].

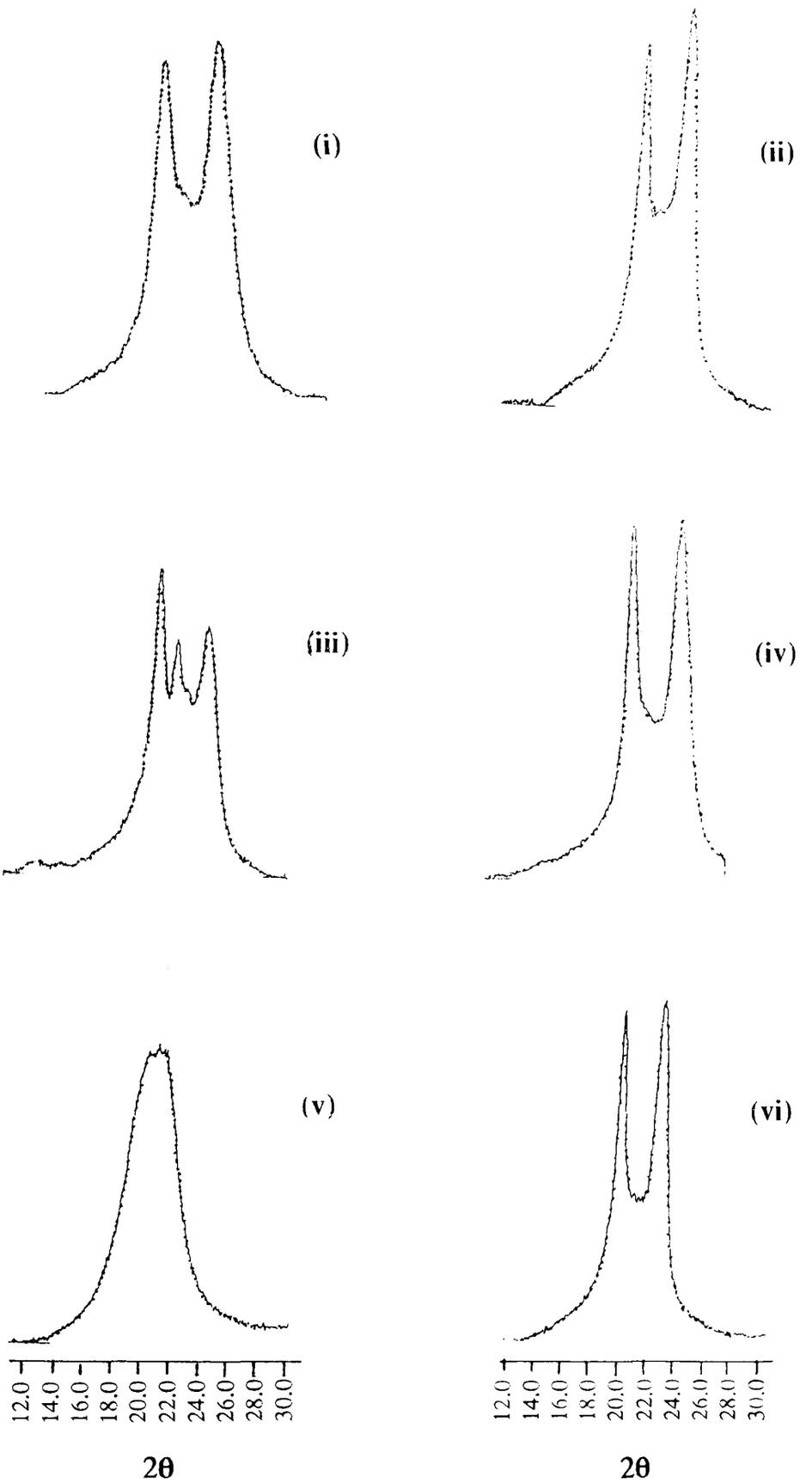

Figure 3.10 WAXD equitorial profile of reactive PA6 variants
(i) water-quenched (ii) water-quenched/annealed (iii) air-cooled
(iv) air-cooled/annealed (v) water-quenched with monomer residue
(vi) Capron-hydrolytic polymerised

However, all the water-quenched and air-cooled samples after annealing treatment at 180°C for 90 minutes, exhibit only α_1 and α_2 peaks on the WAXD profile indicating possibly the presence of only the α crystalline phase of PA6 [Figure 3.10 (ii) and (iv)]. The disappearance of the γ peak for the 150 rpm, air-cooled sample upon annealing treatment of the PA6 agreed with the findings of **Kyotani** [77-79] which stated that the γ crystalline phase of PA6 is thermally unstable and at temperatures above 160°C could transform into either the amorphous or the thermally more stable α form.

It is well established that the α crystalline phase of PA6 is in the extended conformation while the γ phase is in twisted helical conformation as shown schematically in Figure 3.11 [75]. The α crystalline form is the thermally more stable phase which can be obtained by slow cooling of the PA6 melt. On the other hand, the γ phase has been reported to exist under stress-induced conditions such as spinning of PA6 filaments at high speed [83]. The γ phase can also be obtained by fast cooling of the PA6 melt as well as chemically treatment of the α form using iodine [71]. The γ crystalline phase has also been reported to transform into the α phase by melting followed by recrystallisation at slow cooling rate [78] and by annealing the material at temperatures above 160°C [76]. The transformation of γ crystalline phase of PA6 to the α form has been established as a first order crystal-crystal transformation [82].

WAXD profiles of the as-processed water-quenched PA6 materials, which has not been subjected to predrying and residual monomer extraction exhibit only a broad γ phase peak as shown in Figure 3.10 (v). As discussed earlier, after these extrudate samples were subjected to monomer extraction by hot water followed by drying at 110°C for 24 hours, only α crystalline peaks were observed for all the water-quenched and some air-cooled samples.

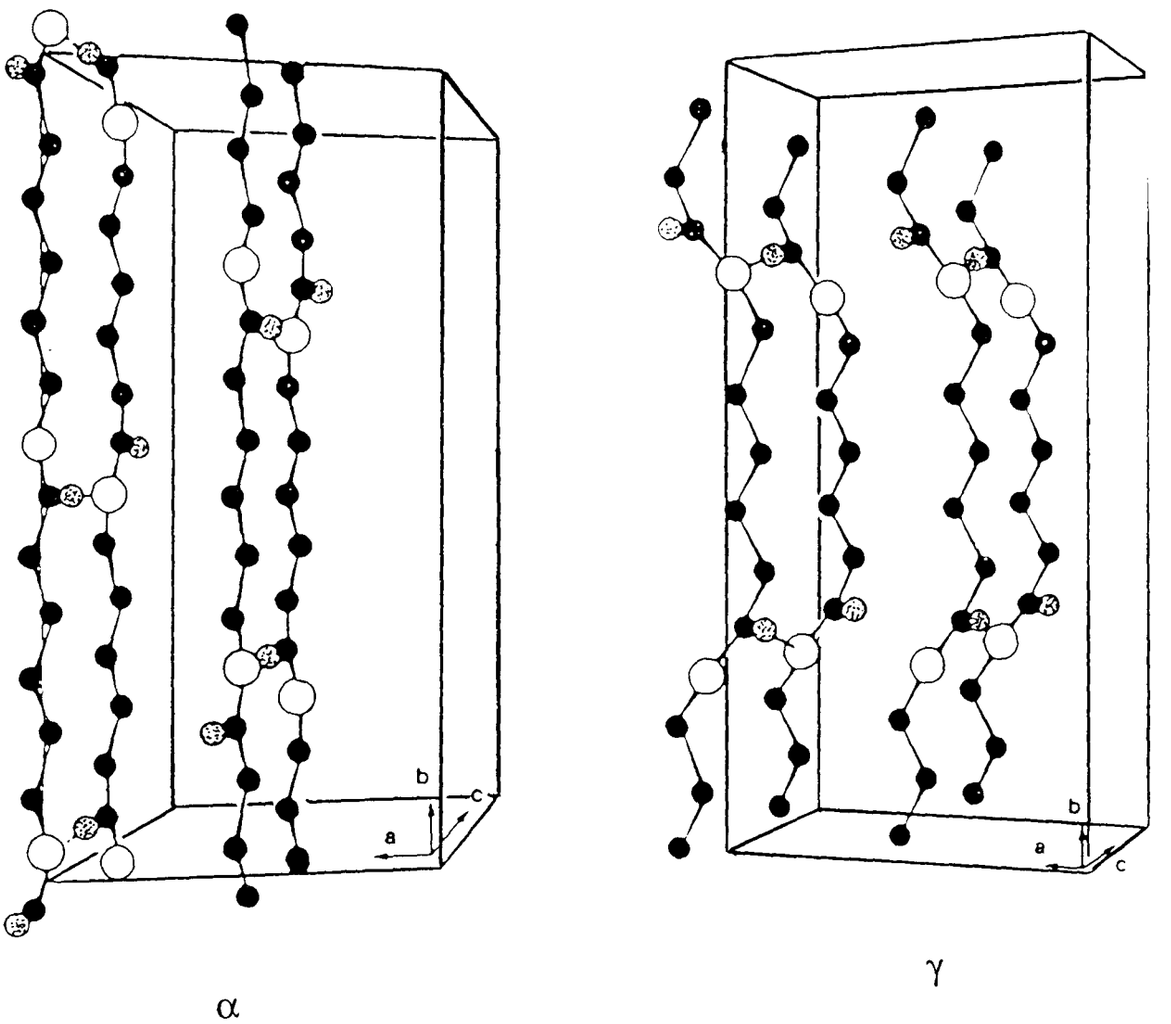

α γ

Figure 3.11 α, γ crystalline structures of polyamide 6

It appeared that the γ phase of the unextracted water-quenched sample has been transformed into the α phase during the extraction/drying process. The presence of caprolactam monomer could not be accounted for the formation of the γ phase since the WAXD profile obtained for the air-cooled but unextracted PA6 samples prepared at low rpm (other than 150 rpm) showed the presence of only α peaks. The conversion of the γ phase to the α phase during the extraction/drying process could be attributed to the breaking up of the hydrogen bonding within the γ phase structure to effect a molecular chain rearrangement to the thermally more stable α phase structure.

The additional γ peak of the 150 rpm, air-cooled sample as shown in Figure 3.10 (iii) suggested that a thermally stable γ peak was obtained under this high shear rate pcocessing condition as compared to others. Nevertheless, this apparently thermally more stable γ phase which "survived" during drying process at 110°C was eventually observed to transform into the α phase during the subsequent annealing treatment at 180°C for 90 minutes.

The WAXD equitorial profile of the commercial nucleated grade PA6 material in Figure 3.10 (vi) showed the characteristic α peaks indicating that the nucleating additives favoured the formation of the α crystalline phase [96].

3.3.4.2 *Differential Scanning Calorimetry*

Polymer melting and crystallisation temperatures as well as the heats of fusion and crystallisation are listed in Table 3.3. The data are representative of all the transition temperatures and heats for the different reactive polymerised PA6 samples prepared using extruder speeds of 50, 70, 90, 120 and 150 rpm since little variation in these values were observed as a function of extruder screw speeds. From the

Table 3.3 DSC thermal data of polyamide 6 variants

Sample*	T_{m1} (°C)	ΔH_{f1} ($J.g^{-1}$)	T_c (°C)	ΔH_c ($J.g^{-1}$)	T_{m2} (°C)	ΔH_{f2} ($J.g^{-1}$)
water-quenched	214.2	87.8	180.1	58.4	213.5	60.8
water-quenched (annealed)	214.9	84.9	179.5	63.0	213.0	64.5
air-cooled	216.2	75.6	181.2	61.2	215.0	62.3
air-cooled (annealed)	216.1	81.2	181.0	59.6	214.5	66.6
Capron +	221.0	65.3	192.0	65.3	214.0	65.3

* Reactive polymerised PA6 extruded at 150 rpm.

\+ Commercial PA6 made by hydrolytic polymerisation.

T_{m1}, T_{m2} Peak endothermic melting temperatures, stage I and II heating cycles.

T_c Peak exothermic crystallisation temperature in cooling cycle.

ΔH_{f1},ΔH_{f2} Heats of fusion, stage I and II heating cycles.

ΔH_c Heat of crystallisation, cooling cycle.

thermogram data it was observed that all the reactive polymerised samples yielded consistent Stage II peak melting temperatures of between 213°-215°C, which is comparable to that obtained for the hydrolytic polymerised commercial grade PA6. However, a noticeable difference in Stage I maximum peak melting temperatures of 5 - 6°C was recorded between the reactive and hydrolytic polymerised PA6 samples. This difference in Stage I melting temperatures is possibly attributed to the higher level of thermally more stable α crystallites in the nucleated commercial grade PA6 material [96].

The peak crystallisation temperatures (T_c) of the reactive polymerised PA6 samples were recorded in the region 180 ± 1°C. This observation infers that the crystallisation rate of these PA6 materials is rather independent of processing conditions such as screw speeds, rate of quenching and annealing treatment. The commercial grade sample has recorded a much higher T_c which can be again possibly attributed to faster rate of crystallisation due to the presence of nucleating agents.

Figure 3.12 shows DSC thermograms of the samples obtained in Stage I and II heating as well as the cooling cycles. During Stage I heating, the water-quenched samples exhibit broad melting peaks which can be attributed to the melting of the smaller, less perfectly formed crystals at lower temperatures [Figure 3.12 (i)]. After annealing these samples at 180°C for 90 minutes followed by slow cooling to room temperature at 23°C, a narrower melting peak with only a slight shoulder at the lower temperature slope was obtained [Figure 3.12 (ii)].

Similar but more obvious shoulder peaks were also observed for all the air-cooled samples except the one extruded at 150 rpm in the Stage I heating thermograms.

(i)

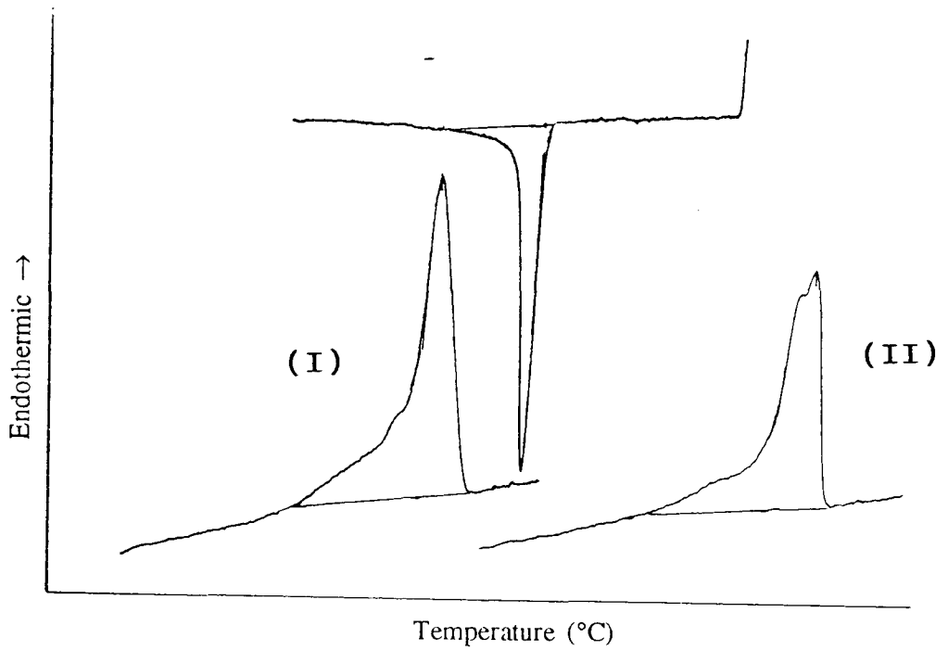

(ii)

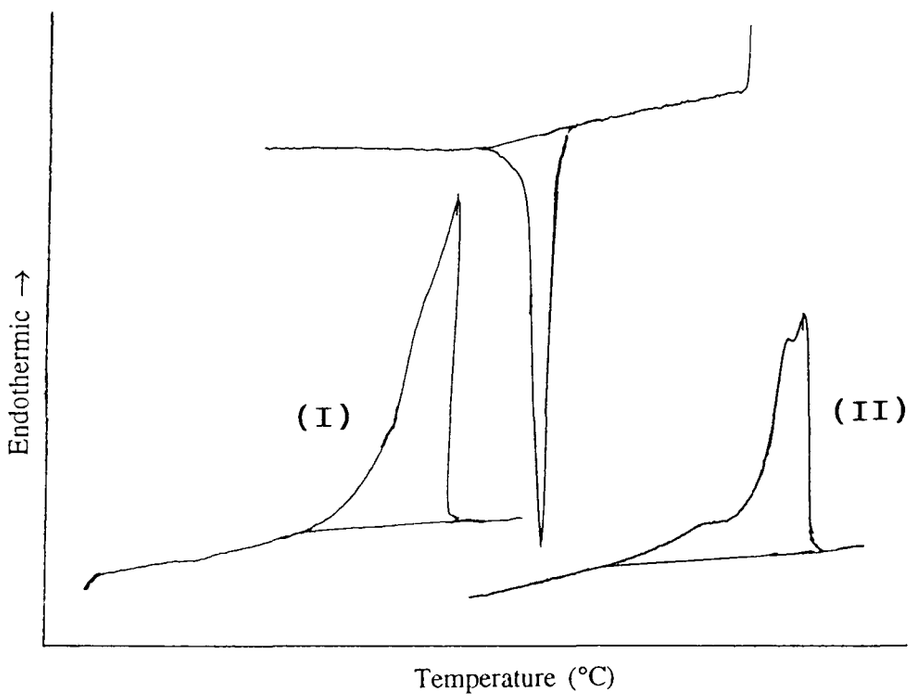

Figure 3.12 DSC thermograms of polyamide 6 variants

(i) reactive polymerised/water-quenched

(ii) reactive polymerised/water-quenched/annealed

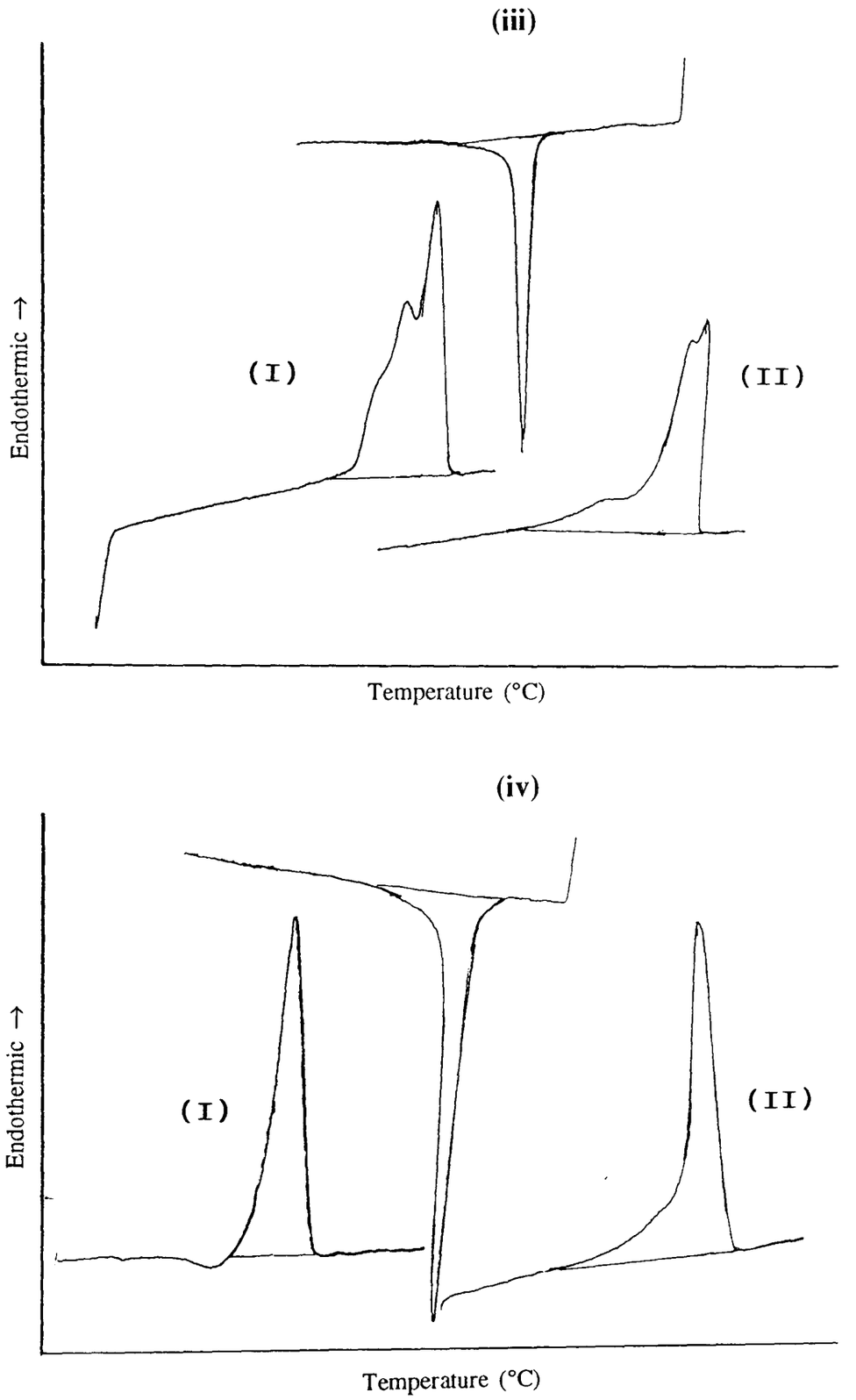

Figure 3.12 DSC thermograms of polyamide 6 variants (cont.) (iii) reactive polymerised/air-cooled (iv) hydrolytic polymerised/water-quenched (Capron)

Hinrichsen [153] studied the thermal properties of solution grown single crystals of PA66 and found that the double melting peaks appeared in the DSC thermograms of every sample he used. He attributed these double melting peaks to the melting, recrystallisation and remelting of the crystallites during DSC scanning. **Wunderlich** *et.al* [154] also reported that double endothermic melting peaks were observed for both melt-grown and solution-grown crystals of PA6 and attributed it again to reorganisation and/or recrystallisation of originally ill-crystallised polymer during the DSC heating.

According to studies on the thermal analysis of PA6 fibres, the double melting peaks of PA6 yarns are considered to be merely the combined result of three processes which occur successively during heating in the DSC apparatus, i.e perfection of the original crystals, partial melting and reorganisation, and finally, complete melting of the recrystallised crystals [101].

During Stage II heating, all reactive polymerised samples regardless of previous history showed rather identical DSC thermograms, with bimodal melting peaks due possibly to the reorganisation or recrystallisation followed by melting of the crystals along the DSC scanning process. This is an interesting observation since all these PA6 materials, irrespective of their thermal history were maintained in a complete molten state during the 15 minutes annealing period after the Stage I heating cycle, prior to the commencement of the cooling cycle. Based on this observation, it is reasonable to postulate that the more obvious double endothermic peaks as observed on the thermogram of the reactive polymerised air-cooled samples extruded at 150 rpm in Stage 1 heating could possibly be attributed to the reorganisation and melting of the imperfect α crystallites formed as a result of $\gamma \rightarrow \alpha$ crystalline phases transition during DSC scanning.

It is remarkable to note that only a single endothermic melting peak is observed for the commercial, nucleated PA6 material in both the heating stages [Figure 3.12 (iv)]. Based on the earlier discussion about the formation of bimodal endothermic melting peaks, it is possible to suggest that more perfect crystallites are formed in the CAPRON material as a result of the nucleating agents incorporated which therefore, only displayed a single melting endothermic peak on the thermogram in both the heating cycles.

Based on the heat of fusion for a 100% crystallinity PA6 material at 188 J g^{-1} [155], the reactive polymerised PA6 samples have recorded crystallinity levels of 32-35 % as compared to a higher crystallinity of 41 % for the commercial, hydrolytically polymerised material. No appreciable difference in crystallinity was recorded for the water-quenched and air-cooled samples upon annealing treatment at 180°C for 90 minutes.

3.3.4.3 *Fourier Transform Infrared Spectroscopy*

Figure 3.13 shows the Fourier transform infrared spectroscopy (FTIR) spectrum of the reactive polymerised PA6 prepared at extruder screw speeds of 50, 90 and 150 rpm (residual monomer extracted and dried at 110°C for 24 hr). For comparison study, the spectrum of the commercial hydrolytic polymerised PA6 material (CAPRON 8202C) is also presented.

Several studies in the literature have dealt with the assignment of characteristic infrared bands for PA6 [156-159]. A broad shoulder is observed in some PA6 samples in the region 3440-3560 cm^{-1} which is attributed to bound water in the amorphous phase. The intense band at 3302 cm^{-1} is assigned to the hydrogen-bonded

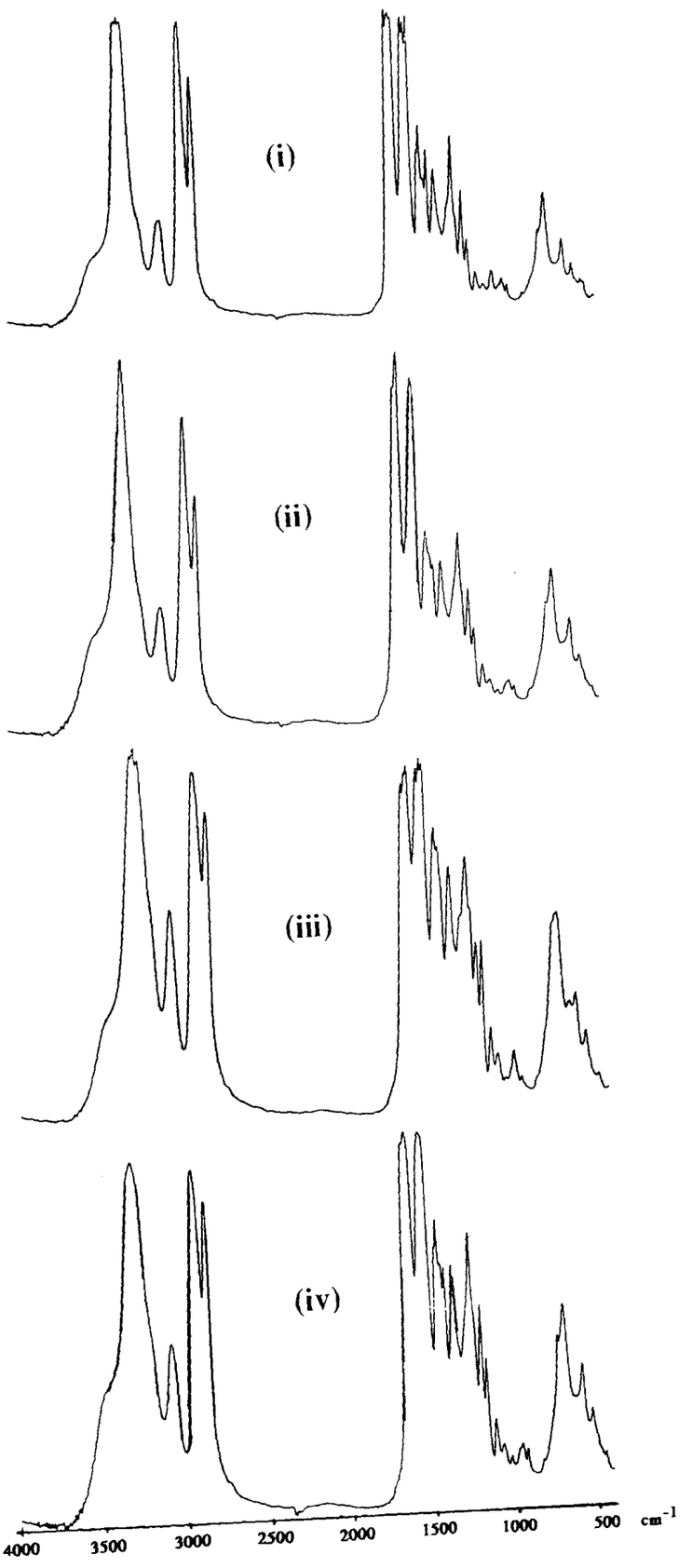

Figure 3.13 FTIR spectrum of polyamide 6 variants (i) Capron (ii) 50 rpm (iii) 90 rpm (iv) 150 rpm

NH band. The 2940 cm^{-1} and 2865 cm^{-1} bands are attributed to the CH_2 assymmetric and symmetric stretching respectively. The C=O amide I band in PA6 is observed at 1642 cm^{-1}, while the amide II band which involves coupling of NH deformation with CN stretching occurs at 1545 cm^{-1}. In addition, four CH_2 deformation bands are observed at 1480, 1465, 1436 and 1417 cm^{-1}.

No FTIR spectrum band in Figure 3.13 could be detected at 3440-3560 cm^{-1} region, indicating the absence of bound water in all the samples examined. An intense band was observed at 3301, 3300 and 3286 cm^{-1} for the 50, 150 and 90 rpm PA6 samples (Table 3.4). It is interesting to note that this shift of hydrogen bonded NH stretching band to lower frequency appears to follow the relative molecular mass of the samples in the ascending order. Commercial grade PA6 material, on the other hand, shows an intense absorption band at 3308 cm^{-1}.

The shift of the hydrogen bonded NH stretching bands to lower frequencies at 3301-3286 cm^{-1} for the reactive polymerised PA6 materials is evident of stronger hydrogen bonding attributed to the increase in molecular mass of the samples. Commercial Capron PA6 material has a relatively lower molecular mass [Section 3.3.2], hence, not surprisingly by similar arguments, the band occurs at a higher frequency of 3308 cm^{-1}. Similar shift in the absorption band of the NH group was also observed by **Ismat** [159] between PA6 and PA6/iodine complex samples.

The CH_2 assymmetric stretching bands occur at 2933, 2936 and 2944 cm^{-1} for the 50, 150 and 90 rpm reactive polymerised samples. In this case, shifting of the bands to higher frequencies was observed with increasing molecular masses of the samples. Similar absorption band for the commercial material occurs at 2940 cm^{-1}. The bands associated with CH_2 symmetric stretching were observed at 2865, 2865 and 2864 cm^{-1} respectively for the samples extruded at 50, 150 and 90 rpm while similar absorption band for commercial PA6 sample is at 2867 cm^{-1}.

Table 3.4 FTIR characteristic absorption bands of Polyamide 6 variants

Band assignment	50rpm	150rpm	90rpm	Capron+	Literature Reference
NH stretching H-bonded /cm^{-1}	3301 (vvs)	3300 (vvs)	3286 (vvs)	3308 (vs)	3302 [159]
CH_2 assymm. (aliphatic) /cm^{-1}	2933 (vs)	2936 (s)	2944 (vs)	2932 (vs)	2940 [157]
CH_2 symm. (aliphatic) /cm^{-1}	2865 (vs)	2865 (s)	2863 (vs)	2867 (vs)	2865 [157]
Amide I, C=O /cm^{-1}	1642 (vs)	1641 (vs)	1630 (vs)	1638 (vs)	1642 [157]
Amide II, NH /cm^{-1}	1548 (vvs)	1542 (vs)	1536 (vvs)	1550 (vs)	1545 [157]
CH_2 deformation /cm^{-1}	1473(s) 1461(s) 1438(s) 1418(s)	1475(m) 1462(m) 1439(m) 1418(m)	- 1461(vs) 1441(vs) -	1475(s) 1462(s) 1438(m) 1418(s)	1480[157] 1465 1438 1417

Band intensity classifications: >4 (vvs); >3 & <4 (vs); >2 & <3 (s); >1 & <2 (m); <1 (w).

+ Commercial PA6 made by hydrolytic polymerisation.

The C=O amide I band for the reactive polymerised PA6 samples are observed at 1642, 1641 and 1630 cm^{-1} while that recorded for Capron sample is at 1638 cm^{-1}. In addition, the amide II bands occur at 1548, 1542 and 1536 cm^{-1} respectively for the 50,150 and 90 rpm samples while the Capron material has the similar absorption at 1550 cm^{-1}. Here again, substantial shifts of absoption bands to lower frequencies were observed especially for the 90 rpm sample which has the highest molecular mass among all the samples included in this study. These results again infer that stronger hydrogen bonding in the 90 rpm sample could possibly accounted for the band shift.

As for the CH_2 deformation bands, four absorptions are recorded for the 50 rpm sample at 1473, 1461, 1438 and 1418 cm^{-1}. Similar CH_2 bands observed for the 150 rpm sample are at 1475, 1462, 1439 and 1418 cm^{-1}. However, only two CH_2 bands at 1461 and 1441 cm^{-1} are observed for the 90 rpm material. Four bands are also observed for the Capron sample at 1475, 1462, 1438 and 1418 cm^{-1}.

A possible explaination for the observation of only two absorption bands in the FTIR spectra of the 90 rpm sample at the CH_2 deformation absorption positions, as compared to four well defined bands recorded for the other samples, is again ascribed to the hydrogen bonding effect as a result of the extraordinary molecular mass associated with this sample. It is likely that molecules in the 90 rpm sample have to assume a more prominent zig-zag type chain contraction conformation which could resulted in "bridges" being formed between the carbonyl group and the amide group in the neighbouring distort sheet. These bridges have the tendency to discrupt hydrogen bonding and possibly accounted for the disappearance of some CH_2 deformation bands. Similar assumptions on zig-zag type chain contraction of molecules was also made by **Matsubara** *et. al* [160] in order to accommodate the large I_3^- ion present in the PA6 iodine complex. The workers also reported only two CH_2 defomation bands at 1463 and 1440 cm^{-1}.

3.3.4.4 *Microscopic Analysis*

Optical photomicrographs of the as-processed water-quenched and air-cooled samples (with monomer residue) prepared from different extruder screw speeds are shown in Figures 3.14 and 3.15 respectively. Poorly defined spherulitic structures are visible for all the samples which appeared to have little variation in diameters with respect to extruder speeds used in the polymerisation process for both the water-quenched and air-cooled materials. However, on comparison of the spherulitic morphology prepared at various melt cooling rates show that the spherulitic diameters of the air-cooled samples seem to be larger than that of the water-quenched samples. These observations are in accordance with the two structural forms of PA6 i.e. α and γ crystalline phases which are preferentially formed under slow and fast cooling conditions respectively. Also, α spherulites are known to exist in large coalesced polyhedral spherulites embedded in a seemingly amorphous matrix as a result of reduced chain mobility due to restriction in the crystallisation process. On the other hand, the spherulitic morphology of the commercial grade Capron PA6 exhibits fine spherulites which has much smaller diameters as compared to the reactive polymerised PA6 samples [Figure 3.16]. This spherulitic morphology has been attributed to the presence of the nucleating agents which could effect heterogeneous nucleation of the Capron spherulites [96].

Generally, PA6 morphology is well known to have high nucleation density followed by rapid radial growth of small spherulites leading to a random mosaic morphology. **Bessell** *et al.* [161] studied the effect of catalyst and initiator concentrations, and hence induction times, on the crystalline morphology of the resulting PA6. The workers concluded that there is little variation of spherulitic diameter with concentration. However, they reported that a large difference in the spherulite size was observed as a result of varying the polymerisation temperature.

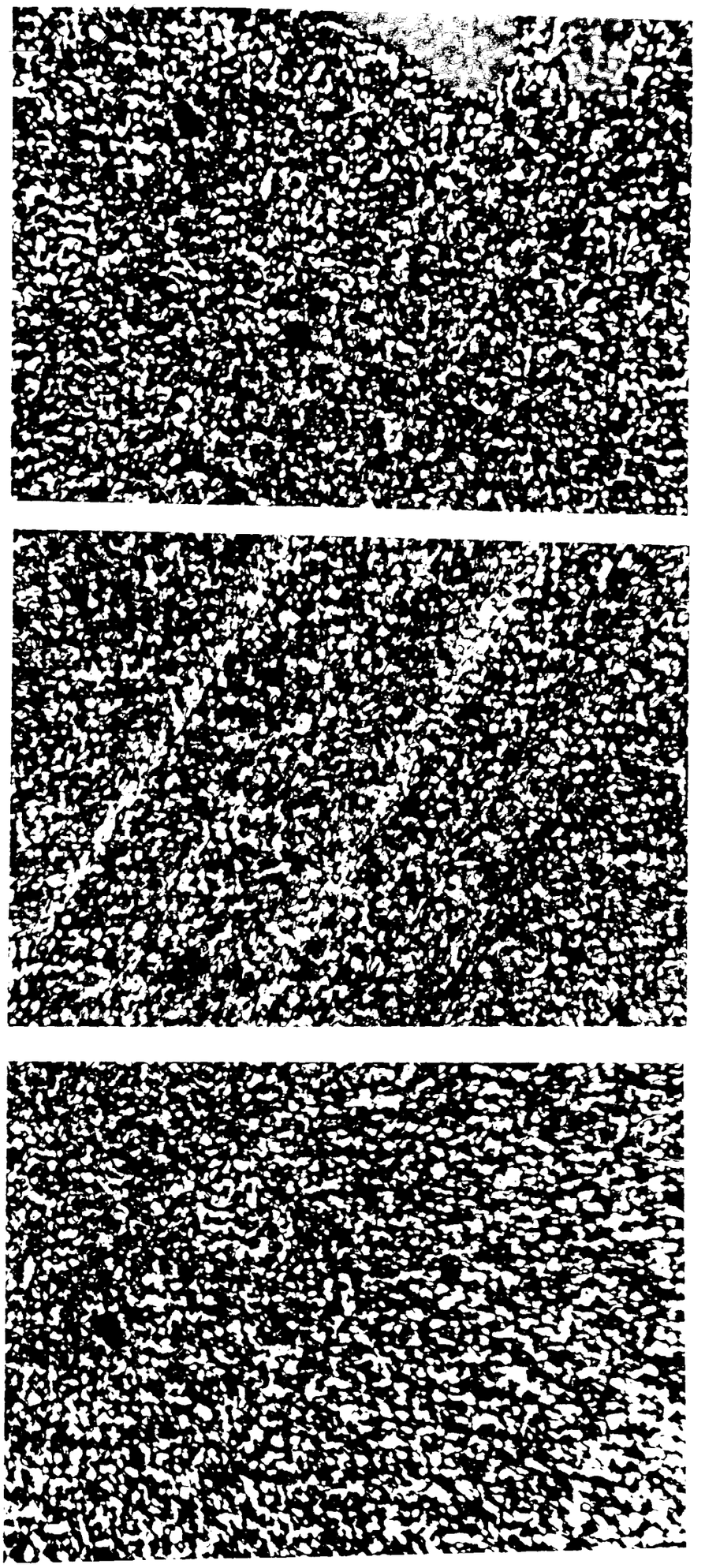

Figure 3.14 Optical micrograph of reactive polymerised PA6 (water-quenched)(i) 50 rpm, (ii) 90 rpm, (iii) 150 rpm

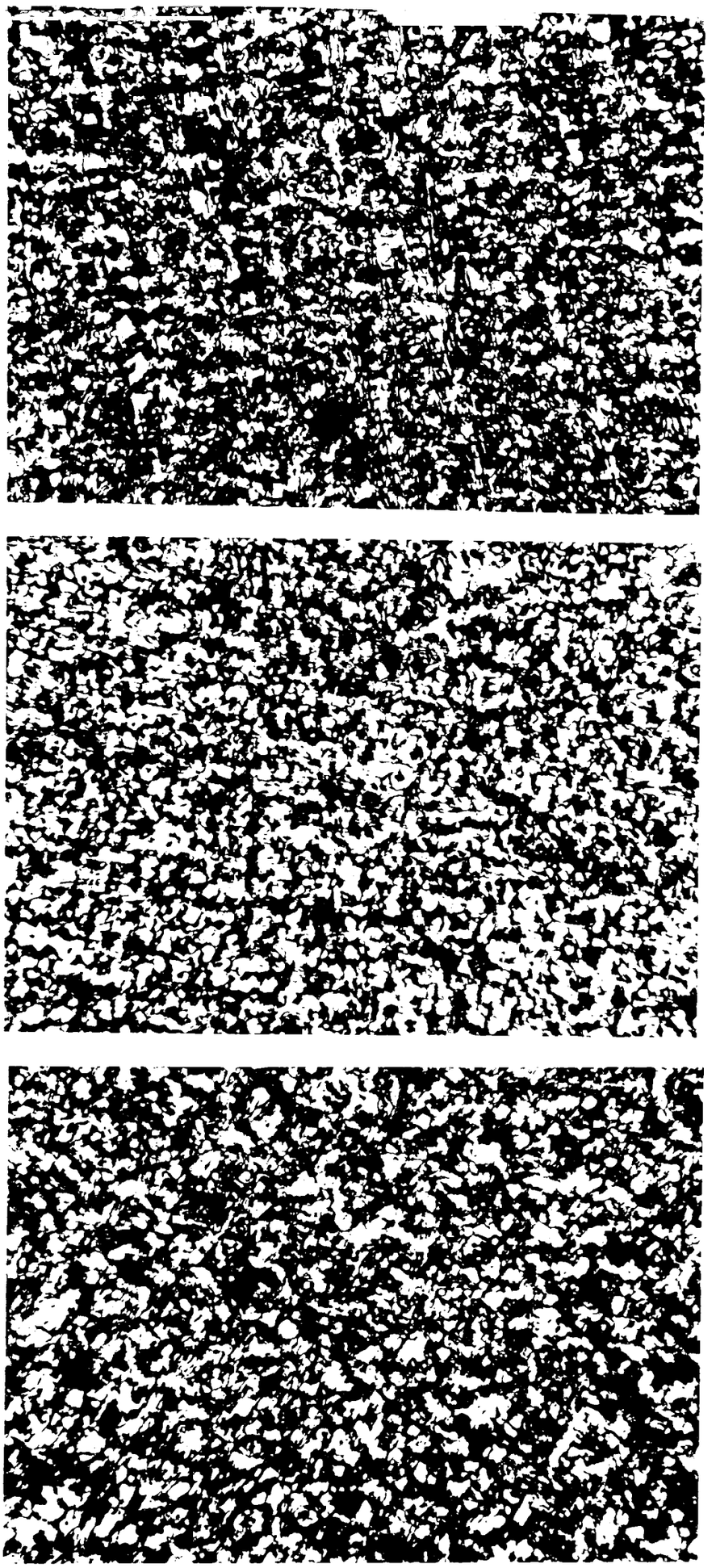

Figure 3.15 Optical micrograph of reactive polymerised PA6 (air-cooled)(i) 50 rpm (ii) 90 rpm (iii) 150 rpm

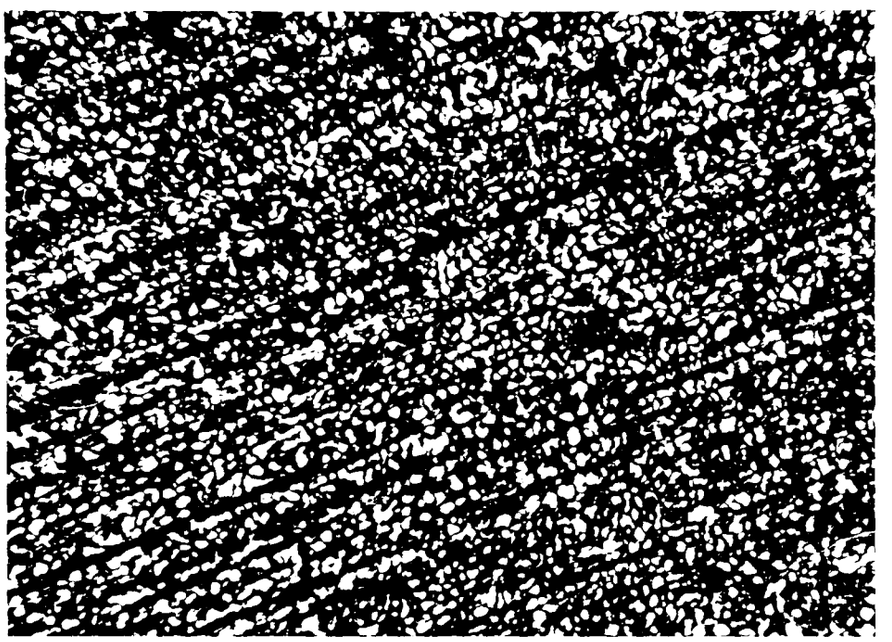

Figure 3.16 Optical micrograph of hydrolytic polymerised PA6 (Capron)

The electron micrograph obtained from transmission electron microscopy (TEM) of the reactive polymerised PA6 prepared by water-quenching is shown in Figure 3.17. A general sheaf-like appearance of a spherulite was observed. Selective staining by phosphotungstic acid (PTA) causes the non-crystalline regions to show a dark contrast, whereas the interior of the crystalline lamellae appears as bright ribbons. Starting from the spherulitic centre (A), the lamellae may be clearly followed up to the spherulite boundary (B) in a diametrical section. The sheaf-like growth seems to arise from progressive branching and spraying apart of the lamellae during growth, connected with segregation processes as well as with the nucleation and growth of subsidiary lamellae in the gaps between the dorminant growing lamellae [162-165]. TEM electron micrograph of the commercial Capron PA6 material prepared under similar experimental conditions also showed similar sheaf-like lamellae structures (Figure 3.18). Electron micrograph of the reactive polymerised PA6 sample obtained from slow cooling in air (Figure 3.19) shows no significant difference in the structure of the lamellae from that of the water-quenched sample.

On the other hand, a better defined lamellar structure (A) was observed for the water-quenched sample which has undergone annealing treatment at 180°C for 90 minutes (Figure 3.20). Here, it is seen that the lamellae are much longer and more distinguisable as compared to those observed for both the air-cooled and water-quenched samples especially in the direction along the spherulite radius. Once originated, the lamella appears to follow the radius of the spherulite until impingement occurs with another spherulite. These observations agreed well with the findings of **Matyi** *et al.* [166] who reported a noticeable increase of the lamellae dimension with annealing at about 140°C but most pronounced changes were recorded with annealing temperature at 170°C.

Scanning electron micrographs of the cryogenically fractured surfaces of the reactive polymerised and Capron PA6 materials are shown in Figure 3.21. A homogeneous

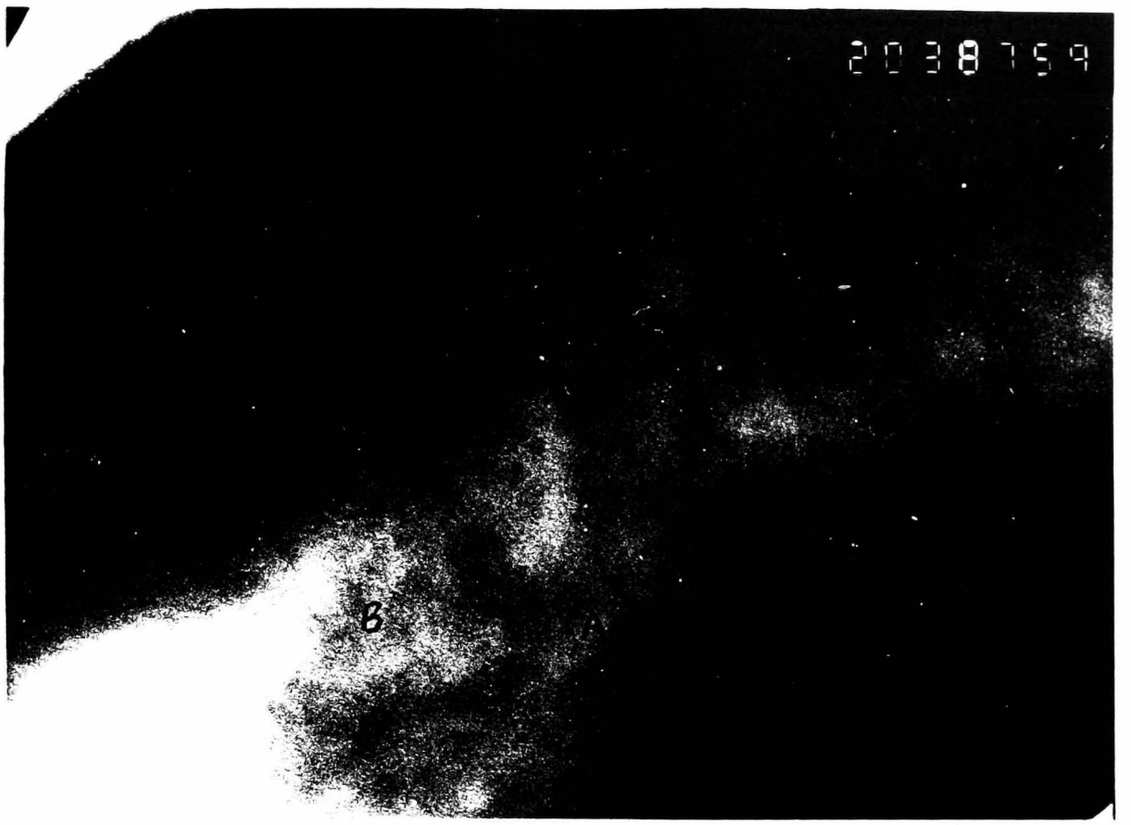

Figure 3.17 TEM micrograph of reactive polymerised PA6 (water-quenched)

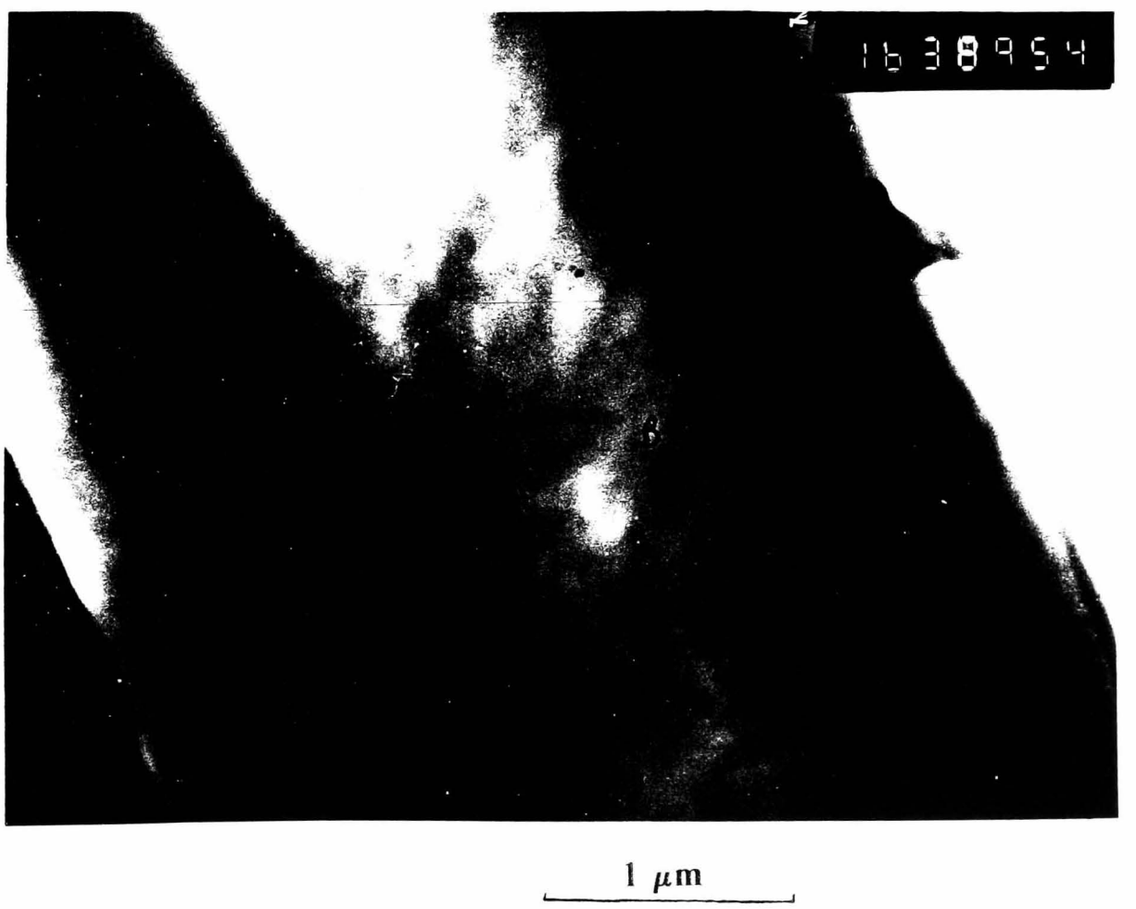

Figure 3.18 TEM micrograph of commercial grade PA6 (Capron)

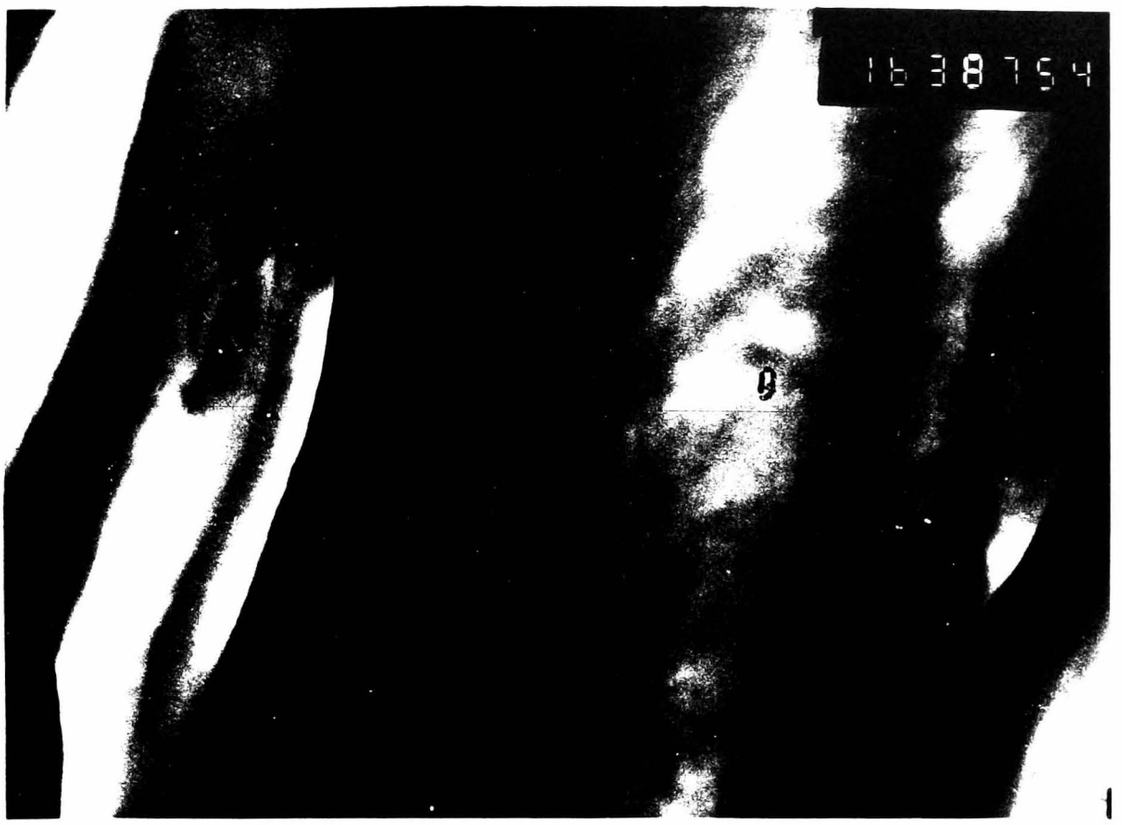

Figure 3.19 TEM micrograph of reactive polymerised PA6 (air-cooled)

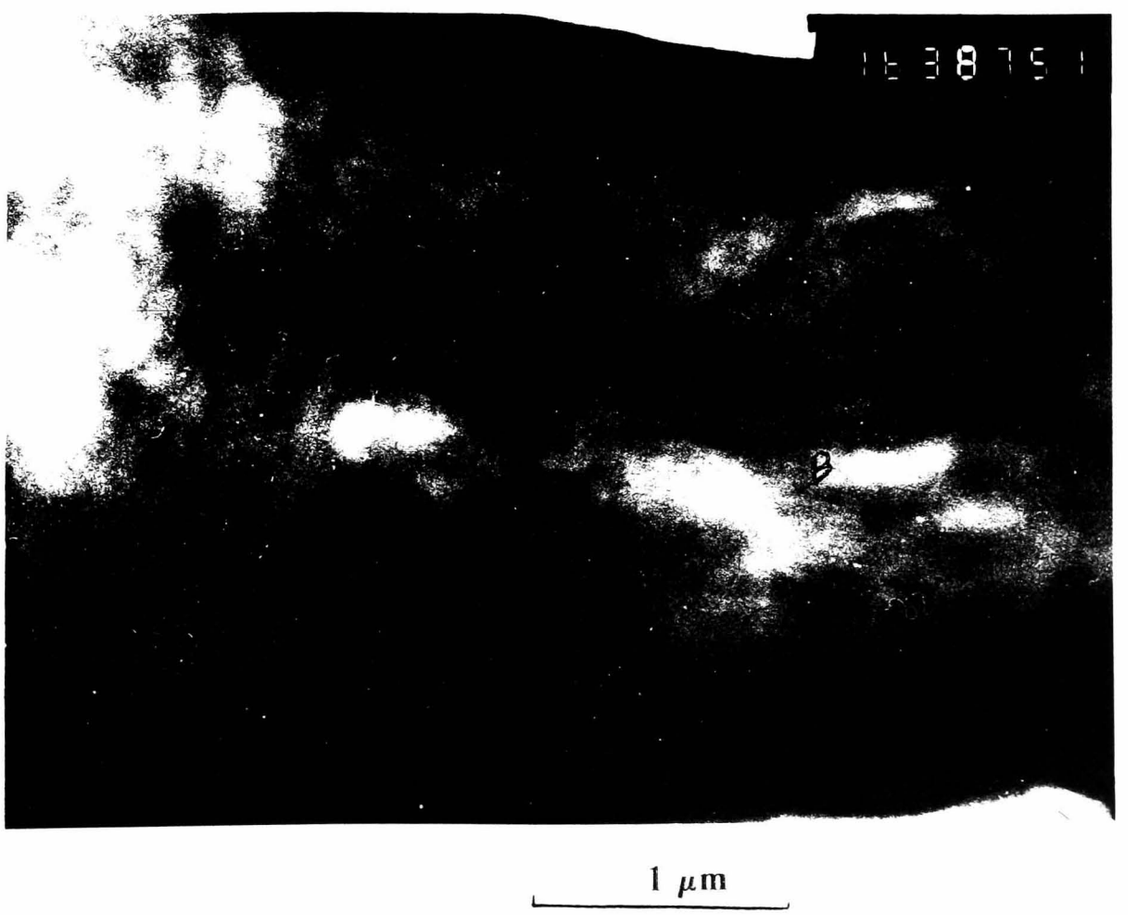

Figure 3.20 TEM micrograph of reactive polymerised PA6 (annealed)

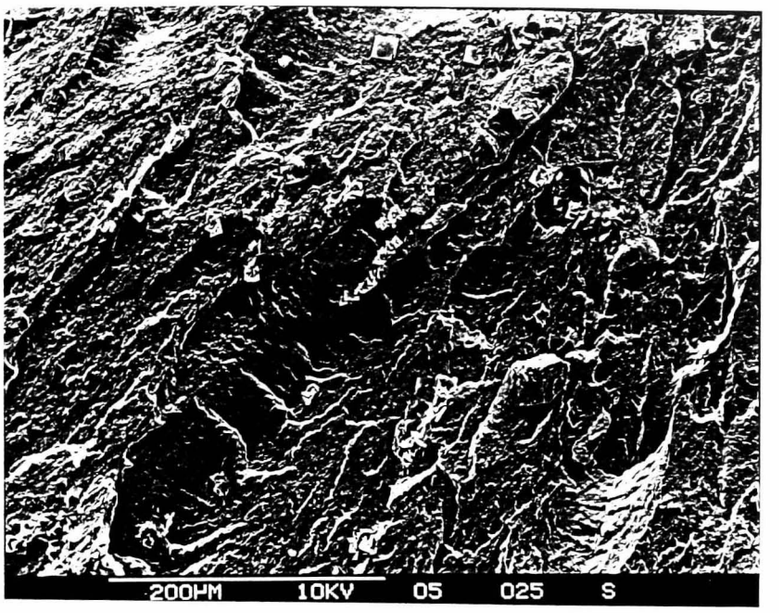

(i) reactive polymerised PA6

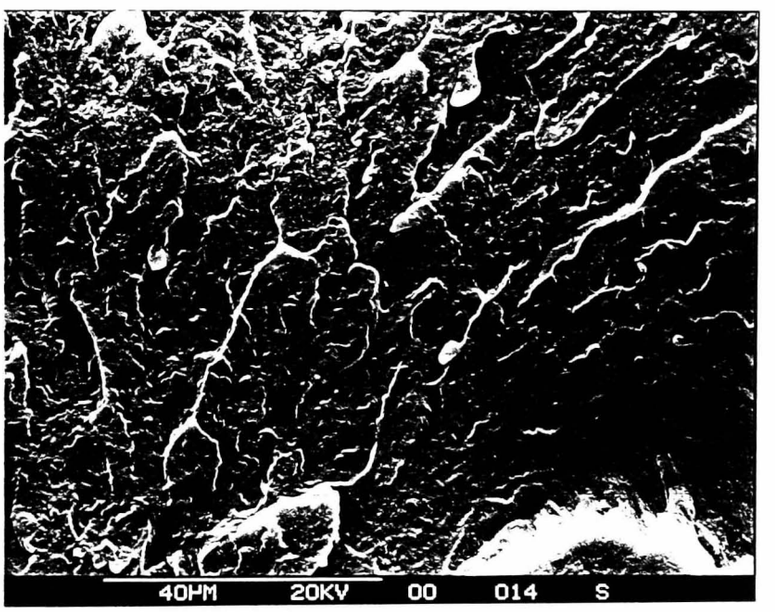

(ii) hydrolytic polymerised PA6 (Capron)

Figure 3.21 SEM micrograph of PA6 variants

morphology is observed in both cases showing characteristics of a brittle fractured mechanism.

3.3.5 Physical Properties

3.3.5.1 Mechanical

A tensile stress-strain curve typical of a PA6 semi-crystalline material is illustrated in Figure 3.22. Generally, stress-strain properties can give an indication of the strength and toughness of a polymeric material. In all cases at the strain rate of 50 mm min^{-1}, ductile rupture behaviour was observed for all the PA6 samples tested, with a well-defined yield point and the crack tip plastic zone extending across the width of the test piece followed by necking. Stress-whitening dominated the necking region in all the samples tested, indicative of submicrometer void formation during yielding.

Mechanical properties of the PA6 variants are summarised in Table 3.5 . The sample obtained at 90 rpm with the highest molecular mass recorded the highest tensile modulus amongst the reactive polymerised PA6 materials prepared. However, this tensile modulus is still lower than that observed for the commercial grade, nucleated Capron sample, indicating that this material has lower stiffness property as compared to the hydrolytic polymerised PA6. This 90 rpm PA6 sample also yield the highest tensile strength amongst the reactive polymerised PA6 series, but is still about 15% lower with respect to the reference commercial sample synthesised by hydrolytic polymerisation. Samples obtained from the lowest and highest screw speeds i.e. at 50 and 150 rpm were observed to yield the lowest tensile strength in relation to their lower molecular mass. Lower level of crystallinity has been recorded for all the reactive polymerised PA6 ($\approx$32% in Section 3.3.4.2) as compared to commercial

Table 3.5 Mechanical properties of polyamide 6 variants

Sample *	Young's Modulus (GPa)	Stress @ yield σ_y (MPa)	Elongation @ Break (%)	Impact Strength ($J.m^{-1}$)	Flexural Modulus (GPa)
50 rpm	2.41	56.2	90.1	82.4	2.53
70 rpm	2.72	68.1	77.3	77.1	2.81
90 rpm	2.74	69.0	75.8	69.4	2.87
120 rpm	2.46	60.2	80.0	80.6	2.49
150 rpm	2.68	66.4	88.7	93.8	2.72
CAPRON +	2.84	76.4	12.2	60.1	3.12

Note: All the samples were tested in "dry as-moulded" condition @ 23°C.

* Reactive polymerised PA6 extruded at different screw speeds.
\+ Commercial PA6 made by hydrolytic polymerisation.

material at 41%, which could probably accounted for the lower tensile strength obtained. The reference commercial PA6 is a nucleated material claimed to yield mainly α crystallites with higher tensile strength [96].

As for the elongation at break ϵ_B properties of the PA6 variants shown in Table 3.5, all reactive PA6 samples recorded higher ϵ_B values with respect to the commercial material. Among the reactive PA6, samples obtained at the lowest and highest screw speeds yield the highest values while the sample prepared at 90 rpm recorded the lowest ϵ_B values.

From the results, it is interesting to observe that in the case of the reactive polymerised PA6 samples, the tensile properties appear to depend on the number average molecular weights whereas the ϵ_B values are inversely proportional to the molecular weight distribution of the samples (Table 3.2). Caprolactam monomer cannot be accounted for the tensile and elongation properties of the reactive polymerised PA6 samples since all the residual monomers have presumably be extracted by hot water prior to the preparation of test specimens.

Increase in molecular mass will lead to an increase in the number of intercrystalline tie chains that run longitudinally in each microfibril and laterally between microfibrils when stretched as in a tensile test. The tie chains are capable to restrain the microfibrils from slipping with respect to each other, thus increasing the tensile strength [167]. This mechanism may probably explained the higher tensile strength properties of the 90 and 70 rpm samples with respect to other reactive PA6 materials since they have recorded the highest molecular mass amongst the series.

On the other hand, it is possible that for these high molecular mass materials, chain entanglement has increased to a point where chain straightening to release imposing stresses is substantially inhibited prior to break, which therefore contributing to the

lower elongation at break properties as compared to the lower masses reactive PA6 counterparts. In addition to increasing chain entanglement, intermolecular forces becomes significant especially with polar polymers such as PA6. For low molecular mass polymers, the intermolecular forces between small molecules are weak in comparison to the primary valence forces. Therefore, chain slippage becomes the primary factor affecting elongation. However, for the high molecular mass materials, it may be easier to break primary valence bonds (chain scission) than to overcome the chain entanglement with significant intermolecular forces. This mechanism can effectively contribute to an overall reduction in ultimate elongation which probably explained the higher elongation at break properties attained by the 50 and 150 rpm reactive PA6 samples with lower molecular mass.

As for the flexural modulus properties, the reactive PA6 samples recorded a similar trend as that obtained for the tensile properties. Samples extruded at 90 and 70 rpm recorded the highest modulus but still some 20% lower than that obtained from the commercial grade material. Here, the higher crystallinity of the commercial grade material may again be ascribed to the more superior stiffness properties.

On the other hand, the Izod impact strength of notched reactive PA6 samples were observed to be much more superior as compared to the commercial material. The higher crystallinity of the commercial material may probably account for its lower impact strength [167]. The lower molecular mass and molecular weight distribution of the 50 and 150 rpm samples may possibly be accounted for their superior toughness properties in the reactive polymerised series. Also, it is possible that the factors which have been discussed earlier causing the decrease in elongation properties with increasing molecular mass with higher intermolecular forces and chain entanglements, can have an important effect on the impact behaviour. This is so, since the total energy required to fracture by impact is a function of the ability of the polymer to elongate [167].

Extensive studies of the mechanical relaxation of polyamides have been conducted in the past few decades for which good review articles are available [168, 169]. Essentially, there are three relaxation processes in the temperature range -160° to 200°C, namely the α, ß and γ transitions occurring at around 60°C, -70°C and -120°C respectively, at a frequency of 1 Hz [170].

The α relaxation is attributed to the movement of large chain segments resulting from the disappearance of hydrogen bonding with increasing temperature in the amorphous region [171]. This transition is considered by many researchers to be the glass transition temperature (T_g) of a polyamide. The ß relaxation has been linked with the crank shaft-type motion involving an unbonded amide group and several methylene carbon groups [172]. The γ transition is a consequence of cooperative motion of the methylene groups between amide linkages [173].

The elastic storage modulus (E') and loss factor (tan δ) data at an experimental frequency of 1 Hz for three reactive polymerised PA6 samples prepared at screw speeds of 50, 90 and 150 rpm as function of temperature are shown in Figure 3.23. Experimental results for Capron material obtained under similar test conditions are also included for comparative studies.

Both the E' and tan δ curves show that there are two defined mechanical relaxations in the testing temperature range between -100°C and 130°C corresponding to the α and ß transitions of PA6 respectively. The loss peak attributable to the γ transition is not observed since it is below the temperature range of the instrument used.

Figure 3.23 shows that the tan δ peak for the glass transition region tends to be higher and narrower for the reactive extruded PA6 samples prepared at 90 and 70 rpm compared to that extruded at 150 rpm. This result can be attributed to the

increased level of hydrogen bonding associated with the 90 and 70 rpm samples which recorded the highest molecular mass.

On the other hand, it is interesting to note that the commercial PA6 sample prepared by hydrolytic polymerisation has recorded a T_g at 60°C which is some 10°C higher than those obtained for the reactive PA6 series. This enhanced T_g is probably attributed to the lower moisture content as well as higher crystallinity of the commercial sample in accordance with the findings of **Rong** *et al.* [174] .

The variation of E' as a function of temperature for the reactive PA6 samples show a gradual decrease of elastic modulus with temperature at the region just below the glass transition range of 50-52°C. On the other hand, the E' value of the hydrolytic polymerised PA6 exhibits a much sharper fall at its glass transition region. This great loss of E' modulus at transition temperature region has been reported with many heterogeneous crystalline polymers [96].

Thermal mechanical loss curves of E' and tan δ for the reactive polymerised PA6 extruded at 150 rpm under different processing conditions are presented in Figure 3.24.

Consider first the results obtained from the as-processed sample which has not gone through the hot water extraction process and still has monomer residue content of some 6% [Figure 3.24 (×)]. The observed loss spectrum showed a prominant α and ß relaxation processes at transition temperatures of 26°C and -73°C respectively. This result illustrates the great influence of the presence of monomer residue on the T_g of PA6 since a shift of about 25°C was recorded as compared to the same PA6 material which has been extracted of its residue monomers [Figure 3.24 (▲)]. The effect of monomer content on the relaxation processes of PA6 has been reported by **Garbuglio** *et al.* [175]. It was concluded that the monomer has the same

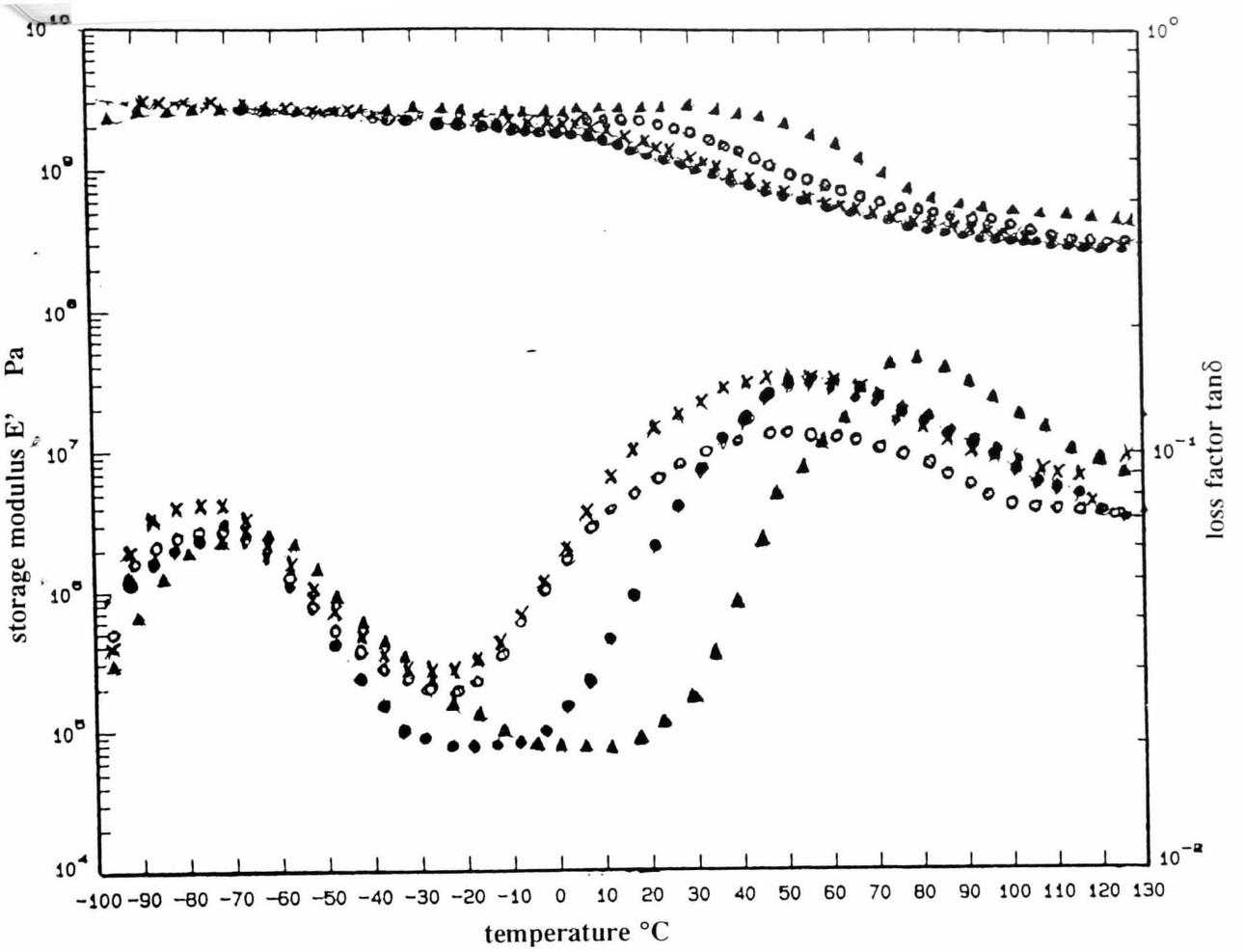

Figure 3.23 Dynamic mechanical spectrum of PA6 variants
(●) 50 rpm (×) 90 rpm (○) 150 rpm (▲) Capron

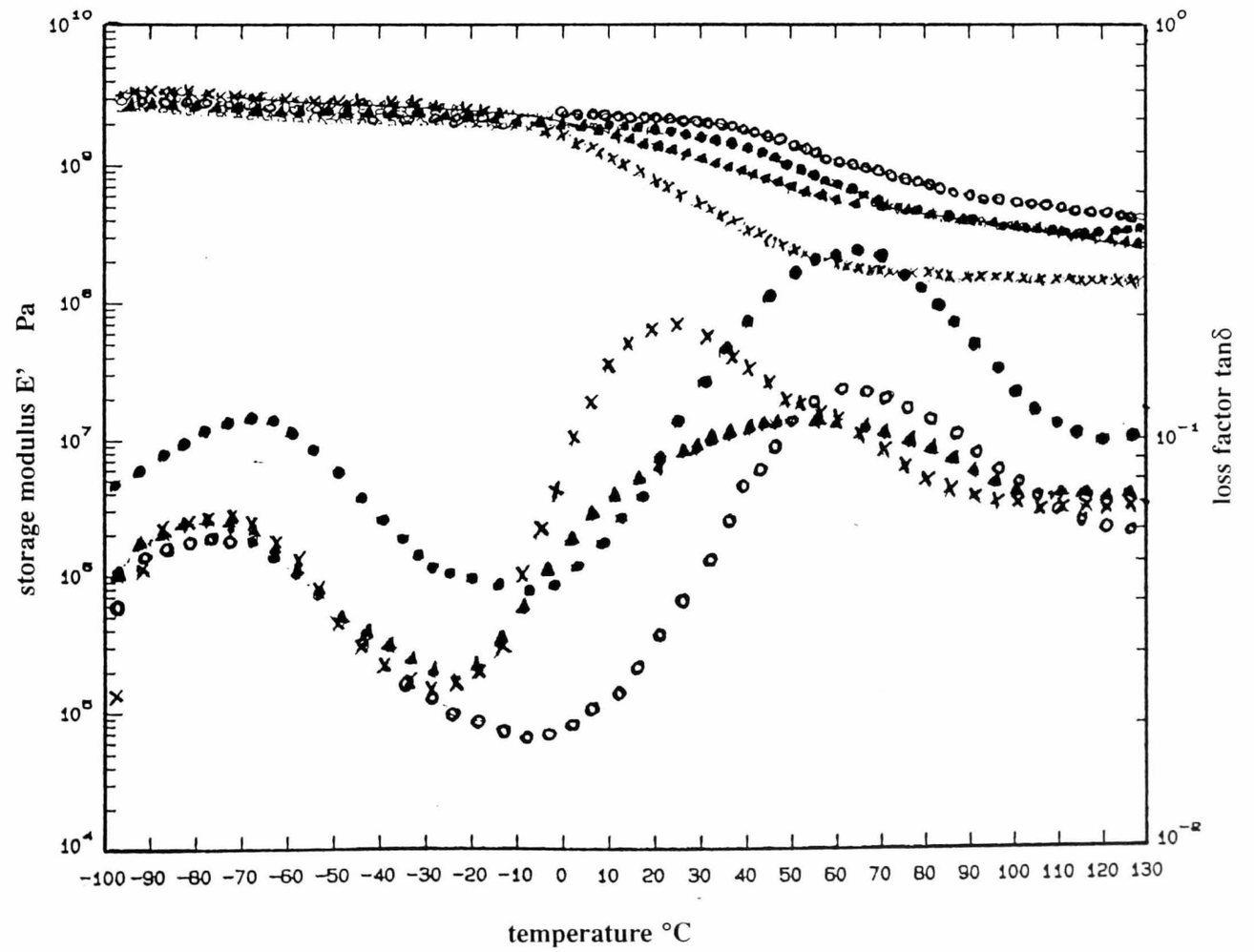

Figure 3.24 Dynamic mechanical spectrum of reactive polymerised PA6 variants prepared under different processing conditions
(✗) water-quenched with monomer residue (▲) water-quenched/monomer extracted
(●) air-cooled (○) water-quenched/monomer extracted/annealed

plasticising effect as water and resulted in shifting of T_g to a 20°- 30°C lower temperature region.

The ß transition of the as-processed (monomer non-extracted) sample was observed to yield the same T_B at -75°C as well as similar peak intensity and structure as that obtained for the extracted PA6. These results suggested that monomer residues apparently has no appreciable influence on the ß transitions of PA6.

On the other hand, the elastic loss modulus E' spectrum show that the as-processed PA6 sample recorded the highest E' intensity at the low temperature ß transition region. However, this modulus intensity was observed to decrease substantially in the higher temperature region of the α transition. This observed increase in low temperature modulus with high monomer residue may attributed to improved chain packing upon disruption of some intermolecular bonds. This is in accord with the findings of **Kotlik** *et al.* [176] who reported that the ß process arises from localised reorientation motions of chain segments involving non-chain bonded, or weakly bonded amide groups. With enhanced levels of diluent such as monomers, increased number of such amide groups are present which may cause a rise in the E' intensity. On the other hand, the abrupt decrease of the elastic modulus at the α transition is mainly attributed to the presence of the monomers which can cause the breakage of intermolecular hydrogen bonds between neighbouring chains and thereby plasticising the polymer by an increase in chain mobility.

The effect of melt cooling rate on the dynamic mechanical spectra of the reactive polymerised PA6 sample is illustrated in Figure 3.24 (•). It is observed for the air-cooled sample, the intensities of both the α and γ transition peaks are higher and more defined as compared to other samples. The T_g of this air-cooled sample is recorded at 59.5°C which is some 10°C higher than that obtained for the water-quenched sample. The ß peak position, however, was observed to be similar to the

other samples. The more highly ordered PA6 structure obtained by slow rate of melt cooling require higher temperature to initiate the molecular dissociation at the glass transition region which probably explain the shift of T_g to a higher temperature. These results implies that ordered regions, in addition to the amorphous domains, can contribute substantially to the molecular relaxation process of the α transition.

The loss factor curve (tan δ) shown in Figure 3.24 (•) for the water-quenched and annealed sample exhibit two fairly sharp relaxation peaks at 60.5°C and - 68°C, corresponding to the α and ß transitions respectively. The data showed a much higher peak intensities with respect to those obtained from either air-cooled or water-quenched samples.

It is commonly accepted that thermal annealing at temperature above 170°C induces a polymorphic transformation from the γ to the α crystalline phase of PA6 [176]. Also, it is known that the effect of annealing not only serve to enhance the degree of hydrogen bonding structures and produce restraints in the PA6 amorphous regions by forming small nuclei, but it can also increase the degree of phase separation as well as to relax the thermal stresses in the material [177].

The mechanism widely accepted for the PA6 α transition is the rupture of hydrogen bonds between the polyamide chains which are formed between the amide C=O groups in one chain and the amide N-H groups in the neighbouring chains. At the α transition, molecular thermal motions can possibly force the dissociation of this interchain hydrogen bonding structure which will correspond microscopically to an appearance of a loss peak at this temperature. Therefore, the more highly ordered structure of the PA6 obtained by annealing treatment will require higher temperature and relaxation energy in order to initiate the molecular dissociation. This mechanism could therefore, probably accounted for the shift of T_g to a higher

temperature as well as the increase in peak height for the α transition of the annealed PA6 material.

In fact, the shift of the α transition for the air-cooled and annealed samples of reactive polymerised PA6 suggests that the ordered regions of semi-crystalline polymers, in addition to the amorphous domains, contribute significantly to the α and γ molecular relaxation processes. This intepretation is substantiated by the observed increase relaxation peaks of the α and γ peaks with annealing.

3.3.5.2 *Melt Flow Index and Moisture Content*

The melt flow indices (MFI) and moisture content of the reactive polymerised and commercial grade PA6 materials are summarised in Table 3.6. MFI is a measure of the fluidity of the molten polymers and is inversely proportional to the polymer molecular mass M_w. The highest and lowest MFI recorded is 7.3 g.10 min^{-1} and 1.5 g min^{-1} for the reactive PA6 material extruded at 50 rpm and 90 rpm respectively. On the other hand, the Capron PA6 has recorded a much higher MFI of 30.4 g.10 min^{-1} indicating that it is less viscous material as compared to the reactive polymerised samples due to its lower molecular mass.

The moisture content of the reactive polymerised PA6 was observed to be slightly higher than that determined from the commercial sample. Reactive polymerised materials with the highest and lowest molecular weights recorded the highest levels of moisture content (1.8%).

Absortion of water in polyamides has been described as a physiochemical process. First, water is absorbed on the surface and when the surface layer is saturated with moisture, absorbed water will start diffusing inside the body. It was found from

Table 3.6 Melt flow index and moisture content of PA6 variants

Sample*	Melt Flow Index (g.10 min.$^{-1}$)	Moisture Content (%)
50 rpm	7.3	1.74
70 rpm	2.3	1.79
90 rpm	1.5	1.82
120 rpm	3.2	1.71
150 rpm	3.9	1.73
CAPRON+	30.4	1.61

* Reactive polymerised PA6 extruded at various screw speeds.

\+ Commercial grade PA6 made by hydrolytic polymerisation.

infrared spectroscopy, X-ray and density studies that moisture diffuses mainly in the amorphous regions rather than into the crystalline regions [178, 179]. Thus, the higher crystallinity of Capron could possibly accounted for its lower moisture content as compared to the reactive polymerised materials.

CHAPTER 4

REACTIVE POLYMERISED POLYAMIDE 6 / EPR BLEND MADE BY REACTIVE EXTRUSION

4.1 Introduction

In this work, a novel process is reported for in-situ reactive blending of 10% by weight of a commercial ethylene propylene copolymer (EPR) elastomer with polyamide 6 prepared by activated anionic polymerisation of ϵ-caprolactam on a fully intermeshing, co-rotating twin-screw extruder. Microstructure and mechanical properties of the elastomer modified reactive polymerised PA6 blend are analysed with respect to extrusion processing variables.

4.2 Experimental

4.2.1 *Materials and Blend Preparation*

ϵ-caprolactam, catalyst and activator used for the preparation of polyamide 6 (PA6) are described in Section 3.2.1.

Ethylene-propylene rubber (EPR) block copolymer was obtained from Exxon Chemicals Corp. [VISTALON, Grade EXXELOR PE 805 with 75% ethylene by weight, $\underset{\sim}{MR} = 5.1$ (10 kg, 230°C)]. This was supplied in pellet form.

For PA6/EPR blend synthesis, batches of 500 gm of the solid feedstock materials were weighed, comprising 90% by weight of ϵ-caprolactam, sodium caprolactamate and activator V5, with 10% of EPR, and thoroughly tumble mixed before being introduced into the K-Tron volumetric feeder of the intermeshing, co-rotating twin-screw extruder of diameter 40 mm and L/D ratio of 21, as described previously (Section 3.2.2).

The same screw configuration and temperature profile was used as for PA6 preparation (Figure 3.2). A fixed screw speed of 150 rpm was employed throughout the in-situ polymerisation and blending extrusion process. The melt extrudate after exiting from the 4 mm die was water-quenched at room temperature, and collected as 60 mm length rods or pellets. These as-extruded blend samples were then extracted with boiling distilled water in a reflux apparatus for 12 hr to remove residual monomer and other low molecular mass oligomers, followed by drying in vacuo at 110°C for another 24 hr.

4.2.2 *Test Specimens Preparation*

Experimental details for injection moulding of test specimens and conditioning prior to characterisation of properties are as described in Section 3.2.3. Some samples were also annealed at 180°C for 90 min in vacuo, followed by slow cooling in air to room temperature while with others, the elastomer phase was extracted with boiling xylene in a Sohxlet apparatus for 12 hr and dried in vacuo at 90°C for a period of 24 hr. All the washed and dried PA6/EPR blend samples were stored in dessicators at room temperature (23°C) for 7 days prior to injection moulding for test specimen preparation and structural analysis.

4.2.3 *Analysis of structural and Physical Property*

Experimental procedures for the structural (WAXD, DSC, IR, scanning electron microscopy) and mechanical properties characterisation are as outlined in Sections 3.2.6. and 3.2.7. All structural analysis and mechanical properties were evaluated at room temperature of 23°C and in a "dry as-moulded" state.

4.3 Results and Discussion

4.3.1 *Structural Analysis*

4.3.1.1 *Wide Angle X-Ray Diffraction*

Wide angle X-ray diffraction (WAXD) equitorial profiles of the reactive PA6/EPR blend and pure EPR material are shown in Figure 4.1. For the blend sample two reflection peaks characteristic of the PA6 α crystalline phase at Bragg angles $2\theta \approx 20.1^{\circ}$ and $2\theta \approx 23.5^{\circ}$ were observed. Another two weak reflection peaks with lower intensities are also detected at $2\theta \approx 14.2^{\circ}$ and $2\theta \approx 16.8^{\circ}$ respectively which are probably associated with the α_1 (110) and α_2 (040) crystalline phases of polypropylene [180].

It is interesting to note that the WAXD profile for the pure EPR [Figure 4.1 (ii)] which showed only a broad reflection peak at Bragg angle $2\theta \approx 20.6^{\circ}$ (d spacing = 4.3Å). This reflection peak may be associated with the crystallinity of the polyethylene (PE) in the EPR main chain [181]. These WAXD results for the reaction PA6/EPR blend suggest possible structural changes with respect to the EPR polymer chain might have occurred during the reactive blending process as the PA6 was synthesised.

WAXD reflection profiles of the PA6/EPR blend after annealing at 180°C for 90 min is as shown in Figure 4.1 (iii). Here again, the two characteristic α peaks of PA6 crystalline phase are observed with narrower peaks and higher reflection intensities indicating some perfection of the PA6 crystallites have occurred during the annealing process. However, in addition to these two α peaks, another reflection peak at Bragg angle $2\theta \approx 21.3^{\circ}$ (d spacing = 4.1Å) can also be seen which is likely to be associated with the γ crystalline phase of PA6. Again, two lower intensity but distinct reflection peaks at Bragg angles $2\theta \approx 14^{\circ}$ and $2\theta \approx 17^{\circ}$ are observed which are associated with PP.

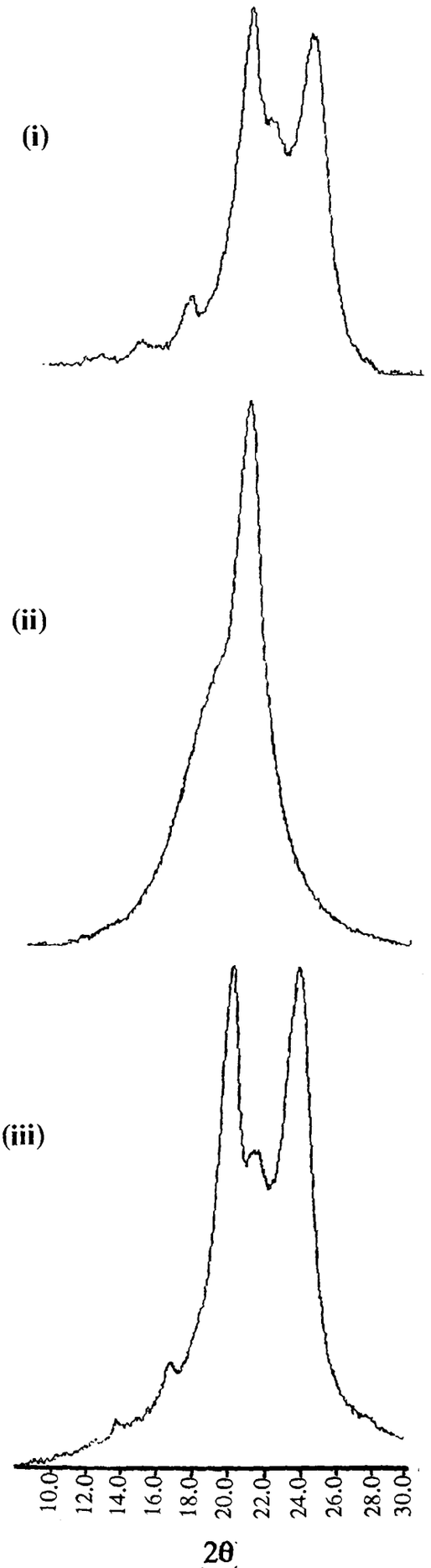

Figure 4.1 WAXD equitorial profile of PA6/EPR blend and EPR copolymer

(i) PA6/EPR (water-quenched) (ii) EPR

(iii) PA6/EPR (water-quenched/annealed)

It is interesting to observe the presence of the PA6 γ reflection peak in the annealed sample as compared to the unannealed one. It is possible that this peak is also present in the unannealed sample but is not detected due to the overlapping effect of the two stronger intensity α peaks. This experimental result from annealing the PA6/EPR sample suggests that a thermally more stable γ phase of PA6 has been formed as a result of the presence of 10% EPR as compared to the γ peak formed by air-cooling the extrudate, since in the latter case, the γ phase disappeared upon annealing [Section 3.3.4.1].

Martuscelli *et al.* [126] also reported WAXD profiles for both the α and γ crystalline phase reflection peaks associated with PA6 in a PA6/EPR blend material prepared by melt mixing a commercial grade PA6 resin synthesised by hydrolytic polymerisation of caprolactam and an amorphous EPR material with 60 mole % ethylene content. However, no reflection peaks associated with the PP or polyethylene (PE) crystalline phase were reported.

4.3.1.2 *Differential Scanning Calorimetry*

Typical DSC thermograms of the reactive PA6/EPR blend and pure EPR pellet are shown in Figure 4.2 with major thermal events summarised in Table 4.1.

For the blend sample, two distinct endothermic melting and exothermic crystallisation peaks were observed in both the heating and cooling cycles corresponding to the transitions of the PA6 and PP crystalline phases respectively [Figure 4.2 (i)]. It is indeed surprise to observe the transition peaks associated with the PP component of the EPR material since a DSC run on the pure EPR sample shows no evidence of crystalline peaks for either the ethylene or propylene component [Figure 4.2(ii)] suggesting that it can be an amorphous material at room temperature. The WAXD reflection profile of the pure EPR material [Figure 4.1 (ii)] however, suggested that the EPR used in this study is in fact, a semi-crystalline

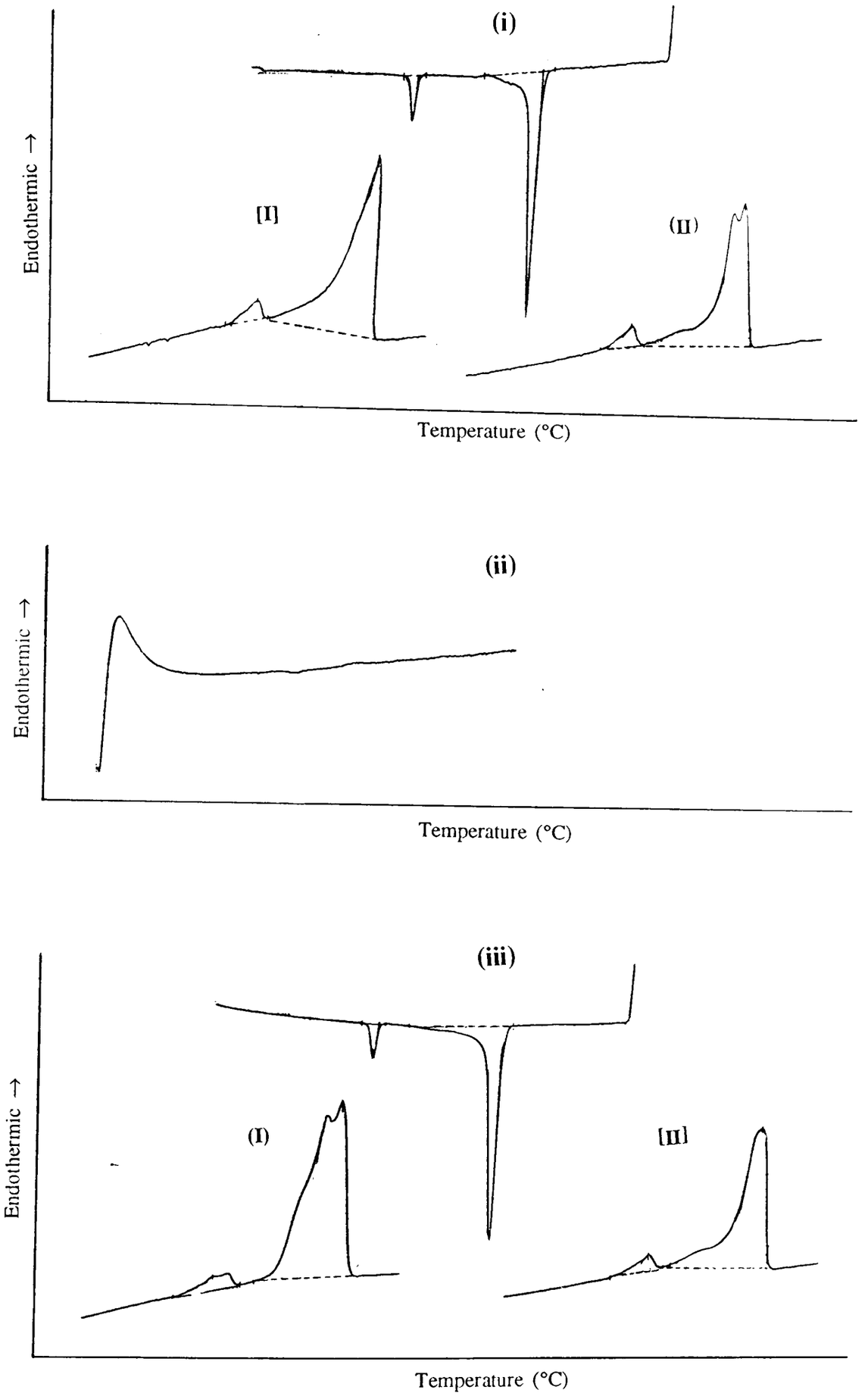

Figure 4.2 DSC thermogram of PA6/EPR and EPR copolymer
(i) PA6/EPR (water-quenched) (ii) EPR copolymer
(iii) PA6/EPR (water-quenched/annealed)

Table 4.1 DSC thermal data of reactive polymerised PA6/EPR, PA6 and PP

Sample*	T_{m1} (°C)		ΔH_{f1} ($J.g^{-1}$)		T_c (°C)		ΔH_c ($J.g^{-1}$)		T_{m2} (°C)		ΔH_{f2} ($J.g^{-1}$)	
	PA6	PP	PA6	PP	PA6	PP	PA6	PP	PA6	PP	PA6	PP
PA6/EPR	216.5	164.7	51.4	3.8	182.5	124.4	52.6	6.0	215.4	161.4	46.1	3.9
PA6/EPR (annealed)	216.7	158.0	81.3	4.8	180.9	123.3	58.7	5.1	214.5	161.8	42.6	3.5
PA6	214.2	-	87.8	-	180.1	-	58.4	-	213.5	-	60.8	-
PA6 (annealed)	214.9	-	84.9	-	179.5	-	63.0	-	213.0	-	64.5	-
PP +	-	161.4	-	86.1	-	112.7	-	98.1	-	158.1	-	99.5

* Reactive polymerised PA6 and PA6/EPR blends

\+ Commercial grade isotactic PP homopolymer

T_{m1}, T_{m2} Peak endothermic melting temperatures, stage I and II heating cycles.

T_c Peak exothermic crystallisation temperatures, cooling cycle.

ΔH_{f1}, ΔH_{f2} Heats of fusion, stage I and II heating cycles.

ΔH_c Heat of crystallisation, cooling cycle.

polymer. It is therefore likely that the melting point of the crystalline PE has been suppressed by the presence of PP component at room temperature [181]. An apparent "transition" region was observed on the heating thermogram of the EPR sample at temperature region of 40°-50°C [Figure 4.2 (ii)], which probably substantiated this proposition.

On the other hand, the observation of the crystalline PP transitions in DSC thermograms suggests the possibility of structural changes to the EPR polymer as a result of intense elongational shear stresses developed during the extrusion/blending process. Among other products, apparently short chains of PP block copolymers might have been formed as a result of chain scission of the EPR main chain which probably have attained sufficient polymer chain length to effect crystallinity, thus constituting the transition and reflection peaks recorded in both the DSC and WAXD profiles. The other workers, **Martuscelli** *et al.* [126] and **Kim** *et al.* [182] however, reported only a transition peak corresponding to PA6 for thermal studies on PA6/EPR and PA6/EPDM mechanical blend materials.

Thermal analysis data in Table 4.1 shows that the PA6 component of PA6/EPR blend has recorded a slightly higher melting temperature (216.5°C) in stage I heating cycle as compared to the pure PA6 material (214.2°C) even though a significantly lower crystallinity is observed as shown by the lower enthalpy of fusion. The results obtained for this reactive blend material suggest that either the molten PP or other EPR component could possibly impart a nucleating effect on PA6 during crystallisation stage of PA6. A shift of the crystallisation temperature (T_c) of PA6 to some 2.5°C higher at 182.5°C was also noted which further substantiate the possible nucleating effect PA6.

Martuscelli *et al.* [126] in their investigation of the thermal and structural properties of PA6/EPR blend by DSC reported the addition of the elastomer to PA6 did not influence the thermal behaviour of the PA6 component. No change in both the peak melting and crystallisation temperatures were observed as compared to the pure PA6

material. However, the workers did not present any enthalpy data to indicate the crystallinity levels of the PA6 component.

Kim *et al.* [182] reported DSC results on the effect of adding functionalised ethylene propylene diene monomer (EPDM) to PA6 which showed a shift of the crystallisation peak temperature of this component to a higher temperature range (4 °C), with evidence for an increased rate of crystallisation.

As for the PP transition peaks in this PA6/EPR reaction blend, both higher melting and crystallisation temperatures have been recorded as compared to the pure PP material [Table 4.1]. The significantly higher crystallisation temperature (about 12 °C higher) obtained for the PP in this PA6/EPR reaction blend suggests that in this case, the presence of solidifying PA6 can possibly influence the nucleation process of PP crystallisation.

Typical DSC thermograms of the annealed PA6/EPR blend are shown in Figure 4.2(iii). Here again, two transition peaks are observed in both the heating and cooling cycles, corresponding to the PA6 and PP phases. In stage I heating cycle, however, a much broader PA6 transition peak is observed with bimodal endothermic melting peaks and 60% higher heat of fusion is also recorded as compared to the PA6 peak of the unannealed PA6/EPR blend sample. Nevertheless, the maximum peak melting temperatures of both the annealed and unannealed samples in the two heating cycles are almost identical suggesting higher crystallinity is probably attributed to the formation of the γ PA6 crystalline phase which has a lower melting temperature and favourably formed as a result of the annealing process as indicated by the WAXD profile discussed earlier.

It is well known that annealing the PA6 at a temperature of 180 °C could promote the growth of the PA6 α crystallites as a result of transformation from the γ phase or amorphous region [91]. However, in this case, it is conceivable to postulate that the increase in enthalpy for the annealed sample recorded in the stage I heating cycle

as compared to the unannealed sample is probably due to the combination of both the perfection of the γ phase as well as the transformation to α phase from the amorphous region of the unannealed sample.

However, during the stage II heating cycle, it is interesting to observe that both the PA6 and PP phases of the annealed sample yield rather similar enthalpy of fusions as well as peak melting temperatures to those recorded by the unannealed samples. These results suggest that in the presence of 10% EPR, γ crystallites and other less perfect α crystallites of PA6 are favourably formed in the continuous matrix. These crystallites are however, not been able to recrystallise in the DSC cooling cycle after they have completely melted at 250°C at the end of the stage I DSC heating. The much lower heats of crystallisation and fusion recorded in the cooling cycle and stage II heating cycle substantiated this reasoning. These observations are also in agreement with the finding of **Khanna** *et al.* [92] who suggest that with nucleated polyamide materials, effects of their processing history are lost after the materials are completely melted and held isothermally for a short period, before being subjected to recrystallisation cycle by cooling down to room temperature.

On the other hand, however, it is significant to observe that when pure PA6 materials are annealed under similar conditions, the crystallinity level is observed to decrease slightly but much higher melt temperatures are recorded for both the stage I and II heating cycles [Table 4.1]. In this aspect, it is plausible to conceive that in the case of a pure PA6 material, the processes of α crystallite perfection, $\gamma \rightarrow \alpha$ crystallite transformation, as well as the trasformation of amorphous polymers to the α crystallites may have occurred simultaneously during the annealing period similar to the observations reported by **Murthy** *et al.* [91].

In the stage II heating cycle, the observation of the bimodal melting peaks in the stage II heating cycles in both the annealed and non-annealed binary blend samples is again possibly attributed to the reorganisation, melting and perfection of the

crystallites along the DSC scan as discussed earlier for the PA6 materials [Section 3.3.4.2].

The endothermic melting peak of the PP phase of the annealed sample also appeared broader but recorded a maximum melting temperature some 7°C lower than the pure unannealed sample although a higher enthalpy was recorded. At the annealing temperature of 180°C, the PP phase of the reactive PA6/EPR blend is in a semi-molten state. As the sample is being cooled down to room temperature after the annealing process, PP will recrystallise as it reaches the temperature region of 124°C where maximum crystallisation has been observed. At this temperature region however, solidified PA6 crystals are present which might induce heterogeneous nucleation of the PP crystallising spherulites and accounted for the higher enthalpy observed. It is possible that as a result of this heterogeneous crystallisation of PP spherulites, less perfect crystals are formed which may have contributed to the lower peak melting temperature as compared to the PP phase of the unannealed sample.

Ethylene and propylene are the basic monomeric units of EPR block copolymer. It is also well known that EPR copolymer can be crosslinked via a free radical mechanism [181]. The tertiary hydrogen on the EPR copolymer main chain is known to be most reactive and can be readily abstracted by a peroxide radical to form a polymer radical which will subsequently combine with adjacent radicals to complete the crosslink. This reaction mechanism forms the basis of crosslinking or vulcanising the EPR thermoplastic elastomer in its commercial applications.

It is reported that all the commercial grades of ethylene propylene diene monomer (EPDM) and EPR materials that contain above 40% ethylene develop crystallinity below ambient temperature if annealed for several hours or weeks. At about 40% ethylene content, the melting peak of PE is suppressed by the comonomer content to its glass transition temperature, T_g at about 38°C. Below 40% ethylene content, the polymer remains amorphous at all temperatures. In no significant case, is the

PP stereo regular enough or of sufficient sequence length to make it crystallised [181]. This statement agrees well with the observed DSC result for pure EPR which shows no PE crystallinity above room temperature, but the WAXD result however, infer that the EPR coplymer used in this reaction blend is in fact, a semi-crystalline with substantial PE crystallinity at room temperature.

In this reactive polymerisation and blending process, however, large shearing forces are being experienced which could cause the polymer chains to undergo severe physical and chemical changes. It is plausible that during the melt blending process, mechano-chemical degradation can occur which could produce chain macro-radicals from both the PA6 and EPR components, as a result of polymer chain scission. These microradicals could possibly react with each other and form either a branched or grafted copolymer or both. Formation of new PP block chains could possibly account for the observed melting and crystallisation peaks in Figure 4.2, which are not observed in pure EPR polymer or in other PA6/EPR blend materials prepared by conventional mechanical mixing where the shearing stresses experienced by the polymers are less severe. It is interesting to note that other WAXD and DSC experiments performed on different EPR materials which have been separately annealed at 140°C for 3 hr and compression-moulded yielded no characteristic reflection profiles as well as the melting and crystallisation peaks associated with PP. These results further substantiate the postulation that chain scission of the EPR chain may have occurred during the extrusion polymerisation and blending process due to extremely higher elongational shear stresses developed.

Baranwal [183] studied mechanochemical degradation of EPDM and EPR copolymers and concluded that at processing temperature >200°C in the presence of shear forces, the polymer main chains are broken down to yield polymer macroradicals. The study reported that the weakest spot in EPDM and EPR polymers is the tertiary hydrogen in the PP repeating units and therefore it is the most susceptible to abstraction during chain scission to yield a radical.

Both the WAXD and DSC results reported by **Martuscelli** *et al.* and **Kim** *et al.* on their PA6/EPR and PA6/EPDM blends only involved the PA6 phase. It is worth noting that the main difference between these two elastomer modified PA6 blend materials and the reactive polymerised PA6/EPR blend used here is the processing conditions used for the blend preparations. The other workers both used a Brabender-like apparatus to melt blend the materials at 260°C/32 rpm and 250°C/10 rpm respectively which as compared to the extrusion processing conditions used for this reactive blending process (235°C/150 rpm) is much less severe being less likely to cause chain scission of the EPR polymer main chain and may form, among other products, crystalline PP block copolymers.

4.3.1.3 *Fourier Transform Infra-red Spectroscopy*

The Fourier transform infrared spectroscopy (FTIR) characteristic absorption bands and spectra of the reactive PA6/EPR blend with 10 wt% composition of elastomer are shown in Table 4.2 and Figure 4.3 respectively.

In order to ascertain qualitatively whether a graft copolymer has been formed during the reactive polymerisation/blending process, the Molau test is applied using 90% formic acid as a solvent [115]. About 200 mg of the PA6/EPR blend materials were placed in about 20 ml of formic acid solution, which is an excellent solvent for PA6 and a non-solvent for EPR. After 5 hours, a milky and colloidal suspension was observed with small pieces of non-soluble particles floating on the solution. The weight of this colloidal suspension together with the undissolved particles was about 21.65 mg which suggests a small amount of graft copolymers have been formed. The spectra and the characteristic absorption bands of this insoluble matter are also included in Figure 4.3 and Table 4.2.

Table 4.2 shows that the characteristic absorption bands of the PA6 component, i.e., NH stretching (3300 cm^{-1}), CH_2 assymmetric/symmetric (2937, 2867 cm^{-1}), C=O

Table 4.2 FTIR characteristic absorption bands of PA6/EPR blend

Band assignment	PA6	PA6/EPR	PA6/EPR*	Literature Reference
NH stretching (H bonded)/cm^{-1}	3300 (s)+	3300 (vs)+	3298 (s)	3302 [159]
CH_2 assymm. (aliphatic)/cm^{-1}	2936 (s)	2937 (vs)	2923 (m)+	2940 [157]
CH_2 symm. (aliphatic)/cm^{-1}	2865 (s)	2867 (s)	2868 (m)	2865 [157]
Amide I, C=O/cm^{-1}	1641 (vs)	1642 (vs)	-	1642 [157]
Amide II, NH/cm^{-1}	1542 (vs)	1552 (vs)	1545 (vs)	1545 [157]
CH_2 deformation/cm^{-1}	1475 1462 1439 1418 (m)	1475 1462 - 1418 (m)	1477 1464 1436 1417 (w)+	1480 1465 1438 1417 [157]
CN stretching/cm^{-1}	-	-	1241 (w)	1238 [157,188]

+ Band intensity classification: >3(vs); >2 & <3(s); >1 & <2(m);<1 (w)

* Insoluble extract from formic acid solution

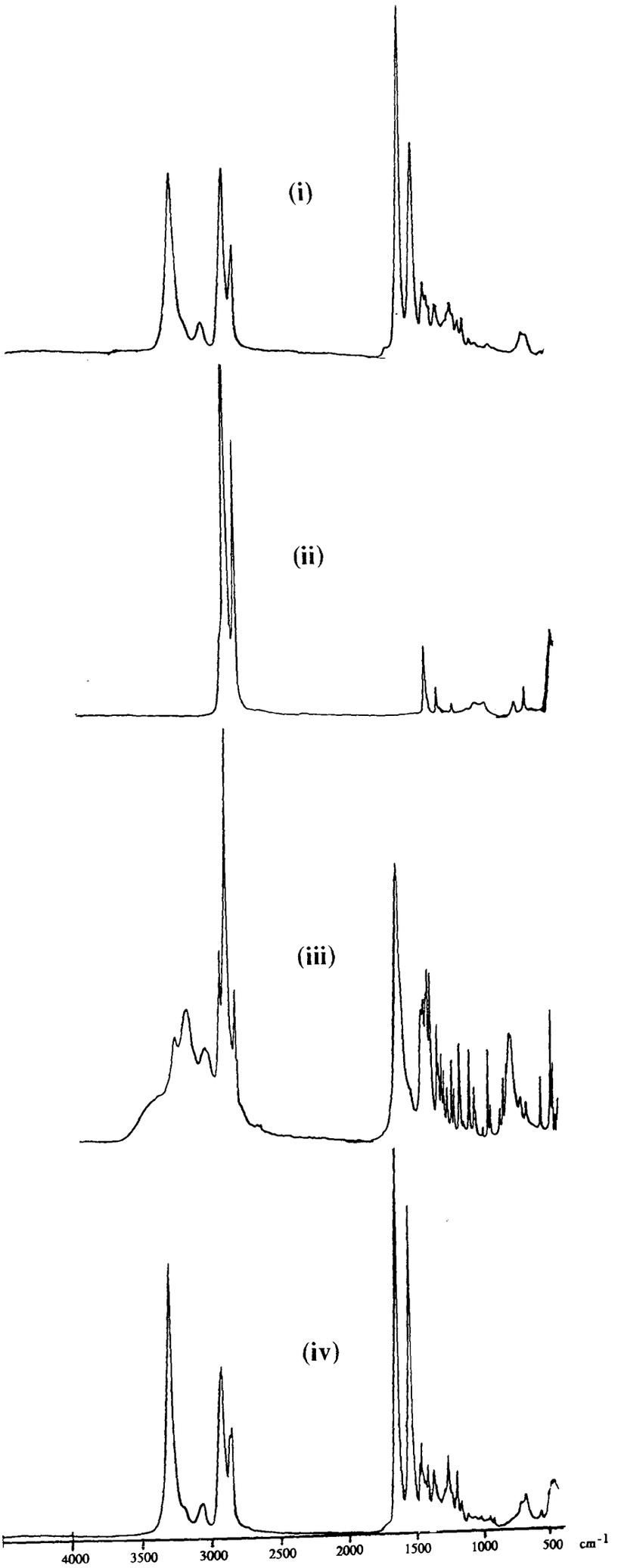

Figure 4.3 FTIR spectrum of PA6/EPR, EPR and caprolactam monomer
(i) insoluble PA6/EPR extract from formic acid solution
(ii) EPR copolymer (iii) caprolactam monomer (iv) PA6/EPR reaction blend

amide I (1642 cm^{-1}), NH amide II (1552 cm^{-1}) and CH_2 deformations (1475, 1462, 1418 cm^{-1}) are all observed on the PA6/EPR blend spectra indicating of course, the presence of PA6. However, it is interesting to observe a slight shift of these bands to higher frequencies as compared to the pure reactive polymerised PA6 sample extruded at 150 rpm under similar processing conditions. A much larger shift to higher frequency is recorded for the NH amide II band which suggests a weakening or destruction of the hydrogen bonds due possibly to a reduction of these characteristic group which involves coupling of NH deformation with CN stretching [159].

The spectra of the insoluble matter obtained from formic acid solution [Figure 4.3 (i)] exhibits characteristic absorption bands associated with PA6 (NH stretching / 3298 cm^{-1}; NH amide II/1545 cm^{-1}) which is most unusual since all the PA6 phase is expected to have dissolved in formic acid solution in this incompatible two phase system. These results imply that a graft copolymer PA6-g-EPR might have formed. The very strong band intensity recorded for the NH amide II stretching deformation (1545 cm^{-1}) and the disappearance of the C=O amide I (1642 cm^{-1}) suggests the presence of shorter PA6 chain with longer -CH_2- sequences, since the PA6 phase is insoluble [184]. These results also indicate possible chain scission of the PA6 polymer chains to form a new imide linkage with a carbonyl group. This postulation is substantiated by the detection of a weak CN amide III absorption band at 1241 cm^{-1}. The spectra of caprolactam monomer is also shown in Figure 4.3 (iii). Both the spectrum of reaction PA6/EPR blend and the insoluble extract from formic acid solution did not exhibit characteristic absorption bands associated with caprolactam, indicating no monomer residues were present in these materials.

As discussed earlier, ethylene and propylene are the two basic monomeric units of EPR block copolymer and their structures as shown in Figure 4.4 are oversimplified since no information is available on the probable distributions of these monomer units which depend very much on the ratio of the monomers employed, the catalyst system and the polymerisation conditions [185]. However, under a high shear

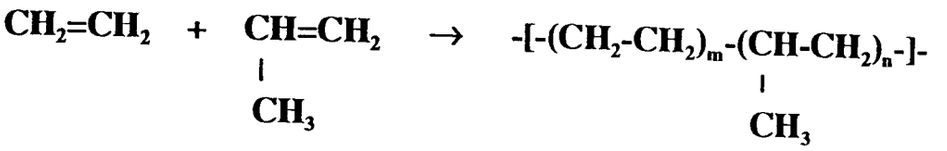

ethylene propylene copolymer

Figure 4.4 Structure of EPR block copolymer

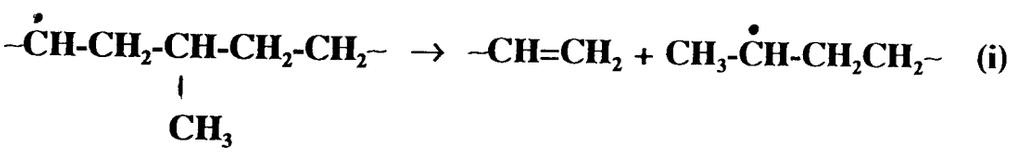

or

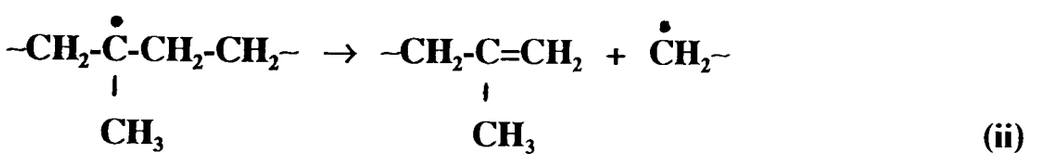

Figure 4.5 Chain scission of EPR copolymer during extrusion processing

extrusion blending process, as experienced in a twin-screw extruder, it is possible that homolytic chain scission can occur along the EPR main chain forming macro-radicals associated with the ethylene and propylene monomeric blocks respectively as shown in Figure 4.5 [186].

In the literature [187], it has been described that during melt blending, polyethylene (PE) chains can break preferentially at branch points, forming secondary radicals which will either react with another PE chain through hydrogen extraction or rearrange to form a new radical and unsaturated groups (C=C or C=O). The reaction terminates when two macro-radicals react between themselves, forming a branched PE molecule. In the presence of oxygen, the double bonds made by the reaction sequence mentioned above can also readily react to form aldehyde end groups. Since the FTIR spectrum of the PA6/EPR blend as well as the insoluble matter obtained from formic acid solution showed no evidence of the band absorption for the aldehyde group at 1735 cm^{-1}, it suggests that C=O functionality of PE has possibly been involved in a chemical reaction during the melt blending process.

Observations of characteristic absorption bands associated with PA6 (3298 and 1545 cm^{-1}) in the insoluble matter extracted from the formic acid solution further substantiate the possibility that a PA6-g-PE graft copolymer has been formed during the reactive blending process. The graft copolymer is likely to be formed from a imide linkage (CN) between the NH group of the PA6 main chain and the C=O group resulting from PE scission chain. This reaction proposed is similar to that reported by **Curto** *et al.* [188] on blending of photo-oxidised PE with PA6. Graft copolymer of PA6-g-PE is assumed to have formed which act as interfacial agents and improve the compatibility of the two phases with enhancement of mechanical properties.

The detection of a weak absorption band at 1241 cm^{-1} from the insoluble formic acid acid extract [Table 4.2] which has been assigned as the amide III (CN) with CH_2

wagging vibration characteristic band by **Rotter** *et al.* [189] and **Arimoto** [157] provides further experimental evidence of the formation of a graft copolymer PA6-g-PE by the imide linkage between the scission polymer chains of PA6 and PE.

Cimmino *et al.* [123] reported the reaction of ethylene propylene monomer elastomer grafted with succinic anhydride (EPR-g-SA) with aliphatic amines such as n-hexylamine leads to amidic or imidic linkages depending on the reaction temperature used. At low temperatures ($< 120^{\circ}C$), amidic linkages are prevalent, whereas at higher temperatures, almost only imidic bonds are present as revealed by infra-red spectroscopy. The workers have considered this reaction mechanism as a model scale reaction of that occurred during the melt blending of PA6 and EPR-g-SA at $260^{\circ}C$, suggesting that likely imide linkages are present in the EPR-g-PA6 graft copolymer formed by combination of the terminal NH_2 group of PA6 and the C=O functional group of succinic anhydride. However, the workers claimed that they cannot exclude the possibility that graft copolymer can also be formed by breaking of the amide bonds of PA6 main chain by means of anhydride or carbonyl groups of the functionalised EPR.

Similarly, **Borggreve** *et al.* [127] studied the infra-red spectrum of a PA6/EPDM-g-MA blend residue extracted from formic acid solution and reported the absence of a strong free-acid absorption band at 1720 cm^{-1} and suggested that a graft copolymer with imide bond has possibly been formed rather than an amide/acid linkage. Their results seem to support the conclusions of **Cimmino**'s model study that imide bonds are preferentially formed at melt blending temperatures exceeding $120^{\circ}C$.

Furthermore, as discussed earlier, it is very likely that two macro-radicals of PE formed by main chain scission can also react with each other to form a branched PE which together with the PA6-g-PE graft copolymer, could possibly account for the non-detection of the PE crystalline phase in the DSC thermogram [Section 4.3.1.2]. **Macknight** *et al.* [190] reported a drastic decrease in the degree of crystallinity for the PE phase of a PA6/ethylene methyacrylic acid blend of compositon 90/10 wt %

and attributed this observation to the formation of branched PE molecules and the formation of the non-crystalline PA6-g-PE graft copolymer.

In contrast to PE chain breakage to form the unsaturated C=C and C=O groups, PP degrades predominantly by chain scission to form $-CH(CH_3)-\dot{C}H-$ and $-\dot{C}(CH_3)CH_2-$ radicals [191, 192]. The first radical, however is believed to be highly reactive with oxygen and can easily transfer into a peroxy radical. As for the second radical, as a result of the hindrance effect of the larger CH_3 group, it is less likely that the NH group of the scissioned PA6 chain can react with either of these PP radicals as compared to a linkage formed between NH and the C=O group of the scissioned PE chain.

Furthermore, from the trade literature of the EPR material supplier [185], it is known that the mole ratio of the PE monomer units to those of the PP is 3:1. Also, it is known from literature that 9.9×10^{18} bonds cm^{-3} were broken during rupture of a PE chain as compared to 2.5×10^{18} bonds cm^{-3} in the case of PP [187]. All these information tends to imply higher possibility of bond formation between the NH group of PA6 and PE rather than PP chain. Finally, both DSC and WAXD structural analysis results have revealed the presence of a crystalline phase associated with PP in the blend material. Presumably all the PE phase materials have therefore either remains in the EPR main chain, or transform into branched molecules or might have reacted with PA6 to form the graft copolymer.

For the PA6 chain structure, as discussed earlier, many workers have reported the reaction between the pendant anhydride of the functionalised elastomer with either the terminal amine group or with the amide bonds of the PA6 main chain to yield a PA6/elastomer graft copolymer. However, it is anticipated that in a highly shear stress dominated reactive extrusion/blending environment, radical initiation by homolytic scission at the C-N linkage is more probable than at the C-C bond of the PA6 polymer main chain, since the C-N bond is known to be weaker than the C-C bond [193]. The strength of the former being about 66 $kcal.mol^{-1}$ as compared to

the bond strength of C-C which is some 82 kcal.mol^{-1}, depending on the polymer structure in which it is located. The C-N bond beta to the carbonyl group will break more preferentially since it is weaker than that alpha to the carbonyl group. It is likely that breakage of this C-N bond in the PA6 main chain is responsible to the shift of the amide II CN absorption band from 1542 cm^{-1} to a higher frequency at 1552 cm^{-1} since less hydrogen bonding effect on the overall crystalline structure of PA6.

4.3.1.4 *Scanning Electron Microscopy*

Figure 4.6 shows scanning electron microscopy (SEM) micrographs of cryogenically fractured surfaces of PA6/EPR material made by reactive blending.

The cryogenically fractured surface of the EPR modified PA6 shows a fracture mechanism that is very familiar to that of the pure reactive polymerised PA6, i.e. with a fast crack propagation zone extended to the whole sample but with a rougher surface indicating a slightly higher energy dissipation than in the case of the pure PA6. Elongated ellipsoidal shape domains and dispersed spherical particles are observed well distributed over the continuous PA6 matrix. The spherical domains diameters ranges from 1-3 μm while the ellipsoidal structures recorded dimensions about 20-30 μm in length and 3-5 μm in thickness. Ellipsoidal formation is due primarily to the difference in viscosities of the blend components during melt flow in the presence of elongational shear forces as well as the reaction temperature during extrusion. Melt flow index of the PA6/EPR blend is recorded at 2.7 (g/10 minutes) which is lower than that of the pure reactive polymerised PA6 at 3.9 (Table 3.6).

The interior walls of the cavities left behind by the ellipsoidal structures from fracture appear to be rough and the structure surfaces showed evidence of polymer

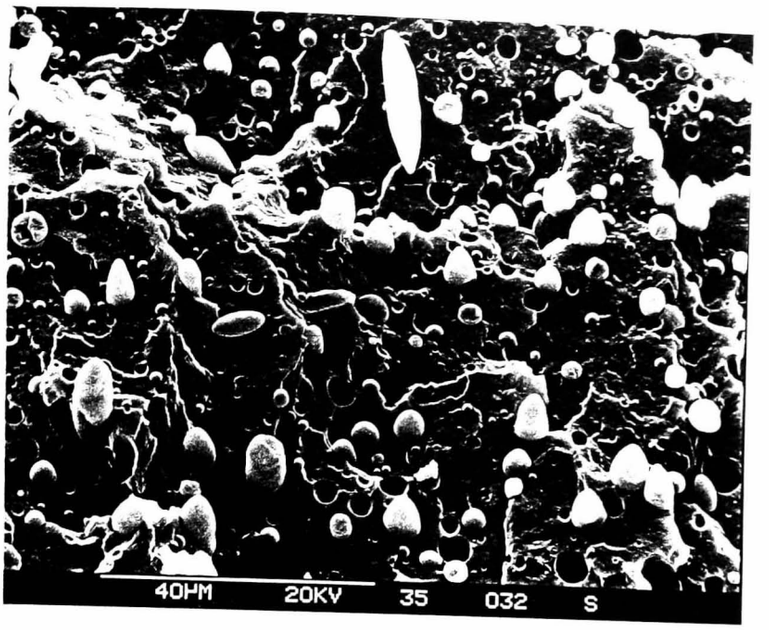

(i) as-fractured

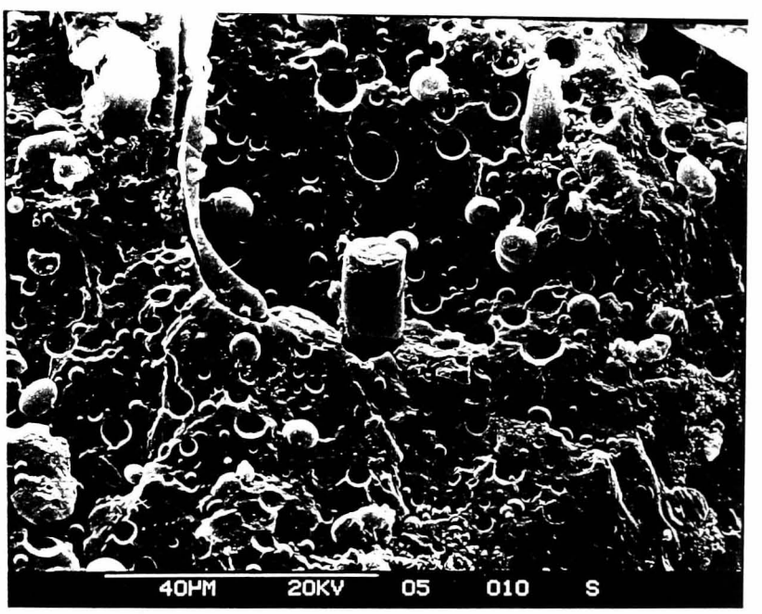

(ii) xylene-extracted

Figure 4.6 SEM micrograph of reaction PA6/EPR 90/10 blend

adhesion which suggests some degree of interaction or adhesion between the PA6 and dispersed EPR phase.

The observation of ellipsoidal shaped domains of the elastomer dispersed phase is rather unexpected. Typical SEM micrographs of cryogenically fractured syrface of a PA6/EPR blend of similar composition by weight (90/10) reported by **Cimmino** *et al.* [124] as a blend exhibiting a "cheese-like" morphology with rubbery spherical shaped domains of about 20 μm average diameter, uniformly distributed throughout the whole PA6 matrix. Also, it was reported that no adhesion was observed at the PA6/EPR interface as indicated by the smoothness of the wall cavities. It is postulated that formation of ellipsoidal structure in this reactive blended PA6/EPR alloy is attributed to the extremely high elongational shear conditions as well as the large difference in the melt viscosities of PA6 and EPR materials.

Orazio *et al.* [194] observed ellipsoidal shape ethylene vinyl acetate copolymer (EVA) domains dispersed in a continuous PA6 matrix for a PA6/EVA blend of 90/10 wt %. The blends were prepared by melt mixing using a single screw extruder at 50 rpm, 220°C and residence time of 10 minutes. The workers reported that on either increasing the extrusion temperature to 260°C or decreasing the extruder residence time to 3 minutes, only spherical droplets of EVA are observed instead of the ellipsoidal domains. These observations suggested that the formation of ellipsoidal shape domains of the dispersed phase are favoured at lower reaction temperatures which can lead to higher blend viscosities as well as longer residence time inside the extruder.

The morphology of the reactive polymerised PA6/EPR blend after xylene extraction of the elastomer phase is shown in Figure 4.6(ii). The disappearance of many ellipsoidal structures after xylene treatment provide evidence that they are in fact, elastomeric based materials since the PA6 phase is known to be not at all affected by xylene. However, it was observed that many of the spherical particles and some

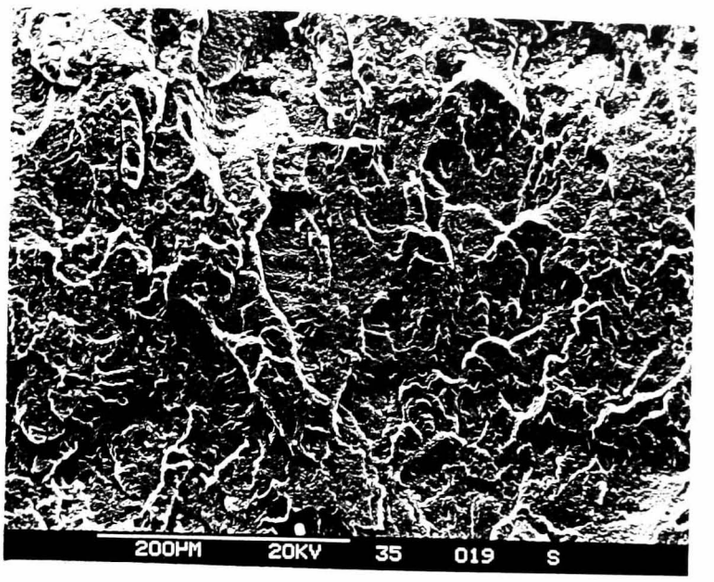

(i) PA6 homopolymer

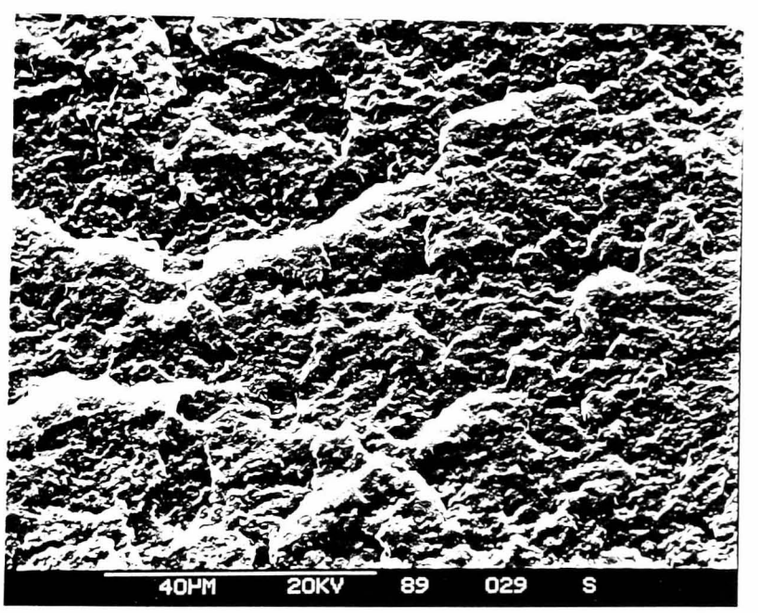

(ii) PA6/EPR 90/10 reaction blend

Figure 4.7 SEM micrograph of cryogenically fractured tensile test specimen

ellipsoidal structures remained intact after xylene treatment, suggesting that these are possibly PA6/EPR graft copolymers which are not affected by the action of xylene.

The fractured surface of the reactive polymerised PA6 homopolymer tensile test piece after injection moulding exhibits a rough topography typical of a fast fracture [Figure 4.7 (i)]. No evidence of stress whitening is observed indicating that the impact energy is mainly related to the yielding process. On the other hand, examination of the fractured surface of the PA6/EPR injection moulded tensile test piece reveals a distinct shear whitening phenomenon which indicate the formation of multi crazes during the fracturing process [Figure 4.7 (ii)]. In addition, the overall blend matrix is observed to be plastically deformed. The homogeneous morphology of the reaction blend surface indicates the inclusion of fine EPR copolymer dispersions in the PA6 continuous matrix. This morphological evidence suggests that the fracture mode of the reactive polymerised PA6/EPR blend material is possibly the result of the combined effect of multicraze propagation and shear yielding, to be followed by a rapid crack propagation involving the rest of the sample.

4.3.2 *Mechanical Properties*

The stress-strain curve for the PA6/EPR blend at room temperature (23 °C) shows a typical behaviour of a semicrystalline polymer similar to that obtained for pure PA6 (Figure 3.22), with a yield point, a cold drawing region and a yield rupture. The modulus E, stress at yield σ_y and elongation at break ϵ_b data for this reaction blend as well as for other elastomer-modified PA6 samples reported in the literature are summarised in Table 4.3 . A slight decrease in E modulus is observed for the blend as compared to pure PA6, probably attributed to the elastomer contribution since it has a modulus almost three decades smaller than that of the PA6 matrix. Also, there is a possibility of the existance of interfacial zones between the PA6 matrix and the elastomer dispersed particles, in which there is likely an increase in

Table 4.3 Mechanical properties of elastomer (10 wt%) modified PA6 blends

Sample	Young's Modulus (GPa)	Stress @ Yield (σ_y)	Elongation @ Break (%)	Impact Strength ($J.m^{-1}$)	Flexural Modulus (GPa)
PA6/EPR[a]	2.46	55.9	182.0	194	2.56
PA6/EPR[b]	2.71	34.3	160.0	-	-
PA6/EPR[c]	2.86	28.2	65.0	152	-
PA6/SEBS[d]	2.61	53.4	60.0	62	-
PA6[a]	2.68	66.4	88.7	93.8	2.72

Note:

(a) reactive polymerised PA6/EPR and PA6 (tested in "dry as-moulded " @ 23°C);
(b) in-situ hydrolytic polymerisation/blending [124];
(c) mechanical blending with plasticorder [125];
(d) mechanical blending of PA6 and styrene-(ethylene-co-butylene)-styrene [135].

free volume which can cause a reduction of modulus [125]. As compared to other elastomer modified PA6 blends, this reaction PA6/EPR blend recorded the lowest E modulus value.

Tensile strength at yield of this elastomer modified PA6 blend (55.9 MPa) is observed to be only slightly lower than that obtained for the pure PA6 (56.4 MPa) but much higher as compared to other blend materials. This extraordinary high yield stress attained may also be attributed to the formation of more perfect PA6 crystallites due to the presence of the EPR phase which is evident from the much higher melting temperature recorded from DSC studies although a lower enthalpy and hence crystallinity is recorded for this blend material [Section 4.3.1.2].

Elongation at break ϵ_b recorded for the reaction blend PA6/EPR material shows an almost 106% increase as compared to the pure PA6 material and also recorded much higher elongation as compared to other blend materials. It is well known that PA6 is a semicrystalline material which would undergo a classical spherutic - fibrous morphological transformation by means of diffuse or localised cold drawing and therefore behaves plastically. The addition of the elastomer phase can effectively modify the deformation behaviour of the PA6 matrix.

One possible explaination for the increase in ϵ_b properties without a decrease in tensile yield stress in the case of the reaction PA6/EPR blend is the formation of an PA6-g-PE graft copolymer located at the PA6/EPR interface and act as an emulsifying agent. In this way, the local stress at yield will be lowered around the elastomeric particles which can eventually lead to an increase in the efficiency of craze termination [132]. This hypothesis can be substanciated by the prominent stress-whitening effect observed on the elongated fractured specimens, indicating diffused craze formation [Figure 4.8].

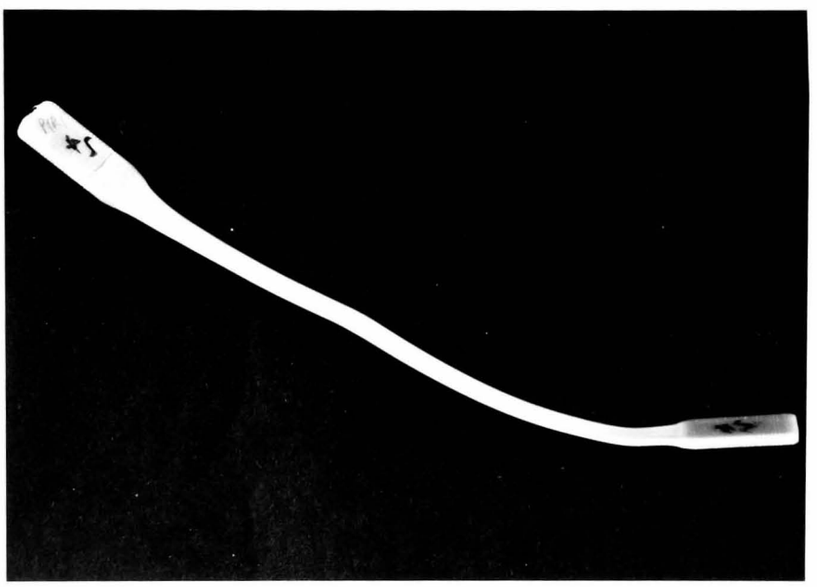

Figure 4.8 Stress whitening of reaction PA6/EPR elongated test specimen

The flexural modulus of the elastomer modified binary blend is about 15% lower than that of the pure PA6 material. This decrease in flexural properties is possibly again attributed to the softening effect due to the elastomer inclusion.

A much higher notched Izod impact strength at 194.4 $J.m^{-1}$ is recorded for the reaction blend material with respect to the pure PA6 material and all other elastomer modified materials. Both the higher elongation at break and impact strength properties of the reaction PA6/EPR blend material suggest that it has much superior toughness property.

Merz *et al.* [195] and **Kunz** *et al.* [196] suggested that the function of the elastomer particle in polyamide blends is to bridge the cracks formed so as to prevent the growth of the crack to catastrophic size which can lead to ultimate failure. On the other hand, **Hobbs** *et al.* [197] and **Wu** [198] claimed that the effectiveness of the rubber particles to toughen polyamides originates from the ability to generate stress concentrations around the particles in an applied stress field. Because of the differences in modulus between the the dispersed elastomer phase and polyamide matrix, the stress will be concentrated around the elastomer particles which would then lead to local nucleation of plastic deformations like crazing or shear banding. When the particles are sufficiently close together, the stress fields will overlap which can account for even an additional toughening effect.

It has been reported that during impact in elastomer modified polyamides, elastomer particles will cavitate or delaminate with an attempt to relieve some of the hydrostatic tension of impact [128]. Based on this argument, it is postulate that the fine structures of the EPR observed in the PA6/EPR blend material after injection moulding can possibly have the effect of dissipating the fracture energy more efficiently so as to divert the fast catastrophic crack formation thereby accounted for the improved toughness properties of this blend. These improved toughness properties are in good agreement with the earlier fractographic analysis, showing that

in the presence of EPR particles, diffuse shear yielding is possibly accompanied by multi-craze formation during the fracture.

Dynamic mechanical spectra of the reactive polymerised PA6/EPR blend and that of a pure EPR sample are shown in Figures 4.9. Several interesting results were observed for the reaction blend PA6/EPR [Figure 4.9 (■)]. Two separate loss factor peaks (tan δ) peaks corresponding to the α and ß transition peaks of PA6 were observed at temperature regions of 55°C and -78°C respectively. Another loss factor peak at T_g 19°C was also recorded which probably belong to PP. It is surprised to note that the transition of the pure EPR at -28°C [Figure 4.9 (▲)] is not been observed in this material. This result again, can possibly support the earlier proposition that during the extrusion process, the EPR chain segment has been modified as a consequence of shear degradation leading to main chain scission to form PP and PE block and random copolymers. The elastic modulus E' of the PA6/EPR blend was observed to exhibit a gradual decrease in modulus through the whole temperature span of measurement.

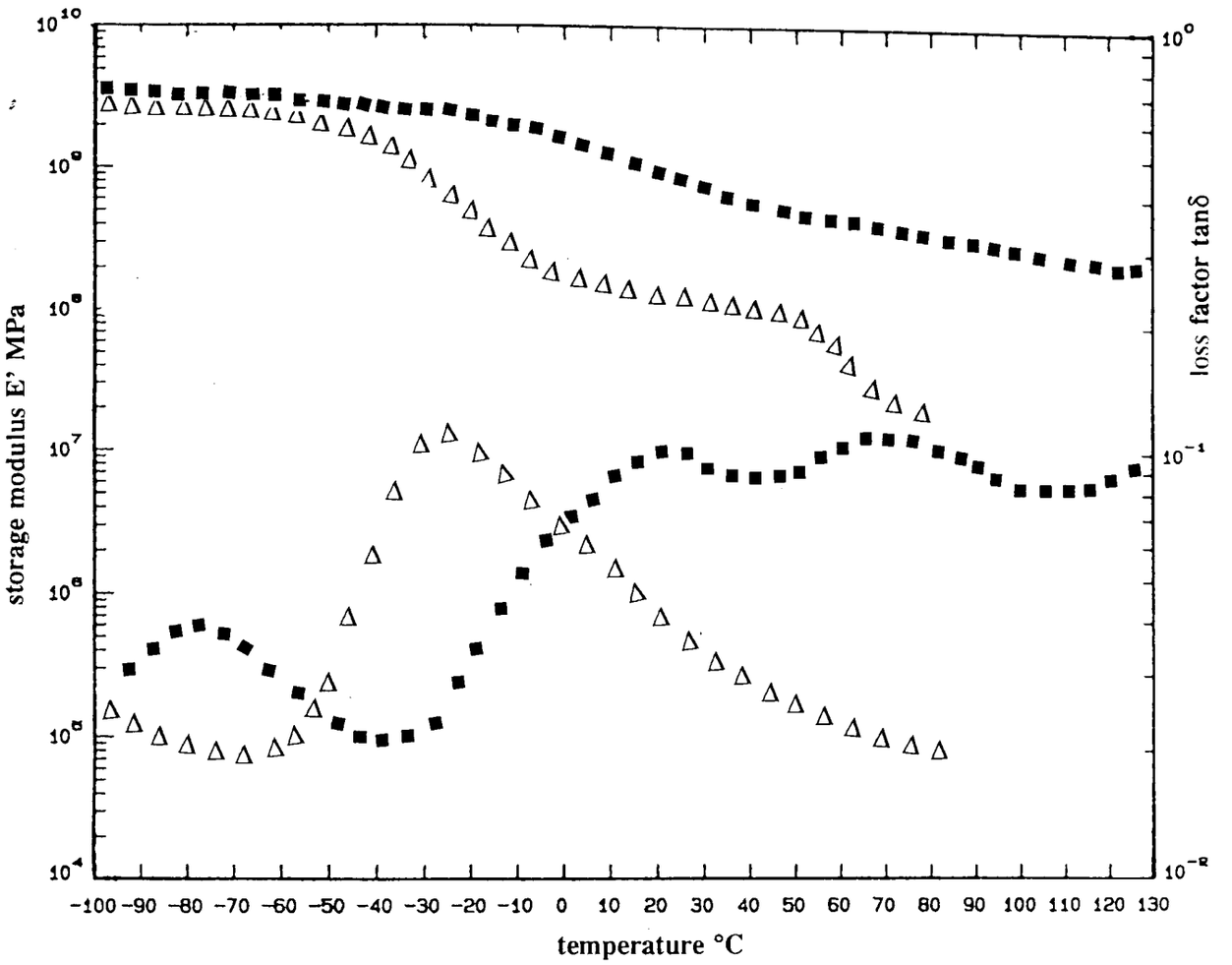

Figure 4.9 Dynamic mechanical spectrum of reaction PA6/EPR 90/10 blend and EPR

(■ PA6/EPR Δ EPR)

CHAPTER 5

REACTIVE POLYMERISED POLYAMIDE 6 / PP BLENDS MADE BY REACTIVE EXTRUSION

5.1 Introduction

In this work, a novel process is reported for in-situ reactive blending of a commercial grade isotactic polypropylene (PP) homopolymer with polyamide 6 prepared by activated anionic polymerisation of ∈-caprolactam on a fully intermeshing, co-rotating twin-screw extruder. A series of reaction blends with compositions 10, 30, 50 and 70% by weight of the PP component were prepared.

To investigate the effect of a commercial functionalised PP compatibiliser on these reaction blend, another series of functionalised reaction blends of PA6/PP-g-MA/PP were also prepared under similar reactive polymerisation conditions. Microstructure and mechanical properties of these reaction PA6/PP blends are analysed with respect to blend compositions and extrusion processing variables.

5.2 Experimental

5.2.1 *Materials and Blend Preparation*

∈-caprolactam, catalyst and activator used for the preparation of polyamide 6 (PA6) are described in Section 3.2.1.

Polypropylene (PP) used was GYM 45 (MFI=9) in powder form, supplied by Imperial Chemical Industries, United Kingdom. The combatibiliser used was maleic anhydride grafted polypropylene copolymer (PP-g-MA), Polybond® 3001 in powder form (6% maleic anhydride, MFI=7), supplied by BP Performance Plastics, United Kingdom.

For the non-compatibilised blends, percentage compositions by weight of PA6/PP i.e. 90/10; 70/30; 50/50 and 30/70 were prepared in batches of 500gm. These blend materials were thoroughly tumble mixed before being introduced into the K-Tron volumetric feeder of the intermeshing, co-rotating twin-screw extruder of diameter 40 mm and a L/D ratio of 21, as described in Section 3.2.2. These non-compatibilised reactive polymerised PA6/PP blends are coded as "reaction" blends.

For the compatibilised blends, similar percentage compositions by weight of PA6 and PP were prepared. In addition, 5% by weight of commercial grade PP-g-MA (in terms of the weight composition of PP in the blend) were also added to the blend material. These blend functionalised PA6/PP blend series are coded as "functionalised reaction" blends.

For both the reaction and functionalised reaction PA6/PP blends, the same extruder configuration and temperature profile was used as for PA6 preparation (Figure 3.2). A fixed screw speed of 150 rpm was employed throughout the in-situ polymerisation and blending extrusion process. The melt extrudate after exiting from the 4 mm die was water-quenched at room temperature, and collected as either 60 mm length rods or pellets. These as-extruded blend samples were then extracted with boiling distilled water in a Soxhlet apparatus for 12 hours to remove residual caprolactam monomer and other low molecular mass oligomers, followed by drying in vacuo at 110°C for another 24 hr. All the washed and dried reaction PA6/PP blend materials were then stored in dessicators at room temperature (23°C) for 7 days prior to injection moulding for test specimen preparation and structural analysis. Some samples after residue monomer extraction and drying were also annealed at 180°C for 90 minutes in vacuo, followed by slow cooling in air to room temperature while with others, the PP phase was extracted with boiling xylene in a soxhlet apparatus for 12 hr and dried in vacuo at 110°C for another 24 hr.

For comparative studies, a commercial PA6/PP material of composition 70/30 with an unknown compatibiliser (ORGALLOY 6000R, supplied by Elf Atochem, France) in pellet form was also used.

Another PA6/PP blend series was also prepared by mechanically blending pellet forms of commercial grades of PA6 and PP in compositions similar to those of the reaction blends using a conventional twin-screw co-rotating extruder. The PA6 used is a hydrolytic polymerised grade material supplied by SNIA, Italy (ASN 27; $\overline{M}_w$=35,000; MFI=25). PP used is an isotactic homopolymer supplied by ICI, U.K. (GY45; MFI=13; $\overline{M}_w$=60,000). The blend extrudates formed were water-quenched and then pelletised. Test specimen were also prepared under similar conditions as described earlier for comparative structural and morphological evaluations with the reaction blends. These mechanical blended PA6/PP materials are coded as "mechanical" blends.

5.2.2 *Test Specimen Preparation*

Experimental details for injection moulding of tensile and impact test specimens and conditioning prior to properties characterisation are as described in section 3.2.2. However, for the PA6/PP blend of composition 30/70, lower temperature settings of 220°C, 220°C, 215°C and 215°C were used at nozzle, front of screw, middle of screw and rear of screw during injection moulding. This was done to avoid degradation of the PP component in the blends.

5.2.3 *Analysis of Structural and Physical Property*

Experimental procedures for the structural (WAXD, DSC, IR, SEM) and physical properties characterisation are as outlined in Sections 3.2.6 and 3.2.7. All structural

analysis and mechanical properties are evaluated in a "dry as-moulded" condition at room temperature of 23°C.

5.3 Results and Discussion

5.3.1 *Reaction and Mechanical PA6/PP Blends*

5.3.1.1 *Wide Angle X-Ray Diffraction*

Typical wide-angle X-ray diffraction (WAXD) equatorial scans for the reaction PA6/PP blends are illustrated in Figure 5.1.

For the 90/10 blend prepared by water-quenching , a mixture of α_1 ($2\theta=19.6^\circ$) and α_2 ($2\theta=23.5^\circ$), and γ reflection ($2\theta=21.3^\circ$) characteristics of PA6 crystalline phases are observed [Figure 5.1 (i)]. This WAXD profile appears to be similar to that obtained for the pure PA6 sample prepared at 150 rpm with air cooling [Figure 3.10 (iii)]. However, as discussed in Section 3.3.4.1, upon annealing treatment of this air-cooled pure PA6 sample at 180°C for 90 minutes, it is observed that the γ crystalline peak has disappeared and assumed to have transformed into the thermally more stable α form [Figure 3.10 (iv)]. In this case, for the water-quenched, reaction PA6/PP blend of composition 90/10, it is rather surprising to observe that both the α and γ characteristic reflection peaks are still present after the annealing treatment. This observation infers that the γ crystalline phase formed in this reaction PA6/PP blend is thermally more stable as compared to that obtained from the air-cooled, pure PA6 material.

Although this water-quenched reaction 90/10 blend contains 10% by weight of PP component, it is however, rather surprising not to observe any characteristic X-ray diffraction peaks associated with the PP homopolymer phase [Figure 5.2 (vi)]. The X-ray diffraction profile of another reaction sample of composition 90/10 but

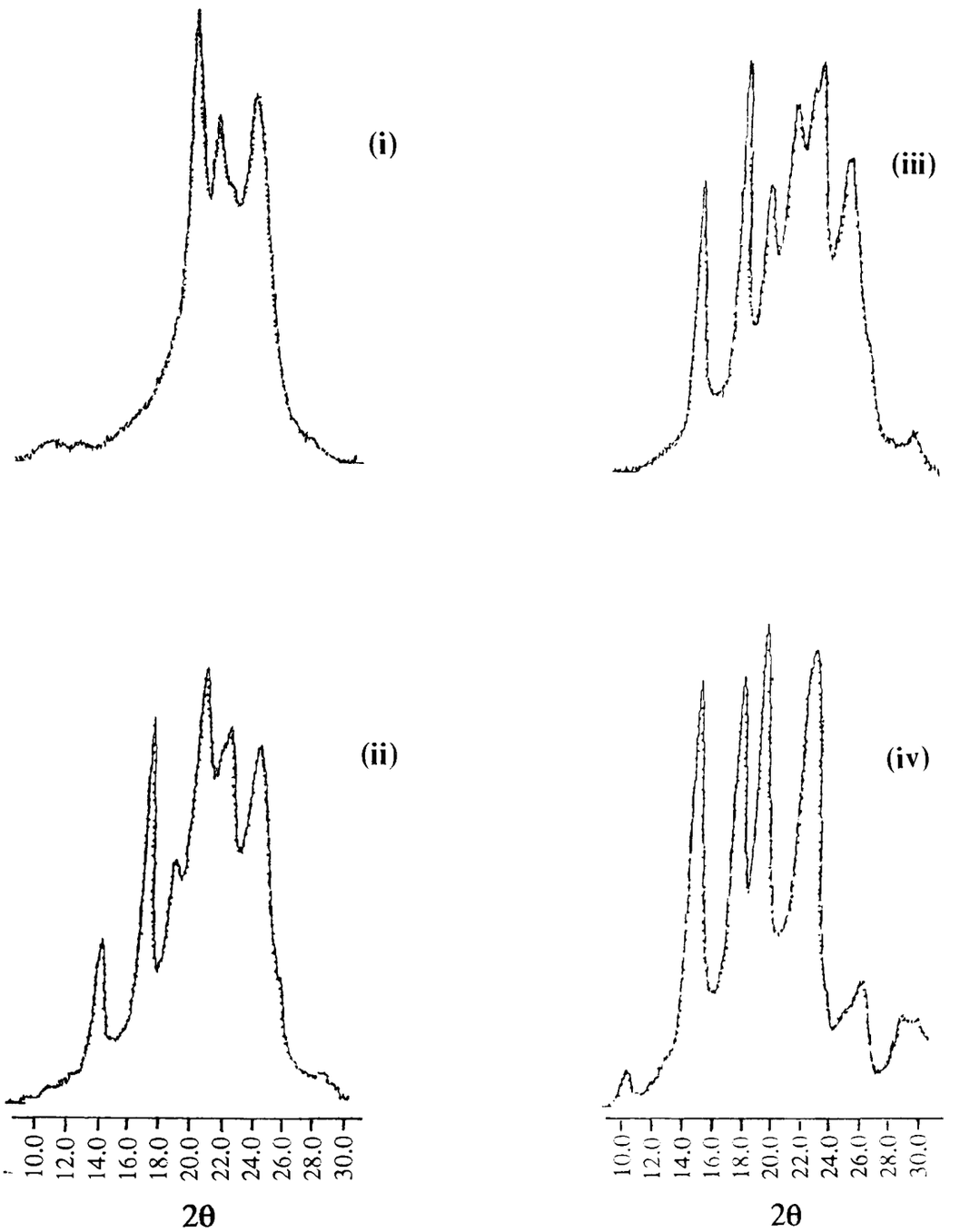

Figure 5.1 WAXD equitorial profile of reaction PA6/PP blends

(i) 90/10 (ii) 70/30 (iii) 50/50 (iv) 30/70

prepared by slow cooling in air after extrusion instead of water-quenching shows only the two characteristic α peaks. No characteristic γ peak of PA6 as well as other reflection peaks associated with the PP phase can be observed.

The WAXD results obtained for the 90/10 reaction blend samples prepared under these different processing conditions suggest that the γ phase of PA6 in this blend of composition 90/10 could only be formed as a result of fast cooling of the hot extrudate melt. **Addonizio** *et al.* [199] also reported the detection of the γ crystalline form of hydrolytic polymerised PA6 in the PA6/EVA blend using X-ray diffraction technique.

The equatorial diffraction profile for the 70/30 reaction PA6/PP blend is as shown in Figure 5.1 (ii). Here, in addition to the two characteristic α peaks of PA6 at Bragg angles $2\theta=19.6^{\circ}$ and 23.4°, four additional reflection peaks associated with the principal isotactic structural form of PP (α form) are also observed at Bragg angles $2\theta=14^{\circ}$; 17°; 19° and 22.5°. It is possible that the γ peak of the PA6 phase at $2\theta=21.3^{\circ}$ is also present but has been totally masked by the more prominent PP peaks. On the other hand, WAXD profile of another reaction PA6/PP blend of composition 85/15 prepared by water-quenching yield reflection peaks similar to those observed for the blend of 70/30. These observations suggest that for the reaction PA6/PP blends, phase separation of the two semi-crystalline components could possibly occurred at PP compositions between 10-15%.

The diffraction profile for the reaction blend with composition 50/50 [Figure 5.1 (iii)] shows continuous reduction of peak intensities for the PA6 α reflections but with corresponding increase in intensities associated with PP reflection peaks especially at $2\theta=22^{\circ}$. However, at this blend composition, the PA6 component still maintains the two α peaks at Bragg angles $2\theta=19.6^{\circ}$ and $2\theta=23.5^{\circ}$.

For the reaction PA6/PP blend of composition 30/70, the diffraction profile as exhibited in Figure 5.1 (iv) shows the disappearance of the PA6 α_1 reflection peak

as well as a much reduced intensity peak of the α_2 reflection. The general diffraction profile of this blend exhibits much similarity to that obtained for a pure isotactic PP homopolymer sample [Figure 5.2 (vi)].

WAXD profile for a commercial grade PA6 material synthesised by hydrolytic polymerisation (ASN 27, SNIA, Italy) is as shown in Figure 5.2 (v). An obvious difference between this profile and that observed for the pure reactive polymerised PA6 material [Figure 3.10 (i)] is that no characteristic α reflection peaks are observed. Instead, only a single broad reflection peak at $2\theta=21.6^{\circ}$ associated with the PA6 γ crystalline phase is obtained.

The diffraction profiles for the mechanical PA6/PP blend materials with similar compositions of 90/10; 70/30; 50/50 and 30/70 are displayed in Figures 5.2 (i) to (iv). As mentioned earlier, the PA6 component used in these blends is prepared by hydrolytic polymerisation.

A single, sharp reflection peak at $2\theta=21.3^{\circ}$ belonging to the γ crystalline form of the PA6 phase is observed for the mechanical blend of composition 90/10, together with two other weak reflections at $2\theta=14^{\circ}$ and $2\theta=16.8^{\circ}$ which are associated with the α peaks of the isotactic PP homopolymer [Figure 5.2 (vi)]. The appearance of these reflection peaks associated with both PA6 and PP phases suggests the formation of an immisible blend with 10% PP composition. These WAXD results are different from that obtained for the reaction blend with similar PP composition as discussed earlier which displayed no PP reflection peaks [Figure 5.1 (i)].

At PA6/PP composition of 70/30, the diffraction profile of the mechanical blend material shows again a gradual increase in peak intensities of the PP component at $2\theta=14.2^{\circ}$ and $2\theta=16.8^{\circ}$, rather identical to that observed for the reaction blend of similar composition [Figure 5.1 (ii)]. In addition, another weak reflection peak at associated with PP can also be seen appearing at Bragg angle $2\theta=19^{\circ}$.

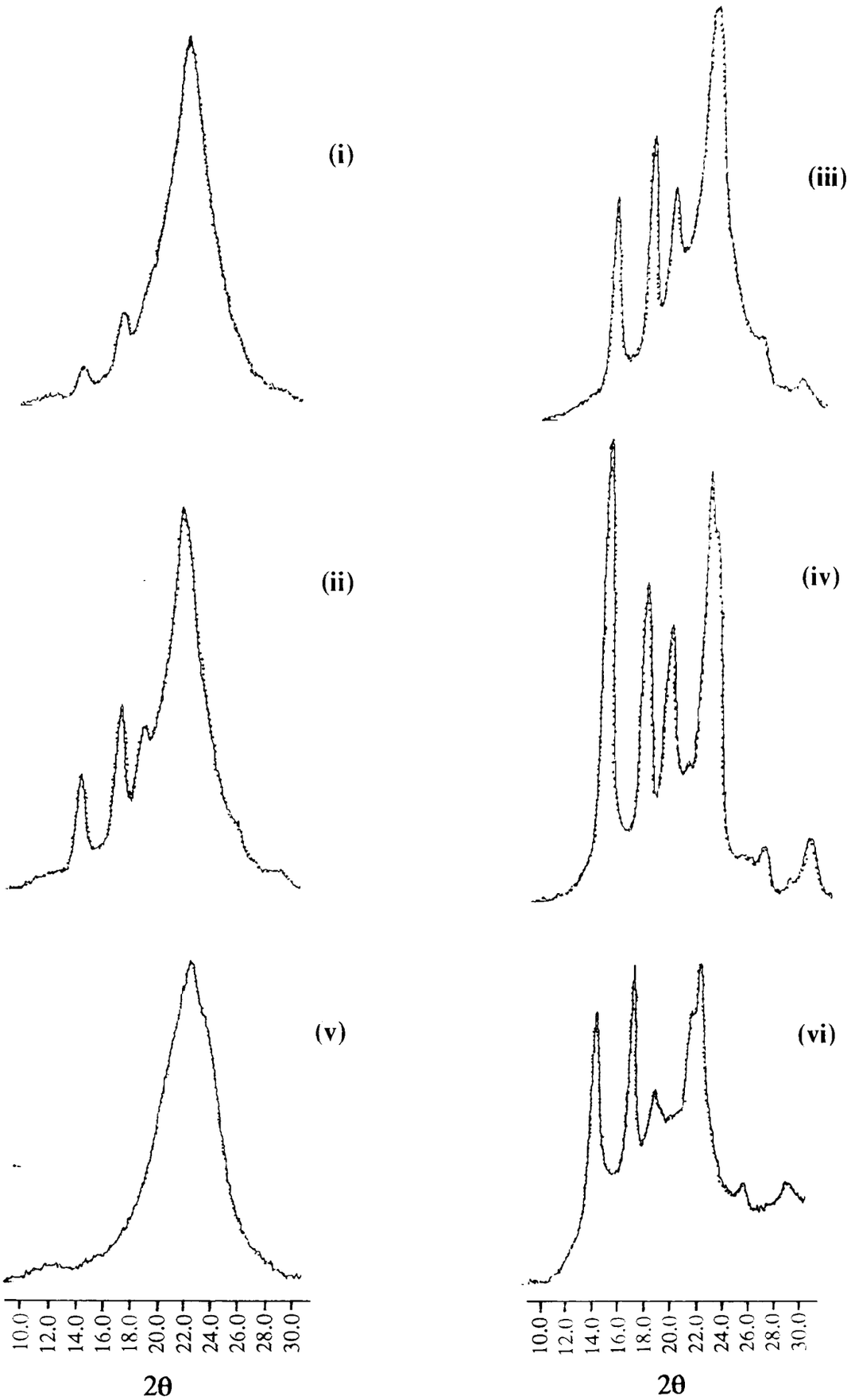

Figure 5.2 **WAXD equitorial profile of mechanical PA6/PP blends, PA6 and PP (i)90/10 (ii)70/30 (iii)50/50 (iv)30/70 (v)hydrolytic polymerised PA6 (vi)PP**

At higher composition of PP i.e. 50 wt % for the mechanical blend of PA6/PP, the reflection peak at $2\theta=19^{\circ}$ has further increased its intensity and caused partial masking of the γ peak associated with PA6 at $2\theta=21.3^{\circ}$. Also, two additional reflection peaks associated with PP which are broader but with lower intensities are observed to emerge at $2\theta=25^{\circ}$ and $2\theta=28^{\circ}$ respectively [Figure 5.2 (iii)].

Finally, for the mechanically blend with composition of 30/70, the WAXD diffraction profile shows complete disappearance of the γ phase of PA6 at $2\theta=21.3^{\circ}$ [Figure 5.2(iv)]. The diffraction profile obtained is in fact, very much similar to that recorded for the pure isotactic PP homopolymer [Figure 5.2 (vi)].

5.3.1.2 *Differential Scanning Calorimetry*

Typical differential scanning calorimetry (DSC) thermograms of the reaction PA6/PP blends are shown in Figure 5.3. Table 5.1 summarises the thermal data of the blend components from the DSC heating and cooling cycles.

For the blend with composition 90/10, only one melting endotherm was observed during both stage I and stage II heating cycles. The cooling thermogram for the sample also yield a single crystallisation exothermic peak [Figure 5.3 (i)]. The maximum melting peak during stage II heating occurred at 209.5°C and the maximum crystallisation temperature recorded is 182.7°C [Table 5.1]. These values correspond well with the melting and crystallisation peaks of the PA6 phase. It is indeed surprise not to observe both the melting and crystallisation peaks of the crystalline PP component which constitute 10% by weight in this blend composition.

The heat of crystallisation for the 90/10 composition blend is 63.4 Jg^{-1} which is similar to that observed for the pure reactive polymerised PA6 extruded at 150 rpm and water-quenched. However, the maximum crystallisation temperature was recorded at 182.7°C as compared to a peak crystallisation temperature of 179.5°C

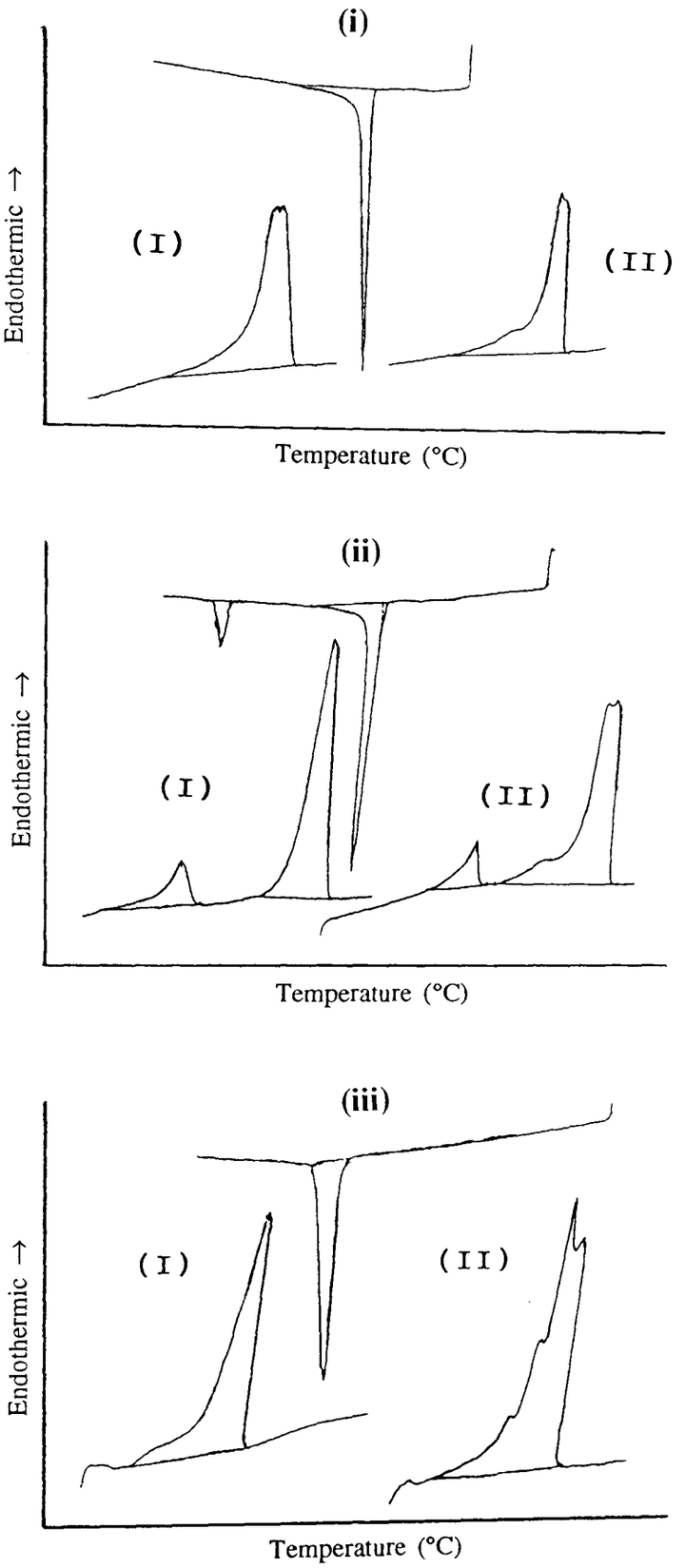

Figure 5.3 DSC thermogram of PA6/PP blends and PP homopolymer

(i) reaction 90/10 (ii) mechanical 90/10 (iii) PP

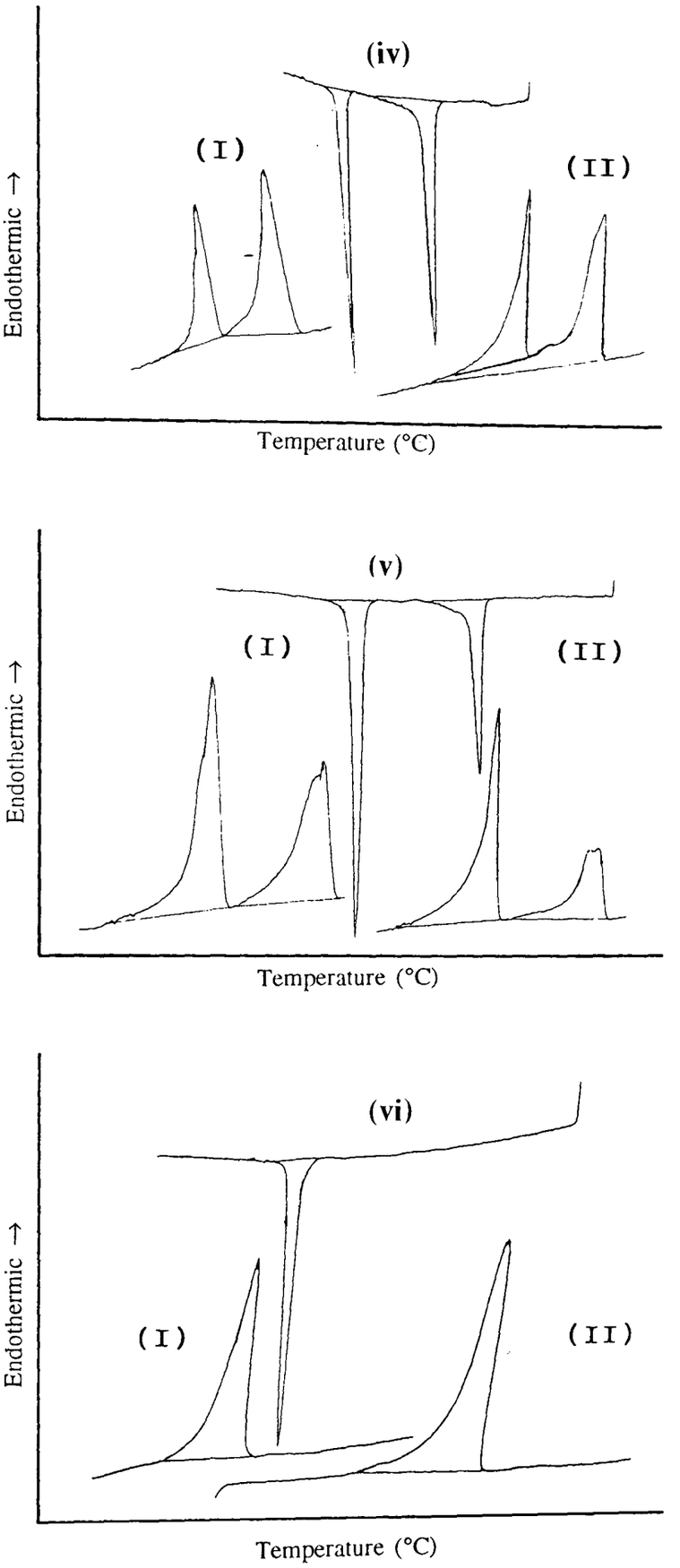

Figure 5.3(cont.) DSC thermogram of PA6/PP blends and PP homopolymer (iv) reaction 70/30 (v) reaction 50/50 (vi) reaction 30/70

Table 5.1 DSC thermal data of reaction PA6/PP blends, PA6 and PP

Sample*	T_{m1} (°C)		ΔH_{f1} ($J.g^{-1}$)		T_c (°C)		ΔH_c ($J.g^{-1}$)		T_{m2} (°C)		ΔH_{f2} ($J.g^{-1}$)	
	PA6	PP	PA6	PP	PA6	PP	PA6	PP	PA6	PP	PA6	PP
90/10	211.6	-	83.9	-	182.7	-	63.4	-	209.5	-	61.2	-
70/30	214.0	162.6	40.6	22.0	179.0	123.3	41.2	28.0	213.2	160.1	34.5	26.9
50/50	214.6	164.4	34.7	21.2	180.6	123.9	37.6	30.3	213.8	161.2	32.4	32.8
30/70	-	162.9	-	71.7	-	115.8	-	77.0	-	163.0	-	76.7
PA6	214.2	-	84.9	-	179.5	-	63.0	-	213.0	-	64.5	-
PP +	-	161.4	-	86.1	-	112.7	-	98.1	-	158.1	-	99.5

Note: * Reaction PA6/PP blend compositions.

\+ Commercial grade isotactic PP homopolymer

T_{m1}, T_{m2} Peak endothermic melting temperatures, stage I and II heating cycles.

T_c Peak exothermic crystallisation temperatures, cooling cycle.

ΔH_{f1}, ΔH_{f2} Heats of fusion, stage I and II heating cycles.

ΔH_c Heat of crystallisation, cooling cycle.

for the pure PA6 material. This enhancement of crystallisation temperature for the PA6 component in the reaction blend of composition 90/10 blend suggests possible nucleation effect of the apparently "amorphous" PP phase on PA6 during crystallisation stage. However, this is a rather unusual observation since at the crystallisation temperature of PA6, PP is still in a molten state!

Maximum endothermic melting temperature of the PA6 phase in the 90/10 blend during stage II heating cycle is observed to be about 4 °C lower than that of the pure reactive polymerised PA6, despite having rather similar level of crystallinity. These results inferred that possible larger and more perfect crystallites were formed during cooling of the pure PA6 material while the presence of 10% PP in the 90/10 blend may effect heterogeneous nucleation of the PA6 crystals which can lead to the formation of higher number of smaller and less perfect crystals.

DSC thermograms recorded for the mechanical PA6/PP blend of similar composition i.e. 90/10, is exhibited in Figure 5.3 (ii). Two distinct endothermic melting and exothermic crystallisation peaks corresponding to both blend components were observed in all the heating and cooling cycles. Observation of these transition peaks for both PA6 and PP indicates phase immisibility between the two semi-crystalline blend components. DSC thermogram for the pure, commercial grade PP homopolymer used in the reaction PA6/PP blends is illustrated in Figure 5.3 (iii) and the thermal data listed in Table 5.1.

The disapperance of the melting endothermic and crystallisation peaks for the PP component of the reactive polymerised 90/10 blend is indeed an unexpected observation. **Lambla** *et al.* [116] reported co-crystallisation phenomenon of a 50/50 composition PA6/PP blend with 7% grafted PP copolymer. The workers observed no crystallisation peak for the PP phase during the cooling cycle of the DSC run. However, distinct endothermic melting peaks of PA6 and PP are detected during both the stage I and stage II heating cycles. Their study concluded that the disappearance of the PP crystallisation peak was attributed to the suppression effect

of the PP crystallisation by the solidifying PA6 crystallites during the DSC cooling scan.

Xanthos *et al.* [200] also reported the absence of a polyethylene terephthalate (PET) crystallisation exotherm for a 65/35 blend of PP/PET with 6% by weight of a reactive acrylic acid grafted PP copolymer. The workers suggested that crystallisation of the PET component in the blend containing the grafted PP could be very slow and possibly occurred over a much larger range of temperatures during the DSC cooling scan. In other words , PET crystallisation was possibly suppressed during the cooling stage. The observation of a distinct PET melting peak in subsequent heating run seems to confirm this proposition.

Frensch *et al.* [201] studied the crystallisation and melting of polyvinylidene fluoride (PVDF) and polyamide 6,6 (PA6,6) by DSC. The workers also reported only one crystallisation exotherm is observed for the 85/15 blend at a temperature of 140°C, i.e. at the crystallisation temperature of the pure PVDF. However, subsequent DSC heating thermogram of this blend exhibits the normal melting endotherms of the blend components i.e. PVDF at 174°C and PA6,6 at 264°C. The workers proposed that the disappearance of the PA6,6 phase in the DSC cooling thermogram could possibly be attributed to co-crystallisation of the two component phases at the crystallisation temperature (140°C) of PVDF.

However, DSC results of our reaction PA6/PP blend with composition 90/10 prepared in this study are rather different from the observations reported above. This is because in our case, both the crystallisation and melting peaks of the PP component are not detected in all the DSC heating and cooling cycles even at very fast and slow heating and cooling rates.

Before attempting to postulate an explaination for this abnormal observation, it is sensible to explore the possible reaction mechanisms of the reactive blend components during the extrusion process. It is well established that polymer micro-

radicals can be formed due to extreme shearing action during the extrusion process. However, the ultimate fate of these radicals and their ability to co-react during the extrusion process are still unpredictable. Therefore, it is plausible to postulate that during this reactive polymerising cum blending process, micro-radicals of both PA6 and PP are formed under high shearing and mixing conditions. Assuming that these radicals will react with each other, then either PA6/PP copolymer or branched molecules of PA6 or PP can possibly be formed. The formation of either a copolymer or a branched PP can possibly be accounted for the disappearance of the melting and crystallisation peaks of the PP componennt in this PA6/PP blend during the DSC scans.

DSC thermograms of the other reaction blends with compositions 70/30 and 50/50 [Figure 5.3 (iv) and (v)] show clearly the presence of two melting and crystallisation peaks in both the heating and cooling cycles. These transition peaks are associated with the two semi-crystalline PA6 and PP components of the blend. The observation of two transition peaks for these blends suggests immisibility of the components at these compositional ratios.

Thermal data in Table 5.1 indicate that both the melting and crystallisation temperatures recorded for the PA6 phase showed no shift with respect to the blend compositions suggesting immisibility between the PA6 and PP components. However, it is significant to observe an enhancement of some 10-11 $^{\circ}$C for the PP crystallisation temperature in these two reaction blends as compared to that obtained for the pure PP homopolymer. These results suggest a strong nucleating effect of the sodifying PA6 on PP during its crystallisation.

The DSC thermogram of the 30/70 reaction PA6/PP blend is as shown in Figure 5.3 (vi). In this blend however, only one melting and crystallisation peak corresponding to the PP phase is observed in all the heating and cooling cycles. It is rather surprising not to observe the presence of a crystalline PA6 phase even at a theoretical blend composition of 30% by weight. An elevation of 3 $^{\circ}$C for the

crystallisation temperature of the PP phase is recorded with respect to the pure homopolymer suggesting again, possible nucleating effect of the non-crystallising PA6 component!

In a subsequent experiment, small pieces of material cut from thin sections of this blend sample were weighted and put inside a thimble for extraction with boiling xylene with the aim of removing the non-polar PP component. After 36 hours of extraction, the residue obtained was thoroughly rinsed with acetone and dried in a vacuum oven at 100°C. The dried residue was found to weigh only about 8 % of the original blend material. FTIR scans were then undertaken on a thin film obtained from the hot pressed extract. Weak absorption bands characteristic of PA6 were recorded [Figure 5.8 (i)]. The extract was also found to be readily dissolve in formic acid indicating the presence of only the PA6 phase.

Results obtained from these tests provide evidence for the presence of PA6 in this reaction PA6/PP blend of composition 30/70. However, since only less than a third of the expected PA6 component by weight was recorded after xylene extraction, indicating possibly much less amount of polymerised PA6 component were present initially in the blend before extraction. It is plausible that lower degree of polymerisation might have occurred during the polymersation/blending process leading to the formation of low molecular weight PA6 polymers which do not have the required minimum repeating units for crystallisation to occur. The presence of these low molecular weight "amorphous" PA6 materials nevertheless, could still impart some nucleating effect on the PP phase as evidenced from the 3°C enhancement of crystallisation temperature observed.

The disappearance of the PA6 crystallisation peak here also could not be explained by either the co-crystallisation or suppression of crystallisation phenamena as discussed earlier [199-201]. This is because no melting peak of the PA6 phase can be detected in both the stage I and II heating cycles.

This observation is however, postulated to be linked to a composite droplet phenomena similar to that reported by **Lavallee** *et al.* [202]. This phenomena is obtained from a two component system through a phase inversion mechanism whereby the dispersed phase (PA6) can contained small inclusions of the continuous matrix (PP) component. One of the effects of this dispersion structure of immisible blends is predicted to be total inhibition of crystallisation for the minor phase of the blend. This explaination could probably accounted for the disappearance of both the crystallisation and melting peaks of the PA6 component in the DSC thermograms [Figure 5.3 (vi)]. This phase inversion mechanism will be discussed in more detail with reference to the morphology of this reaction blend in Section 5.3.1.4.

5.3.1.3 *Fourier Transform Infrared Spectroscopy*

Application of infrared spectroscopy in characterisation of polymer blends is extensive. Fourier transform infrared spectroscopy (FTIR) is used to study hydrogen bonding as well as for identification of the mechanism of specific interaction in polymer blends. In general, these interactions not only affected the -OH absorption region (3500 to 3600 cm^{-1}) but also the C=O stretching (1737 cm^{-1}), the $-CH_2-$ symmetric stretching (2886 cm^{-1}) as well as the finger-printing frequency region (1300 to 650 cm^{-1}) and others [203].

The infrared spectra for the reaction PA6/PP blends prepared at compositions of 90/10, 70/30, 50/50 and 30/70 are shown in Figure 5.4. For comparative study, the infrared spectra of the mechanical PA6/PP blends of compositions 90/10 and 70/30, a pure PP homopolymer and a commercial grade PA6/PP alloy material (Orgalloy 6000R) are also exhibited in Figure 5.5.

As discussed in Section 3.3.4.3, the infrared spectrum for pure PA6 is characterised by free N-H stretching in the band region 3302 cm^{-1}, amide I (C=O) stretching at 1640 cm^{-1} and amide II at 1545 cm^{-1} which corresponds to coupling of NH

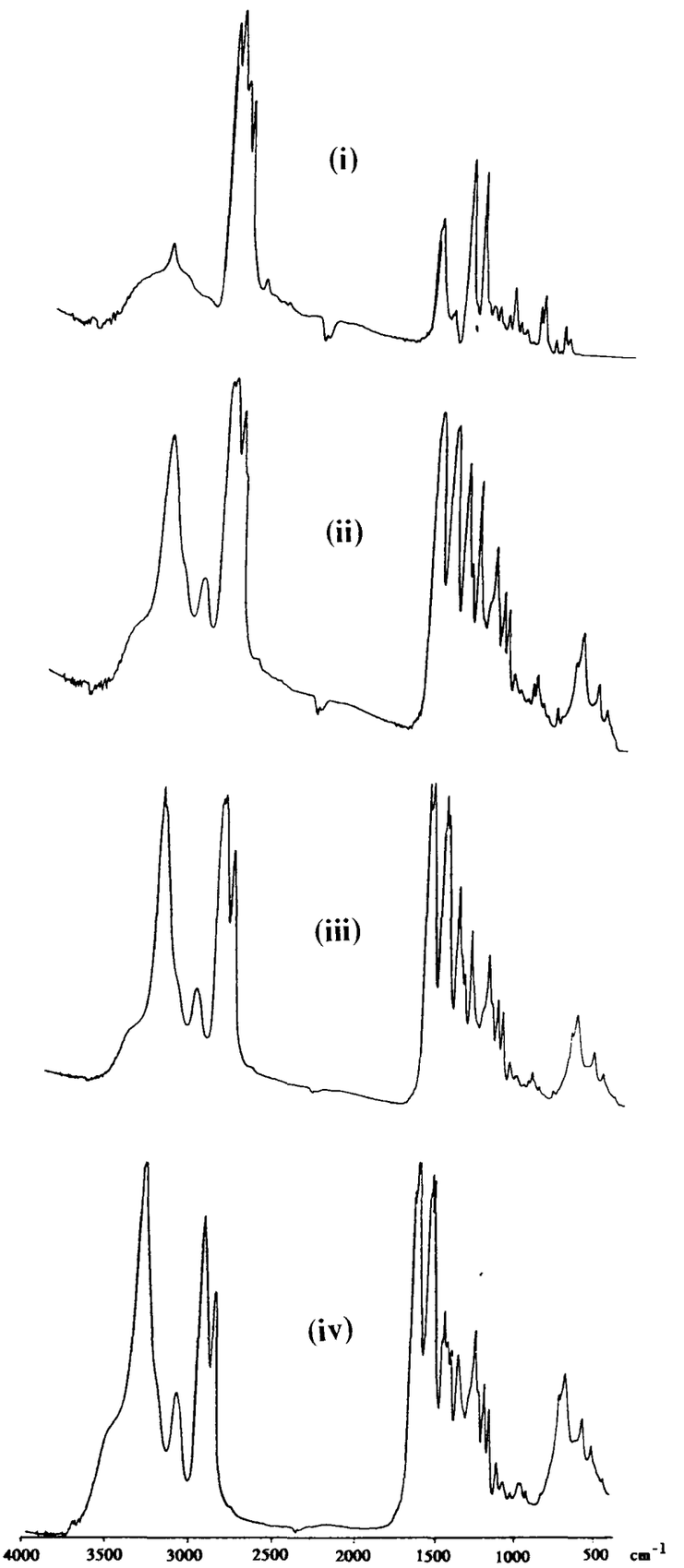

Figure 5.4 FTIR spectrum of reaction PA6/PP blends (i) 30/70 (ii) 50/50 (iii) 70/30 (iv) 90/10

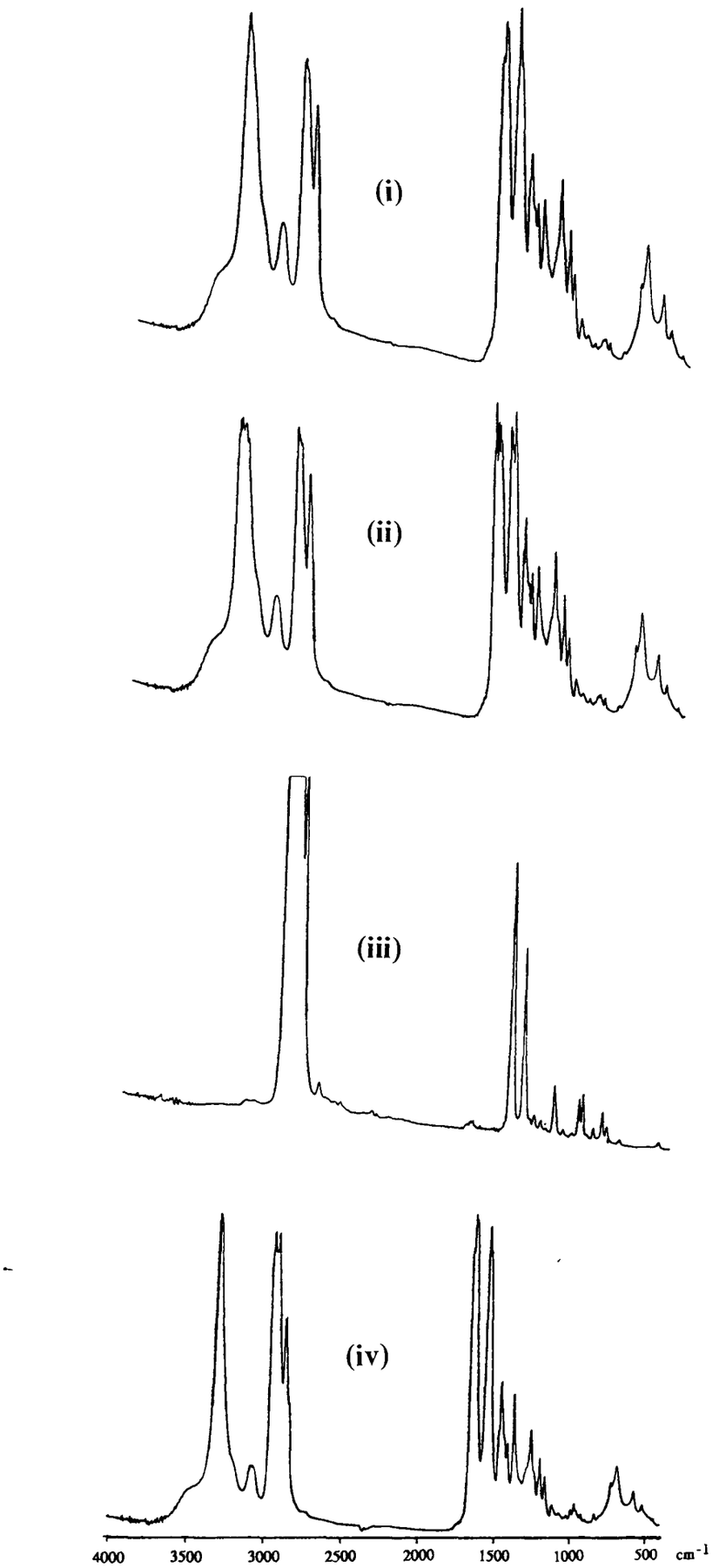

Figure 5.5 FTIR spectrum of mechanical PA6/PP, PP and commercial PA6/PP

(i) 90/10 (ii) 70/30 (iii) PP (iv) commercial PA6/PP

deformation with C-N stretching [Table 3.4]. Since we are interested in examining any possible interaction between the PA6 and PP phases in these blends, as well as to understand the reaction mechanisms involved, it is therefore also important to consider both the aliphatic -CH_2- stretching mode at 2860-2880 cm^{-1} and the olefinic -CH_2- stretching at band region 2900-3100 cm^{-1}. Table 5.2 summarises these characteristic bands associated with PA6 and PA6/PP blends.

No appreciable shift of the absorption band at 3300 cm^{-1} to lower frequencies is observed for all the reaction PA6/PP blends implying that the concomitant decrease in PA6 component of the blends has apparently no influence on the NH stretching deformation. However, shifts of the band at 1641 cm^{-1} to lower frequencies are observed for all the blends with respect to the pure reactive polymerised PA6. These observations suggest that changes in the blend composition has a significant effect on the C=O Amide I stretching deformation due possibly to the disruption of the hydrogen bonding as a result of less C=O groups present in blends of lower PA6 content.

As for the aliphatic -CH_2- stretching band region, a slight shift to lower frequencies at around 2934-2865 cm^{-1} is observed for the reaction blend sample of composition 90/10. On the other hand, reaction PA6/PP blends of other compositions recorded an increase in absorption frequencies suggesting minimum interaction effect on the CH_2 stretching deformation.

Similarly for the characteristic absorption band at 2903 cm^{-1} due to olefinic -CH_2- stretching, shifts of bands to higher frequencies are observed for all the blend samples with respect to the pure PP spectra. This observation again suggests no appreciable interaction exists between the blend components in the olefinic -CH_2- region.

However, it is really surprising to observe again a distinct absorption band at 1239 cm^{-1} with medium band intensity corresponding to a CN stretching deformation for

Table 5.2 FTIR charateristic absorption bands of reaction and mechanical PA6/PP blends

Band Assignments	Reaction PA6/PP Blends					PA6/PP Mechanical Blends			PP
	100/0+	90/10+	70/30+	50/50+	30/70+	100/0*	90/10*	70/30*	100/0
NH stretching (H bonded)/cm^{-1}	3300 (s)	3300 (vs)	3301 (vs)	3299 (m)	3301 (w)	3304 (m)	3302 (vs)	3306 (vs)	-
C=O amide I stretching/cm^{-1}	1641 (vs)	1636 (vs)	1632 (vs)	1634 (m)	1641 (w)	1634 (m)	1640 (vs)	1657 (vs)	-
CH_2 assym. (aliphatic)/cm^{-1}	2936 (s)	2934 (vs)	2938 (vs)	2948 (m)	2952 (w)	2932 (m)	2940 (vs)	2947 (vs)	2939 (vs)
CH_2 symmetric (aliphatic)/cm^{-1}	2865 (s)	2864 (s)	2866 (s)	2868 (m)	2872 (w)	2867 (m)	2867 (s)	2867 (vs)	2880 (vs)
Olefinic CH_2 stretching/cm^{-1}	-	2922 (m)	2922 (vs)	2922 (m)	2919 (m)	-	-	2923 (vs)	2903 (vs)
CN stretching deformation/cm^{-1}	-	1239 (m)	-	-	-	-	-	-	-

Note: Band intensity (code) : >3 (vs); >2 & <3 (s); >1 & <2 (m); <1 (w)

\+ PA6/PP blend composition (reaction blend).

* PA6/PP blend composition (mechanical blend).

the PA6/PP blend of composition 90/10. This absorption band is similar to the band observed earlier in the reactive polymerised PA6/EPR blend of composition 90/10 [Section 4.3.1.3]. The pure PA6 samples as well as all other reaction PA6/PP blends however, do not exhibit this particular absorption band. As discussed earlier in the case of the PA6/EPR blend, this unique absorption band can possibly provide some experimental evidence on the likely formation of a PA6/PP copolymer between the amide group of PA6 and the PP chain.

It is well known that when large elongational shear forces are involved in a process, mechano-chemical degradation can occur which will produce chain radicals [187]. The subsequent reaction then propagates through hydrogen extraction on a near polymer chains and terminates when two radicals react between themselves. In this way, branched molecules are possibly formed. When the system being processed is formed of two components such as PA6 and PP in the present study, the situation is more complex. Now two types of macroradicals can be formed. They, in turn, can either react with themselves or with radicals of different chemical nature forming, respectively, branched molecules and various types of graft copolymers [190].

It has been shown that [190] in an extrusion blending system involving polymers such as polyamides, including PA6 and polyolefins, macroradicals are formed. It has also been reported that PA6 tends to form radicals more easily than polyolefins in a homolytic chain scission process. The C-N bond in PA6 is known to be weaker than a C-C bond in polyolefins, the strength of the former being about 66 $kcal.mol^{-1}$, whereas the latter is about 85 $kcal.mol^{-1}$. Also the homolytic scission of the peptide (C-N) link depends very much on the structure in which it is located. The C-N band alpha to the carbonyl is stronger than that beta to the carbonyl group [193]. The radical density of the polymers, as expected, depends very much on the shearing forces imposed.

However, while the occurance of macroradicals during extrusion process employing large shearing forces is well established, the ultimate fate of these radicals and their ability to co-react is not necessarily preditable. **Braun** *et al.* [204] found no evidence of graft copolymers in a PA6/HDPE blend prepared by melt mixing in an extruder apparatus. They concluded, therefore that the macroradicals formed during the mixing process react only with themselves. Hence, it was of considerable interests in the present investigation to compare the relative abilities of PA6 and PP to form graft copolymers as well as branched homopolymers during blending under elongational shear stresses at elevated temperatures.

First, let us consider the possibility of two PA6 radicals react between themselves to form branched molecules. Molau tests conducted by dissolving 500 mg of PA6 granules in 25ml of 90% formic acid solution (Section 3.3.2) showed a colourless solution after 2 hours at room temperature of 23 °C. The complete solubility of PA6 in formic acid solution provide convincing evidence that no PA6 branched molecules are formed during the reactive polymerisation of ∈-caprolactam to PA6. In other words, macroradicals of PA6 extruded at 150 rpm possibly do not recombine among themselves to form branched structures during the extrusion process. The absence of the branched PA6 molecules in this reactive polymerised sample is the main reason that make it possible for our viscosity number determination in accordance with procedures of ISO 372 [Section 3.3.2]. As discussed earlier, ISO 372 does not recommend the use of this standard for PA6 prepared by anionic polymerisation due primarily to the problem of its insolubility in formic acid solution, presumably as a result of branching.

Next, let us consider the possibility of combination of PP radicals to form branched PP molecules. During the extrusion blending process, possibility also exist for PP macroradicals to react with another PP chain through hydrogen extraction or decomposition to form another new radical and an unsaturated group. The reaction will terminate when two macroradicals react between themselves, forming a branched PP molecule. It is well known that in the presence of oxygen, the double

bonds formed by the reaction sequence above can react to form aldehyde end groups and the carbonyl stretching vibration will exhibit an IR absorption band at the region 1720 cm^{-1}. Indeed, it is remarkable to observe that only the IR spectra of our reaction PA6/PP blend of composition 90/10 exhibits a weak band at 1719 cm^{-1} indicating very likely the formation of a highly branched PP.

The disappearance of the PP melting and crystallisation peaks in the DSC heating and cooling thermograms for this reaction blend sample [Figure 5.3 (i)] as well as the disappearance of the PP X-ray diffraction peaks in the WAXD profile [Figure 5.1 (i)] could possibly be ascribed to this highly branched chain which has the effect of discrupting the PP crystallite lattice and impede crystallisation of the polymer.

It has been reported that if a physical mixture of PA6 and polyethylene (PE) which is practically free of graft copolymers, is put into pure formic acid, the PA6 component will dissolve completely, leaving the PE component to precipitate in the form of coarse, white flakes in the solution. However, if the same solubility experiment is carried out with a PA6/PE blend which contain a certain amount of graft copolymer, or with a physical mixture to which graft copolymers of PA6/PE have been added, then a colloidal suspension will be observed without any insoluble precipitation. This solubility test is often being referred to as the Molau test [115].

Molau tests are conducted on the reaction blends of PA6/PP with different compositions by introducing 200 mg of the blend materials (sectioned into thin slides of thickness ~25 μm) into 50 ml of 90% formic acid at room temperature of 23 $^{\circ}$C. Pure reactive polymerised PA6 as well as the mechanical PA6/PP blend of composition 90/10 are also introduced into the formic acid to serve as controls.

For the reactive polymerised sample with composition 90/10, a colloidal suspension was observed floating in the upper portion of the solution after a reaction time of 5 hours, rather similar to the one observed for the reaction PA6/EPR 90/10 blend. No undissolved particles were visible [Figure 5.6 (ii) and (iii)]. However, the test

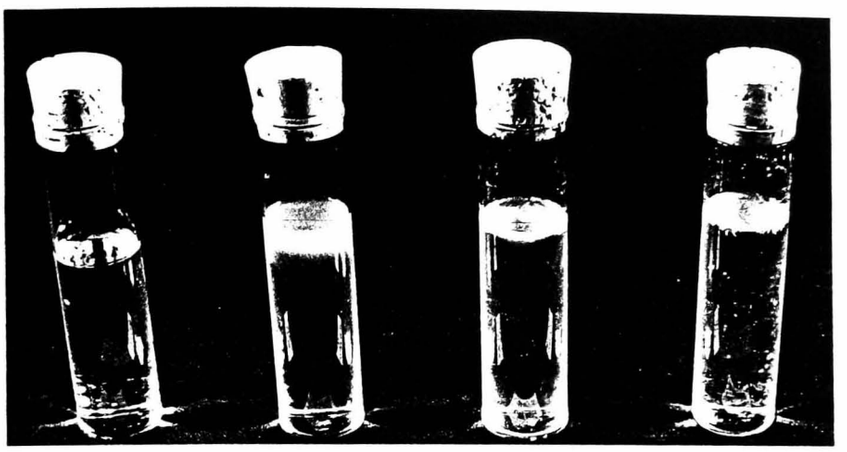

(i) (ii) (iii) (iv)

Figure 5.6 Molau tests for PA6 variants and blends

(i) reaction PA6 (ii) reaction PA6/PP 90/10
(iii) reaction PA6/EPR 90/10 (iv) mechanical PA6/PP 90/10

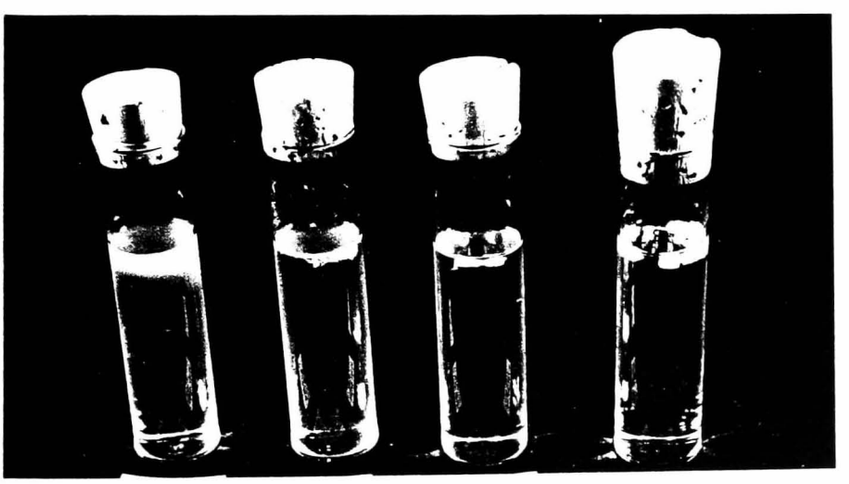

(i) (ii) (iii) (iv)

Figure 5.7 Molau tests for reaction PA6 blends

(i) 90/10 (ii) 85/15 (iii) 70/30 (iv) 50/50

result obtained for the mechanical blend of similar composition shows the presence of undissolved white flake-like particles floating on top of the solution [Figure 5.6 (iv)]. On the other hand, a clear solution is obtained for the pure reactive polymerised sample indicating complete miscibility of PA6 in formic acid [Figure 5.6 (i)]. As discussed earlier, this result also discards any doubt on the formation of branched PA6 which otherwise will not completely dissolve in the acid.

Another Molau tests are performed with similar amount of other reaction PA6/PP blend samples with compositions 85/15, 70/30 and 50/50. The results of Molau tests on the 85/15 blend showed a combination of turbid solution with small undissolved particles floating on top of the solution [Figure 5.7 (ii)] which is different from that of the 90/10 sample which showed no evidence of undissolved particles [Figure 5.7 (i)]. This observation agreed well with the findings of DSC and WAXD which displayed transition and reflection peaks of crystalline PP. As for the 70/30 and 50/50 blend samples, a clear solution with flake-like white particles floating on top were obtained in both cases [Figure 5.7 (iii) and (iv)]. FTIR spectra obtained from these undissolved particles confirmed that they are just PP material having being phase-separated by formic acid solution which has dissolved the PA6 phase.

In another Molau test, thin slices of the reaction PA6/PP blend materials with composition 90/10 were enclosed inside a stainless steel wire gauge of mesh size 0.1mm and submerged into 90% formic acid. After five hours, the "gel-like" material retained inside the gauge was removed and thoroughly rinsed with fresh formic acid, followed by methanol and distilled water. Similar procedures were repeated three times and the remaining gel material was then vacuum dried for 24 hours. FTIR spectrum were undertaken on this thin sheet of undissolved "gel" material as well as the undissolved white particles floating on the formic solution from the mechanical blend of 90/10.

FTIR spectra of the "gel" material showed the characteristic bands associated with PA6 while that obtained from the flakes showed predominantly a PP spectrum [Figure 5.8 (iii)]. These results confirmed the presence of a PA6/PP copolymer in the reaction PA6/PP blend of composition 90/10 which does not dissolve in formic acid. On the other hand, a physical mixture of PA6 and PP as obtained in the case of the mechanical PA6/PP blend can be readily separated into the two individual phases by formic acid since it only react with the polar component of the blend i.e the PA6 phase.

As discussed above, FTIR spectra [Figure 5.8 (iii)] obtained from the turbid suspension of the reaction PA6/PP blend of composition 90/10 shows characteristic bands of PA6. The absorption bands occuring at 3290 cm^{-1} (N-H stretching vibration), 1635 cm^{-1} and 1539 cm^{-1} (C=O stretching, amide bands I and II) suggest that a number of PA6 chains are bonded to the PP polymer chain to form possibly a PA6/PP copolymer, which is not affected by the formic acid solution. The shifts of these characteristic PA6 absorption bands to lower band frequencies present extra evidence on possible interactions between the PA6 and PP molecules in this graft copolymer. Also, the spectra of the formic acid extract sample shows a C-N stretching deformation absorption band at 1213 cm^{-1} which can possibly corresponds to the C-N band at 1239 cm^{-1} for the original undissolved reaction PA6/PP blend sample but has been shifted to lower band frequency as a result of formic acid extraction [Table 5.2].

The existance of the characteristic PA6 deformation bands and the detection of an unique CN band at region 1213-1239 cm^{-1} therefore suggest the possible formation of a PA6/PP graft copolymer as a result of macroradicals reaction.

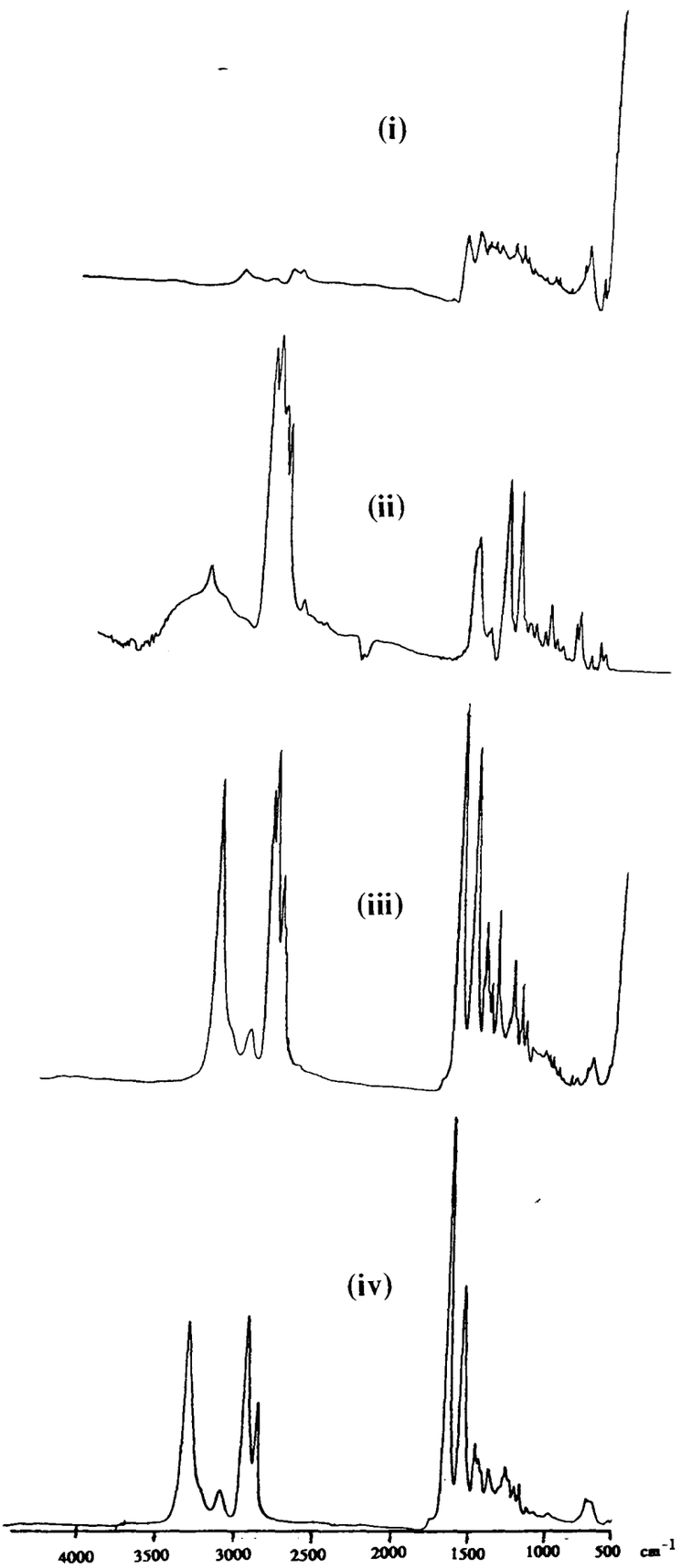

Figure 5.8 FTIR spectrum of insoluble extracts from Molau test

(i) 30/70 extract (after xylene extraction) (ii) reaction 30/70
(iii) 90/10 extract (after formic acid extraction) (iv) reaction 90/10

5.3.1.4 *Scanning Electron Microscopy*

The scanning electron microscopy (SEM) micrographs of the cryogenically fractured surfaces of the reaction and mechanical PA6/PP blend samples with composition 90/10 are shown in Figure 5.9.

For the reaction blend sample, the 10% PP phase (exists in an amorphous state as evidenced from DSC and WAXD results) is seen to disperse homogeneously over the continuous PA6 matrix. The morphology of this blend [Figure 5.9 (i)] is unexpectedly homogeneous and appears identical to that observed for the pure, reactive polymerised PA6 [Figure 3.21 (i)]. The apparent disappearance of the dispersed PP phase in the blend morphology could possibly be accounted for the absence of PP crystallinity in DSC [Figure 5.3 (i)] as well as the characteristic reflection peaks associated with the PP phase in the WAXD profile [Figure 5.1 (i)].

On the other hand, SEM micrograph of the mechanical PA6/PP blend with similar composition of 90/10 obtained by mechanically blending commercial grades of hydrolytic polymerised PA6 and PP using a conventional twin-screw extruder shows discrete PP spherical particles of dimensions 5-10 μm diameters distributed evenly over the continuous PA6 matrix [Figure 5.9 (ii)]. Clean detachment of these PP spherical particles from the continuous PA6 matrix is also evident suggesting very little interfacial adhesion between the two incompatible phases. This two phase incompatible morphology observed is similar to that reported by **Ide** *et al.* [104] and was described as clusters of PP "islands" in a sea of PA6. The workers explained the formation of this coarse morphology in terms of the large interfacial tension existed between the two incompatible phases.

SEM micrographs of the xylene etched samples of PA6/PP blends of composition 90/10 are shown in Figure 5.9 (iii) and (iv). For the reaction blend sample, the morphology shows fragmented lacy sheets of PA6 with fine holes lying on the continuous PA6 matrix. These holes are presumably occupied earlier by the

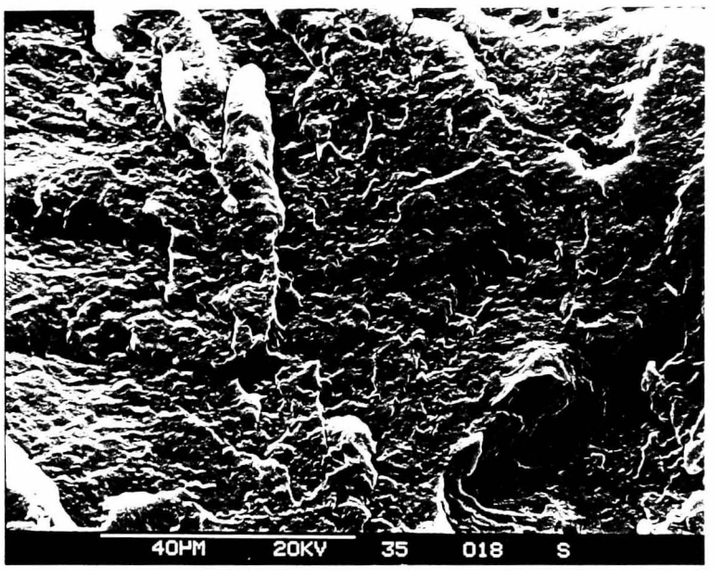

(i) reaction blend (as-fractured)

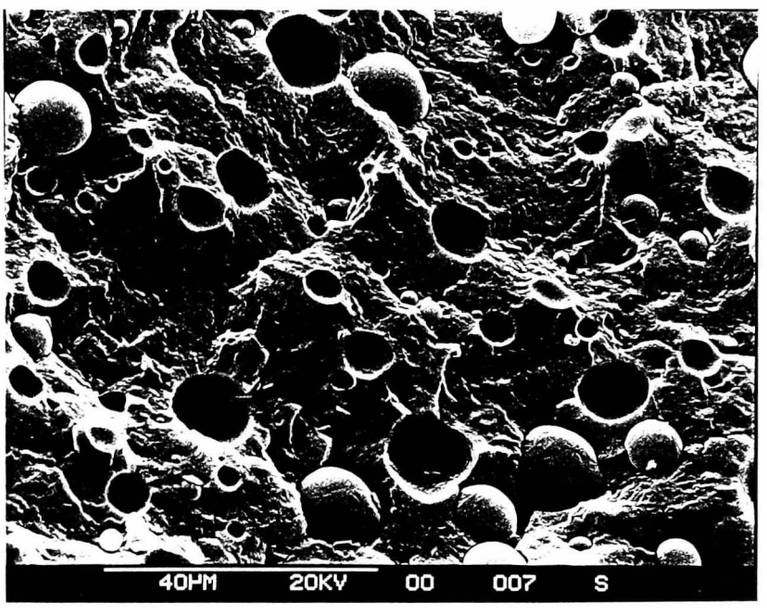

(ii) mechanical blend (as-fractured)

Figure 5.9 SEM micrograph of PA6/PP 90/10 blends

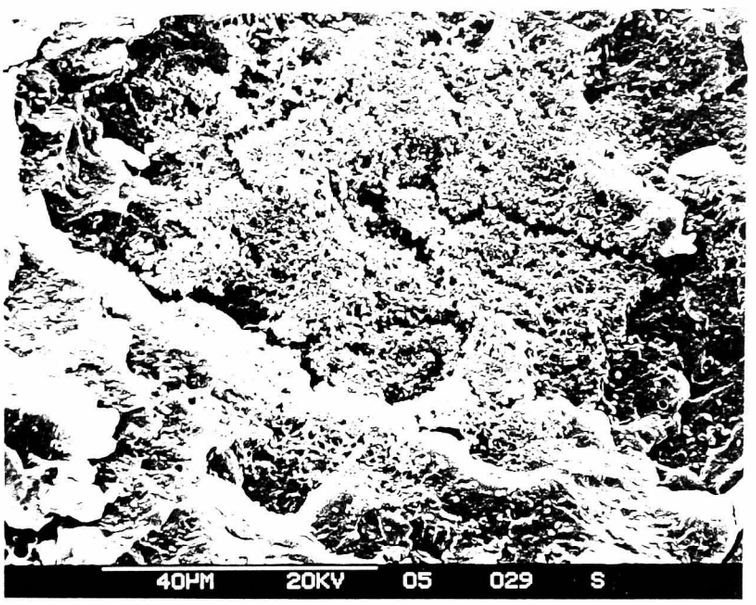

(iii) reaction blend (xylene-extracted)

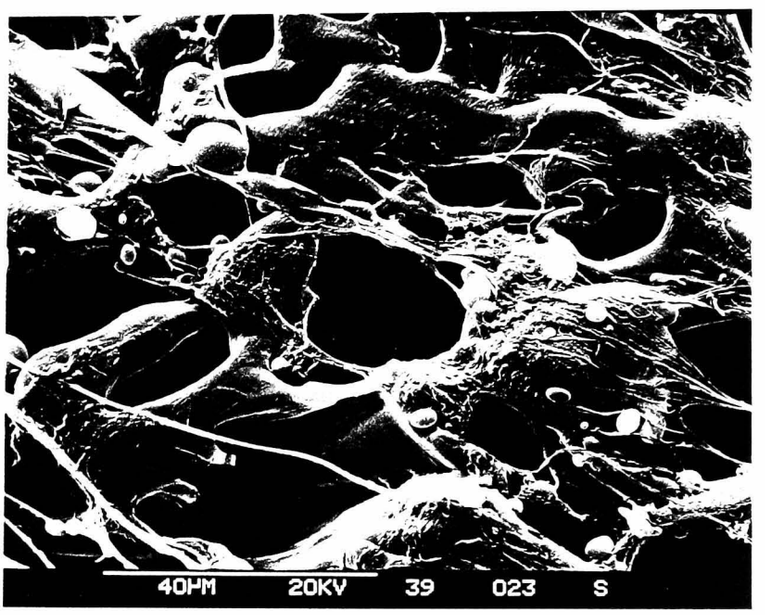

(iv) mechanical blend (xylene-extracted)

Figure 5.9(cont.) SEM micrograph of PA6/PP 90/10 blends

"amorphous" PP materials which have been dissolved by xylene. The etching effect observed on the blend morphology of this reaction sample provide excellent evidence that the PP dispersed phase is in fact present in the continuous PA6 matrix but could not be observed on the SEM micrograph. In the case of the mechanical blend sample, large spherical cavities of diameters 2-10 μm are observed which suggest poor interfacial adhesion between the PP dispersed phase and the continuous PA6 matrix.

On the other hand, SEM micrograph of the cryogenically fractured surface of a reaction 90/10 blend tensile test specimen exhibits a totally different morphology as shown in Figure 5.9(v). Here, an incompatible blend morphology is obtained with small PP spherical particles dispersed over the continuous PA6 matrix. This is a most unusual observation since as discussed above, a homogeneous blend morphology is observed from the same material in the as-extruded form. Both DSC and WAXD results of the injection test piece sample however, again did not yield evidence of PP crystallinity as well as X-ray diffraction peaks. It appears that the PP discrete particles observed from the morphology of the fractured injection test piece are still exist in an "amorphous" state!

The SEM micrograph of the reaction PA6/PP blend of composition 70/30 shows a typical blend morphology of two incompatible phases where PP spherical domains are dispersed in the continuous PA6 matrix [Figure 5.10 (i)]. The many smooth voids observed suggest that poor adhesion between the phases as a result of PP particles being pulled out during the cryogenic fracture process. The diameters of the dispersed spherical PP particles are in the range 0.5-5.0 μm. Other than spherical particles, some rod-like PP fibrillar structures with diameters of 3-5 μm are also observed. It is assume that these elongated PP structures are formed as a consequence of large elongational shear forces and the melt viscosity differences between the two phases which can cause the dispersed phase droplets to be frozen before they are subjected to "recoil or breaking-up" process to form spherical particles [206].

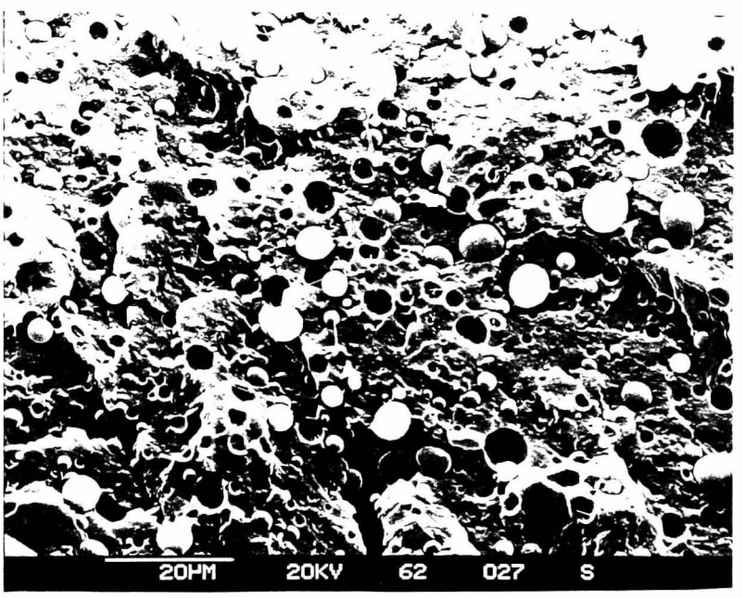

(v) reaction polymerised injection sample (as-fractured)

Figure 5.9(cont.) SEM micrograph of PA6/PP 90/10 blends

Utracki *et al.* [203] reported the formation of PA6 fibres in a HDPE/PA6 blend of composition 70/30 obtained from a capillary flow experiment and attributed the fibrillar formation to the higher melt viscosity of the dispersed PA6 phase. However, to-date no open literature has ever reported the formation of fibrillar structures for PA6 and polyolefin blends prepared from laboratory-scale extruder experiments.

It has been proposed that a higher viscosity dispersed phase can enhance the formation of fibrillar or rod-like structures, whereas a less viscous dispersed phase tends to form small droplets [203]. It is postulated that for this reaction blend material of composition 30% PP, certain degree of branching or cross-linking of the PP macro-radicals formed by mechanical degradation due to high shearing forces can possibly occurred. The branched molecules will then cause an increase in molecular size and hence melt viscosity of the PP phase. The increase in viscosity ratio formed between the dispersed (PP) and matrix (PA6) phases may subsequently affect the melt flow characteristics and ultimately favours the formation of some fibrillar structures instead of spherical particles for the dispersed PP phase.

SEM micrograph of the mechanical PA6/PP blend of similar composition 70/30 shows a conventional two phases incompatible blend morphology with only discrete PP spherical particles dispersed over the continuous PA6 matrix [Figure 5.10 (ii)]. Numerous cavities of dimensions 5-15 μm are observed on the fracture surface presumably due to pull-out of the PP particles during the fracture process. It is interesting, however, not to observe any rod-like PP structures on the PA6 matrix.

Figure 5.10 (iii) shows the SEM micrograph of the 70/30 reaction PA6/PP blend after etching with xylene. An array of cavities previously occupied by the PP dispersed phase are seen on the surface of the continuous PA6 matrix. Most of these cavities are small with diameters of 1-2 μm. Larger elongated cavities can also be observed which are of dimensions 10-15 μm length. These elongated cavities

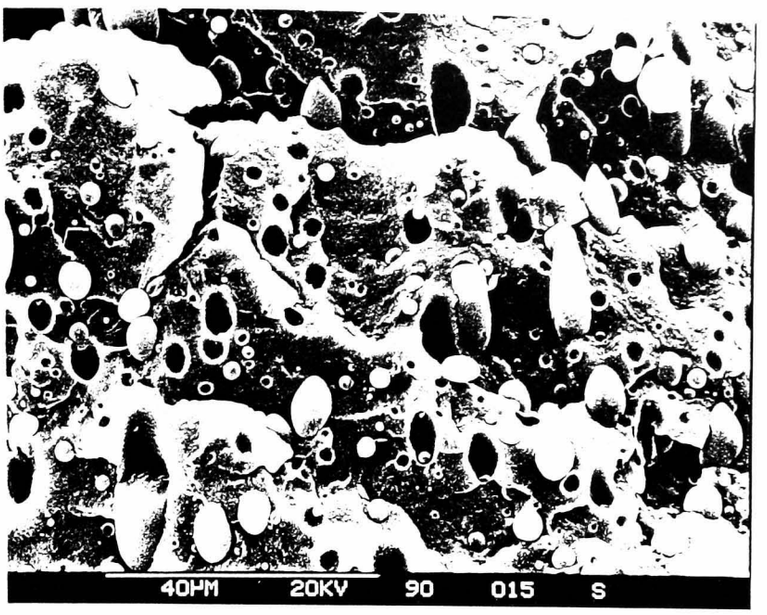

(i) reaction blend (as-fractured)

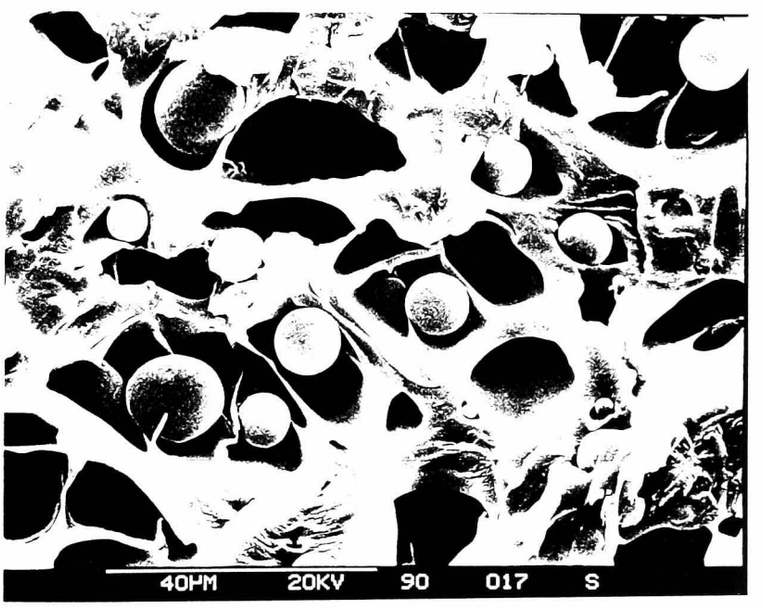

(ii) mechanical blend (as-fractured)

Figure 5.10 SEM micrograph of PA6/PP 70/30 blends

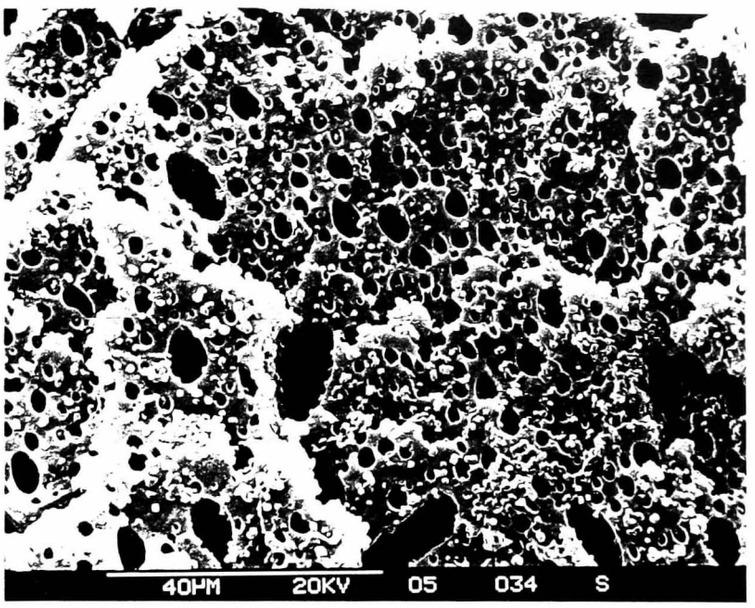

(iii) reaction blend (xylene-extracted)

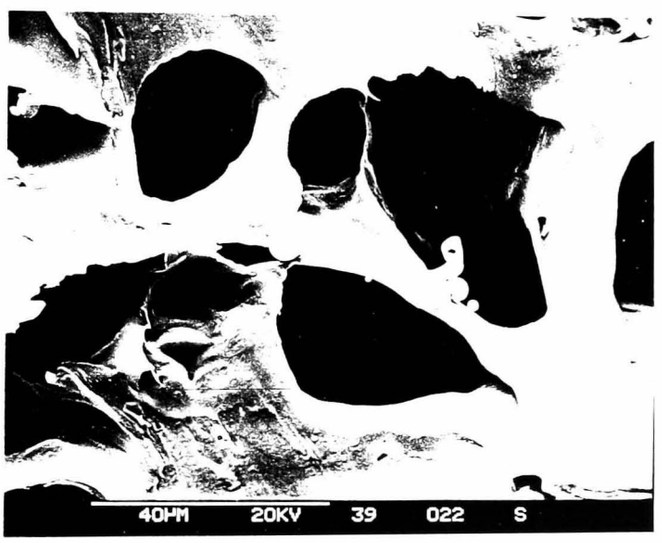

(iv) mechanical blend (xylene-extracted)

Figure 5.10(cont.) SEM micrograph of PA6/PP 70/30 blends

could possibly formed from clusters of dispersed PP particles either in spherical or fibrilllar structures.

The morphology of the xylene-etched mechanical blend 70/30 material is shown in Figure 5.10 (iv). Large cavities, previously occupied by PP particles are observed on the micrograph. The different morphology obtained from xylene treated surfaces of these two blends discussed above suggests that the reaction blend prepared from a polymerising PA6 can yield a finer PP dispersed phase as compared to that obtained from a conventional mechanical blend of similar composition but using commercial grades of PA6 and PP materials. When this blend material is subjected to etching with formic acid which is a solvent for the continuous PA6 phase, micro-fibrils of PP are observed [Figure 5.10 (v)].

The morphology of the reaction PA6/PP blend with composition 50/50 is as shown in Figure 5.11 (i). Again a two phase incompatible blend morphology is observed with PP fibrillar structures dispersed over the continuous PA6 matrix. In this blend morphology however, no discrete spherical particles of PP particles can be seen. Generally the fibrillar structures have diameters about 3-4 μm but larger clusters with diameters of 25 μm can also be observed. The cavities left over from cryogenic fracture process again depicted smooth internal surfaces, suggesting minimum interfacial adhesion between the two phases.

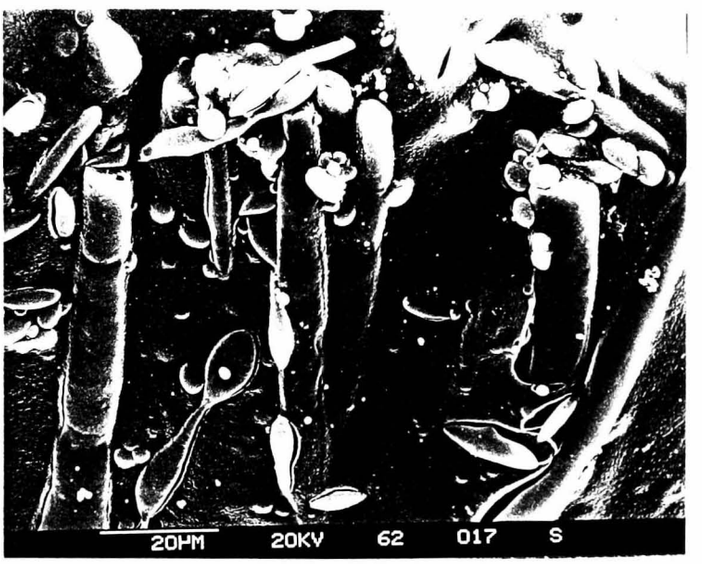

(v) formic acid-extracted

Figure 5.10(cont.) SEM micrograph of PA6/PP 70/30 blends

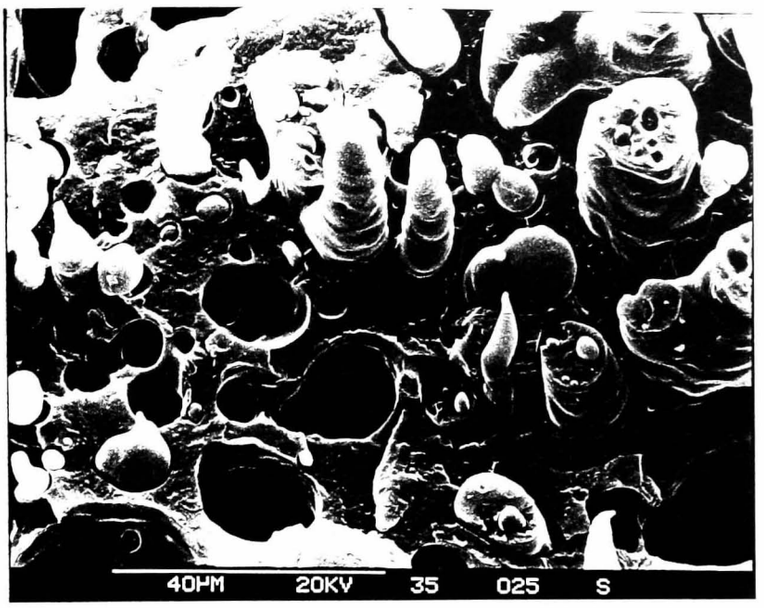

(i) as-fractured

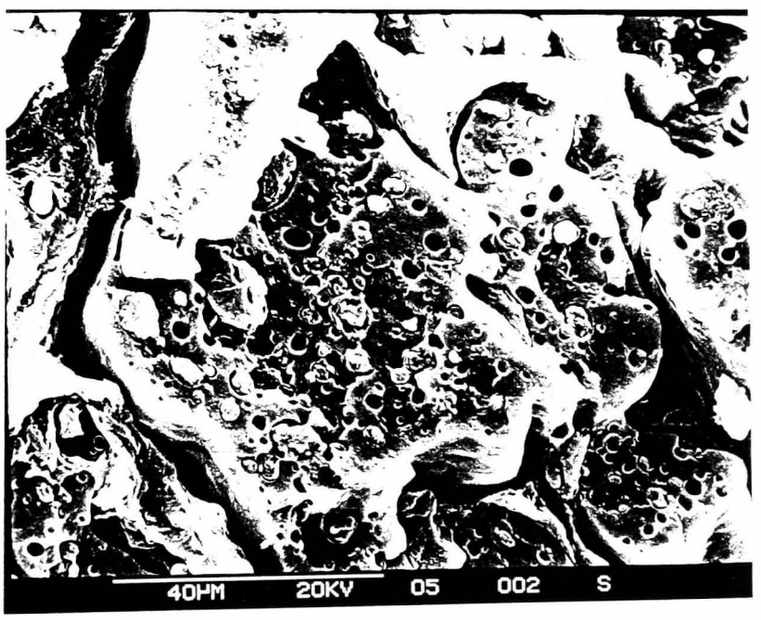

(ii) xylene-extracted

Figure 5.11 SEM micrograph of reaction PA6/PP 50/50 blend

The morphology of the reaction PA6/PP blend materials up to compositions of 50/50 are found to obey the rheological "viscosity-volume fraction" equation stated below [207]:

$$(\eta_1/\eta_2).(\varnothing_2/\varnothing_1) \quad \begin{cases} > 1 & \text{PHASE 2 continuous} \\ < 1 & \text{PHASE 1 continuous} \\ \approx 1 & \text{DUAL PHASE continuity} \end{cases}$$

where η = polymer melt viscosity

$\varnothing$ = volume fraction of component phase

This rheological equation states that phase 2 is continuous when the left hand side of the equation is greater than unity and similarly, phase 1 is continuous when the quantity is less than unity. Dual phase continuity arises when the quantity is approximately unity.

From melt flow index measurements [Table 3.6], η_{PA6}=3.9 and η_{PP}=9.

Then, at PA6/PP blend of composition 50/50,

$$(\eta_{PA6}/\eta_{PP}).(50/50) = 3.9/9 \text{ i.e. } < 1$$

Therefore as predicted, PA6 is the continuous phase. Similar calculations show that for the blends with compositions of 90/10 and 70/30, PA6 again forms the continuous matrix phase.

The morphology of the reaction PA6/PP blend of composition 50/50 after xylene extraction is as shown in Figure 5.11 (ii). The blend morphology shows the disappearance of majority of the PP fibrillar structures as a result of xylene extraction. It can be observed that large boundary cleavage regions are present on

the continuous PA6 matrix surface which could possibly accounted for the inferior mechanical properties [Section 5.3.1.6] for this blend sample.

Electron micrographs of the reaction PA6/PP blend with composition 30/70 is as shown in Figure 5.12 (i). A complex blend morphology is observed in this case where clusters of "honey-comb" globules are observed scattered over the continuous matrix. Neither fibrillar structures nor spherical particles can be seen on the fracture surface. On closer examination of the hollow "honey-comb" globules revealed evidence of fine sub-inclusions of another interpenetrating network-like layers scattered over the entire interior surface of the structures.

The boundary regions of the continuous matrix surrounding each of those globules is smooth indicating again minimum or no adhesion between the phases. The rather spacious boundary cleavages are postulated to have occurred as a result of recoiling action of the honey-comb structures during the cryogenic fracturing process. The interior wall surfaces of the empty cavities on the continuous matrix also exhibited network structures. These cavities are presumably formed from clean pull-out of the honey-comb globules without subsequent recoiling during fracture.

The morphology of this blend is similar to the composite droplet morphology reported by **Lavallee** *et al.* [202] and **Sorensen** [208]. This composite morphology is defined as a two component system where the dispersed phase contains small inclusions of the matrix component. These researchers concluded that similar blend morphology can only be obtained through phase inversions of the blend components at certain viscosity ratio and compositional ratios stated in the viscosity-volumn ratio equation [206].

Using the rheological viscosity-volume fraction equation and from melt flow indices measurements again, $\eta_{PA6}=3.9$; $\eta_{PP}=9$; $\varnothing_{PA6}=30\%$; $\varnothing_{PP}=70\%$, we have

$$(\eta_{PA6}/\eta_{PP}).(\varnothing_{PP}/\varnothing_{PA6}) = (3.9/9)x(70/30) \approx 1$$

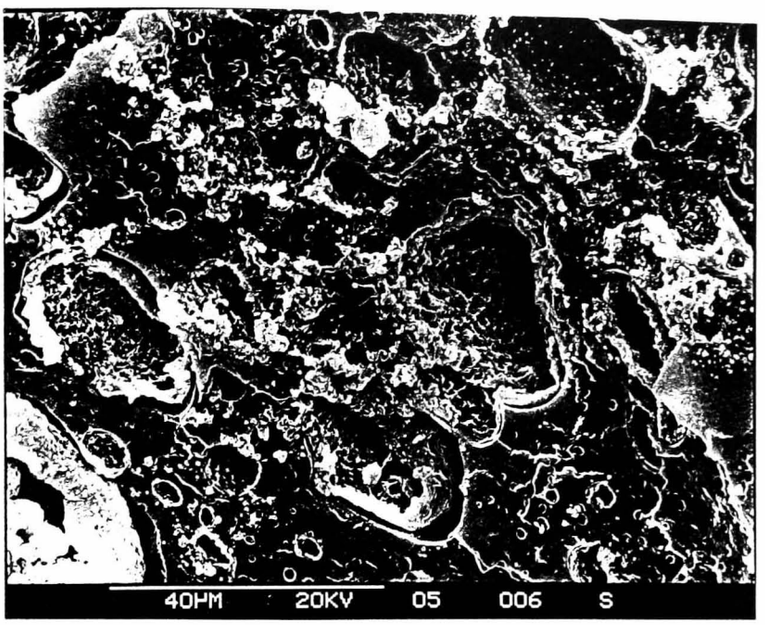

(i) as-fractured

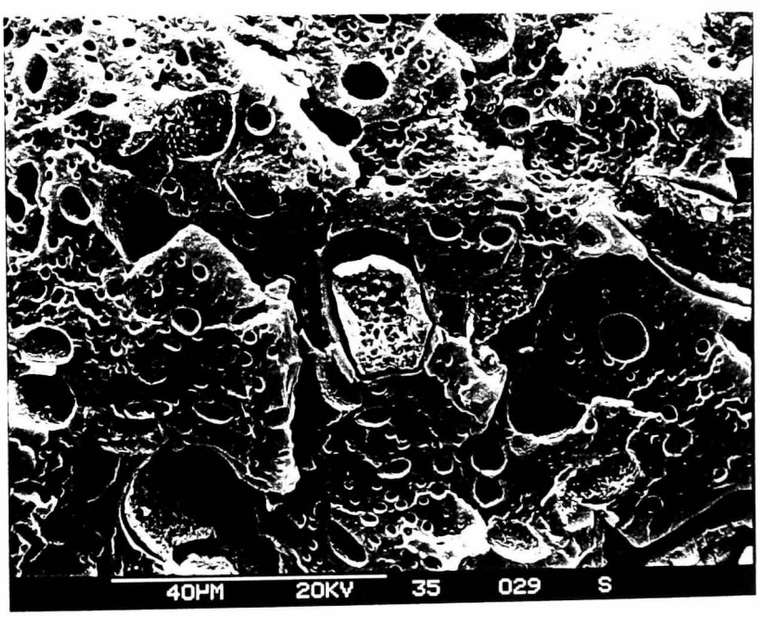

(ii) xylene-extracted

Figure 5.12 SEM micrograph of reaction PA6/PP 30/70 blend

This relationship implies that at this particular blend composition, the reaction blend is approximately exist in a state of DUAL PHASE CONTINUITY which has been defined as a region of space where each of the two phases maintains some degrees of continuity [206]. At this composition of 30/70, phase inversion between the reaction blend components PA6 and PP phases has possibly occurred and PA6 materials are now presumed to disperse over the continuous PP matrix. From this argument, it is therefore logical to suggest that the honey-comb structures are basically PA6 phase with inter-penetrating network structures of PP.

Electron micrograph of the 30/70 reaction blend etched with xylene is as shown in Figure 5.12 (ii). It is observed that the honey-comb globules did not seem to have affected much by xylene providing evidence that it could possibly be composed of majority PA6 phase. The PP continuous matrix surface also appears to be not much affected by xylene. This could possibly attributed to the fact that xylene etching treatment is not strong enough to dissolve the PP phase which is now constituting the major crystalline phase. This hypothesis is confirmed when boiling xylene is used which readily dissolves the blend material leaving behind flakes of PA6 material which has been confirmed by FTIR analysis [Figure 5.8 (i)].

On etching this blend sample with fuming formic acid, only cavities with smooth interior linings are observed suggesting the removal of the PA6 which formed majority portion of the "honey-comb" structures [Figure 5.12 (iii)]. This morphological observation with formic acid etching also provide additional experimental evidence on the presence of "amorphous" PA6 in this reaction PA6/PP blend of 30/70.

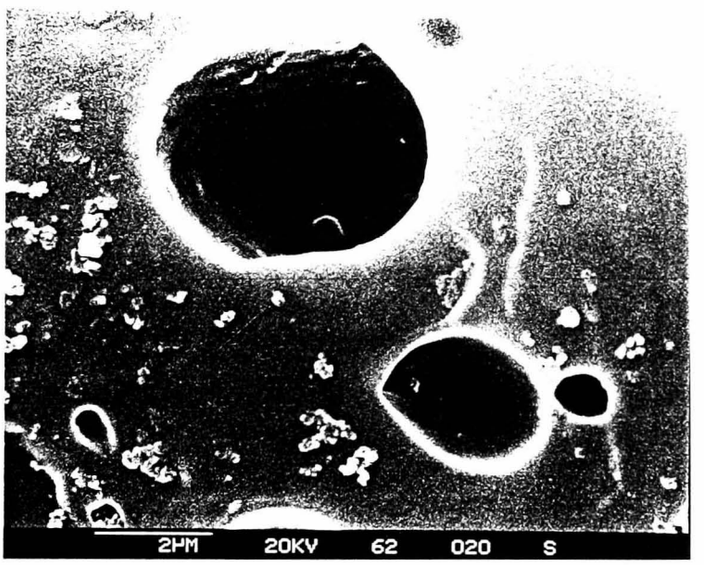

(iii) formic acid-extracted

Figure 5.12(cont.) SEM micrograph of reaction PA6/PP 30/70 blend

5.3.1.5 *Melt Flow Index and Moisture Content*

The melt flow indices (MFI) and moisture content of the reaction PA6/PP blends are listed in Table 5.3.

Higher MFI values for the blends are observed with higher compositions of PP implying lower melt viscosity of the material. Comparing the MFI of the PA6/PP blends with that of the pure reactive polymerised PA6 samples reveals some interesting observations. PA6/PP blend with composition 90/10 exhibits only slightly higher MFI value (5.2 g min^{-1}) as compared to that obtained from a pure PA-6 extruded at 150 rpm (3.9 g min^{-1}). The blend with composition 70/30, on the other hand, recorded a value rather similar to that of the pure PA6 material extruded at 50 rpm. As discussed in Section 3.3.2, PA6 extruded at 50 rpm yields the lowest molecular weight in the reactive polymerised PA6 series. Therefore these MFI results indicate that incorporation of PP into the PA6 matrix has the effect of reducing the molecular weight of the PA6 phase leading to lower melt viscosity. No MFI value is obtained for the blend with composition 30/70 since the experimental condition used (235 °C) is too severe for the material.

5.3.1.6 *Mechanical Properties*

The stress-strain curves obtained for the reaction PA6/PP blend materials show decreasing necking behaviour with increasing PP compositions. The mechanical properties of the blends are summarised in Table 5.4.

The blend material of composition 90/10 recorded the highest tensile strength of about 53 MPa which is slightly lower than that attained by the pure reactive polymerised PA6 sample extruded at 150 rpm. The tensile strengths of other reaction PA6/PP blends with higher PP composition recorded only half the values as that obtained by the 90/10 material. These rather inferior properties could

Table 5.3 Melt flow index and moisture content of reaction PA6/PP blends

Sample*	Melt Flow Index (g.10 min.$^{-1}$)	Moisture Content (%)
90/10	5.2	1.42
70/30	7.1	1.35
50/50	11.3	1.30
30/70	-	1.21
PA6+	3.9	1.73
CAPRON++	30.4	1.61

* Reaction PA6/PP blends

\+ Reactive polymerised pure PA6 extruded @ 150 rpm

++ Commercial grade PA6 made by hydrolytic polymerisation.

Table 5.4 Mechanical properties of reaction PA6/PP blends

Sample	Young's Modulus E (GPa)	Stress @ Yield σ_y (MPa)	Elongation @ Break (%)	Impact Strength ($J.m^{-1}$)	Flexural Modulus (GPa)
90/10	2.52	52.7	115.6	80.2	1.73
70/30	1.43	30.1	18.6	61.8	1.52
50/50	1.12	27.8	10.5	57.8	1.48
30/70	0.83	25.2	11.7	32.4	1.31
PA6*	2.68	66.4	88.7	93.8	2.72

Note: All tests evaluated in "dry as-moulded " conditions @ 23°C;

* Reactive polymerised PA6 extruded @ 150 rpm.

possibly be attributed to incompatibility between the crystalline phases of PA6 and PP. On the other hand, the smaller difference in tensile strength between pure PA6 and the reaction blend of composition 90/10 could be due to the presence of the amorphous state of the PP phase (as indicated by experimental results obtained from DSC and WAXD) which could possibly enhance some degree of homogeneity in this blend material.

The elongation at break properties of the blend materials show that the 90/10 blend sample has recorded almost 40% increase in elongation as compared to the pure reactive polymerised PA6. However, the elongation properties of other blends were observed to have much lower values with regard to the pure PA6 which could possibly be accounted again by the non-compatibility and inhomogeneity of the two crystalline components.

The flexural modulus of the reaction PA6/PP blends are observed to decrease gradually with increasing amount of PP composition presumably due to the inclusion of the softer PP phase.

For the Izod impact propeties, the 90/10 composition blend records only slightly lower impact value as compared to the pure PA6 sample but this value obtained is still better than the other pure reactive polymerised PA6 materials extruded at various extruder screw speeds (Table 3.6). A gradual decrease in impact properties with increasing amount of PP in the blends suggest again incompatibility of the two component phases.

Dynamic mechanical data for the reaction PA6/PP blends i.e. the storage modulus (E') and the loss factor (tan δ) as a function of temperature, are shown in Figure 5.13.

The loss factor curve (tan δ) for the reaction blend with composition 90/10 exhibits only a single, broad relaxation peak at about 50.5°C which corresponds well to the

glass transition temperature or α transition of PA6 [Figure 5.13 (e)]. Another sharp relaxation peak is also observed at -77°C (ß peak) which has been known to be caused by a crank-shalf type of motion involving an unbonded amide group and several methylene carbon groups of PA6.

It is interesting to observe that the transition temperatures of these two peaks are similar to that obtained from the pure, reactive polymerised PA6 sample extruded at 150 rpm [Figure 3.23 (iii)]. It is also surprise not to observe the α relaxation peak associated with the 10% PP component which has been reported to occur at temperature region of 7° - 9°C. This α relaxation peak of PP is generally recognised to be the glass-rubber relaxation of the amorphous portion of the pure PP material. The ß relaxation of the PP phase reputed to occur at -80°C is also not being observed which could possibly be overlapped by the ß relaxation of PA6 in the region -77°C.

The loss factor curve for the 70/30 reaction blend as shown in Figure 5.13 (d) exhibits again a broad α relaxation peak for the PA6 phase at about 60.7°C. However, in addition to this broad peak, a slight "shoulder" can be detected at a temperature region of 5.9°C which correspond possibly to that of the α relaxation peak of the PP component. At the lower end of the temperature scale, another broader relaxation peak is observed at about -70°C. This broad transition peak is possibly due to overlapping of both the ß relaxation peaks associated with the PA6 and PP phases.

For higher composition of PP at blend of 50/50, the loss factor curve of the material exhibits two distinct damping peaks at the α transition zones [Figure 5.13 (f)]. The transition peak which occur at a higher temperature of 65.9°C belongs to the PA6 component while the lower temperature peak at 6.3°C is attributed to the PP phase. The shape of the PA6 transition peak is observed to be much pronounced and narrower as compared to that recorded for either the 90/10 or 70/30 blends discussed earlier.

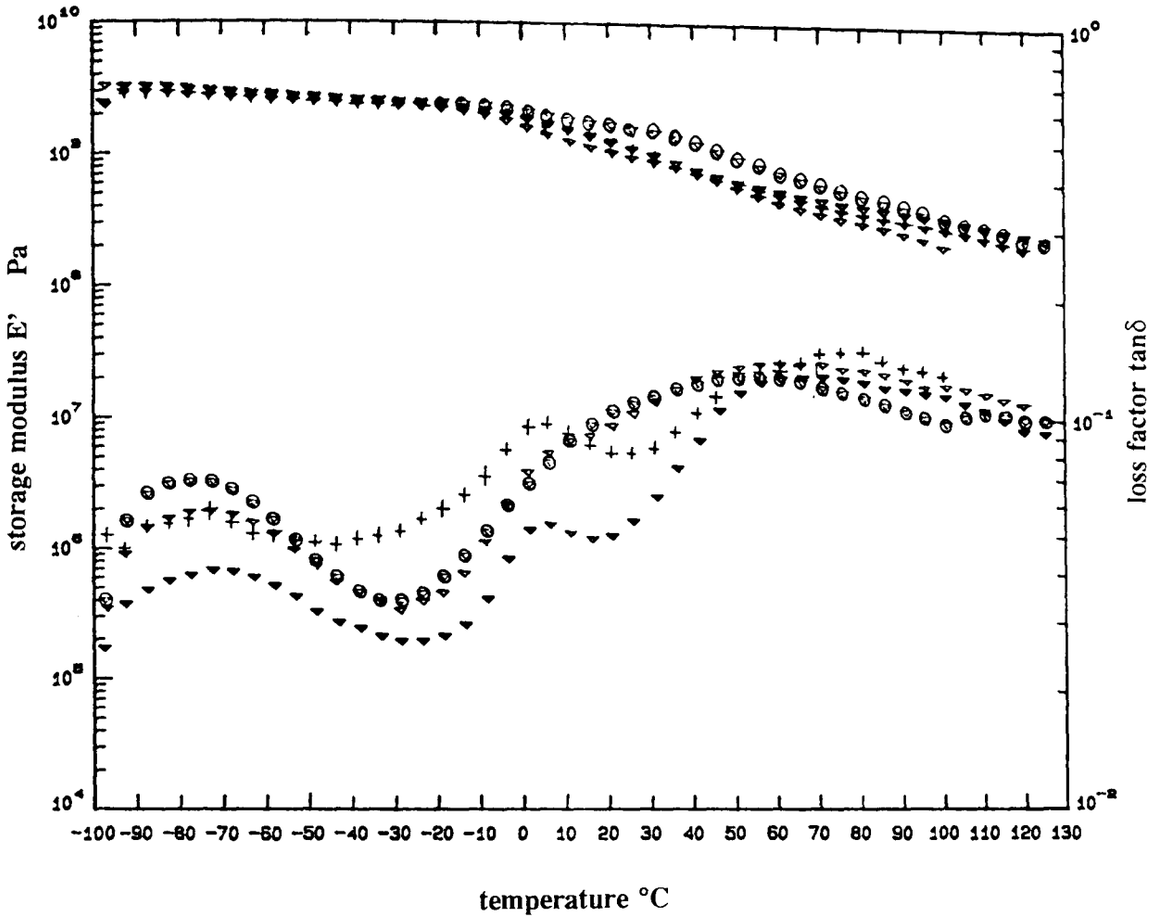

Figure 5.13 Dynamic mechanical spectrum of reaction PA6/PP blends (o) 90/10 (▽) 70/30 (▼) 50/50 (+) 30/70

The appearance of two distinct maxima peaks at the α transition zones of the reaction 50/50 blend suggests that the two blend components are incompatible at molecular level and possibly exhibit a two-phase morphological feature. Certain degree of compatibility could possibly exists in the blends with compositions 90/10 and 70/30, although the former blend shows much better compatibility since no relaxation peak for PP is observed.

The loss factor curve for the 30/70 blend is as shown in Figure 5.13 (+). Here again, two distinct α transition peaks are detected at temperatures of 69.5°C and 6.9°C belonging to the PA6 and PP phases respectively. This result again indicates non-compatibility of the two phases in the blend.

It is interesting to observe that the glass transition temperatures (T_g) or peak maxima of the PP phase in blend compositions of 70/30, 50/50 and 30/70 does not change appreciably i.e. from 5.9°C to 6.9°C. On the other hand, a large increase in T_g of the PA6 phase is recorded i.e. from 60.6°C to 69.5°C. These T_g values observed can possibly provide some experimental evidence that these reaction PA6/PP blends are non-compatibilised systems and the degree of incompatibility tend to affect the PA6 component more than that of the PP phase.

The rather similar T_g values recorded for both the pure PA6 and the blend of composition 90/10 at temperature of 50.7°C as well as the non-detection of the PP α relaxation peak suggest partial miscibility of PA6 and PP phases in molecular level at this reaction blend compositon. This is indeed a very unusual observation since PA6 and PP are widely known to be incompatible phases. The different peak structures of the α transitions observed in the pure and blend PA6 materials could possibly be attributed to the influence of the 10% PP component which can affect the crystalline structure or crystallinity of the PA6 phase as described by **Takayanagi** *et al.* [212].

A sudden increase of T_g of PA6 phase from 50.5°C to 60.6°C was observed for the blend with composition 70/30 as well as the partial detection of the α transition peak for PP at 5.9°C suggest that blend components could be immisible at PP composition $\geq 10\%$. This immisibility observation agrees well with the WAXD and DSC results discussed earlier which showed the appearance of PP reflection peaks as well as the melting and crystallisation peaks in a reaction blend of composition $>10\%$.

As for the mechanical PA6/PP blend of composition 90/10 prepared by mechanical blending in a twin-screw extruder, two distinct α transition peaks are observed at -10°C and 42°C which again correspond to the PP and PA6 phases respectively. These results suggest that the reaction PA6/PP blend of composition 90/10 has better compatibility between the two phases as compared to the mechanically blend sample since no appreciable α transition peak of PP could be observed.

5.3.2 Functionalised Reaction PA6/PP Blends

5.3.2.1 *Wide Angle X-Ray Diffraction*

WAXD diffraction profiles of all the functionalised reaction PA6/PP blend samples with 5 wt% PP-g-MA are shown in Figure 5.14.

For the blend with composition 90/10/5, two α peaks of PA6 component at Bragg angles $2\theta=19.6^\circ$ and $2\theta=23.5^\circ$ and a less obvious γ peak at $2\theta=21.3^\circ$ are observed together with two other characteristic diffraction peaks of PP at $2\theta=13.9^\circ$ and $2\theta=16.8^\circ$ [Figure 5.14 (i)]. This diffraction profile is different from that obtained from the non-functionalised reaction blend of similar composition where no reflection peaks associated with the PP phase were observed [Figure 5.1 (i)]. The appearance of the PP characteristic peaks in this functionalised blend suggests that

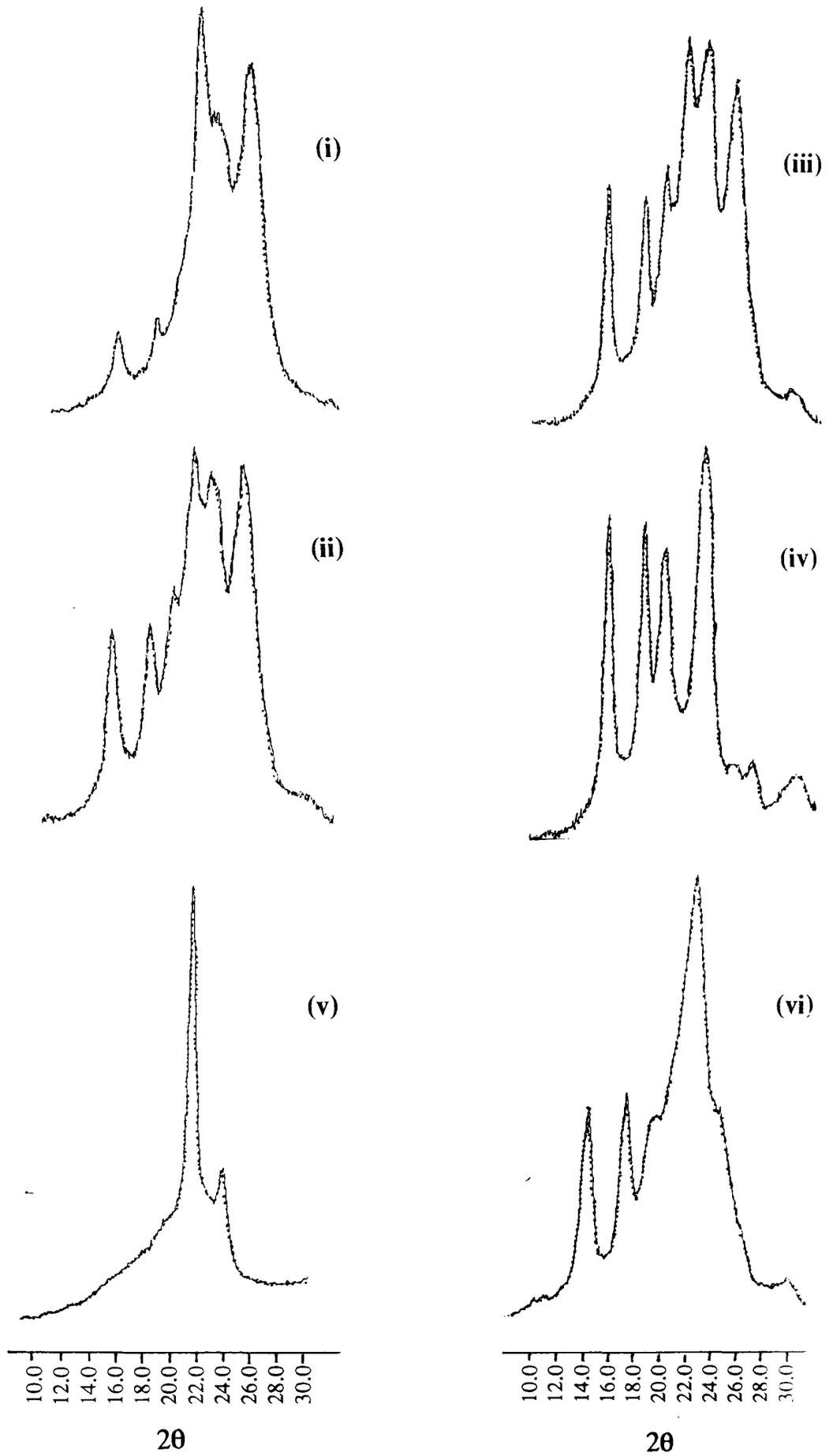

Figure 5.14 WAXD profile of functionalised reaction PA6/PP blends (i) 90/10 (ii) 70/30 (iii) 50/50 (iv) 30/70 (v) PP-g-MA (vi) Orgalloy

addition of 5% PP-g-MA has the effect of transforming the apparently "compatibilised" blend into an immisible two phase system.

WAXD of other functionalised reaction PA6/PP blends with compositions 70/30, 50/50 and 30/70 however, show similar profiles as compared to those obtained from the non-functionalised reaction blend series. These results inferred that apparently there is little change with regard to the development of the crystallite structures for PA6 and PP phases in the presence of 5% compatibiliser PP-g-MA.

The diffraction profile of the compatibiliser PP-g-MA shown in Figure 5.14 (v) is observed to be different from that obtained from the pure PP homopolymer suggesting modification of the PP crystalline structure. On the other hand, it is interesting to note that the diffraction profile of the commercial grade PA6/PP blend (Orgalloy 6000R-Elf Atochem) with composition 70/30 and an unknown compatibiliser shows only the characteristic PA6 γ peak and two other reflection peaks associated with the PP component [Figure 5.14 (vi)]. The diffraction profile for this commercial blend material resembles very much that of the mechanically blend sample of similar composition i.e. 70/30 [Figure 5.2 (ii)]. This similarity arises possibly due to the use of hydrolytic polymerised PA6 component in both blend materials.

5.3.2.2 *Differential Scanning Calorimetry*

Typical DSC thermograms of the reaction PA6/PP blends with 5% by weight of functionalised PP (PP-g-MA) are shown in Figure 5.15 and the corresponding thermal data are presented in Table 5.5.

The functionalised reaction blend with composition 90/10 shows two distinct melting and crystallisation peaks associated with the PA6 and PP components in both the heating and cooling cycles [Figure 5.15 (i)]. The results of the Molau test for this

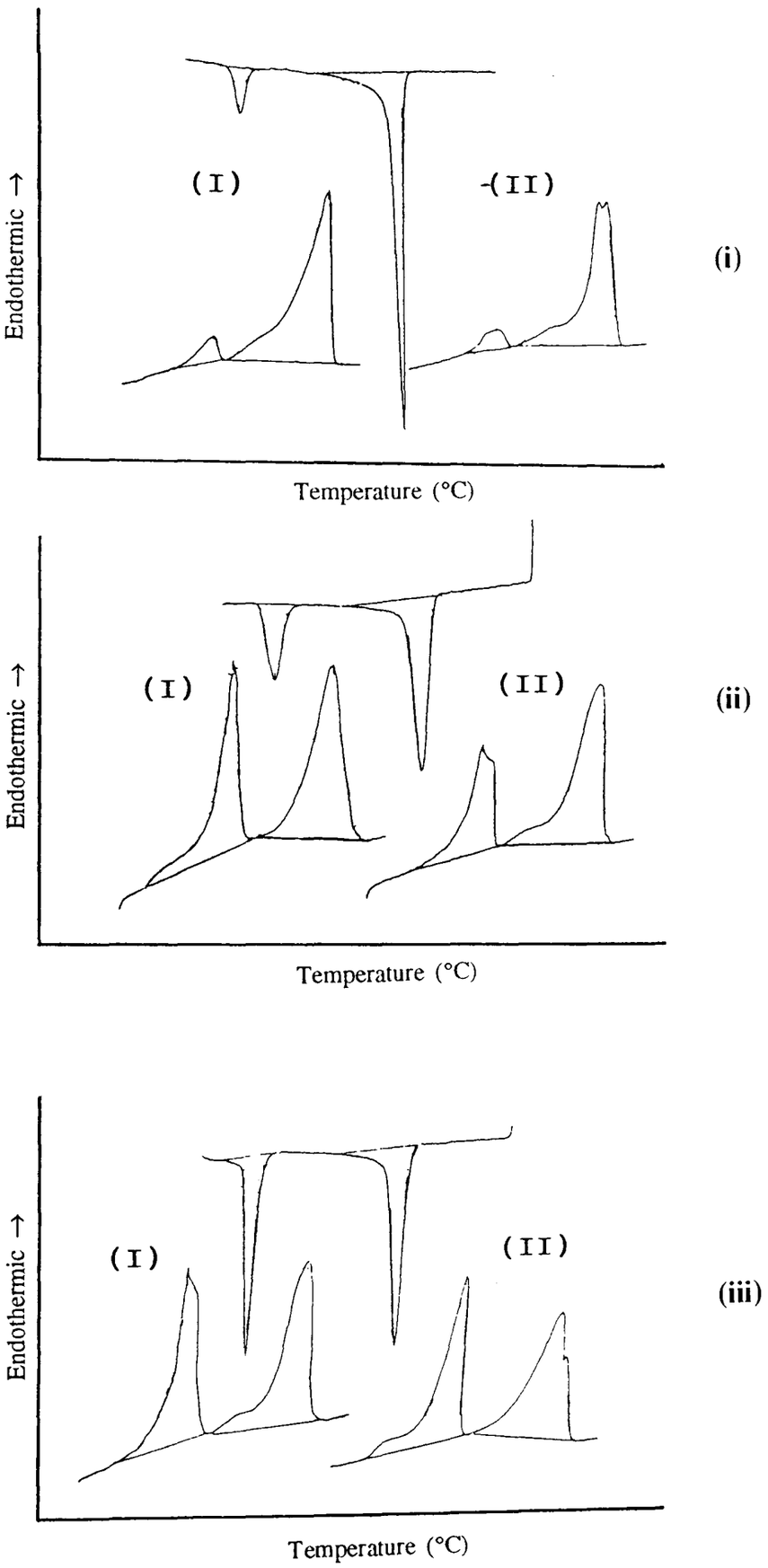

Figure 5.15 DSC thermogram of functionalised reaction PA6/PP blends

(i) 90/10/5 (ii) 70/30/5 (iii) 50/50/5

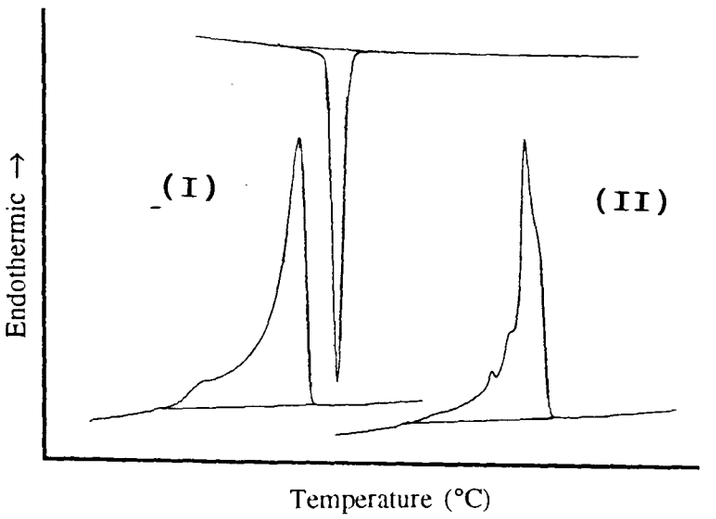

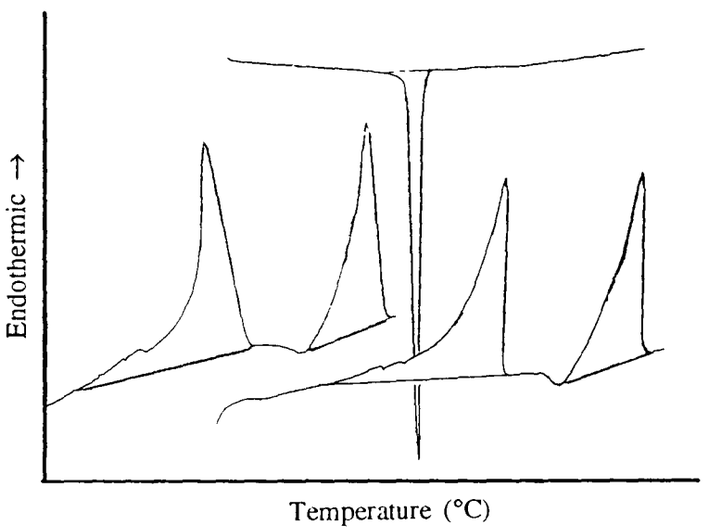

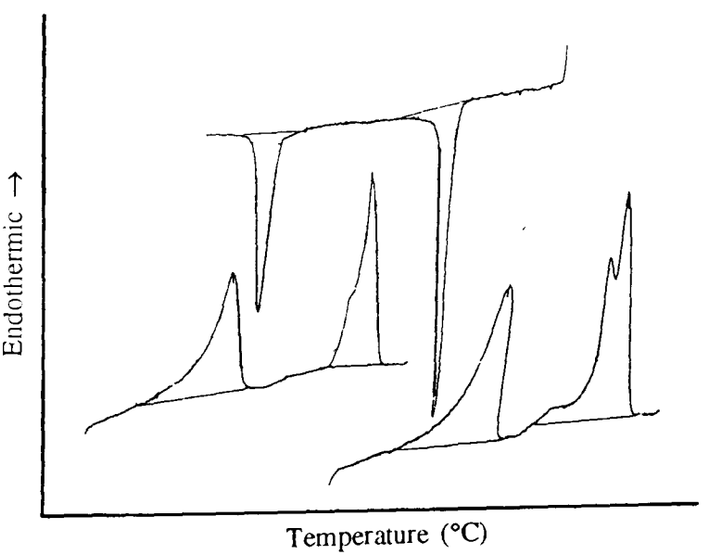

Figure 5.15 (cont.) DSC thermogram of functionalised reaction PA6/PP blends (iv) 30/70/5 (v) Orgalloy (vi) Orgalloy (annealed)

Table 5.5 DSC thermal data of functionalised reaction PA6/PP blends

Sample*	T_{m1} (°C)		ΔH_{f1} ($J.g^{-1}$)		T_c (°C)		ΔH_c ($J.g^{-1}$)		T_{m2} (°C)		ΔH_{f2} ($J.g^{-1}$)	
	PA6	PP	PA6	PP	PA6	PP	PA6	PP	PA6	PP	PA6	PP
90/10/5	219.7	167.9	66.5	5.5	182.4	113.6	57.2	7.8	217.4	163.2	52.9	5.7
70/30/5	216.9	165.0	36.4	30.2	182.5	113.4	34.9	24.8	216.9	162.2	31.4	26.8
50/50/5	209.6	164.4	37.7	26.0	182.0	113.0	38.6	26.2	215.2	160.5	33.6	27.8
30/70/5	-	160.0	-	61.5	-	112.7	-	61.3	-	162.2	-	65.4
PA6	214.2	-	84.9	-	179.5	-	63.0	-	213.0	-	64.5	-
Orgalloy +	220.7	161.8	51.4	34.8	188.0	112.8	39.9	27.3	219.7	159.6	36.8	30.2

Note: * Functionalised reaction PA6/PP blend compositions with 5 wt % PP-g-MA.

+ Commercial grade PA6/PP alloy R6000

T_{m1}, T_{m2} Peak endothermic melting temperatures, stage I and II heating cycles.

T_c Peak exothermic crystallisation temperatures, cooling cycle.

ΔH_{f1}, ΔH_{f2} Heats of fusion, stage I and II heating cycles.

ΔH_c Heat of crystallisation, cooling cycle.

blend material (Section 5.3.2.3) yield a combination of turbid solution with small flake-like particles floating on top indicating the presence a PA6/PP copolymer.

On comparing the thermal data of this functionalised reaction blend with the non-functionalised reaction blend of similar composition i.e. 90/10 in Table 5.1, it is observed that, the melting temperatures for the PA6 phase of the functionalised blend are about 8°C higher than that of the non-functionalised one although rather similar crystallisation temperatures were recorded for this blend. On the other hand, the heat of crystallisation for this functionalised sample is observed to be some 10% lower than that of the non-functionalised one. These results imply that the presence of the compatibiliser PP-g-MA probably has the effect of enhancing the crystallisation process of the PA6 phase by contribution to the nucleation of larger and more perfect crystallites. The lower heat of crystallisation recorded is possibly attributed to the formation of fewer crystallites.

As for the PP phase, an increase of 5-7°C is observed for the melting temperatures as compared to the PP homopolymer [Table 5.1] although rather equivalent crystallisation temperatures are recorded for both the samples. These results suggest that the solidified PA6 phase in the presence of PP-g-MA could possibly influence the crystallisation process of PP leading to the formation of larger and more perfect crystallites and resulting in higher melting temperatures. On the other hand, crystallisation temperature equivalent to that of the pure PP materials was recorded suggesting no nucleating effect of the sodified PA6 in the presence of PP-g-MA.

Two distinct melting and crystallisation peaks are also observed for the 70/30 functionalised reaction PA6/PP blend [Figure 5.15 (ii)]. Here again, the PA6 phase recorded melt temperatures about 3-4°C higher than that of the non-functionalised counterpart despite having a 15% lower crystallinity. The higher melt temperatures observed with lower degree of crystallinity again suggest the formation of larger and more perfect crystallites for the PA6 phase of this functionalised reaction PA6/PP blend. A higher crystallisation temperature is also noted for this functionalised

material indicating some molecular interaction between the the PA6 and PP phases in the presence of the compatibiliser PP-g-MA resulting in higher rate of crystallisation for PA6.

For the PP phase, only slightly higher melt temperatures (2-3°C) are observed for the functionalised blend sample as compared to the non-functionalised one. However, it is remarkable to observe a much lower crystallisation temperature for PP in this blend (~9°C) with respect to the PP component in the non-functionalised reaction blend of similar composition. In fact, the crystallisation temperatures observed for the PP phase in both the functionalised reaction blends 90/10 and 70/30 are similar to that recorded for the pure PP homopolymer (Table 5.1).

However, it is significant to observe rather equivalent melt and crystallisation temperatures for the PA6 and PP phases in these two functionalised blends of compositions 90/10 and 70/30. These thermal results indicate minimum miscibility between the PA6 and PP phases at these compositions although the presence of the 5 wt% of PP-g-MA could possibly impart higher effect on the nucleation process of the PA6 component. It is also interesting to note that although PP-g-MA has minimum effect on the crystallisation process of PP, it has in fact, "retard" the nucleating effect of the solidifying PA6 on PP crystallites as exemplified in the reaction PA6/PP blend of composition 70/30 (Table 5.1). Nevertheless, the PP component in these functionalised blends of 90/10 and 70/30 still recorded higher melt temperatures as compared to the pure PP homopolymer.

DSC thermogram for the functionalised reaction blend of composition 50/50 is as shown in Figure 5.15 (iii) which depicts both the melting and cystallisation peaks of the blend components. Thermal data in Table 5.5 again shows slightly higher melting and crystallisation temperatures of the PA6 phase as compared to those of the non-functionalised sample. These results again confirm the nucleating effect of the PP-g-MA on the PA6 blend component. No appreciable differences in melt temperatures were observed for the PP phase between the functionalised and the

non-functionalised blend samples although again a much lower temperature of crystallisation (~9 °C) was obtained for the functionalised material.

As for the functionalised reaction blend of 30/70, the DSC thermogram in Figure 5.15 (iv) shows again the presence of only one transition peak in both the cooling and heating scans associated with the PP crystalline phase, similar to the one observed for the reaction blend of similar composition discussed earlier [Figure 5.3 (vi)]. Here again, the absence of the PA6 crystallinity could possibly be attributed to the "droplet" morphology effect and/or the formation of short PA6 chains which are "amorphous". (Section 5.3.1.2).

Thermal data for the PP phase of this functionalised reaction blend again shows a crystallisation temperature (~113 °C) similar to those recorded for the other blends with lower PP content. Also, a higher stage II melting temperature is observed with respect to the pure PP homopolymer.

DSC thermogram for the commercial grade PA6/PP alloy (Orgalloy R6000) shows two melting endotherms in the heating cycles associated with the blend components [Figure 5.15 (v)]. However, it is rather surprising to observe only a single crystallisation peak belonging to the PP phase. The absence of the PA6 crystallisation peak is presumably attributed to co-crystallisation effect by the PA6 component as discussed earlier in Section 5.3.1.2 [116]. The fact that no co-crystallisation or suppression of crystallisation effect is observed for our functionalised reaction blends of similar compositions i.e. 70/30 suggests the addition of the 5% compatibiliser PP-g-MA in this blend may not have produced an effective compatibilising reaction between the PA6 and PP phases.

5.3.2.3 *Fourier Transform Infrared Spectroscopy*

FTIR spectrum of the functionalised reaction PA6/PP blends with 5% functionalised PP (PP-g-MA) are shown in Figure 5.16 and the major characteristic absorption bands listed in Table 5.6.

No appreciable shift in band frequencies are recorded in all the blend samples at NH and amide I (C=O) stretching deformations. However, for the 90/10 functionalised reaction blend only, substantial shifts of absorption bands to lower frequencies are recorded for both the aliphatic CH_2 symmetric (2862 cm^{-1}) and assymmetric (2930cm^{-1}) stretching deformations. Blend samples with other compositions exhibited only slight shift in frequencies at these two absorption regions.

As for the olefinic CH_2 stretching deformation region, however, similar trends are observed. In this case, all blend samples except the 90/10 material show an increase in absorption band frequency suggesting minimum interaction between the PA6 and PP molecular components in blends with PP component $>10\%$.

It is however, significant to observe the presence of a C-N stretching deformation band at 1240 cm^{-1} for all the functionalised PA 6/PP blends except the one with composition 30/70. This is a significant observation since earlier we have also recorded an unique C-N stretching deformation band at 1239 cm^{-1} for the non-functionalised reaction PA6/PP blend with 10% PP (Section 5.3.1.3) as well as the reactive polymerised PA6/EPR blend of similar composition (Section 4.3.1.3). However, the slightly lower band frequency recorded for the reaction sample as compared to these obtained for the functionalised series at 1240 cm^{-1} suggest different C-N band may be present in the non-functionalised and functionalised blend samples.

In view of these findings, we postulated that in the presence of PP-g-MA, PA6/PP copolymer is formed as a result of amidation between the amide group of the PA6

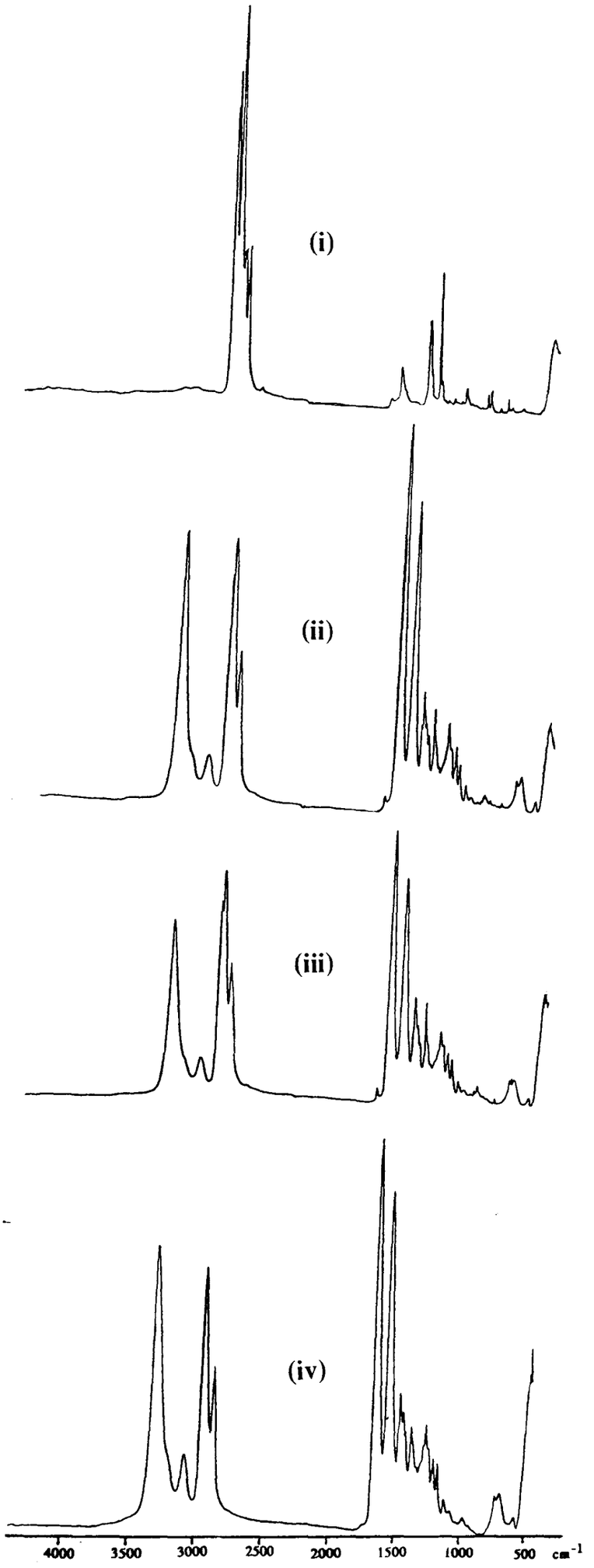

Figure 5.16 FTIR spectrum of functionalised reaction PA6/PP blends (i) 30/70 (ii) 50/50 (iii) 70/30 (iv) 90/10

Table 5.6 FTIR characteristic bands of functionalised reaction PA6/PP blends

Band Assignment	Functionalised reaction PA6/PP Blends			
	90/10/5*	70/30/5*	50/50/5*	30/70/5*
NH stretching (H bonded)/cm^{-1}	3296 (s)	3300 (m)	3299 (m)	3299 (w)
Amide I, C=O stretching/cm^{-1}	1639 (s)	1639 (s)	1639 (s)	1674 (w)
CH_2 assymm. (aliphatic)/cm^{-1}	2930 (s)	2948 (m)	2945 (m)	2951 (m)
CH_2 symm. (aliphatic)/cm^{-1}	2862 (m)	2866 (m)	2866 (w)	2868 (w)
Olefinic CH_2 stretching/cm^{-1}	-	2922 (m)	2928 (m)	2920 (m)
CN stretching/cm^{-1}	1240 (m)	1240 (w)	1240 (w)	-

Band intensity (Code): >3 (vs); >2 & <3 (s); >1 & <2 (m); <1 (w)

* Functionalised reaction PA6/PP blends with 5 wt% PP-g-MA

chain and the carbonyl group of PP-g-MA. The proposed reaction mechanism is as shown in Figure 5.17. In this case, it is unlikely that macroradicals of PA6 and PP can be produced as a result of reduced elongational shear force in the extruder by the presence of 5% PP-g-MA which has been proven to impart some plasticising effect on the molten melt. Improvement of extrusion processability as well as the increased MFI values recorded for the functionalised blends (Section 5.3.2.5) further substantiate this proposition.

Molau test results conducted on the functionalised reaction PA6/PP blends using both formic acid and xylene are shown in Figure 5.18 . Blends of compositions 90/10, 70/30 and 50/50 in formic acid exhibit a combination of turbid solution with small flake-like particles floating on top. The blend composition with 70% PP in xylene however, shows only a clear xylene solution. It is probable that the turbid emulsions observed for the blend samples with PP composition <70% in formic acid are ascribed to the dispersive action of the PA6/PP-g-MA copolymer formed [115]. The observation of these turbid emulsions in the functionalised reaction blends of compositions 90/10, 70/30 and 50/50 corresponds well with the presence of the C-N absorption band obtained from the FTIR spectrum of these samples.

These infrared and Molau test results can also substantiate our earlier postulation that a PA6/PP graft copolymer as well as a branched PP are formed by macroradical combinations in the case of the non-functionalised reaction PA6/PP blend material with 10% PP. However, in the case of the functionalised PA6/PP blends of compositions 90/10, 70/30 and 50/50, only a copolymer of PA6/PP-g-MA is formed. No branched PP is presumed to have formed in these functionalised samples since no characteristic IR deformation band for aldehyde at 1730 cm^{-1} is detected .

The appearance of WAXD reflection peaks and the melting and cooling transition peaks in DSC thermograms (Section 5.3.1.1 and 5.3.1.2) for the PP component in all the functionalised reaction blends further substantiate the argument that no

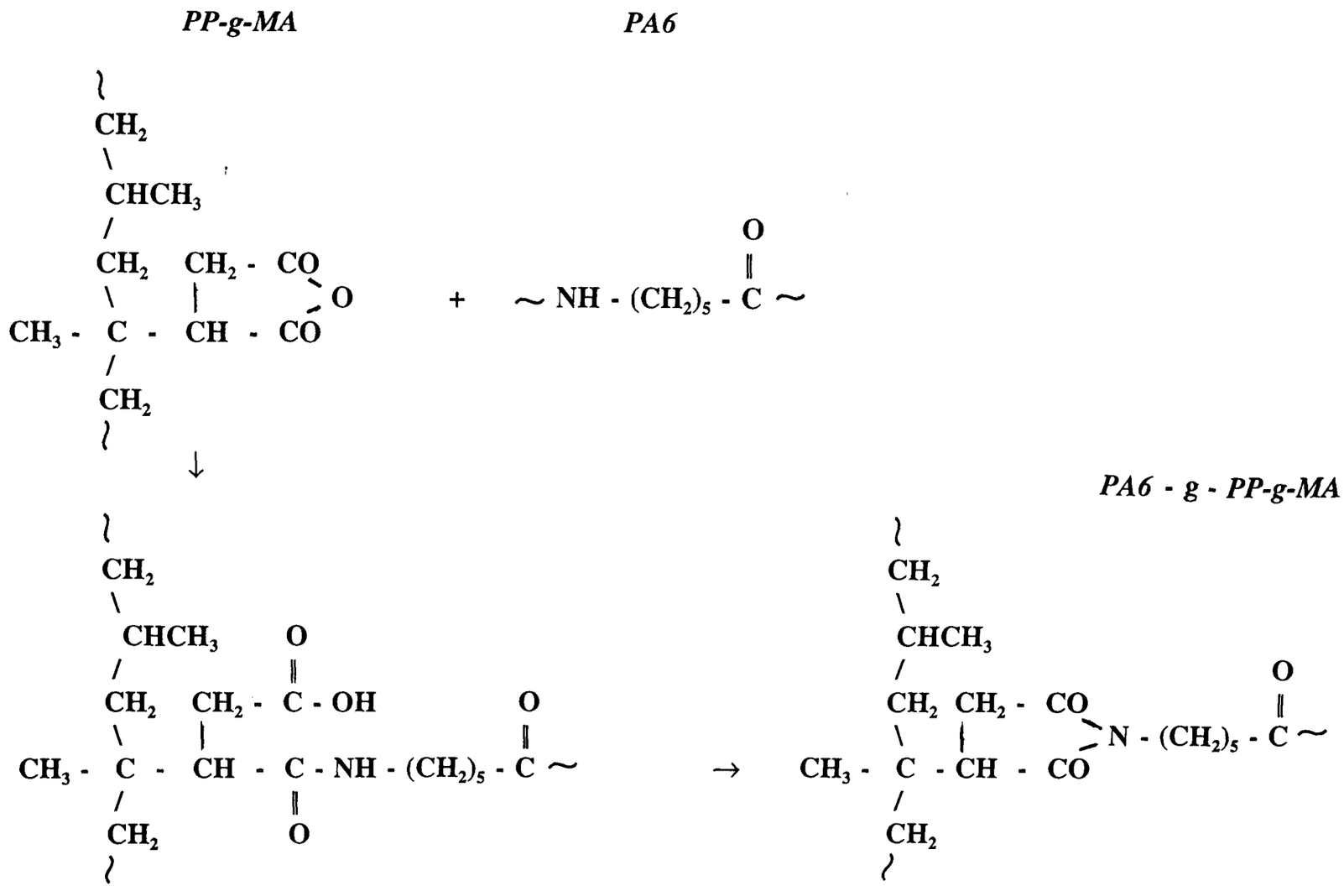

Figure 5.17 Schematic compatibilisation reaction between modified PP and PA6

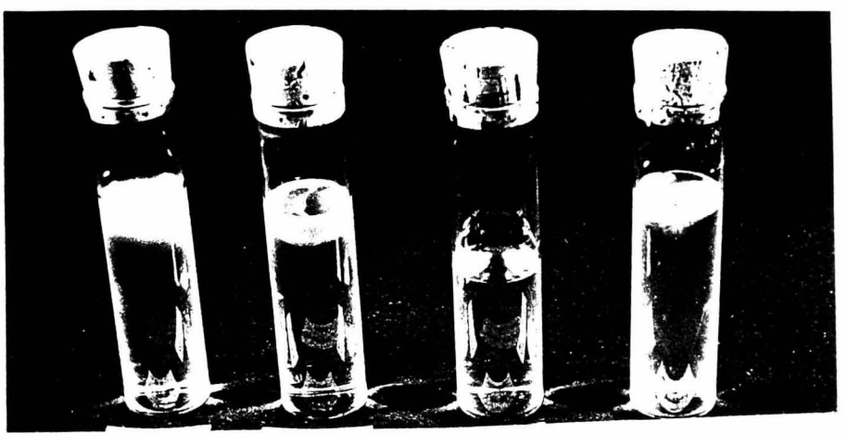

(i) (ii) (iii) (iv)

Figure 5.18 Molau tests for functionalised reaction PA6/PP blends

(i) 90/10 (ii) 70/30 (iii) 30/70 (iv) 50/50

branched PP molecules are present in these materials which will otherwise impede the formation of PP crystallinity.

5.3.2.4 *Scanning electron Microscopy*

SEM micrographs of the functionalised reaction PA6/PP blend of composition 90/10 with 5% PP-g-MA is shown in Figure 5.19 (i). Fine spherical particles with dimensions 0.5-1.5 μm of the dispersed PP phase are observed to scatter over the PA6 continuous matrix. This morphology is different from that observed for the reaction 90/10 blend without PP-g-MA which shows a homogeneous texture rather similar to that of the pure reactive polymerised PA6 material [Figure 5.10 (i)]. This is an interesting observation since the addition of a compatibiliser in this "misible" reaction blend of PA6 and PP has apparently caused a phase-separation of the two crystalline components.

The appearance of the fine PP dispersed particles on the continuous PA6 matrix could probably be accounted for the detection of PP melting and crystallisation peaks (DSC) as well as the characteristic reflection peaks observed on the WAXD profiles for this sample. Small cavities are also observed on the PA6 matrix which are probably caused by removal of the PP particles during the fracture process.

Micrograph of the same blend material after etching with xylene is shown in Figure 5.19 (ii). A "blurred" morphology is observed with patches of white powder and flakes presumably PA6 materials left behind after the neighbouring dispersed PP particles have been removed.

The morphology of the functionalised reaction blend of composition 70/30 is shown in Figure 5.20 (i). The dispersed PP phase are seen as solid fibrillar structures of diameters 1-20 μm scattered over the continuous PA6 matrix. Bundles of irregular shape PP structures can also be observed. The cavity surfaces formed as a result of

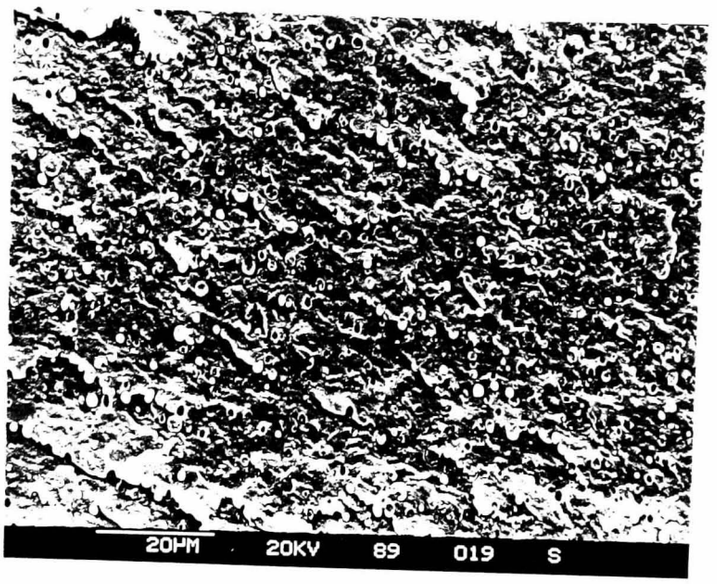

(i) as-fractured

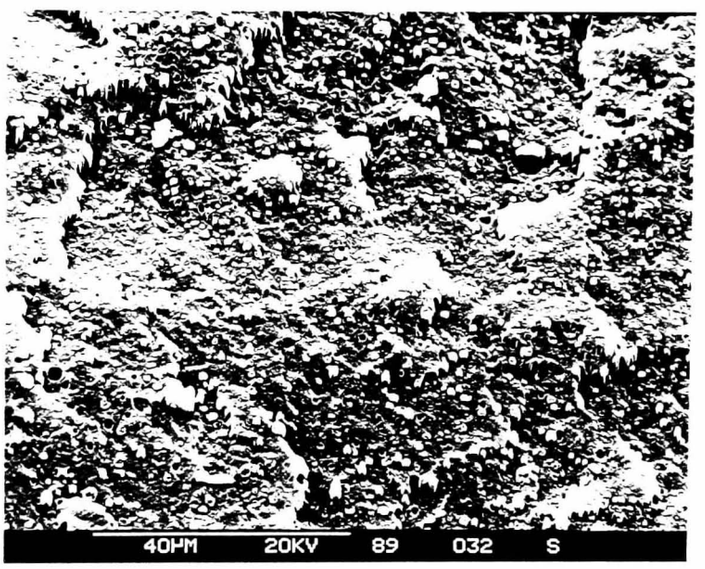

(ii) xylene-extracted

Figure 5.19 SEM micrograph of functionalised PA6/PP 90/10 blend

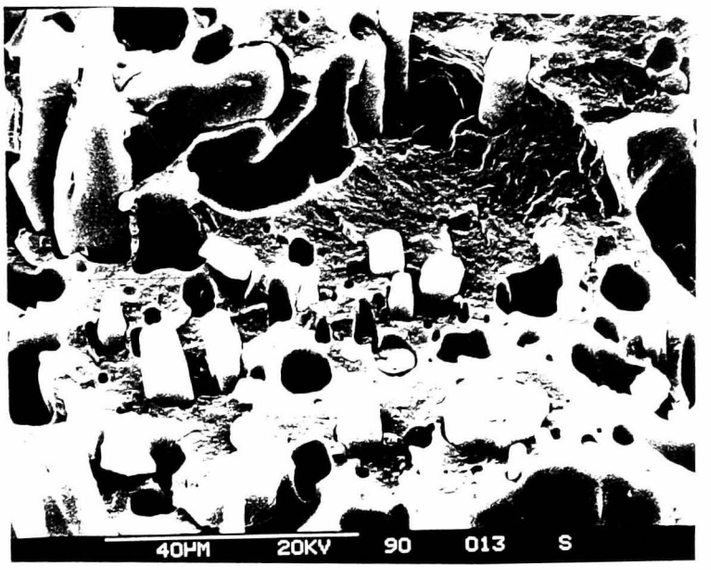

(i) as-fractured

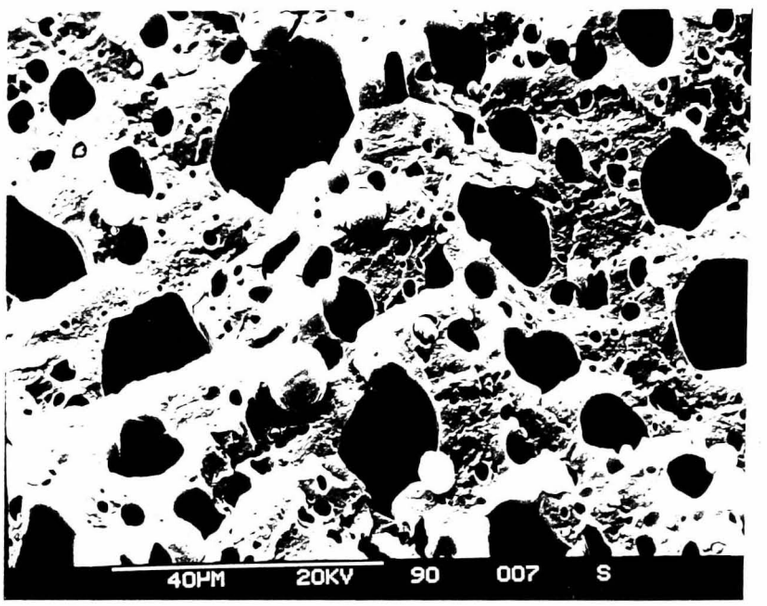

(ii) xylene-extracted

Figure 5.20 SEM micrograph of functionalised PA6/PP 70/30 blend

fibres pull-out are smooth suggesting again little adhesion between the phases in the blend. Also, it is observed that most of the fibres were broken indicating that the adhesion force between the phases might possibly be stronger than the fibre strength.

Comparing the micrograph of this sample with that of the reaction blend of similar composition but without PP-g-MA reveals that in addition to the fibrillar structures, some small size spherical PP particles can also be seen on the latter blend morphology. Apparently, incorporation of 5% compatibiliser has effectively enhanced the formation of fibrillar structures of PP instead of spherical particles. This could possibly be due to the plasticising effect of the PP-g-MA which can produce a profound effect on the viscosity of the blend components. Better processability of the blend materials with PP-g-MA is also observed during the reactive extrusion stage. Blend extrudates with smoother surfaces were obtained which provides experimental evidence on the effect of the compatibiliser on the viscosity of the melt.

The morphology of the 70/30 functionalised PA6/PP blend after etching with xylene shows a discontinuous network of discrete PA6 bundle structures [Figure 5.20 (ii)]. From the micrograph, it appears that some of the PP dispersed particles have been occluded inside the PA6 bundles which in turn are surrounded by another boundary layer of PP materials.

SEM micrograph of the functionalised reaction 50/50 blend is shown in Figure 5.21 (i). PP globular structures of diameters 1-8 μm are dispersed over the continuous PA6 matrix. These globular structures are different as compared to the large fibrillar structures observed for the reaction blend of similar composition [Figure 5.11 (i)]. Cavities, possibly formed by pull-out of the PP structures are observed to have smooth internal surfaces suggesting again minimum interfacial adhesion between the two phases.

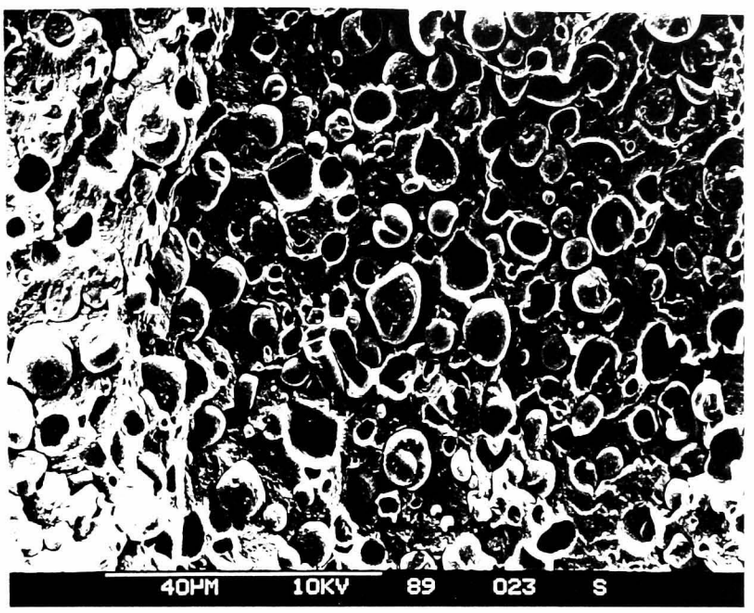

(i) as-fractured

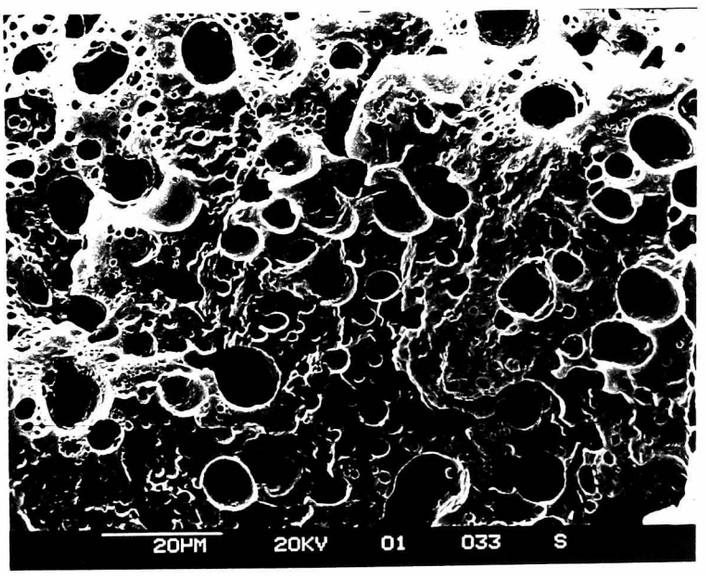

(ii) xylene-extracted

Figure 5.21 SEM micrograph of functionalised PA6/PP 50/50 blend

The morphology of this functionalised blend after extraction with xylene is shown in Figure 5.21 (ii). Large cavities with smooth internal surfaces are seen scattered over the entire PA6 matrix. Some PP particles can still be observed which probably might have escaped the xylene treatment.

The morphology of the functionalised reaction 30/70 blend is shown in Figure 5.22 (i). Again some "honey-comb" shape PA6 structures are seen dispersed on the continuous PP matrix similar to those observed for the reaction blend of similar composition but without the compatibiliser [Figure 5.12 (i)]. Many cavities are present presumably formed by pulling-out of these structures during fracture. It is interesting to observe some kind of network structures at the interior surface region of the cavities indicating possible interfacial adhesion between the phases or possibly the formation of a graft copolymer [Figure 5.22 (iii)].

The morphology of this blend after xylene etching exhibits a layer of lacy sheet structures over the continuous PP matrix [Figure 5.22 (ii)]. These lacy sheets are probably PA6 network materials formed from disintegration of the attached PP as a result of xylene action. Again, the effect of xylene etching is observed not strong enough to cause total dissolution of the continuous PP matrix.

Micrographs of the commercial grade PA6/PP blend (Orgalloy) is shown in Figure 5.23 (i). A rather homogeneous and seemingly co-continuous morphological structure is observed. Dispersed particles of PP could hardly be distinguished from the continuous PA6 matrix. The morphology of this commercial material after xylene extraction shows evenly distributed arrays of small cavities left behind after extraction of the PP phase [Figure 5.23 (ii)].

Many researchers have mentioned about interpenetrating polymer network (IPN) structures while discussing the droplet or phase continuity morphology [206, 210, 211]. Interpenetrating polymer network is defined as the network formed when a

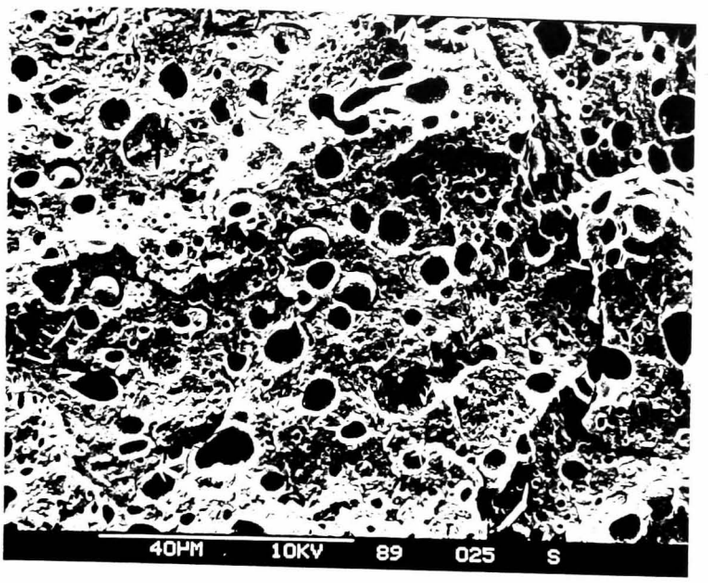

(i) as-fractured

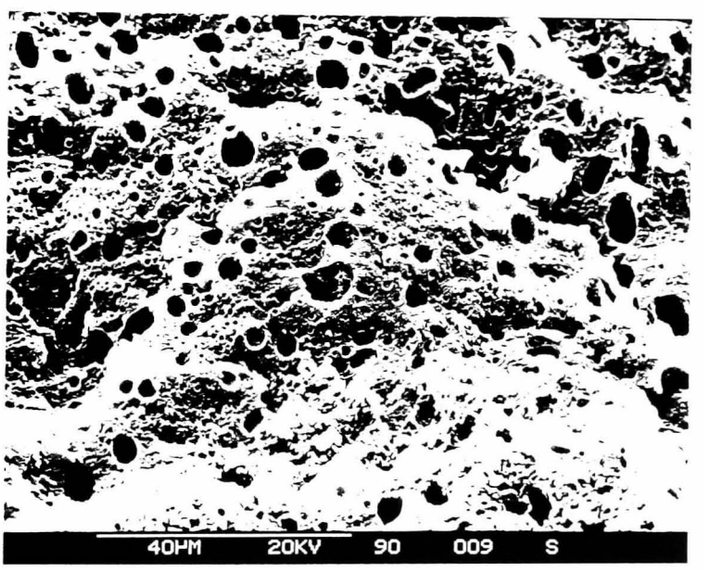

(ii) xylene-extracted

Figure 5.22 SEM micrograph of functionalised PA6/PP 30/70 blend

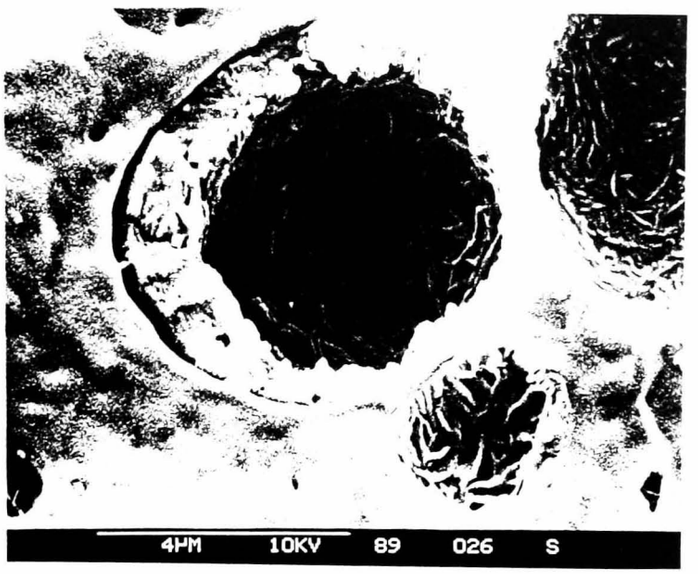

(iii) xylene-extracted

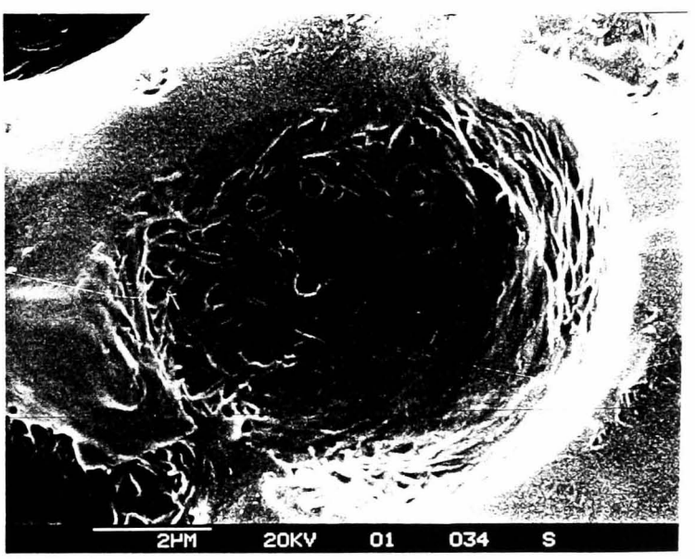

(iv) formic acid-extracted

Figure 5.22(cont.) SEM micrograph of functionalised PA6/PP 30/70 blend

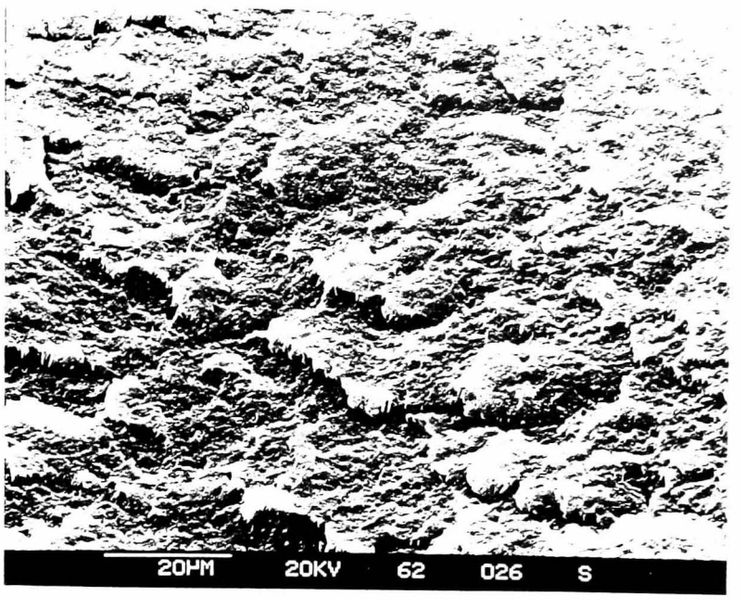

(i) as-fractured

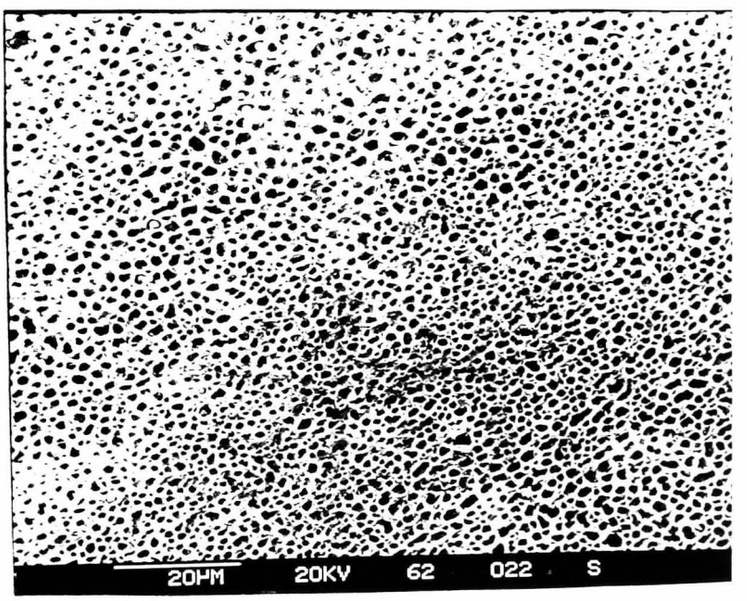

(ii) xylene-extracted

Figure 5.23 SEM micrograph of commercial grade PA6/PP blend (Orgalloy)

pair of intimately mixed polymeric network is prepared in which at least one network is synthesised and/or crosslinked in the presence of the other [206].

The reaction PA6/PP blends used in these experiments were in fact, obtained by blending the PP component with ϵ-caprolactam during in-situ polymerisation process to form PA6. This in-situ polymerisation cum blending processes fits perfectly well with the defination of IPN mentioned above. However, the blend morphology as revealed by SEM micrographs shows that possible IPN structures for these reaction and functionalised reaction blends can only formed at a specific composition of 30/70 (PA6/PP). This particular phase composition for the formation of IPN agrees well with the prediction of dual phase continuity stated in the rheological viscosity-volume fraction equation discussed earlier.

This is a remarkable observation since it is well known that phase inversion or partial phase inversion ending in dual phase continuity can provide critical steps in the manufacture of several important commercial polymeric products such as high impact polystyrene and thermoplastic elastomers [211].

5.3.2.5 *Melt Flow Index and Moisture Content*

The melt flow index (MFI) and moisture content of the functionalised reaction PA6/PP blends are summarised in Table 5.7.

Higher MFI values are recorded for the functionalised blends as compared to the reaction blends without the compatibiliser providing good experimental evidence on the plasticising effect of the PP-g-MA used (Table 5.7). However, it has been reported that reductions of MFI i.e. increases of polymer melt viscosity were observed for certain PA6/PP blends (comprising < 40% PP) compatibilised with different amounts of acrylic acid and maleic anhydride. This observation has been attributed to the formation of a PA6-g-PP graft copolymer and the viscosity effect

Table 5.7 Melt flow index and moisture content of functionalised reaction PA6/PP blends

Sample*	Melt Flow Index (g.10 min.$^{-1}$)	Moisture Content (%)
90/10/5	6.8	1.32
70/30/5	18.4	1.31
50/50/5	30.2	1.30
30/70/5	-	1.21
PA6+	3.9	1.73
Orgalloy++	24.7	1.30

* Functionalised reaction PA6/PP blends with 5 wt% PP-g-MA.

\+ Reactive polymerised pure PA6 extruded @ 150 rpm

++ Commercial grade PA6/PP alloy (R6000)

is more obvious with increasing PA6 content [212]. The increase of MFI observed in our functionalised reaction blends as compared to the reaction blends again suggests minimum compatibilisation effect of the PP-g-MA compatibiliser on the PA6 and PP phases.

Slightly lower moisture contents were recorded for the functionalised blend materials of compositions 90/10 and 70/30 as compared to the reaction blends of similar compositions, presumably due to the formation of more perfect PA6 crystallites as discussed earlier [Section 5.3.2.2]. Moisture content for the other functionalised blends with compositions of >30% showed similar levels of moisture content as those observed for the reaction blend series.

5.3.2.6 *Mechanical Properties*

Mechanical properties of the functionalised reaction PA6/PP blends are summarised in Table 5.8.

Generally lower E modulus is recorded for all the functionalised samples except the blend with composition 70/30 as compared to those of the reaction series. This exceptional high rigidity is attained probably due to the presence of more perfect crystallites of the PA6 phase as shown by the much higher endothermic melting temperature recorded for this blend [Table 5.1 and 5.5].

Tensile strengths of the functionalised reaction blends with compositions 90/10 and 70/30 are observed to be slightly higher as compared to the corresponding reaction blends with similar compositions. This higher tensile property could possibly be again attributed to the presence of more perfect crystallites of the PA6 phase in the functionalised blends.

Table 5.8 Mechanical properties of functionalised reaction PA6/PP blends

Sample+	Young's Modulus E (GPa)	Stress @ Yield σ_y (MPa)	Elongation @ Break (%)	Impact Strength ($J.m^{-1}$)	Flexural Modulus (GPa)
90/10/5	2.18	54.1	21.4	84.7	1.68
70/30/5	1.48	49.2	19.2	67.5	1.55
50/50/5	0.65	25.8	25.2	45.8	0.82
30/70/5	0.58	20.1	4.9	31.7	0.71
Orgalloy*	1.81	43.5	270.0	108.0	1.92

Note: All samples tested in "dry as-moulded" conditions @ 23°C.

* Commercial grade PA6/PP (70/30) alloy R6000.

+ Functionalised reaction PA6/PP blends with 5% PP-g-MA.

The tensile strengths of the other blends with 5% PP-g-MA i.e. 50/50 and 30/70 however, recorded much lower values as compared to similar reaction blends without the compatibiliser.

As for the elongation at break properties, the functionalised reaction blend with composition 90/10 exhibits much poorer result as compared to the reaction blend counterpart. This could be explained by the formation of separate crystalline phases of PA6 and PP as detected by DSC, WAXD and the Molau test results. The functionalised blends of other compositions recorded elongation at break properties rather similar to the corresponding reaction blend series.

These tensile and elongation properties discussed above are extraordinary since many researchers have reported improved properties for the PA6/PP blends with incorporation of a compatibiliser [104, 106, 203]. It is however, important to differentiate that all the previous work done on PA6/PP blends were based on lower molecular weight commercial grade PA6 synthesised by hydrolytic polymerisation of ∈-caprolactam. Most of the works reported for PA6/PP blends were prepared using either a Barblender mixer or twin-screw extruder with specific screws designed only for mixing. The work reported here however, involves the simultaneous processes of in-situ polymerisation and blending of the reacting PA6 and PP phases which is different from those of "direct" blending between the PA6 and PP polymers with a compatibiliser. The PA6 material used in these reaction experiments is an activated anionic polymerised product and has an average molecular mass some 20-30% higher than that of the commercial PA6 materials. As shown by DSC and WAXD experiments, different crystalline structural forms are associated with these in-situ formed PA6 materials which can have an appreciable influence on their mechanical properties.

Izod impact properties of the functionalised reaction blends with compositions 90/10 and 70/30 recorded only slightly lower impact strengths as compared to the reaction blends without compatibiliser. However, with increasing PP content, the

functionalised blends recorded much lower impact properties presumably due to more severe phase inhomogeneity of the two crystalline phases.

The higher impact value attained by the commercial grade PA6/PP blend (Orgalloy) further substantiated the argument that non-compatibility of the PA6 and PP phases in all these functionalised reaction blends is the primary reason for the much inferior impact properties recorded.

Almost similar flexural modulus values are observed for the functionalised blends of compositions 90/10 and 70/30 with respect to the reaction blends of similar compositions. The high rigidity of these two functionalised blend samples can again be attributed to the formation of more perfect crystallites. On the other hand, functionalised blends of higher PP compositions recorded much lower modulus properties as compared to the non-functionalised series.

The flexural modulus of the commercial grade PA6/PP blend (Orgalloy) has a value of 1.92 GPa which is much higher than all the reaction PA6/PP blends. This superior flexural properties is attributed to the formation of a PA6-g-PP graft copolymer located at an interface between the PA6 and PP phases. This copolymer can act as an interfacial agent to reduce interfacial tension between the two incompatible phases thereby enhancing phase homogeneity of the incompatible components [214].

Dynamic mechanical spectrum of the functionallised reaction blends are shown in Figure 5.24.

Incorporation of 5% functionalised PP into the reaction blends has the effect of producing rather similar glass transition temperature, T_g of the PA6 component in all the blend compositions at about 69.5°C. Similar observation has also been reported by **Ultracki** *et al.* [214] for the commercial grade PA6/PP blend (Orgalloy R6000) in a melt flow study on immisible blends who concluded that the

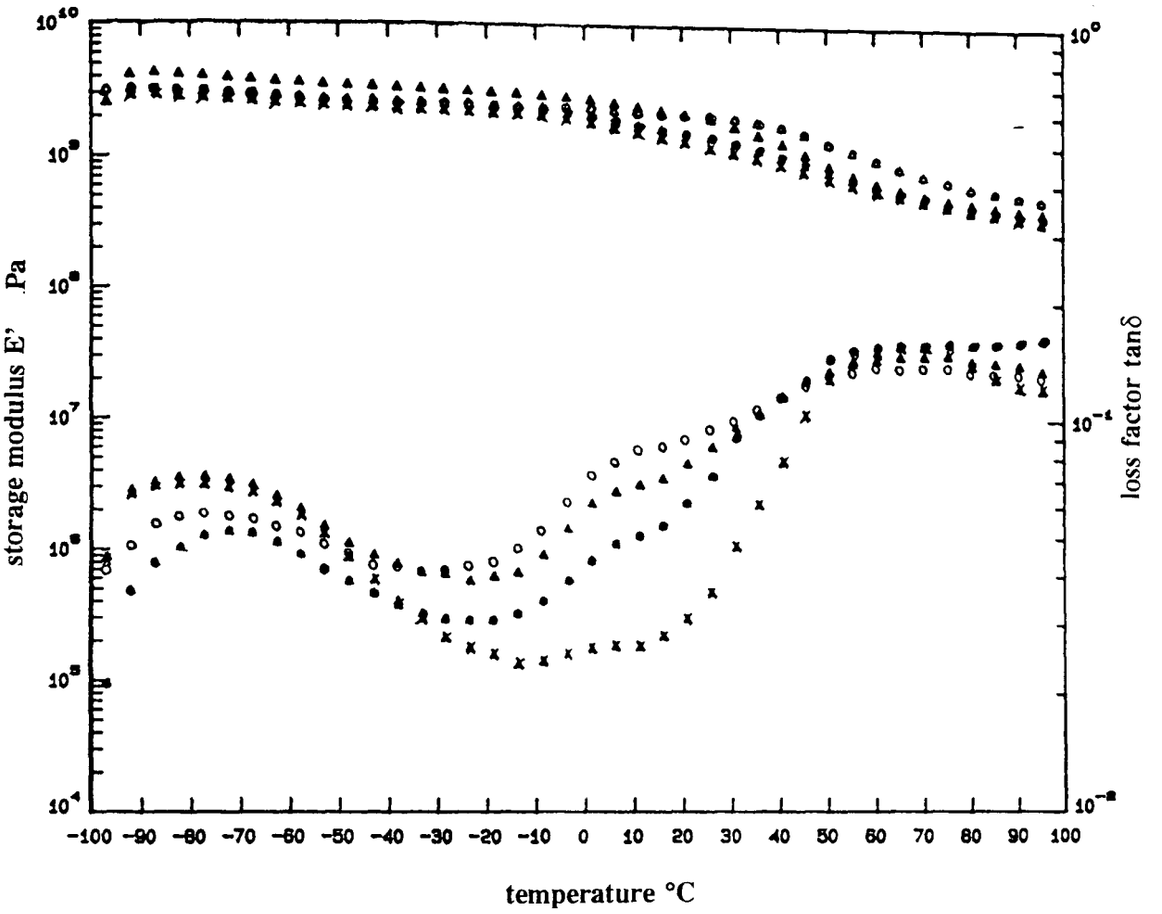

Figure 5.24 Dynamic mechanical spectrum of functionalised reaction PA6/PP blends (×) 90/10 (▲) 70/30 (○) 50/50 (•) 30/70

compatibilisation effect has affected the PA6 phase more than the PP. Furthermore, on checking the difference in the α relaxations of the PA6 phases between the functionalised and non-functionalised blends, it is revealed that the damping peaks in the functionalised samples become broader at compositions of 50/50 and 30/70. At these compositions, the blends exhibit only a shoulder-type peak on the low temperature side of the α transition zone [Figure 5.24]. The reaction blends of similar compositions but without compatibiliser, on the other hand, still maintain a well shape α damping peak of the PA6 phase [Figure 5.13]. These results at first glance can be easily interpreted in terms of partial miscibility of the PA6 and PP phases at these blend compositions but as shown by SEM morphologies, these functionalised reaction blends are not compatible and still maintains a two-phase morphology feature.

The storage modulus E' data seems to provide more evidence for the partial miscibility in the functionalised reaction blends studied since their values tend to decrease nearly linearly with increasing PA6 content in the blends over the whole compositions. These results could possibly be attributed to the fact that the PP-g-MA compatibiliser used has effectively increase the interfacial adhesion between it and the PA6 phase, and possibly also enhance improved compatibility between PA6 and PP phases. This proposition has been confirmed by SEM observations which showed smaller dispersed phase particles as compared to the non-functionalised blends.

Also, as mentioned earlier, the α transition peak maxima, T_g of the PA6 phase in all the compositions of the functionalised reaction blends was observed to have shifted to a higher temperature of 69.5 $^{\circ}$C as compared to a T_g of about 60 $^{\circ}$C for the non-functionalised reaction blends of compositions < 50% PP. The fact that the tanδ relaxation peaks of PP remain relatively unchanged for both the reaction and functionalised blend series at about 6-9 $^{\circ}$C, suggests that the compatibiliser used seems to impart a greater influence on the PA6 phase as compared to PP. This observation tends to agree with the results of DSC studies discussed earlier.

CHAPTER 6

CONCLUSIONS AND SUGGESTIONS FOR FURTHER WORK

6.1 Conclusions

(1) Polyamide 6 materials prepared by reactive polymerisation of ϵ-caprolactam, using various extruder screw speeds yield different molecular weights, molecular weight distributions and residual monomer contents. The molecular mass obtained was generally much higher than commercial PA6 polymers formed by hydrolytic polymerisation. Reactive polymerised PA6 materials also exhibited superior impact and elongation properties but have lower tensile strength and flexural modulus. It seems probable that this difference in mechanical behaviour arises from variation in molecular weight and/or crystallinity associated with the different synthesis processes.

(2) DSC and WAXD results indicated possible formation of a meta-stable PA6 γ crystalline phase structure obtained at extruder speed of 150 rpm and with slow melt cooling conditions, in addition to the α crystalline form. It is suggested that this thermally unstable γ crystalline state transforms into the more stable α phase upon annealing at a temperature of 180°C for a period of 90 minutes.

(3) Reactive polymerised PA6 modified with 10 wt% of EPR copolymer has been successfully synthesised using a fully intermeshing, co-rotating twin-screw extruder. This reaction blend material exhibits superior tensile and impact strength properties compared to the pure PA6. Enhancement of these mechanical properties is attributed to the formation of a PA6-g-PE graft copolymer located possibly at the PA6/EPR interface which can function as an emulsifying agent to compatibilise the two blend phases. Experimental evidence for this graft copolymer has been obtained from FTIR and phase solubility studies.

(4) DSC, DMA and WAXD results suggested structural modification of the EPR copolymer has occurred during the polymerisation/blending process in the extruder resulting in the formation of a crystalline PP phase and an amorphous PE component. A polymer chain scission mechanism for both the PA6 and EPR reaction components is proposed with the generation of macroradicals responsible for the formation of the graft copolymer as well as the crystalline PP and amorphous PE phases.

(5) Reaction PA6/PP blends of different compositions are prepared during in-situ polymerisation of ∈-caprolactam in the reactive extrusion process using a twin-screw extruder. Structural, morphological and mechanical studies on the reaction blend with 10% PP showed apparent "miscibility" of the phase components which is an unexpected observation since PA6 and PP crystalline phases are well known to be incompatible with each other due to polarity and structural differences. It is postulated that a branched PP and/or a PA6-g-PP graft copolymer with C-N imide linkage has been formed as a result of mechano-degradation reaction due to severe elongational shear stress experienced during the reactive extrusion process. Again, the formation of macroradicals are proposed as a consequence of polymer main chain scission. Reaction blends with higher PP composition however, showed the usual incompatibility behaviour with coarse blend morphology and inferior mechanical properties. Phase inversion phenomena for the blend components is observed at a composition of 30% PA6 which also exhibited evidence of interpenetrating network structures in the blend morphology.

(6) Functionalised reaction PA6/PP blends were also prepared with the incorporation of 5 wt% commercial compatibiliser. Phase separation of the PA6 and PP components were observed for all the blend compositions from DSC, WAXD, DMA and SEM studies. No improvement of mechanical properties was observed as compared to the reaction blends without compatibiliser. However, both FTIR and phase solubility studies revealed

the formation of a PA6-PP-g-MA graft copolymer which has effectively lowered the interfacial tension between the phases as evidenced from the reduced particle size of the dispersed phase observed in the SEM micrographs. This compatibilisation reaction is however, appeared to be only effective betwen the functionalised PP compatibiliser and the PA6 phase, as a result of which a two phase polymer system still exist, i.e. PA6-g-PP-g-MA and PP with much inferior mechanical behaviours.

6.2 Suggestions for Further Work

(1) The present study engages an extruder screw design with a L/D ratio of 21 and an average residence time of 80-92 seconds. It is interesting to investigate the effect of an extended material residence time in the reaction zone of the screw profile on the PA6 molecular weight and molecular weight distributions by using higher L/D ratios of possibly 25 and 29 which may provide an efficient means of controlling the molecular weight of PA6 other than engaging different screw speeds. Alternatively, it is also of interest to extend the compression/metering zone of the extruder to accomodate a longer reaction/mixing time for the blend components. In this way, it may be possible to induce greater chain scission of the polymeric melts which can possibly lead to improved compatibilisation in the PA6 blends with EPR and PP as postulated by this study.

The slight yellowing appearance observed on the PA6 extrudate obtained suggests the possibility of oxidation reaction of the polymer melt. It is therefore important to conduct this reactive polymerisation process either in an inert nitrogen blanket or with the inclusion of small quantities of an antioxidant in the reactant formulation to minimise the degradation effect attributed to oxygen.

(2) SEM studies on our reaction PA6/EPR blend with 10% elastomer suggest the formation of a two phase polymer system. Preliminary work carried out during the reactive extrusion of this blend with the inclusion of a commercial compatibiliser (5 wt% PP-g-MA) has produced a homogeneous blend morphology with minute elastomeric domains dispersed over the continuous PA6 matrix, suggesting excellent compatibilisation has occurred between the phases. It will be interesting therefore, to conduct further study on the relationship between the interfacial adhesion and elastomer particle size with respect to the toughness behaviour of this elastomer modified PA6 blend.

The influence of higher elastomer composition and compatibiliser content of the reaction PA6/EPR blend on the product final performance properties need to investigate further for a better understanding of the toughness mechanism introduced by the elastomer phase.

(3) The extraordinary observation on the formation of an "apparent miscible" reaction blend of PA6/PP at 10% PP composition shall be investigate further using analytical technique such as solid state ^{13}CNMR for an enunciation of this polymer structure and possibly confirm the reaction mechanism involved leading to the formation of the PA6-g-PP graft copolymer.

Only limited compatibilisation reaction was observed in all the functionalised reaction PA6/PP blends and resulted in a coarse morphology with poor mechanical properties. It is therefore of interest to investigate the effect of higher composition (>5%) of the compatibiliser used on the blend behaviour. Binary functionalised reaction PA6/PP-g-MA blends instead of the ternary blends as discussed in this study may produce a better compatibilisation of the phases with good performance properties.

(4) Some preliminary experiments on the effect of incorporating 10% by weight of short glass fibres into the polymerising PA6 have shown an enhancement

of tensile and flexural modulus properties of the PA6 composite. Both WAXD and DSC investigations also revealed the effect of the glass fibre on the formation of an additional thermal stable γ crystalline phase which may have influence the mechanical behaviour of the composite. Further work on the effect of higher glass fibre content on the structure and properties of the resulting composite is necessary to establish the reinforcement mechanism involved.

REFERENCES

1. Biesenberger, J.A., and Sebastian, D.H., *"Principles of Polymer Engineering"*, Wiley-Interscience, New York (1983).
2. Brown, S.B., and C.M. Orlando, *"Reactive Extrusion"* in Encycl. Polym. Sci. Eng., J.I. Kroschwitz, ed., Wiley, New York, ***14,*** 169 (1988).
3. Wielgolinski, L., and J. Nangeroni, *Adv. Polym. Tech., **3,*** 99 (1983).
4. Kowalski, R.C., American Chemical Society Polym. Div. Topical Workshop on *"Polymerisation and Polymer Modification by Reactive Processing"*, May 21-24 (1985), Bermuda.
5. Eise, K., *Plast. Compounding, **January/February,*** 44 (1986).
6. Frund, jr., Z.N., *Plast. Compounding, **September/October,*** 24 (1986).
7. Kamal, M.R., and M.E. Ryan, *Adv. Polym. Technol., **9,*** 321 (1989).
8. Ratzsch, M., *Makromol. Chem. Macromol. Symp., **12,*** 165 (1987).
9. Lambla, M., *Polym. Process Eng., **5,*** 297 (1988).
10. Tzoganakis, C., *Adv. Polym. Technol., **9,*** 321 (1989).
11. White, J.L., W. Seydlowski, K. Min, and M.H. Kim, *Adv. Polym. Technol., **7,*** 295 (1987).
12. Rauwendaal, C.J., *Polym. Eng. Sci., **21,*** 1092 (1981).
13. Janssen, L.P.B.M., in *Proceedings of the 3rd International Conference on Reactive Processing of Polymers,* Strasbourg, France, 151 (1984).
14. Mack, W.A., *Chem. Eng., **99*** (1972).
15. Siadat, B., M. Malone, and S. Middleman, *Polym. Eng. Sci., **19,*** 787 (1979).
16. Stober, K.E., and J.L. Amos, *U.S. 2,530,409* (Dow-1950).
17. Martens, M.M., and White, D.H., paper presented at the *79th AIChE National Meeting, Houston, TX* (1975).
18. Streetman, W.E., *U.S. 4,497,934* (American Cyanamid-1985).
19. Tadmor, Z., and C.G., Gogos, *"Principle of Polymer Processing"*, John Wiley, New York, (1979).
20. Hyun, M.E., and S.C. Kim, *Polym. Eng. Sci., **28,*** 743 (1988).

21. Mizuno, S., and T. Adachi, *U.S. 4,254,010* (Dainippon Ink and Chemicals-1981).
22. Gozdz, A.S., and W. Trochimczuk, *J. Appl. Polym. Sci., 25,* 947 (1980).
23. Tucker, C.S., and R.J. Nichols, *Plast. Eng., 43,* 27 (1987).
24. Gouinlock, E.V., H.W. Marciniak, M.H. Shatz, E.J. Quinn, and R.R. Hindersiun, *J. Appl. Polym. Sci., 12,* 2403 (1968).
25. Schuddemage, H.D., H. Jastrow, and H. Barsh, *US 4,007,234* (1977).
26. Komazawa, H., T. Mori, Y. Ikenaga, H. Hotta, and T. Nakashima, *US 4,390,684* (1983).
27. Stuber, N.P., and M. Tirell, *Polym. Process Eng., 3,* 71 (1985).
28. Kotnour, T.A., R.C. Barber, and W.L. Kruegen, *US 4,619,979* (1986).
29. Engler, D.A., and A.R. Maistrovich, *EPA 160,397* (1985).
30. Ganzeveld, K.J., and I.P.B.M. Janssen, *Polym. Eng. Sci., 32,* 457 (1992).
31. Rauwendaal, C., *"Polymer Extrusion"*, Hanser Publisher, New York (1986).
32. Kalyon, D.M., and H.N. Sangani, *Polym. Eng. Sci., 29,* 1018 (1989).
33. Hornsby, P.R., *Plast. Compounding, 56, September/October* (1988).
34. Hornsby, P.R., *Plast. Rubber Processing Appl., 7,* 237 (1987).
35. Ess, J.W. and P.R. Hornsby, *Polym. Testing, 6,* 205 (1986).
36. Takekoshi, T., and J.E. Kochanowski, *US 4,011,198* (1977).
37. Banucci, E.C., and G.A. Mellinger, *US 4,073,773* (1978).
38. Schmidt, L.R., and E.M. Lovgren, *US 4,421,907* (1983).
39. Kosanovich, G.M., and G. Salee, *US 4,465,819* (1984).
40. Xanthos M., *"Reactive extrusion"*, Hanser Publisher, New York, 87 (1992).
41. Sutter, H., M. Beek, F. Haas, and G. Marwede, *GB 1,347,088* (1974).
42. Bruzzone, M., S. Gordini, and K. Wyllic, *US 4,714,747* (1987).
43. Carbonaro, A., S. Gordini, and S. Cucinella, *EPA 127,236* (1984).
44. Heinemeyer, B.W., and S.D. Tatum, *US 4,612,156* (1986).
45. Seddon, R.M., W.H. Russel, and K.B. Rollino, *US 3,253,818* (1966).
46. Semandik, M., and D.M. Braunstein, *US 4,105,637* (1978).
47. Todd, D.B., *Polym. Process Eng., 6,* 15 (1988).

48. Illing, G., *US 3,536,680* (1970).

49. Bartilla, T., D. Kirch, J. Nordmeier, E. Promper, and Th. Strauch, *Adv. Polym. Technol.*, **6,** 339 (1986).

50. Menges, G., and T. Bartilla, *Polym. Eng. Sci.*, **27,** 1216 (1987).

51. Berghaus, U., and W. Michaeli, *Soc. Plast. Eng. ANTEC Tech. Pap.*, *36*, 1929 (1990).

52. Van Buskirk, B., and M.K. Akkapeddi, *Polym. Prepr. Am. Chem. Soc. Div. Polym. Chem.*, **29(1),** 333 (1988).

53. Hergenrother, W.L., and A.W. Greenstreet, *EPA 155,995* (1985).

54. Kubanek, V., Z. Sterbacek, J. Kralicek, J. Marik, and B. Casensky, *GB 2,096,155* (1982).

55. Biensan, M., and P. Potin, *US 4,067,861* (1987).

56. Joyce, R.M., and D.M. Ritter, *US 2,251,519* (1941).

57. Hall, H.K., *J. Am. Chem. Soc.*, **80,** 5404 (1958).

58. Sebenda, J., O. Wichterle, and M. Kralicek, *J. Adv. Polym. Sci.*, **2,** 578 (1961).

59. Sebenda, J., *J. Macromol. Sci. Chem.*, **A6,** 1145 (1972).

60. Sebenda, J., *Prog. Polym. Sci.*, **6,** 123 (1978).

61. Sebenda, J., and V. Kouvil, *Eur. Polym. J.*, **8,** 437 (1972).

62. Stea, G., and G.B. Gechele, *Eur. Polym. J.*, **6,** 233 (1970).

63. Desai, M.R., M.V. Pondya, and C.S. Shah, *Polym. Internatioanal,* **29,** 137 (1992).

64. Iobt, S.A., *Polym. Eng. Sci.*, **25,** 425 (1985).

65. Lin, D.J., J.M. Ottino, and E.L. Thomas, *Polym. Eng. Sci.*, **25,** 1155 (1985).

66. Cimini, R.A., and D.C. Sundberg, *Polym. Eng. Sci.*, **26,** 560 (1986).

67. Brill, R., *Phys. Chem.*, **B53,** 61 (1942).

68. Wallner, L.G., *Monatsch. Chem.*, **79,** 279 (1948).

69. Holmes, D.R., C.W. Bunn, and D.J. Smith, *J. Polym. Sci.*, **17,** 159 (1955).

70. Kinoshita, Y., *Makromol. Chem.*, **33,** 1 (1959).

71. Arimoto, H., *J. Polym. Sci., A-2,* 2283 (1964).

72. Roldan, L.G., and H.S. Kaufman, *J. Polym. Sci. Polym. Lett. Ed., **B1,*** 603 (1963).

73. Ziabicki, A., *Kolloid-Z, **167,*** 132 (1959).

74. Illers, H.K., H. Haberkorn, and P. Sinak, *Makromol. Chem., **158,*** 285 (1972).

75. Parker, J.P., and P.H. Lindenmeyer, *J. Appl. Polym. Sci., **21,*** 821 (1977).

76. Stepaniak, R.F., A. Garton, D.J. Carlsson, and D.M. Wiles, *J. Appl. Polym. Sci., **23,*** 1747 (1979).

77. Kyotani, M., and S. Mitsushashi, *J. Polym. Sci., Part A-2, **10,*** 1497 (1972).

78. Kyotani, M., *J. Macromol. Sci.-Polym. Phys. **B11(4),*** 509 (1975).

79. Kyotani, M., *J. Polym. Sci.-Polym. Phys. Ed., **17,*** 103 (1979).

80. Hirami, M., *J. Macromol. Sci.-Phys. **B19(2),*** 205 (1981).

81. Hirami, M., *J. Macromol. Sci.-Phys. **B23(4-6),*** 397 (1984).

82. Murthy, N.S., S.M. Arahoni, and A.B. Szollosi, *J. Polym. Phys. Ed., **23,*** 2549 (1985).

83. Heuvel, H.M., and R. Huisman, *J. Appl. Polym. Sci., **26,*** 713 (1981).

84. Ishibashi, J., and T. Ishii, *J. Appl. Polym. Sci., **20,*** 335 (1976).

85. Gurato, G., A. fichera, F.Z. Grandi, P. Zannetti, and P. Canal, *Makromol. Chem., **175,*** 953 (1974).

86. Koyama, K., J. Suryadevara, and J.E. Spuriell, *J. Appl. Polym. Sci., **31,*** 2203 (1986).

87. Miyasaka K., and K. Makishima, *J. Polym. Sci. Part A-1, **5,*** 3017 (1967).

88. Bankar, V.G., J.E. Spruiell, and J.L. White, *J. Appl. Polym. Sci., **21,*** 2341 (1977).

89. Park, J.B., K.L. Derries, and W.V. Statton, *J. Makromol. Sci.-Phys. **B15(2),*** 229 (1978).

90. Stamhuis, J.E., S.D. Sjoerdsma, and A.J. Rennings, *J. Macromol. Sci.-Phys. **B22(3),*** 383 (1983).

91. Murthy, N.S., H. Minor, and R.A. Latif, *J. Macromol. Sci.-Phys.* ***B26(4),*** 427 (1987).

92. Khanna, Y.P., and A.C. Reimschuessel, *J. Appl. Polym. Sci.,* ***35,*** 2259 (1988).

93. Khanna, Y.P., A.C. Reimschuessel, A. Banerjie, and C. Altman, *Polym. Eng. Sci.,* ***28,*** 1600 (1988).

94. Khanna, Y.P., R. Kumar, and A.C. Reimschuessel, *Polym. Eng. Sci.,* ***28,*** 1607 (1988).

95. Khanna, Y.P., R. Kumar, and A.C. Reimschuessel, *Polym. Eng. Sci.,* ***28,*** 1612 (1988).

96. Khanna, Y.P., C. Knoll, G. Chomya, *US 4,749,736* (1988).

97. Brucato, V., G. Crippa, and S. Piccarolo, *Polym. Eng. Sci.,* ***31,*** 1411 (1991).

98. Kyotani, M., *J. Macromol. Sci.-Phys.* ***B21(2),*** 275 (1982).

99. Lee, W.J., B.K. Fukai, and J.C. Seferis, *Soc. Plast. Eng. ANTEC Proceeding,* 942 (1987).

100. Engler, P., and S.H. Carr, *Polym. Eng. Sci.,* ***19,*** 779 (1979).

101. Todoki, M., and T. Kawaguchi, *J. Polym. Sci.-Polym. Phys. Ed.,* ***15,*** 1067 (1977).

102. Todoki, M., T. Kawaguchi, *J. Polym. Sci.-Polym. Phys. Ed.,* ***15,*** 1507 (1977).

103. Utracki, L.A., and B. Schlund, *Polym. Eng. Sci.,* ***27,*** 367 (1987).

104. Ide, F., and A. Hasegawa, *J. Appl. Polym. Sci.,* ***18,*** 963 (1974).

105. Liang, B.R., J.L. White, J.E. Spruiell, *J. Appl. Polym. Sci.,* ***28,*** 2011 (1983).

106. Willis, J.M., and B.D. Favis, *Polym. Eng. Sci.,* ***28,*** 1416 (1988).

107. Willis, J.M., V. Caldas, and B.D. Favis, *J. Mat. Sci.,* ***26,*** 4742 (1991).

108. Park, S.J., B.K. Kim, and H.M. Jeong, *Eur. Polym. J.,* ***26(2),*** 131 (1990).

109. Dagli, S.S., M. Xanthos, and J.A. Biesenberger, *Soc. Plast. Eng. ANTEC '90 Proceedings,* 1924 (1990).

110. Mishio, T., Y. Suzuki, K. Kojima, and M. Kakugo, *J. Polym. Eng.*, ***10,*** 123 (1991).

111. Modic, M.J., and L.A. Pottick, *Soc. Plast. Eng. ANTEC '91 Proceedings,* 1907 (1991).

112. Holsti-Miettinen R., and J. Seppala, *Polym. Eng. Sci.*, ***32,*** 868 (1992).

113. Ishida, H., and N. Scherbakoff, *Makromol. Chem. Macromol. Symp.*, ***50,*** 157 (1991).

114. Adur, A.M., and R.C. Constable, *Compalloy '92, USA* (1992).

115. Molau, G.E., *J. Appl. Polym. Sci., Part A,* ***3,*** 1267 (1965).

116. Lambla, M., R.X. Yu, and Y.P. Zhu, *Soc. Plast. Eng. ANTEC '91,* 1051 (1991).

117. Oliver, E.J., *US 4,594,386* (1986).

118. Hammer, *US 4,017,557* (1977).

119. Oliver, E.J., and B. Ronge, *US 5,003,003* (1991).

120. Flexman Jr. E.A., *Polym. Eng. Sci.*, ***19(8),*** 564 (1979).

121. Wu, S., *J. Appl. Polym. Sci.-Polym. Phys. Ed.*, ***21,*** 699 (1983).

122. Wu, S., *Polymer,* ***26,*** 1855 (1985).

123. Cimmino S., D.R. Greco, G. Maglio, M. Malinconico, C. Mancarella, E. Martuscelli, and G. Ragosta, *Polym. Eng. Sci.*, ***24,*** 48 (1984).

124. Cimmino S., L. Dorazo, D.R. Greco, G. Maglio, M. Malinconico, C. Mancarella, E. Martuscelli, P. Musto, R. Palumbo, and G. Ragosta, *Polym. Eng. Sci.*, ***25,*** 193 (1985).

125. Cimmino S., F. Coppola, L. D'Orazio, D.R. Greco, G. Maglio, M. Malinconico, C. Mancarella, E. Martuscelli, and G. Ragosta, *Polymer,* ***27,*** 1874 (1986).

126. Martuscelli, E., F. Riva, C. Sellitti, and C. Silvestre, *Polymer,* ***26,*** 270 (1985).

127. Borggreve, R.J.M., R.J. Gaymans, J. Schijer, and J.F. Ingen Housz, *Polymer,* ***28,*** 1489 (1987).

128. Borggreve, R.J.M., R.J. Gaymans, and A.R. Luttmer, *Makromol. Chem. Macromol. Symp.*, ***16,*** 195 (1988).

129. Borggreve, R.J.M., R.J. Gaymans, *Polymer, **30,*** 63 (1989).

130. Borggreve, R.J.M., R.J. Gaymans, and J. Schijer, *Polymer, **30,*** 71 (1989).

131. Borggreve, R.J.M., R.J. Gaymans, and H.M. Eichenwald, *Polymer, **30,*** 78 (1989).

132. Greco, R., M. Malinconico, E. Martuscelli, G. Ragosta, and G. Scarinzi, *Polymer, **28,*** 1185 (1987).

133. Greco, R., M. Malinconico, E. Martuscelli, G. Ragosta, and G. Scarinzi, *Polymer, **29,*** 1418 (1988).

134. Greco, R., N. Lanzetta, G. Maglio, M. Malinconico, E. Martuscelli, R. Palumbo, G. Ragosta and G. Scarinzi, *Polymer, **27,*** 299 (1986).

135. Oshinski, A.J., H. Keskkula, and D.R.Paul, *Polymer, **33,*** 268 (1992).

136. Oshinski, A.J., H. Keskkula, and D.R.Paul, *Polymer, **33,*** 277 (1992).

137. Lawson, D.F., W.L. Hergenrother, and M.G. Matlock, *J. Appl. Polym. Sci., **39,*** 2331 (1990).

138. Mandy, F., *Plast. and Rubber, **1,*** 119 (1976).

139. Jakopin, S., *Adv. Polym. Tech., **3(4),*** 365 (1982).

140. Thomason, L.J., and A.A. Van Rooyen, in *"Controlled Interphases in Composite Material", Elsevier Science Publishing Co., H. Ishido ed.*, 423 (1990).

141. Folkes, M.J., and S.T. Hardwick, *J. Mat. Sci. Letter, **3,*** 1071 (1984).

142. Otaigbe, J.U., and W.G. Harland, *J. Appl. Polym. Sci., **36,*** 165 (1988).

143. Goettler, L.A., and W.J. Neff, *Polym. Eng. Sci., **7,*** 383 (1986).

144. Ishida, H., and G. Rotter, *Proc. 43rd Ann. Tech. Conf. Composite Inst., SPI, Session 6-A, Cincinnati, USA* (1988).

145. Gechele, G.B., and A. Mattiussi, *Eur. Polym. J., **1,*** 47 (1965).

146. Anton, A., *J. Appl. Polym. Sci., **7,*** 1629 (1963).

147. Ongemach, G.C., V.A. Dorman-Smith, and W.E. Beier, *Anal. Chem., **38,*** 123 (1966).

148. Ongemach, G.C., and A.C. Moody, *Analy. Chem.*, ***39,*** 1005 (1967).

149. Hedrick, R.M., J.D. Gabbert, and M.H. Wohl, *Am. Chem. Soc.*, 135 (1985).

150. Kao, S.V., and G.R. Allison, *Polym. Eng. Sci.*, ***24,*** 645 (1984).

151. Samanta, S.R., *J. Appl. Polym. Sci.*, ***45,*** 1635 (1992).

152. Schaefgen, J.R., and C.F. Trivisonno, *J. Am. Chem. Soc.*, ***73,*** 4580 (1951).

153. Hinrichsen, M., *Makromol. Chem.*, ***166,*** 291 (1973).

154. Wunderlich, B., and F.N. Liberti, *J. Polym. Sci., Part A-2,* ***6,*** 833 (1968).

155. Inoue, M., *J. Polym. Sci., Part A,* ***1,*** 2697 (1963).

156. Kinoshita, Y., *Makromol. Chem.*, ***33,*** 1 (1959).

157. Arimoto, H., J. *Polym. Sci., A-2,* 2283 (1964).

158. Bradburry, E.M., and A. Elliot, *Polymer,* ***4,*** 47 (1963).

159. Ismat, A., *J. Polym. Sci., Part A-1,* ***9,*** 199 (1971).

160. Matsubara, I., and J.H. Magill, *Polymer,* ***7,*** 199 (1966).

161. Bessell, T.J., D. Hull, and J.B. Shortall, *J. Mat. Sci.*, ***10,*** 1127 (1975).

162. Galeski, A., A.S. Argon, and R.E. Cohen, *Makromol. Chem.*, ***188,*** 1195 (1987).

163. Galeski, A., A.S. Argon, and R.E. Cohen, *Makromol.*, ***21,*** 2761 (1988).

164. Martinez-Salazar, J., and C.G. Cannon, *J. Mat. Sci. Letters,* ***3,*** 693 (1984).

165. Schaper, A., R. Hirte, C. Ruscher, R. Hillebrand, and E. Walenta, *Colloid Polym. Sci.*, ***264,*** 649 (1986).

166. Matyi, R.J., and B. Crist, J. Polym. Sci., *Phys. Ed.*, ***16,*** 1329 (1978).

167. Nunes, R.W., J.R. Martin, and J.F. Jahoran, *Polym. Eng. Sci.*, ***22,*** 205 (1982).

168. McCrum, N.E., B.E. Read, and G. Williams, in *"Anelastic and Dielectric Effects in Polymer Solid",* John Wiley & Sons, London, (1967).

169. Woodward, A.E., and J.A. Sauer, *Adv. Polym. Sci.*, ***1,*** 114 (1958).

170. Rele, V.B., and Y.S. Papir, *J. Macromol. Sci.-Phys.*, ***B 13(3),*** 405 (1977).

171. Woodward, A.E., and J.A. Sauer, *J. Colloid Sci.*, ***12,*** 363 (1957).

172. Papir, Y.S., S. Kapur, C.E. Rogers, and E. Baer, *J. Polym. Sci., A-2,* ***10,*** 1305 (1972).

173. Curtis, A.J., *J. Res. Nat. Bur. Stand.,* ***65A,*** 185 (1961).

174. Rong, T., and H.L. William, *J. Appl. Sci.,* ***30,*** 2575 (1985).

175. Garbuglio, C., G. Ajroldi, T. Casiraghi, and G. Vittadini, *J. Appl. Polym. Sci.,* ***15,*** 2487 (1971).

176. Kotlik, P., V. heidingsfeld, and J. Zelinger, *J. Polym. Sci.-Polym. Chem. Ed.,* ***12,*** 2639 (1974).

177. Wichterle, O., *Makromol. Chem.,* ***35,*** 174 (1960).

178. Dharia, A., and S.J. Grossman, *Soc. Plast. Eng. ANTEC '87 Proceedings,* 590 (1987).

179. Tirrell, D., S.J. Grossman, and O. Vogl, *Makromol. Chem.,* ***180,*** 721 (1979).

180. Cheremisinoff, N.P., Ed. *"Handbook of Polymer Science & Technology",* ***2,*** 507 (1990).

181. Strate, G.V., Ed., *"Encyclopaedia of Polymer Science & Engineering",* John Wiley & Sons, New York, ***vol.6*** (1986).

182. Kim, J.W., and S.C. Kim, *Polym. for Adv. Technologies,* ***2,*** 177 (1991).

183. Baranwal, K., *J. Appl. Polym. Sci.,* ***12,*** 1459 (1968).

184. Serpe, G., J. Jarrin, and R.F. Daren, Polym. Eng. Sci., 30, 562 (1990).

185. VISTALON Ethylene-Propylene Rubber user guide, *Exxon Chemicals Company,* 1990.

186. De Vito, G., N. Lanzetta, G. Maglio, M. Malinconico, P. Musto, and R. Palumbo, *J. Polym. Sci., Polym. Chem. Ed.,* ***22,*** 1335 (1984).

187. Casale, A., and R.S. Porter, *"Polymer Stress Reaction",* ***vol.1,*** Academic Press, New York, 1978.

188. Curto, D., A. Valenza, and F.P. Mantia, *J. Appl. Polym. Sci.,* ***39,*** 865 (1992).

189. Rotter G., and H. Ishida, *J. Polym. Sci., Part B, Polym. Phys.,* ***30,*** 489 (1992).

190. Macknight, W.J., and R.W. Lenz, *Polym. Eng. Sci., 25,* 1124 (1985).

191. Baldwin, F.P., and G. Ver Strate, *Rubber Chem. Tech., 45(3),* 834 (1972).

192. Borsig, E., A. Fiedlerow, and M. Lazar, *J. Macromol. Sci., Chem. A., 16,* 513 (1981).

193. Straus, S., and L.A. Wal, *J. of Research, National Bureau of Standards, 60(11),* 39 (1958).

194. D'Orazio, L., C. Mancarella, E. Martuscelli, A.Y. Casale, A. Fillippi and K. Speroni, *J. Mat. Sci., 21,* 989 (1986).

195. Merz, E.H., Claver, G.C., and M. Baer, *J. Polym. Sci., 22,* 325 (1956).

196. Kunz, S., P.W. Beaumont, and M.F. Ashby, *J. Mat. Sci., 15,* 1109 (1980).

197. Hobbs, S.Y., R.C. Bopp, and V.H. Watkins, *Polym. Eng. Sci., 23,* 1982 (1983).

198. Wu, S, *Polymer, 26,* 1855 (1985).

199. Addonizio, M.L., L.D. Orazio, and E. Martuscelli, *Polymer, 32,* 109 (1991).

200. Xanthos, M., M.W. Young, and J.A. Biesenberger, *Polym. Eng. Sci., 30,* 355 (1990).

201. Frensch, H., and B.J. Jungnickel, *Plastics, Rubber & Composites Processing & Applications, 1,* 16 (1991).

202. Lavallee, C., and B.D. Favis, *ANTEC '91 Proceedings, Soc. Plast. Engineers,* 973 (1991).

203. Utracki, L.A., "Polymer Alloys and Blends", Hanser Publishers, Munich, 112 (1990).

204 Braun, D., and U. Eisenlohr, *Kunstoffe, 65,* 139 (1975).

205. Alle, C.N., and J.L. Jorgensen, *Rheol. Acta, 19,* 104 (1980).

206. Scott, C.E., and C.W. Macosko, *Polym. Bulletin, 26,* 341 (1991).

207. Jordhamo, G.M., J.A. Manson, and L.H. Sperling, *Polym. Eng. Sci., 26,* 517 (1986).

208. Sorensen, I.W., ACS, *Polym. Mat. Sci. & Eng., 185,* 201 (1985).

209. Glotin, M., R. Parsy, and P. Abadie, *FR. Appl. No 003877,* 24.03.88.

210. Miles, I.S., and A. Zurek, *Polym. Eng. Sci.*, ***20,*** 796 (1988).

211. Sperling, L.H., C.S. Heck, and J.H. An, *American Chemical Society series,* ***395,*** 230 (1989).

212. Takayanagi, M., and T. Matsuo, *J. Macromol. Sci., Phys.* ***B1(3),*** 407 (1967).

213. La Mantia, F.P., *Adv. in Polym. Tech.*, ***12(1),*** 47 (1993).

214. Utracki, L.A., and P. Sammut, *Polym. Networks & Blends,* ***2(1),*** 23 (1992).

APPENDICES

Sodium Caprolactamate

Introduction

Sodium caprolactamate is specially manufactured for use in anionic polymerisation to nylon-6.
Together with the accelerator V5*, sodium caprolactamate is used to control the speed and quality of the anionic polymerisation process.

Formula

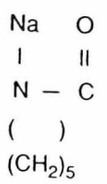

Appearance

Solid, white product.
Strongly hygroscopic.

Physical properties

Density at 20°C	1100 kg/m^3
Melting range (at 135°C completely molten)	80-135°C.

Application

The reaction mixture for the anionic polymerisation of nylon-6 consists of AP-lactam, sodium caprolactamate and accelerator V5.
The amount of sodium caprolactamate and accelerator V5 to be added is determined by many factors like e.g. thickness and construction of end product, temperatures used, performance requirements etc.
As an average 2-4% (by weight) sodium caprolactamate is used.
Sodium caprolactamate is added to the molten AP-lactam.
Because of the high sensitivity to moisture the material has to be handled very carefully.
The average processing temperatures used for the mixture of accelerator V5 and AP-lactam is 100°-130°C.

The mould temperature 130°-170°C.

Packing

1. Iron drums with an airtight and waterproof lid, PE-innerbag, bag with drying agent.
   Nett weight: 10, 20 or 50 kgs.
2. Cardboard box with PE/Aluminium innerbag.
   Nett weight: 2 kgs.

Safety precautions

Fire should be extinguished by water spray.
At temp. >300°C toxic NO_2-vapours are formed.
The use of protective gloves, goggles and clothing is recommended in order to avoid prolonged contact with the skin (splashing) when handling the hot molten product.
Good ventilation or dust extraction-equipment should be applied wherever vapour, dust or fine particles are present.

Toxicity

Oral LD 50 (rat) 5400 mg/kg.
Skin irritation (rabbit) none.

* see separate Product Information Sheet.

Accelerator V5

Introduction

The accelerator V5 is specially manufactured for use in the anionic-polymerisation to nylon-6.
Together with the catalyst, sodium caprolactamate* the accelerator V5 is used to control the speed and quality of the anionic polymerisation process.

Formula

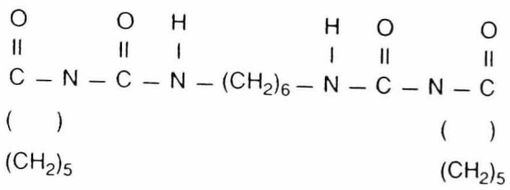

Appearance

Solid, white product.
Hygroscopic

Physical properties

Density at 20°C	1200 kg/m^3
Melting range	80-130°C

Application

The reaction mixture for the anionic polymerisation of nylon-6 consists of AP-lactam, sodium caprolactamate and accelerator V5.
The amount of sodium caprolactamate and accelerator V5 to be added is determined by many factors like e.g. thickness and construction of endproduct, temperatures used, performance requirements etc.
As an average 1-3% (by weight) accelerator V5 is used.
Accelerator V5 is added to the molten AP-lactam.
Because of the sensitivity to moisture the material has to be handled very carefully.
The average processing temperatures used for the mixture of accelerator V5 and AP-lactam is 100°-130°C.
The mould temperature 130°-170°C.

Packing

1. Iron drums with an airtight and waterproof lid, PE-innerbag, bag with drying agent.
   Nett weight: 10, 20 or 50 kgs.
2. Cardboard box with PE/Aluminium innerbag.
   Nett weight: 2 kgs.

Safety precautions

Fire may be extinguished by using foam or powder.
The substance decomposes very slowly upon heating at temperatures >180°C, forming caprolactam and isocyanate.
At temp. >300°C toxic NO_2-vapours are formed.
The use of protective gloves, goggles and clothing is recommended in order to avoid prolonged contact with the skin (splashing) when handling the hot molten product.
Good ventilation, or dust extraction-equipment should be applied wherever vapour, dust or fine particles are present.

Toxicity

Oral LD 50 (rat) 5400 mg/kg.
Skin irritation (rabbit) none.

* see seperate Product Information Sheet.

DSM Chemicals

Material Safety Data Sheet

AP-Caprolactam (molten at 80 °C)

Synonyms: E-Caprolactam, 2 Oxohexamethylene imine.

Formula: $CH_2(CH_2)_4CONH$

Section 1 Manufacturer's name: Fibre Intermediates

Address:	Mauritslaan 49, 6129 EL Urmond The Netherlands
Emergency telephone number:	31-4490-65555
Telephone number for information:	31-4490-63881
Telex number:	36777
Fax number:	31-4490-63853
Date prepared:	Sept. 1988.
Signature of preparer:	J.T.J. van Goolen

Ir. J.T.J. van Goolen
Business Director
DSM Fibre Intermediates

Section 2 Hazardous ingredients/identity information

(Hazardous components) and CAS number	Weight %
Caprolactam CAS (105-60-2)	min. 99.5
Water	min. 0.015
Acidity/Alkalinity	max. 0.05 meq/kg
Ash	max. 10 mg/kg

Section 3 Physical/chemical characteristics

Boiling point (°C):	270.0
Boiling point (°F):	518.0
Vapour pressure (20 °C/68 °F) in mbar:	< 1
Vapour density (air = 1):	3.9
Specific gravity (80 °C/176 °F):	1.0
Melting point (°C):	69.0
Melting point (°F):	156.0
Evaporation rate (butyl acetate = 1):	n.a.
Solubility in water (25 °C/77 °F):	525 g/100 ml.
Appearance and odour:	Colourless liquid.

APPENDIX II

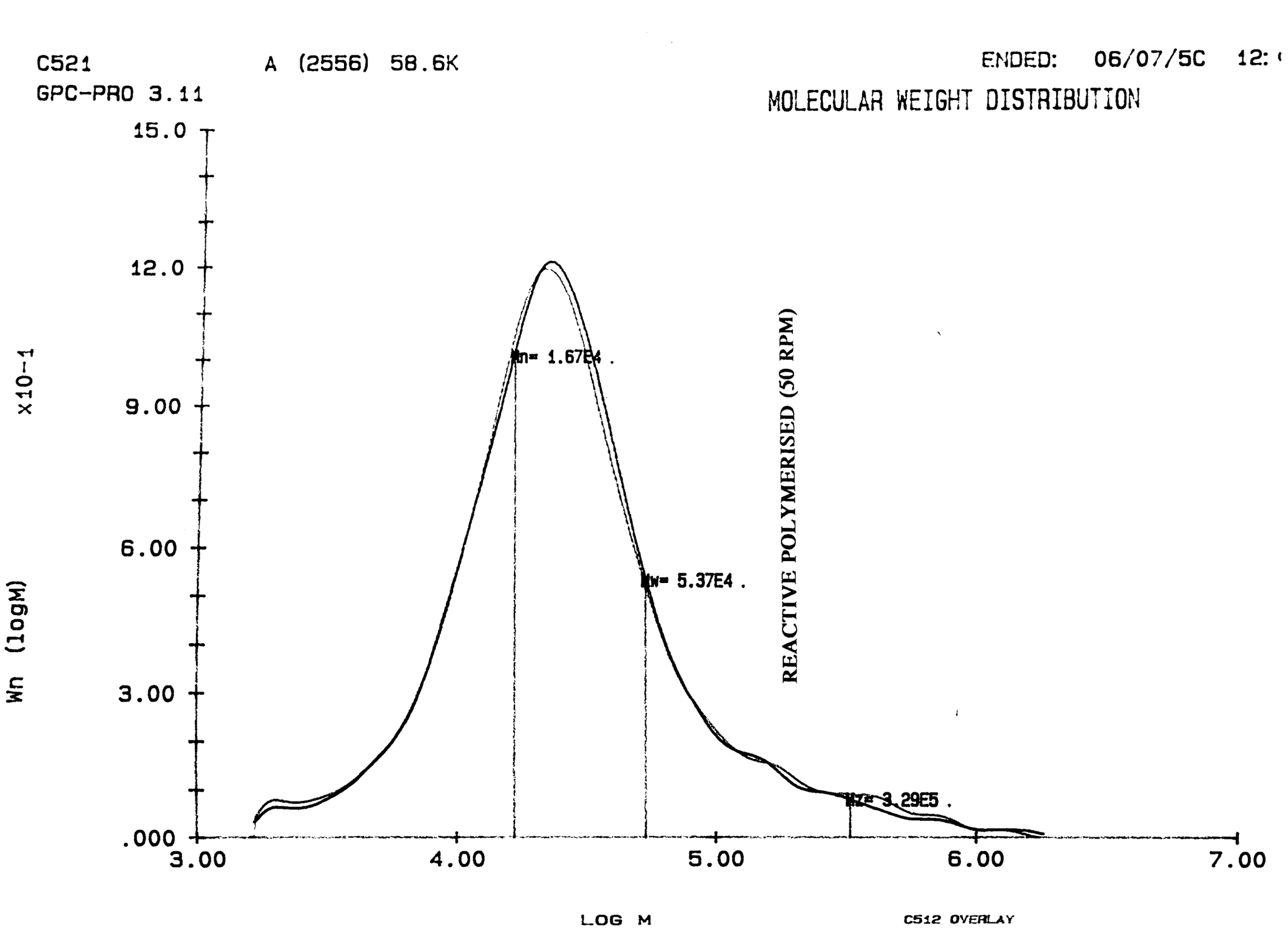
C521
A (2556) 58.6K
ENDED: 06/07/5C 12:
GPC-PRO 3.11
MOLECULAR WEIGHT DISTRIBUTION
15.0
12.0
9.00
6.00
3.00
.000
x10-1
Wn (logM)
Mn= 1.67E4 .
Mw= 5.37E4 .
Mz= 3.29E5 .
REACTIVE POLYMERISED (50 RPM)
3.00
4.00
5.00
6.00
7.00
LOG M
C512 OVERLAY

APPENDIX II

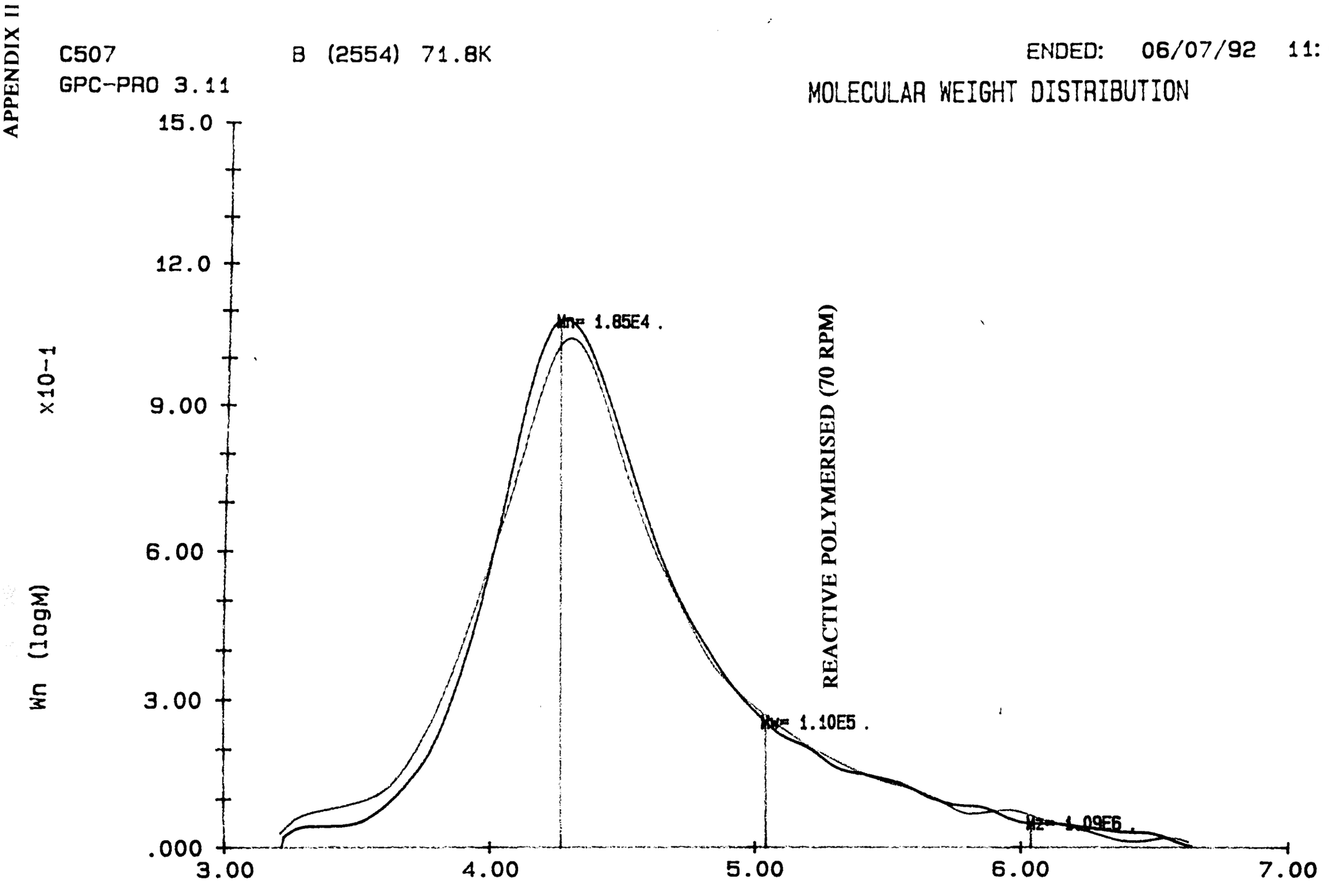
C507
B (2554) 71.8K
ENDED: 06/07/92 11:
GPC-PRO 3.11
MOLECULAR WEIGHT DISTRIBUTION
15.0
12.0
9.00
6.00
3.00
.000
x10-1
Wn (logM)
Mn= 1.85E4 .
Mw= 1.10E5 .
Mz= 1.09E6 .
REACTIVE POLYMERISED (70 RPM)
3.00
4.00
5.00
6.00
7.00

APPENDIX II

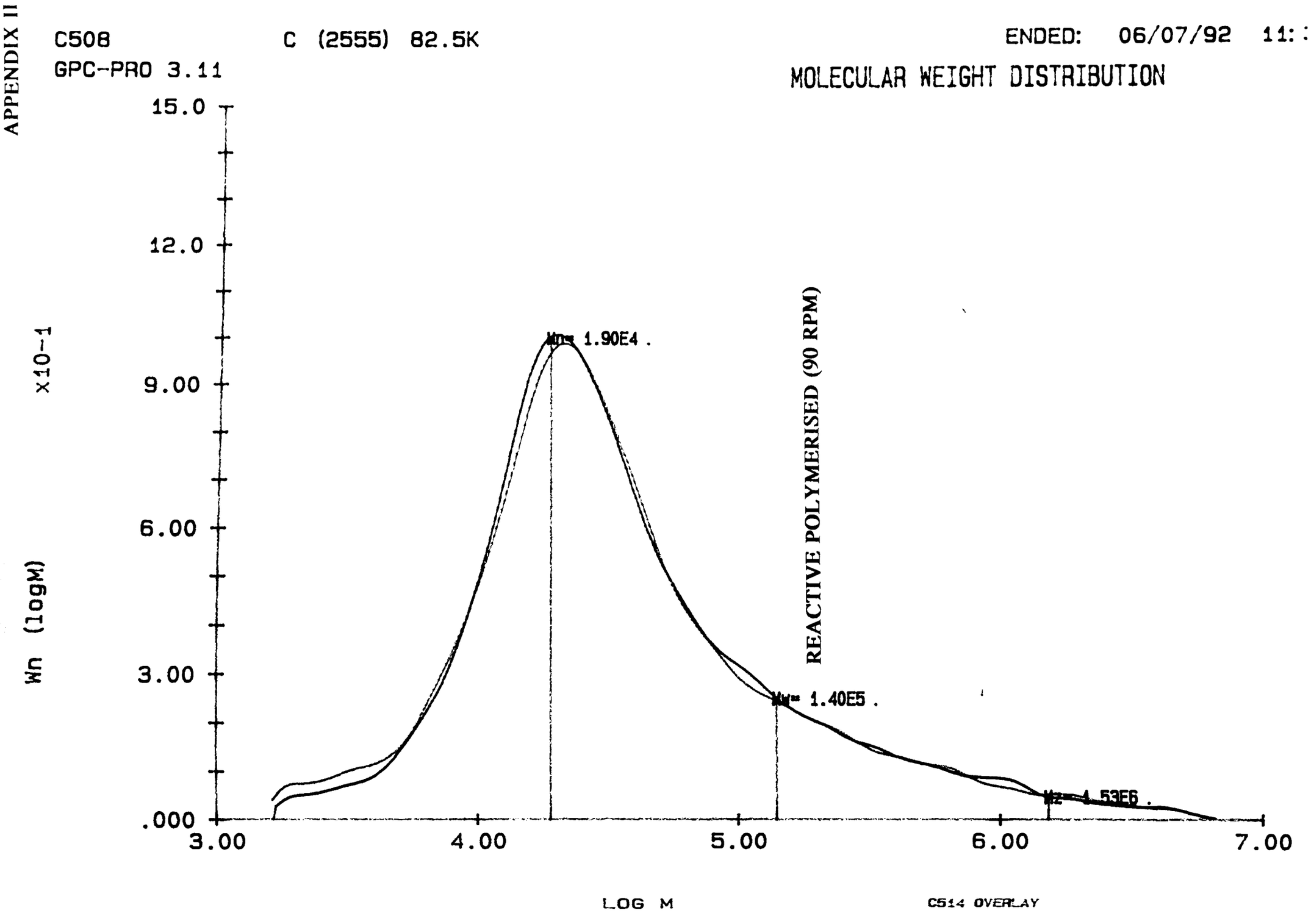
C508
C (2555) 82.5K
ENDED: 06/07/92 11:
GPC-PRO 3.11
MOLECULAR WEIGHT DISTRIBUTION
15.0
12.0
9.00
6.00
3.00
.000
x10-1
Wn (logM)
Mn= 1.90E4 .
Mw= 1.40E5 .
Mz= 4.53E6 .
REACTIVE POLYMERISED (90 RPM)
3.00
4.00
5.00
6.00
7.00
LOG M
C514 OVERLAY

APPENDIX II

C515 D (2556) 56.2K ENDED: 06/07/5C 0E: :

GPC-PRO 3.11

MOLECULAR WEIGHT DISTRIBUTION

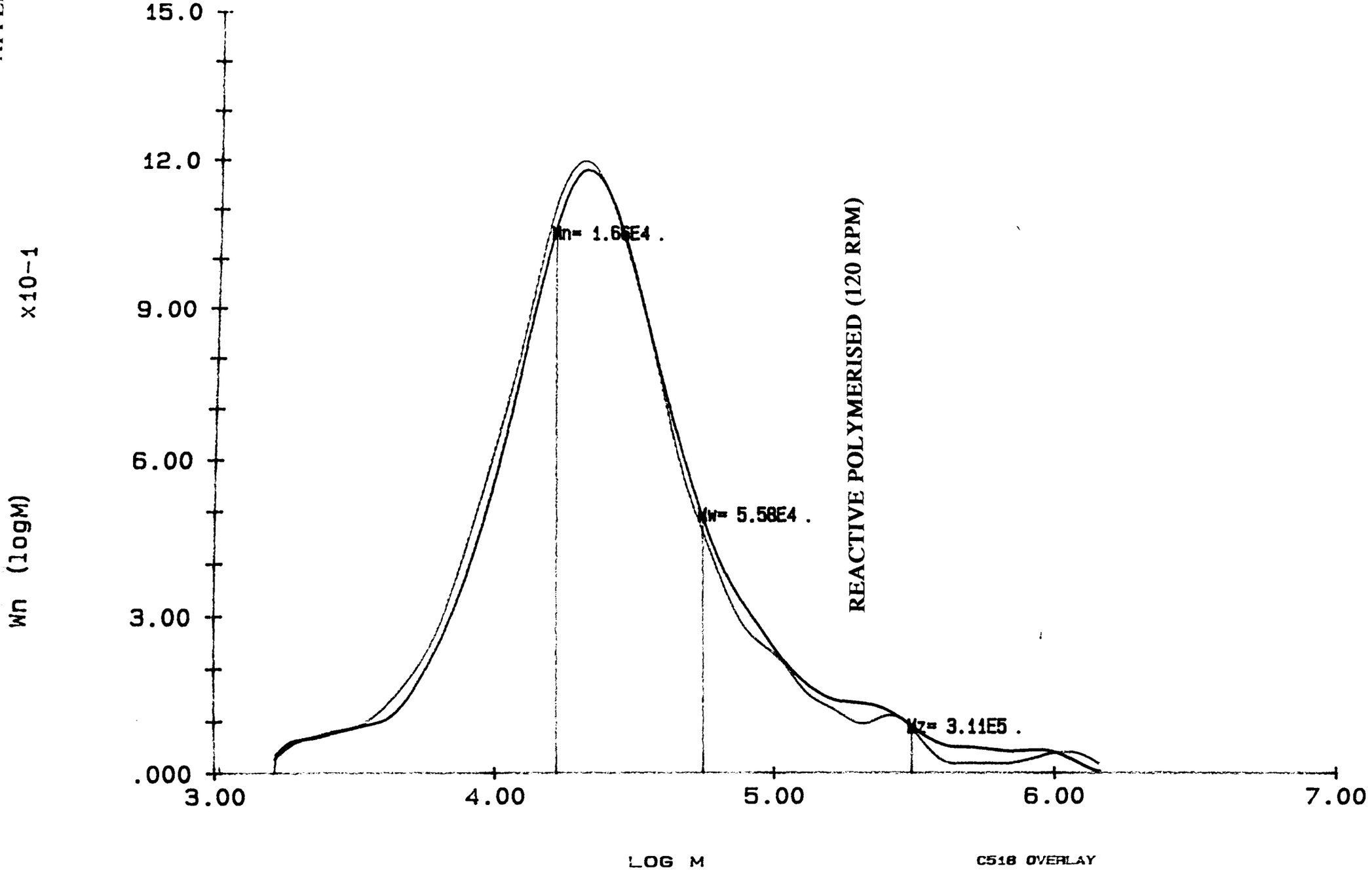

APPENDIX II

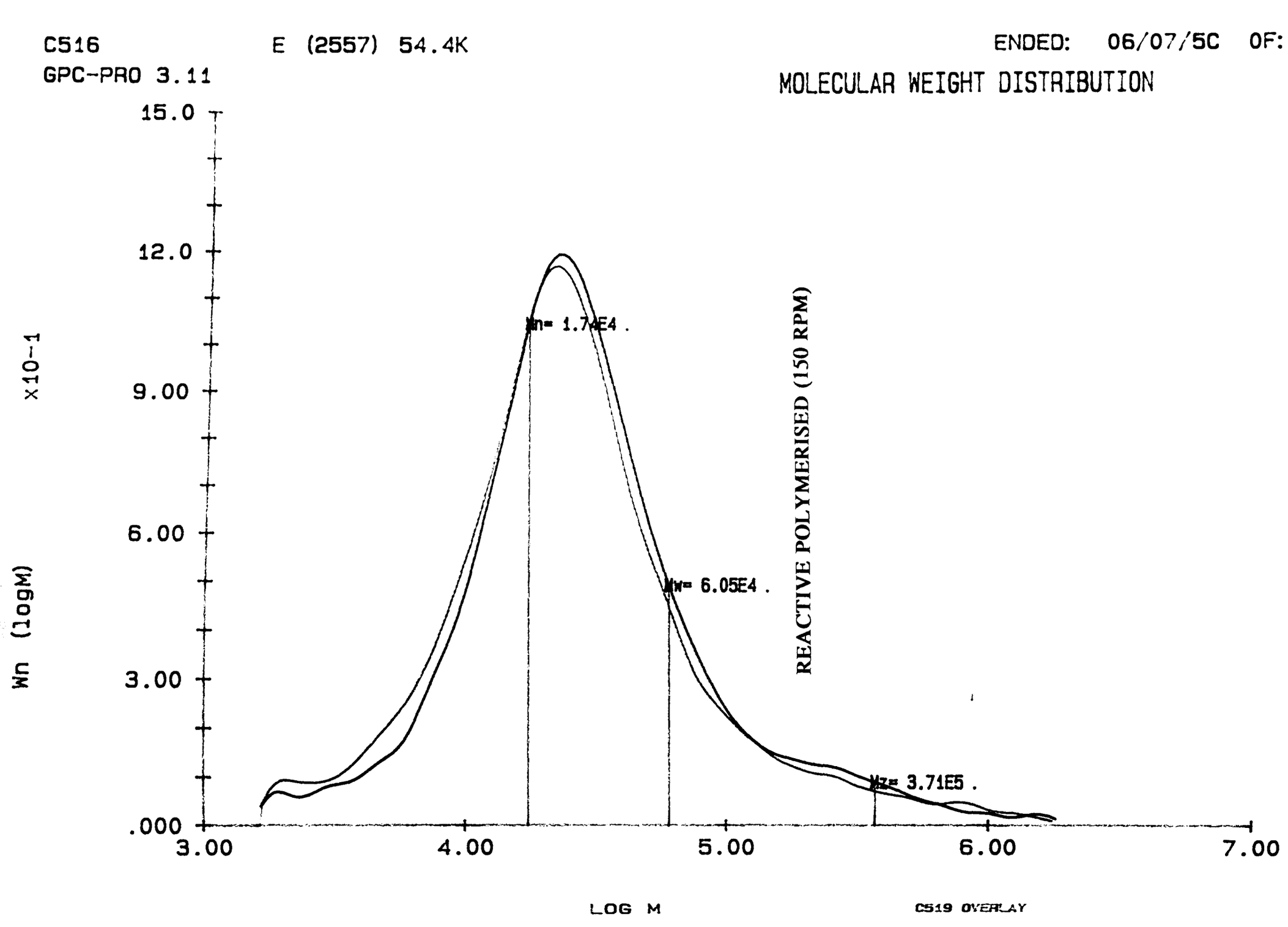
C516
E (2557) 54.4K
ENDED: 06/07/5C 0F:
GPC-PRO 3.11
MOLECULAR WEIGHT DISTRIBUTION
15.0
12.0
9.00
6.00
3.00
.000
x10-1
Wn (logM)
Mn= 1.74E4 .
Mw= 6.05E4 .
Mz= 3.71E5 .
REACTIVE POLYMERISED (150 RPM)
3.00
4.00
5.00
6.00
7.00
LOG M
C519 OVERLAY

APPENDIX II

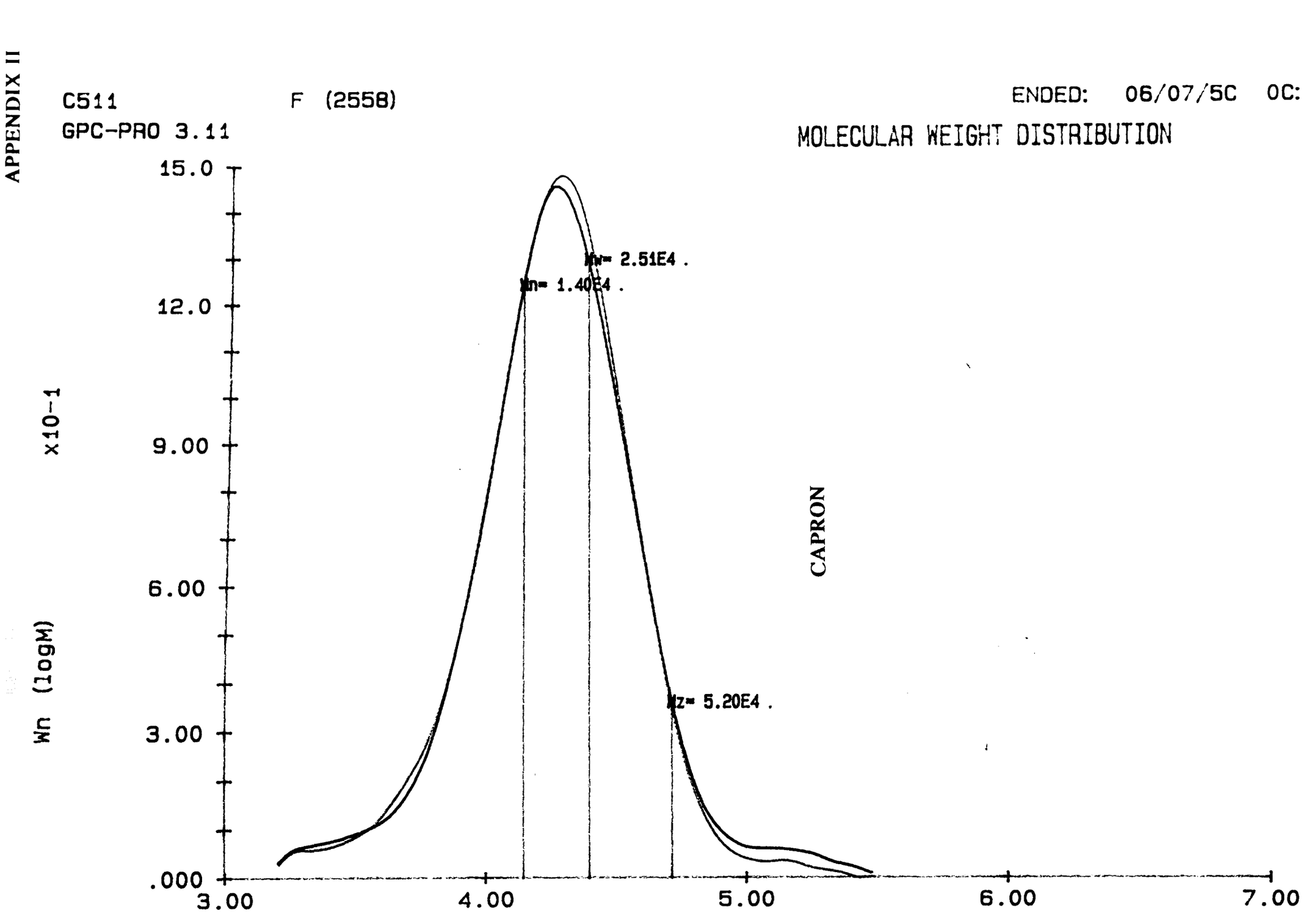
C511
F (2558)
ENDED: 06/07/5C 0C: :
GPC-PRO 3.11
MOLECULAR WEIGHT DISTRIBUTION
15.0
12.0
9.00
6.00
3.00
.000
x10-1
Wn (logM)
Mw= 2.51E4 .
Mn= 1.40E4 .
Mz= 5.20E4 .
CAPRON
3.00
4.00
5.00
6.00
7.00

PPS-9

THE POLYMER PROCESSING SOCIETY

NINTH ANNUAL MEETING

Manchester, England

April 5-8, 1993

EXTENDED ABSTRACTS & FINAL PROGRAMME

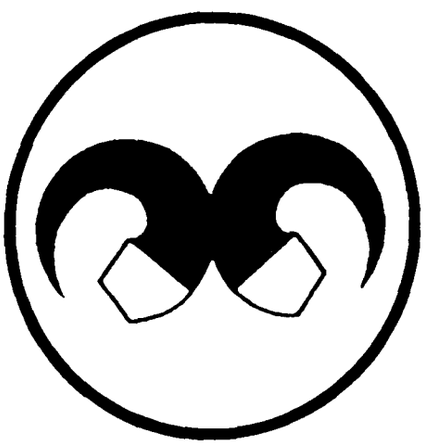

SPONSORS

INSTITUTE OF MATERIALS
INSTITUTION OF CHEMICAL ENGINEERS
INSTITUTION OF MECHANICAL ENGINEERS
DOW EUROPE SA
COURTAULDS plc

CHARACTERISATION OF POLYAMIDE 6 SYNTHESISED IN A TWIN-SCREW EXTRUDER

P.R. Hornsby, J.F. Tung and K. Tarverdi
(Wolfson Centre for Materials Processing,
Brunel University, Uxbridge, Middx, UK)

Continuous anionic polymerisation of catalysed ε-caprolactam has been undertaken on an intermeshing co-rotating twin-screw extruder. Resulting products were characterised to determine the effects of processing conditions on polymer structure and properties.

Polyamide 6 (PA6) was prepared with an optimised screw and barrel configuration, to permit necessary feeding, mixing, devolatilising and pumping requirements, using various screw speeds and barrel temperature profiles, altered to influence the thermal and shear history of the reaction mixture. PA6 melt extrudate was produced as a 4mm diameter rod, which was either rapidly water quenched or allowed to cool slowly in air. Some compositions were also prepared containing 10% by weight of chopped glass fibre, introduced in the extruder together with the caprolactam monomer.

Representative samples of PA6 were analysed by differential scanning calorimetry (DSC) under controlled conditions of heating (up to 250°C) and cooling, to assess crystallisation and melting phenomena. A second melting thermogram was then obtained (stage 2) under the same conditions as the first heating run. Some samples were annealed at temperatures up to 180°C for 90 min. prior to analysis by DSC.

DSC thermograms were influenced by the material composition, method of preparation and annealing procedure, reflecting the extent and form of crystalline order present. For example, during initial heating by DSC (stage 1) both unreinforced water quenched and glass fiber-reinforced water quenched samples exhibited broad melting peaks, suggesting the presence of less well ordered lower melting point crystalline material. After annealing at 180°C for 90 min. followed by slow cooling to room temperature narrowing of these peaks occurred. A noticeable increase in maximum crystallisation temperature was observed in samples polymerised in the presence of glass fibre due to the nucleating effect of this additive.

Complementary wide angle X-ray diffraction (WAXD) studies undertaken on water quenched and most air cooled samples of PA6 extrudate revealed two sharp peaks, characteristic of α- crystalline phases with interplanar spacings of d_{200} = 4.44 Å and d_{002} = 3.82 Å. However WAXD profiles obtained from fibre-reinforced materials, contained an additional reflection peak corresponding to a crystal inter-planar spacing of d_{100} = 4.24 Å consistent with the presence of the γ crystalline form of PA6. On annealing composite PA6 samples at 180°C for 90 min, both α and γ crystalline peaks increased in intensity.

Molecular weight and molecular weight distribution of PA6 samples were determined by solution viscometry and gel permeation chromatography respectively. Residual monomer content was measured by gas chromatography. Both molecular weight and molecular weight distribution were influenced by polymerisation conditions in the extruder, yielding

values of $\bar{M}_v$ up to 100kg mol^{-1} and polydispersity index of up to 6.

Monomer residue also varied from approximately 6% in same unreinforced PA6 samples to about 3% when glass fibre was present.

Selected mechanical properties of PA6 samples were measured using standard test procedures, on injection moulded test pieces after extraction of residual monomer and storage of specimens at 50% relative humidity (23°C). Some results are shown below, which also includes data measured on commercial PA6 resin (CAPRON 8202C - Allied Signal Inc), made by hydrolytic polymerisation. Unreinforced PA6 made by reactive extrusion exhibited superior impact and elongational properties under tensile deformation, but have slightly reduced tensile strength compared to commercial polymer.

TENSILE STRENGTH

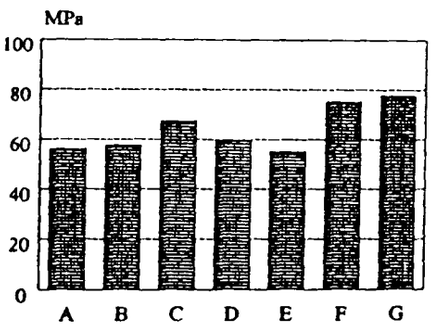

ELONGATION AT BREAK

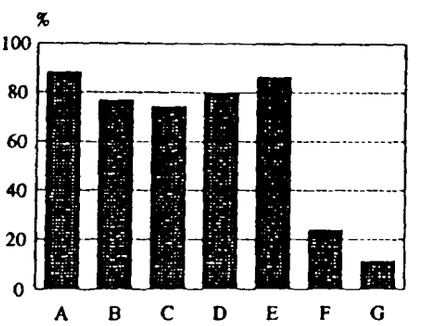

IZOD IMPACT RESISTANCE

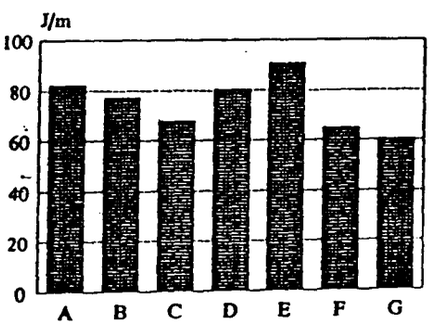

A - E : PA6 made @50,70,90,120,150rpm

F: 10% glass-filled PA6 made @90rpm

G: commercial grade PA6

ANTEC 93

"Be In That Number"

NEW ORLEANS MAY 9-13, 1993

VOLUME III
1993

Society of Plastics Engineers

CONFERENCE PROCEEDINGS

Plastics Engineering

CHARACTERIZATION OF POLYAMIDE 6 SYNTHESISED IN A TWIN-SCREW EXTRUDER

P.R. HORNSBY, J.F. TUNG AND K. TARVERDI

Department of Materials Technology
Brunel University
Uxbridge, Middlesex UB8 3PH, U.K.

1. INTRODUCTION

Polyamide 6 (PA6) can be prepared by the activated anionic polymerisation of ε-caprolactam in the presence of alkaline catalysts, such as alkali carbonates, hydrides or organo-metallic compounds [1]. Rates of reaction are rapid, enabling synthesis of high molecular weight PA6, in only a few minutes compared to many hours of reaction time using an alternative hydrolytic polymerisation process [2].

Continuous anionic polymerisation of ε-caprolactam may be undertaken in a twin-screw extruder,through appropriate control of the process parameters and in particular, the screw geometry and necessary functional characteristics of the machinery, such as the nature of feeding, melting, mixing, reacting and devolatilization zones [3]. Procedures have been reported for combined polymerisation of ε-caprolactam in a twin-screw extruder together with die forming of the resulting PA6 into a semi-finished product, with claimed economic and technical benefits [4].

Polymerisation of caprolactam in the presence of glass fibre reinforcement has also been considered previously both using reactive injection moulding and twin-screw extrusion melt impregnation technologies [5], with the aim of enhancing fibre-wetout by the PA6 and interfacial adhesion.

Very limited attention has been given, however, to the influence of polymerisation processing conditions, or the presence of included fibre reinforcement, on the molecular mass, residual monomer content and crystalline morphology of the PA6 formed in this way, which will have a critical bearing on its physical properties.

This paper will address these issues through detailed characterisation of PA6, made using different processing conditions on a co-rotating intermeshing twin-screw extruder.

2. EXPERIMENTAL

2.1 Polymerisation of ε-Caprolactam

Samples of PA6 were prepared on a 40mm screw diameter co-rotating twin-screw extruder (BTS 40-Betol Machinery) by anionic polymerisation of ε-caprolactam monomer (DSM Chemicals Ltd) containing 3% by weight of sodium caprolactamate catalyst and 2% by weight of accelerator (V-5 DSM Chemicals and Fertilizers). The extruder configuration and barrel temperature profiles [Figure 1] were choosen to accommodate the changing materials characteristics from melting the ε-caprolactam feedstock, monomer polymerisation in the reaction-zone and melt conveying of the PA6 reaction product. Screw speeds were varied between 50 and 150 rpm, thereby altering material residence time within the barrel, whilst maintaining constant conditions of both material feed rate to the extruder and barrel temperature profile. PA6 extrudate, die formed as a 4mm diameter rod, was either water quenched or allowed to cool slowly in air to room temperature.

Some samples of PA6 containing short glass fibre reinforcement were made in a similar way, by combining 10% by weight of sized, chopped glass strand (with 6mm nominal fibre length) into the monomer/ catalyst/ accelerator system as a premix. The pelletised samples were subsequently extracted with boiling distilled water overnight to remove residue monomer before drying in vacuo at 90°C for 6 hours. The dried samples were then stored in dessicators, maintained in an atmosphere of 50% humidity, prior to properties evaluation.

2.2 Structural Characterisation

Representative samples of PA6 with differing processing history were analysed on a Perkin-Elmer DSC-2B differential scanning calorimeter, by thermal cycling under specified conditions of heating and cooling to assess melting and crystallisation phenomena. During the first heating cycle (Stage 1) between 6 and 8 mg of sample was heated from 40°C to 250°C at a rate of 10°C min^{-1}, in order to monitor melting behaviour, then maintained at 250°C for 15 minutes before cooling to 40°C at a rate of 5°C min^{-1} to determine the onset of crystallisation. A second melting thermogram was then obtained (Stage 2), using the same conditions as the first heating run. Some samples were annealed at temperatures up to 180°C for 90 minutes , prior to analysis by DSC.

Complementary wide angle X-ray diffraction (WAXD) profiles were also obtained on a Philips PW1050 Goniometer to further elucidate the influence of processing , compositional and annealing variables on crystalline order produced.

2.3 Determination of Mechanical Properties

Tensile and impact test specimens were prepared by injection moulding technique in accordance with ISO 1874-2. For comparison, samples made from a commercial PA6 resin (CAPRON 8202C - Allied Signal Inc.), were also prepared. Tensile testing was undertaken on a Lloyd L1000S tensometer at a strain rate of 50mm min^{-1} in accordance with ASTM D638 procedures. Izod impact testing was conducted on notched specimens at 25°C in accordance with ASTM D256 procedures.

2.4 Determination of Molecular Weight and Residual Monomer Residue Content

MW and MWD was determined using gel permeation chromatography. The caprolactam monomer residue content of the as-processed samples prepared from different processing conditions were evaluated using a modified gas chromatography technique.

3. RESULTS AND DISCUSSION

3.1 DSC Analysis

Polymer melting and crystallization temperatures are listed in Table 1. These values are representative of transition temperatures for the different PA6 samples prepared using extruder speeds of 50, 70, 90, 120 and 150 rpm since little variation in transition temperatures was seen as a function of screw speed. It is observed that all the samples yield consistent Stage 2 peak melting temperatures of between 213°C-215°C, which is comparable to commercial grade PA6 resins prepared by hydrolytic polymerisation process. However, a noticeable increase in maximum crystallisation temperatures (T_c) was recorded for the short glass fibre reinforced samples as compared to unfilled PA6. This observation suggests that the glass fibre nucleates PA6 during melt crystallization. Differences in endothermic melting temperatures obtained between Stage 1 and Stage 2 heating profiles were also recorded for the

reinforced samples.

Figure 2 shows DSC thermograms of the samples obtained from Stage 1 and Stage 2 heating cycles. During Stage 1, both the unreinforced water quenched and glass reinforced water quenched samples exhibit broad melting peaks [2(a) and (e)], which can be attributed to melting of the smaller, less perfectly organised crystals at lower temperatures. After annealing these samples at 180°C for 90 minutes followed by slow cooling to room temperature, a narrower melting peak with only a slight shoulder at the lower temperature slope was obtained [2(b) and (f)]. The shoulder is more pronounced however, for the annealed,reinforced samples [Figure 2(f)]. Similar but more obvious shoulder peaks were also observed for the air-cooled samples [2(c) and (d)]. These lower temperature melting peaks are tentatively attributed to the melting of the γ crystalline phase of PA6. During Stage 2 heating, all samples regardless of previous history showed rather similar DSC thermograms, with bimodal melting peaks possibly due to melting of α and γ crystalline phases of PA6, resulting from slow cooling and subsequent reheating the samples during the second DSC scan. The heats of fusion and crystallization for all the PA6 samples, including the commercial grade, were observed to be about 60-65 Jg^{-1} which is equivalent to about 31%-34% crystallinity.

3.2 *WAXD Analysis*

WAXD reflection profiles of water quenched PA6 samples are shown in Figure 3 (a). Two sharp peaks are observed characteristic of α crystalline phases with interplanar spacings of d_{200}=4.44Å and d_{002}=3.82Å corresponding to Bragg angles (2θ) of ≈20° and ≈23° respectively. All the air-cooled samples prepared, except for material extruded at 150 rpm, showed similar WAXD pattern to the water quenched materials. The WAXD profile of the sample made at 150 rpm has an additional reflection peak at a Bragg angle (2θ) of 21° which is characteristic of a PA6 γ peak [Figure 3(c)]. However, all the water quenched and air-cooled samples upon annealing, yield only two peaks on the WAXD profiles indicating the presence of only the α crystalline phases [Figure 3(b) and(d)]. The disappearance of the γ peak for the 150 rpm air-cooled sample upon annealing agrees with the finding of Kyotani [6] which stated that the γ crystalline phase of PA6 is unstable at temperatures above 160°C and could possibly transform into either an amorphous or the more stable α form.

The WAXD profiles for glass fibre reinforced samples prepared at various extruder screw speeds are as shown in Figure 3 (e) and (f). In addition to the two sharp α peak reflections, another reflection peak with lower intensity is observed at Bragg angles (2θ) of 21°, corresponding to a crystal inter-planar spacing of d_{100}=4.24Å which is again consistent with the presence of the γ crystalline form of PA6 [Figure 3(e)]. This observation supports the view that the presence of glass fibre during polymerisation of ε-caprolactam nucleates the polymer, leading to formation of an additional γ phase in PA6. This finding is in agreement with the with the DSC analysis discussed earlier. Furthermore, it is observed that on annealing the composite PA6 sample at 180°C for 90 minutes, both the α and γ peaks remain but with increased intensity [Figure 3(f)]. This finding is in contrast with the WAXD profile for the sample extruded at 150 rpm which also has an additional γ peak which disappeared upon annealing as discussed earlier [Figure 3(c) and 3(d)].

3.3 *Determination of Mechanical Properties*

Figure 4 compares mechanical properties of PA6 samples produced at different extruder screw speeds together with results for the commercial polymer. The unreinforced sample, obtained at 90 rpm, has the highest tensile strength, but is still about 30% lower than that for the commercial sample [G in Figure 4 (a)]. Incorporation of only 10% by weight of short glass fibre has the effect of raising the tensile strength to a level comparable to that of the commercial material [F in Figure 4 (a)]. By contrast, all the unreinforced samples recorded much higher elongation at break than either the short fibre reinforced variant or commercial grade [Figure 4(b)]. An improvement in toughness is also evident from the Izod impact resistance values depicted in Figure 4 (c). PA6 samples prepared at screw speeds of 150 rpm yielded the highest impact properties, about 30% greater than that of the commercial resin.

3.4 *Molecular Weight and Residual Monomer Content*

The molecular weight and molecular weight distribution (expressed as a polydispersity index) of the samples prepared at different extruder screw speeds were measured. Samples prepared at screw speeds of 70 and 90 rpm exhibits the highest molecular weights in the region 100 Kg mol^{-1} and high MWD of about 6. Samples obtained at other speeds also yield MW of 54-62Kg mol^{-1} which is about 80% higher than those obtained from commercial PA6 materials.

Unreinforced PA6 samples prepared at lowest and highest extruder speeds apparently possess the highest monomer residue contents (approximately 6%). It is however, interesting that much lower monomer residue contents are associated with the glass fibre reinforced samples (approximately 3%).

4. CONCLUSIONS

PA6 materials prepared by reactive polymerisation of caprolactam, using various extruder screw speeds yield different MW, MWD and residual monomer contents. The molecular weights obtained are generally much higher than commercial PA6 materials formed by hydrolytic polymerisation. Reactive polymerised PA6 materials also exhibit superior impact and elongation properties but have lower tensile strength. DSC and WAXD results indicated possible formation of a meta-stable γ crystalline phase structure obtained at a screw speed of 150 rpm and slow melt cooling conditions, in addition to the α crystalline forms. It is suggested that this thermally unstable γ crystalline state transforms into the more stable α phase upon annealing at a temperature of 180°C. On the other hand, it is observed that incorporating short glass fibres into the monomer during polymerisation can also induce the formation of the γ phase in addition to the α crystalline forms. This γ phase, is however, observed to be more stable and is apparently not be affected by subsequent annealing conditions. The glass fibres present in the PA6 samples may possible act as nucleating agents during melt crystallisation as evident from an increase of crystyallisation temperature of the cooling PA6 melt.

5. REFERENCES

1. Joyce,R.M.& Ritter,D.M.,U.S. Patent 2,251,519, 1941
2. K.Kircher,"Chemische Reaktionen bei der Kunstoffverarbeitung", p.101, Carl Hanser Verlag.
3. G.Menges & T.Bartilla, Polym.Eng.& Sci, 27, 16 1987.
4. U.Berghaus & W.Michaeli, Proceedings from ANTEC '90. Chicago p.1929-33.
5. T.Bartilla, D.Kirch, J.Nordmeier, E.Promper & Th.Strauch, Advances in Polym. Techn., 3, 339, 1986.
6. Kyotani,M., J. Macromol. Sci-Phys., B11(4), 509, 1975

Table 1 Peak melting and crystallisation temperatures of Polyamide 6

sample type	peak melting temperature (°C)		peak crystallisation temperature (°C)
	stage 1	stage 2	
water quenched	214.2	213.5	180.1
water quenched annealed	214.9	213.0	179.5
air-cooled	216.2	215.0	181.2
air-cooled annealed	216.1	214.5	181.0
water quenched glass	218.0	214.1	183.0
water quenched glass annealed	217.6	213.0	183.7

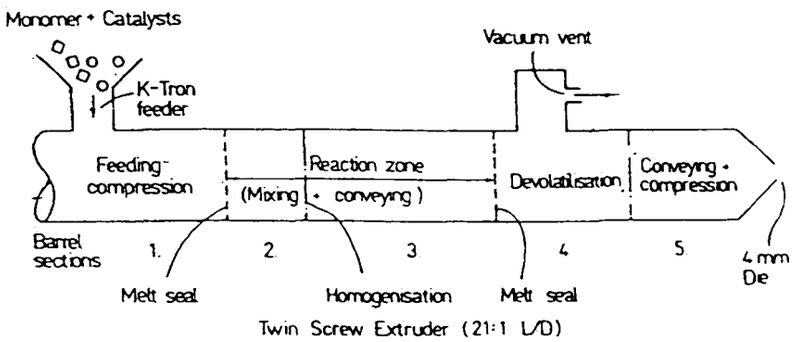

Figure 1 Schematic Diagram of Extruder for Polymerisation of PA6

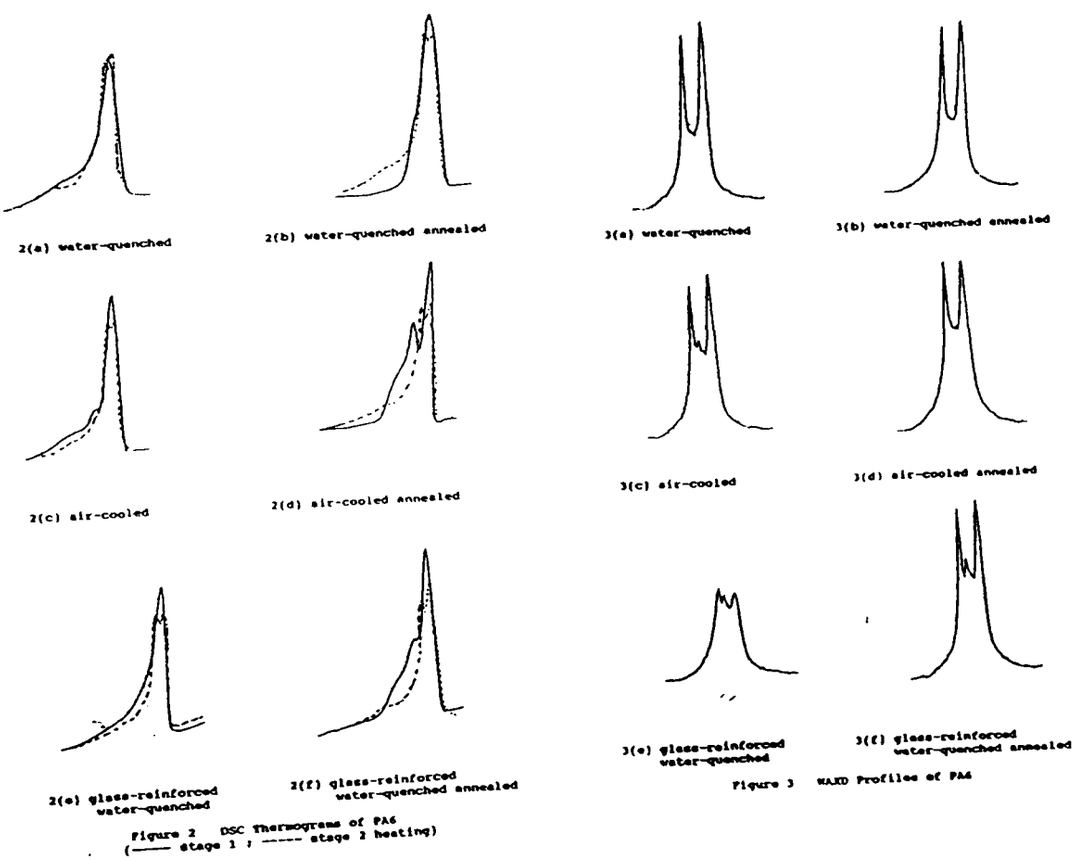

Figure 2 DSC Thermograms of PA6 (—— stage 1 ; ----- stage 2 heating)

Figure 3 WAXD Profiles of PA6